CHEMICAL REVIEWS

pubs.acs.org/CR Review

Coinage-Metal-Based Cyclic Trinuclear Complexes with Metal−Metal Interactions: Theories to Experiments and Structures to Functions

Ji Zheng, Zhou Lu, Kun Wu, Guo-Hong Ning,* and Dan Li*

Cite This: *Chem. Rev.* 2020, 120, 9675−9742 Read Online

ACCESS | Metrics & More | Article Recommendations | Supporting Information

ABSTRACT: Among the d^{10} coinage metal complexes, cyclic trinuclear complexes (CTCs) or trinuclear metallocycles with intratrimer metal−metal interactions are fascinating and important metal−organic or organometallic π-acids/bases. Each CTC of characteristic planar or near-planar trimetal nine-membered rings consists of Au(I)/Ag(I)/Cu(I) cations that linearly coordinate with N and/or C atoms in ditopic anionic bridging ligands. Since the first discovery of Au(I) CTC in the 1970s, research of CTCs has involved several fundamental areas, including noncovalent and metallophilic interaction, excimer/exciplex, acid−base chemistry, metalloaromaticity, supramolecular assemblies, and host/guest chemistry. These allow CTCs to be embraced in a wide range of innovative potential applications that include chemical sensing, semiconducting, gas and liquid adsorption/separation, catalysis, full-color display, and solid-state lighting. This review aims to provide a historic and comprehensive summary on CTCs and their extension to higher nuclearity complexes and coordination polymers from the perspectives of synthesis, structure, theoretical insight, and potential applications.

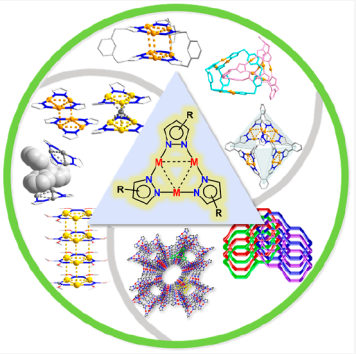

CONTENTS

Received: January 5, 2020
Published: August 11, 2020

https://dx.doi.org/10.1021/acs.chemrev.0c00011
Chem. Rev. 2020, 120, 9675−9742

1. INTRODUCTION

1.1. Historical and Broader Backgrounds

Coinage-metal-based cyclic trinuclear complexes (CTCs) represent a unique class of trinuclear metallocycles with M(I)−M(I) interactions and highly adjustable metal−organic or organometallic π-acidity/basicity. Such complexes are constructed from Au(I)/Ag(I)/Cu(I) cations and a series of angular ditopic anionic bridging ligands, including pyrazolate (Pz), imidazolate (Im), 1,2,4-triazolate (Trz), pyridinate (Py), and carbeniate (Cb) (Figure 1).[1−6] This family of transition-metal complexes has also been extended to coordination oligomers and coordination polymers based on secondary building units (SBUs) of cyclic trinuclear units (CTUs).[5,7]

Research of this family of the simplest polynuclear metal clusters does not only embrace fundamental theoretical insights and innovative applications but it is also highly complex. Indeed, since the first Au(I) CTC was reported by Vaughan in 1970,[8] investigations about CTC systems of coinage metals have covered a wide range of fundamental and applied research fields, including acid−base chemistry, metalloaromaticity, metal−metal interaction, supramolecular assemblies, excimers and exciplexes, host/guest chemistry, and metal−organic optoelectronics.[1−6,9−19]

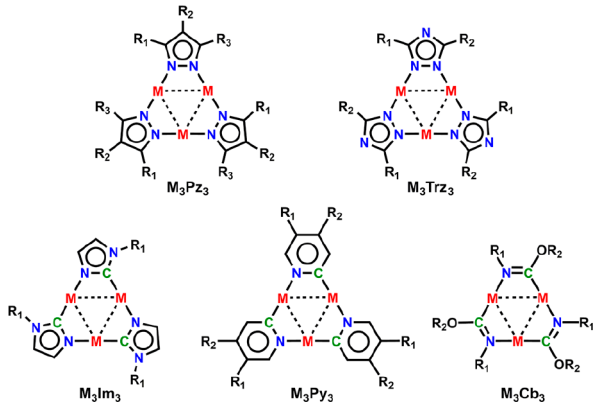

Figure 1. Representative cyclic trinuclear Au(I)/Ag(I)/Cu(I) complexes examined in this Review with coordinated atoms in the nine-membered rings highlighted in red for metal, blue for N, and green for C. The positions of substituents usually modified in the literature have been denoted as R_1, R_2, or R_3.

CTCs and CTU-based materials represent an active family in the long-standing debate of coinage-metal-based M(I)−M(I) interactions. Because of the linear two-coordinate metal centers, close intratrimer metal−metal distances, and near-planar conformations, as well as the ease of synthesis and modification of ligands and metal clusters, CTCs and CTU-based materials are considered to be a valuable platform to investigate multiple ligand-supported and ligand-unsupported homometallic and heterometallic M(I)−M(I) interactions and the related supramolecular aggregations.[12,14−17,19] A recent achievement was the construction of a heterometallic Au/Cu CTC, exhibiting a pair of polar covalent Au−Cu bonds with extremely short Au−Cu distances of 2.8750(8) Å in a chairlike dimer-of-trimer configuration.[20] The pioneering work of Dias, Omary, Cundari, Coppens, and co-workers highlighted the remarkably strong tendency of excimer formation with intermolecular Au(I)−Au(I) and Cu(I)−Cu(I) interactions for triggering bright phosphorescence.[21−25] In addition, CTCs are remarkable metal−organic (or organometallic) π-acids/bases,[5] and their π-acidity/basicity, as well as electron/hole-transporting properties, can be fine-tuned through chemical modification, as clarified by Omary, Cundari, and co-workers.[23] The 2018 reports by Hahn et al. demonstrated that the binding energies of the Au(I) and Ag(I) CTCs adducts could be considerably higher than those of the previously reported π-acid/π-base adducts.[26,27]

The multiple noncovalent interactions and relevant luminescence and charge-transporting properties have opened a vast area of potential applications. Since the beginning of CTC investigations, complexation and reactivities have been two of the most concerned aspects that have been extensively reviewed.[1−6] Related cases have been reported very recently, including reversible chemisorption/desorption of ethylene gas with low overall heat of adsorption and the activation of terminal alkynes to afford 1,4-substituted 1,2,3-triazoles in good yields under mild reaction conditions.[28,29] In addition, since 1997, luminescence properties and relevant potential applications have become emerging interests in the family of CTCs. In that year, the unique solvent-stimulated luminescence behavior—namely, solvoluminescence—was reported for the hexagonal crystalline phase of $Au_3(MeN{=}COMe)_3$ (a Au_3Cb_3 complex) by Balch and co-workers.[30,31] Remarkably abundant luminescence behaviors have been discovered and well-studied. One attractive research area is the modulation of emission colors

https://dx.doi.org/10.1021/acs.chemrev.0c00011
Chem. Rev. 2020, 120, 9675−9742

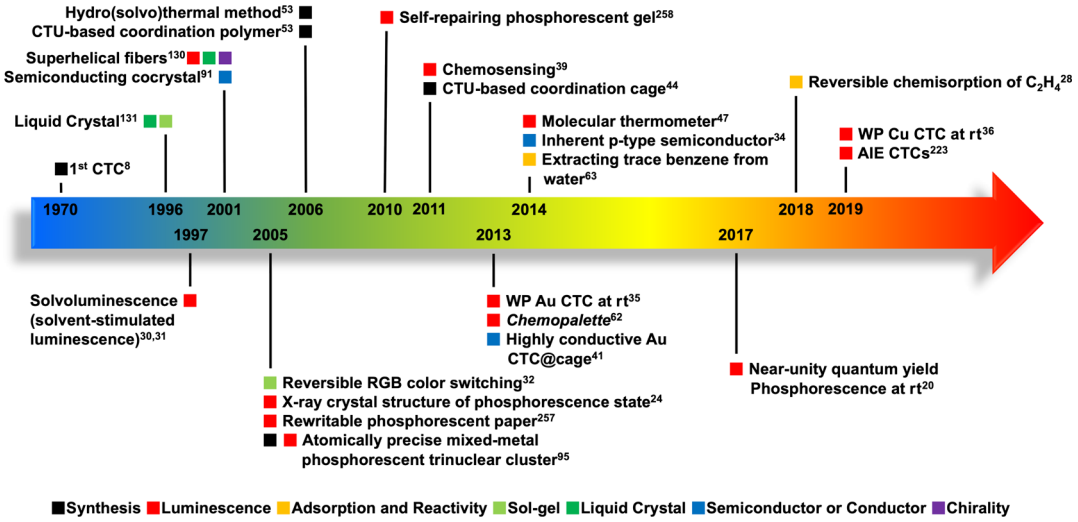

Figure 2. Milestones in the development of CTCs and CTU-based coordination cages and polymers of d^{10} monovalent coinage metal cations. [Abbreviations: RGB = red−green−blue, WP = white-phosphorescent, rt = room temperature, AIE = aggregation-induced emission.]

under physical or chemical stimuli. A typical case is $Cu_3[3,5\text{-}(CF_3)_2Pz]_3$ (CF_3 = trifluoromethyl), which exhibits luminescence thermochromism, solvatochromism, and concentration luminochromism, realizing a variety of phosphorescence colors that cover almost all the visible region.[21−23] In 2005, Aida and co-workers presented the reversible switch of red−green−blue (RGB) phosphorescence color triggered by the sol−gel transition and addition/removal of Ag(I) ions based on a dendritic Au_3Pz_3 complex.[32] Moreover, the emerging single-phase white-light-emitting materials are gaining significant importance in organic light-emitting diode/device (OLED) and light-emitting diode (LED) emitters, which have important applications in many fields, such as sensing, labeling, imaging, and anticounterfeiting methodologies.[33] The above-mentioned hexagonal Au_3Cb_3 was demonstrated as a white-phosphorescent emitter at room temperature (rt) by Cundari, Gnade, Omary, and co-workers in 2014.[34] In the family of pyrazolate CTCs, Li's group presented Au(I) and Cu(I) CTCs as examples of single-phase white-phosphorescent emitters at rt by modulating monomeric and excimeric dual emissions.[35,36] In addition, high quantum yield (QY) is a long-term goal in pushing CTCs toward lighting and display applications. $Cu_3[3,5\text{-}(CF_3)_2Pz]_3$ emits bright excimeric phosphorescence at rt with a phosphorescence QY approaching 80%.[20] A near-unity phosphorescence QY was achieved by Omary's group in 2017 via the construction of heterometallic Au/Cu CTCs.[20,37] Moreover, by doping Au(I) and Cu(I) CTCs in a polymer matrix, Elduque, Giménez, and co-workers achieved phosphorescence QYs of 90% in 2018.[38] CTCs are also capable of serving as effective chemical sensors. The nonemissive $Ag_3[3,5\text{-}(CF_3)_2Pz]_3$ drop-cast film exhibits reversible, fast, and highly sensitive detection toward aromatic vapors,[39] while $Au_3(3\text{-Me-}5\text{-COOH-Pz})_3$ is an effective phosphorescent sensor to detect Ag(I) cations over 15 other metal cations in aqueous media.[40] In addition to luminescence materials, CTCs act as electron conductors and semiconductors for potential applications in optoelectronics. Hexagonal $Au_3(MeN{=}COMe)_3$ was confirmed as a typical *p*-type semiconductor and subsequently fabricated in an organic field-effect transistor (OFET) in 2014.[34] By enclosing Au(I) CTC guests in coordination prism hosts, Kiguchi, Fujita, Tada, Watanabe, and co-workers demonstrated that such host−guest adducts are highly conductive molecular wires with electron transport comparable to that observed through metal atom wires and absolute conductance values significantly higher than those of metal-linked organic wires.[41]

The unique affinity and/or luminescence properties of CTCs have inspired researchers to move forward to construct a series of CTU-based coordination cages[42−52] and polymers.[53−68] Since the introduction of the hydro(solvo)thermal method into the construction of the CTC family in 2006, CTU-based coordination cages, polymers, and supramolecular aggregates have been feasibly prepared.[5,53] Over the past 10 years, exciting progresses have been demonstrated, including a dual-emitting $Cu_6{-}Cu_2{-}Cu_6$ cluster as a self-calibrated and wide-range luminescent molecular thermometer,[47] an exceptionally water-stable metal−organic framework (MOF) with hydrophobic nanospaces for extracting trace aromatic pollutants from water,[63] flexible MOFs for aborting several unsaturated hydrocarbons in a single-crystal-to-single-crystal manner,[54] and a luminescent sensor toward various organic compounds.[65]

The historical developments of CTCs and CTU-based materials of d^{10} monovalent coinage metals are summarized in Figure 2 and will be described and discussed in detail in this review.

1.2. Scope and Organization

Since 1997, few reviews that focus on or are related to monovalent d^{10} coinage-metal-based CTCs and CTU-based materials have been presented.[1−7,9,10,12−19,33,69] Indeed, such reviews have been restricted to individual research groups, limited aspects, or a specific era. Thus, this Review aims to contribute a comprehensive, critical, and informed narrative of the theoretical studies, syntheses, structures, rich photophysical properties, and other important properties, as well as relevant potential applications of neutral homometallic and heterometallic cyclic M_3L_3 complexes (M = Au(I), Ag(I), and Cu(I) cations; L = Pz, Im, Trz, Py, and Cb anions) and CTU-based materials. Mixed-valent and heterometallic clusters of metals other than Au(I), Ag(I), and Cu(I) are excluded from the scope of this Review, unless they arise from or result in Au(I)/Ag(I)/Cu(I) CTCs.

As an important counterpart in the family of d^{10}-metal CTCs, Hg(II) CTCs with μ-C,C-donor ligands (e.g., *ortho*-phenylene, perfluoro-*ortho*-phenylene, and *closo*-carborane

https://dx.doi.org/10.1021/acs.chemrev.0c00011
Chem. Rev. 2020, 120, 9675−9742

$C_2B_{10}H_{10}^{2-}$cage) date back to 1968.[70] Previous publications by Shur et al. and Taylor et al. have well reviewed the coordination chemistry and complexing properties of Hg(II) CTCs, especially for perfluorinated $Hg_3(o\text{-}C_6F_4)_3$, first and widely used as receptors of anionic and aromatic species.[71,72] Herein, we no longer discuss the above-mentioned properties; however, luminescence and potential applications of Hg(II) CTCs are enclosed as supplements of coinage d^{10}-metal CTCs.

2. THEORETICAL STUDIES

2.1. Nature of Metal−Metal Interactions

The first Au(I) complex displaying a short Au−Au distance in the solid state was reported in 1988 and later, the term of "aurophilicity" was introduced by Schmidbaur to describe Au(I)−Au(I) bonding.[73−75] Since then, metal−bonding (metallophilic interaction/bonding) between monovalent coinage-metal cations has been attracting significant attention.[12,14−16,18,19] Such closed-shell attraction usually plays an essential role in the chemistry and fascinating geometrical and electronic structural diversity, as well as many potential applications in materials science, catalysis, and medicinal chemistry of Au(I)/Ag(I)/Cu(I) coordination compounds and their supramolecular aggregates.[12,14−16,18,19]

The mechanism of coinage-metal-based M(I)−M(I) interactions is still a subject of long-standing debate. For decades, it has been realized that the Au(I)−Au(I) bonding energies usually approach those of standard hydrogen bonding.[12] Indeed, by combining the binding energies obtained from gas-phase experiments and high-level quantum calculations on a series of dimeric Au(I) complexes, Růžička, Roithová, Rulíšek, and co-workers recently suggested that strong aurophilic interactions could be comparable or even greater than strong hydrogen bonds.[76] On the other hand, although usually weaker than Au(I)−Au(I) interactions, Ag(I)−Ag(I) and Cu(I)−Cu(I) interactions are still noticeably stronger than normal van der Waals (vdW) interactions.[15,18] In addition, the closed-shell d^{10} electronic configurations should result in (i) Pauli repulsion, rather than covalent bonds, between open-shell species and (ii) Coulomb repulsion, rather than electrostatic attraction, between oppositely charged ions.

Strong attractions between closed-shell cations are usually unexpected and thus, the attraction between d^{10} coinage metal cations is considered one of the most remarkable chemical interactions ever reported. In 1978, an orbital hybridization mechanism was proposed by Hoffmann and co-workers to explain the Cu(I)−Cu(I) bonding in a series of Cu(I) coordination compounds based on the extended Hückel theory (EHT).[77] Later, they suggested that such a mechanism was also partially suitable for dinuclear and polymeric Au(I) complexes.[78] The hybridization picture refers to the orbital hybridization between occupied n d orbitals and empty $(n+1)$ s orbitals, thus leading to an open-shell electronic configuration and allowing the formation of metal−metal covalent bonds. Within the framework of molecular orbital (MO) theory, it can also be expressed as more electrons occupying metal−metal bonding than antibonding orbitals or the combination of filled strong metal−metal bonding and weak metal−metal antibonding orbitals. However, using high-level theoretical calculations, Pyykkö and co-workers argued that the hybridization mechanism could not account for these M(I)−M(I) interactions.[79−81] Instead, they suggested that the electron correlation, strengthened by the relativistic effect, played an essential role and the M(I)−M(I) interaction was attributed to the London dispersion effect, although such an attraction could be remarkably stronger than the normal vdW interactions.

Over the past decades, reported insights into M(I)−M(I) interactions have extended from dinuclear to polynuclear systems, homometallic to heterometallic systems, and ground to excited states, leading to a more extensive and deeper understanding of metallophilic bonding and pushing the debate into new stages.[14−16,18,19]

2.1.1. Simple Models: Dinuclear and Dimeric Mononuclear Complexes. Dinuclear supramolecular complex systems, including dinuclear and dimeric mononuclear compounds, represent the smallest chemical entities to exhibit M(I)−M(I) interactions. In this section, a series of representative dinuclear and dimeric mononuclear complexes have been selected to demonstrate the latest progress on the understanding of the nature of ligand-supported and ligand-unsupported M(I)−M(I) interactions in dinuclear systems.

Figure 3a shows typical structures of a dimeric mononuclear Au(I) compound with a pair of intermolecular Au(I)−Au(I)

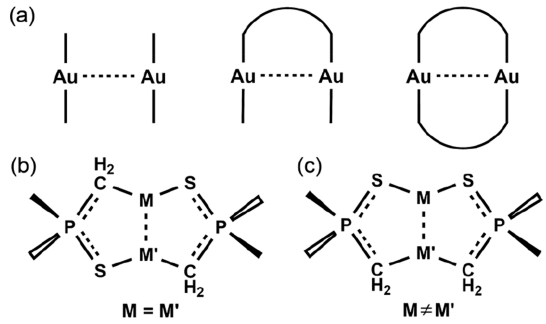

Figure 3. Representative chemical structures of (a) dinuclear supramolecular complex systems with ligand-unsupported and ligand-supported Au(I)−Au(I) interactions and (b) cyclic homobimetallic or (c) heterobimetallic Au(I)/Ag(I)/Cu(I) complexes in ref 37.

contacts and dinuclear Au(I) compounds with intramolecular Au(I)−Au(I) contacts. Cyclic dinuclear Au(I) complexes were among the earliest indicatives of ligand-supported aurophilicity,[12] which were constructed by bridging ligands containing S or P atoms (e.g., bis(diphenylphosphino)methane (dppm)).[82−84] They showed unusual twists in the eight-membered ring structures arising from the attractions between two Au atoms, later described as aurophilicity.[12]

Recently, based on their similar molecular frameworks (Figure 3b), Omary's group provided in-depth comparisons, from theoretical aspects, between ligand-supported homometallic and heterometallic M(I)−M(I) (M = Au, Ag, and Cu) interactions at both ground and excited states.[37] Computational studies were conducted on a series of dinuclear complexes with ligand-supported metal−metal bonding, sharing the formula $MM'[MTP(H)]_2$ (where M and M′ refer to the same and different M(I) cations, respectively, and MTP(H) refers to $H_2CPH_2S^-$ anions). The calculations were performed at the high level of theory using the second-order Møller−Plesset perturbation method (MP2) and cc-pVTZ as the basis set, with pseudopotentials added for Au and Ag. All optimized homobimetallic and heterobimetallic complexes exhibited metal−metal distances shorter than the sum of the vdW radii, and the distances of the heterobimetallic complexes were even shorter than the sum of covalent radii. By combining the geometrical and electronic analysis data (especially orbital

https://dx.doi.org/10.1021/acs.chemrev.0c00011
Chem. Rev. 2020, 120, 9675−9742

analysis and total electron density plots), the following important deductions were made: (i) heterometallic metal−metal interactions are stronger than homometallic interactions, among which Au−Cu bonding is the strongest; (ii) the covalent bonding character plays a more significant role in the heterometallic metal−metal interactions. This was related to the greater number of metal−metal bonding orbitals, over antibonding orbitals, of the occupied frontier molecular orbitals (FMOs), while the same number of bonding and antibonding orbitals resulted in zero formal bond order in homometallic metal−metal interactions; and (iii) the asymmetric bridging ligands introduce covalent bonding character in metal−metal bonding, even in homobimetallic complexes. In addition, natural bond order analysis revealed that the net electron donations were from Au(I) to Cu(I) and Ag(I) in the heterometallic models, indicating that Au(I) acts as a Lewis base and Ag(I) and Cu(I) serve as Lewis acids. This is related to another interesting chemical concept, and readers can refer to the review article by Braunschweig, which focuses on Lewis pairs consisting of Lewis acidic metals and Lewis basic transition metals.[84] The differences between homobimetallic and heterobimetallic M(I)−M(I) interactions also lead to differences in the transition energies and the nature of excited states.

Compared to the above-mentioned cyclic dinuclear compounds, the dimeric mononuclear complexes are more important chemical entities for demonstrating the spontaneous attraction between M(I) cations, i.e., the ligand-unsupported M(I)−M(I) interactions. A representative example is $(H_3P-Au-Cl)_2$, reported by Schwarz and co-workers in 2004, for which DFT calculations suggested that orbital mixing was responsible for the Au−Au bonding in perpendicular $(H_3P-Au-Cl)_2$ (Figure 4a) and the orbital interaction energy was as large as −21 kcal/mol.[85] However, their results were based on a simple local Xα exchange potential (S-LDF) DFT calculation and, thus, could be attributed to the fortuitous cancellation of errors.

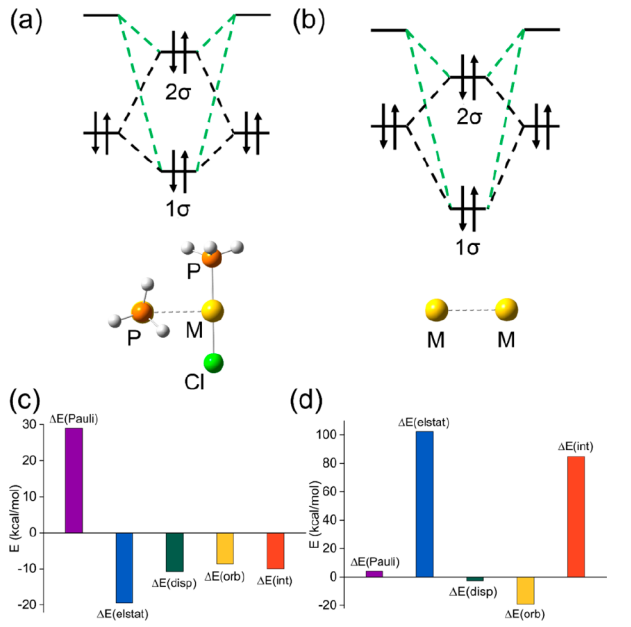

Figure 4. Calculated models and corresponding MO levels of (a) molecular perpendicular $(H_3P-M-X)_2$ and (b) naked dimeric M(I) ions with the M−M distance in the equilibrium (optimized) geometries of $(H_3P-M-Cl)_2$. EDA results for (c) $(H_3P-Au-Cl)_2$ and (d) the naked Au(I) dimer. Data are taken from ref 86.

Recently, Nitsch, Guerra, and co-workers provided a comprehensive comparison for molecular perpendicular $(H_3P-M-X)_2$ (M = Au, Ag, and Cu; X= F, Cl, Br, and I) at the ZORA-BLYP-D3(BJ)/TZ2P level of theory.[86] The dispersion-corrected density functional theory (DFT-D3) developed by Grimme renders a significantly superior performance in describing the dispersion force, compared to many traditional DFT methods (e.g., BLYP, B3LYP, and PBE0), which cannot account for long-range correlation effects.[87] Energy decomposition analysis (EDA) was used therein to divide the dimerization energy (ΔE(dim)) of $(H_3P-M-X)_2$ formation into the interaction energy between the deformed (H_3P-M-X) fragments (ΔE(int)) and the preparation or strain energy of these deformed fragments (ΔE(prep)). Moreover, ΔE(int) was further broken down to the Pauli-repulsive orbital interaction (ΔE(Pauli)) between same-spin electrons, electrostatic interaction (ΔE(elstat)), interaction caused by the dispersion force (ΔE(disp)), and orbital interaction (ΔE(orb)) from charge transfer (CT; interaction between occupied orbitals on one fragment with unoccupied orbitals on the other fragment, including donor−acceptor interactions) and polarization (empty−occupied orbital mixing on one fragment, because of the presence of the other fragment). It was found that ΔE(elstat) played the most important role in stabilizing $(H_3P-M-X)_2$, while ΔE(orb) played a minor but not negligible role in the attraction energy terms (Figure 4c). The dimer cannot be formed without ΔE(orb), because of the strong two-orbital, four-electron Pauli repulsion. Interestingly, by removing the ligands, the resulting dimer of naked M(I) cations highlighted the essential role of ΔE(orb) (Figure 4d). As expected, the simple M(I) ions were repulsive, because of strong Coulomb repulsion. However, by fixing the M−M distances to values equal to those in the equilibrium (optimized) geometries of $(H_3P-M-Cl)_2$ (e.g., 3.15 Å in $(H_3P-Au-Cl)_2$), they found that the orbital interaction was larger than the Pauli repulsion and dispersive attraction, indicating that the net MO attraction arising from orbital hybridization was more significant than ΔE(disp) in stabilizing the dimer.

The investigation of metal−metal bonding in dinuclear systems provides important information to better understand the nature of metal−metal bonding in polynuclear systems. However, the study of bimetallic M(I)−M(I) interactions is still ongoing (e.g., the heterobimetallic M(I)−M(I) bonding in excited states is less explored). In addition, complex polynuclear systems may result in different hypotheses and interpretations from those of dinuclear systems; this debate is still ongoing.

2.1.2. Two-Plus-One, More-Than-Three: Cyclic Trinuclear Complexes. Beyond dinuclear systems, cyclic trinuclear Au(I)/Ag(I)/Cu(I) compounds and their aggregates often exhibit abundant intratrimer (ligand-supported) and intertrimer (ligand-unsupported) metal−metal interactions or bonding at the ground and/or excited states.

The Pz, Trz, Im, Cb, and Py ligands act as short and rigid bridges for linking metal cations within the CTCs, resulting in intratrimer metal−metal distances ranging from 3.10 Å to 3.50 Å for most homometallic Au(I)/Ag(I)/Cu(I) CTCs, based on the available X-ray crystal data and theoretical optimized geometries. Usually, the intratrimer Au(I)−Au(I) and Ag(I)−Ag(I) distances are close to or even shorter than the corresponding sum of vdW radii (3.32 Å for Au and 3.44 Å for Ag), indicating notable metal−metal interactions at the ground states. In

https://dx.doi.org/10.1021/acs.chemrev.0c00011
Chem. Rev. 2020, 120, 9675−9742

contrast, their Cu analogues have intratrimer Cu−Cu distances that are significantly longer than the sum of the vdW radii of Cu (2.80 Å). The vdW radii of Au (1.66 Å), Ag (1.72 Å), and Cu (1.40 Å) are provided by Bondi.[88]

Few computational efforts have been made to shed light on the nature of intratrimer metal−metal bonding for homometallic Au(I)/Ag(I)/Cu(I) CTCs; however, such interactions (if they exist) are usually considered to be typical closed-shell interactions. In 2015, Caramori et al. conducted a comprehensive computational study on a series of Au(I)/Ag(I)/Cu(I) CTC molecules and cations constructed from five-/six-membered heterocyclic ditopic ligands, including Pz and Py.[89] Their results suggested that the intratrimer metal−metal interactions did not exist in these metallotriangles.

Compared to the intratrimer metal−metal distances, the lack of restriction from rigid bridging ligands renders a much wider range of intertrimer metal−metal distances, from values approaching the sum of the vdW radii of metals to distances of >5 Å. For CTCs with certain metals, it is reasonable to assume that the one with the shortest metal−metal distances may exhibit intertrimer M−M interactions with partial covalent contributions. For instance, the crystal structure of Au_3(1-EtIm)$_3$ (1-EtIm = 1-ethylimidazolate) reported by Omary and co-workers in 2017 displayed the shortest intertrimer Au−Au distances (3.067 Å at 100 K) among the Au(I) CTCs reported to date, which were much shorter than 3.32 Å.[90] Indeed, several Au(I) CTCs have been reported to comprise intertrimer Au−Au distances of <3.32 Å. A remarkable representative was reported by Fackler and co-workers in 2001.[91] They found that the intertrimer Au−Au distances of Au_3(1-BzIm)$_3$ (1-BzIm = 1-benzylimidazolate) decreased from 3.347−3.558 Å in the single-component crystal to 3.152 Å in its co-crystal, in which each Au_3(1-BzIm)$_3$ dimer was sandwiched by two 7,7,8,8-tetracyanoquinodimethane (TCNQ) monomers (see Figure 5). They

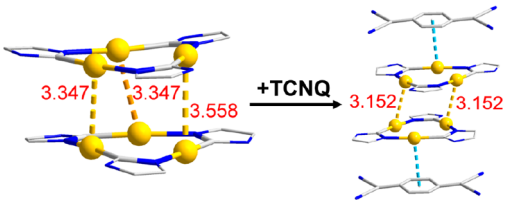

Figure 5. Dimer of Au_3(1-BzIm)$_3$ before and after adducting with TCNQ. The Bz groups and hydrogen atoms have been omitted from the figure for the sake of clarity. Numbers in red refer to intertrimer Au−Au distances (Å). Data are taken from ref 91.

also suggested the formation of Au(II)−Au(II) covalent single bonds due to the partial oxidation of Au(I).[91] Such partial oxidation resulted from electron transfer from Au_3(1-BzIm)$_3$ to the strong π-accepting TCNQ, supported by the darker color of the co-crystal, in contrast to the colorless Au_3(1-BzIm)$_3$ and light-orange TCNQ crystals.

To date, among the unsolvated crystals of Ag(I) CTCs, the shortest intertrimer Ag−Ag contact was reported by Fackler and co-workers in 2005.[92] The crystal structures of Ag_3(3,5-Ph_2Pz)$_3$ (Ph = phenyl) present Ag−Ag contacts as short as 2.9786(11) Å at 110 K, which are much shorter than the sum of vdW radii of Ag atoms (3.44 Å). Their preliminary DFT calculation at the B3LYP level of theory showed antibonding character between the d-orbitals of different Ag atoms in most of the metal-centered occupied FMOs of Ag_3(3,5-Ph_2Pz)$_3$ (Figure 6), indicating that the covalent bonding did not account for the

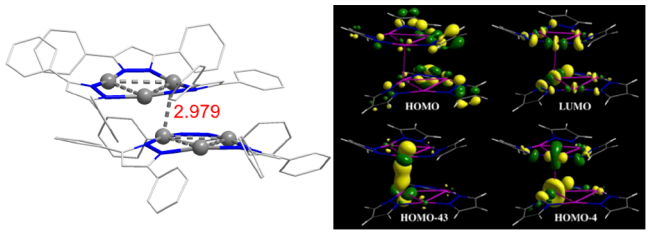

Figure 6. (Left) Dimer-of-trimer model taken from the unsolvated crystalline Ag_3(3,5-Ph_2Pz)$_3$ and (right) contours of selected orbitals based on the simplified dimer model by replacing Ph groups with H atoms (isovalue = 0.05). Number in red refers to intertrimer Ag−Ag distances (Å). [All H atoms have been omitted from the figure for the sake of clarity.] [Reprinted with permission from ref 92. Copyright 2005, Elsevier, Amsterdam.]

short Ag−Ag contacts. Thus, the short Ag−Ag interactions were assigned as London dispersion forces, which are common in homometallic metal−metal interactions based on d^{10} coinage metal ions. Interestingly, the Ag−Ag distance 2.9786(11) Å is considerably shorter than the shortest reported Au−Au distance (3.067 Å in Au_3(1-EtIm)$_3$). Thus, unsolvated crystalline Ag_3(3,5-Ph_2Pz)$_3$ seems an unusual case for presenting Ag−Ag interactions stronger than Au−Au interactions, even though Au atoms normally exhibit a stronger relativistic effect and smaller vdW radius than Ag atoms. Therefore, we believe that further bonding analysis on short Au(I)−Au(I) and Ag(I)−Ag(I) contacts/interactions are required to decipher the origins of the bonding/bond nature.

In the Cu(I) CTC family, only the unsubstituted Cu_3Py_3 crystals exhibit intertrimer Cu−Cu contacts (2.7624(6) Å at 180 K) shorter than 2.80 Å; however, no reliable computational studies have been performed to elucidate the nature of the Cu−Cu interactions in Cu_3Py_3 crystals.[93] Among the other Cu(I) CTCs reported to date, the shortest intertrimer Cu−Cu contact was reported by Li and co-workers in 2016.[94] In one of the polymorphs (**Br-*α***; formulated as Cu_3[4-(4′-Br-Ph)-3,5-(Me)$_2$Pz]$_3$), an extremely short intertrimer Cu−Cu contact (2.856 Å at 293 K and 2.817 Å at 100 K), approaching the vdW radii of Cu atoms, was observed in the dimer, assisted by parallelogram-like Br_4 halogen bonding and rigid Pz ligands. Notably, Cu−Cu contacts of <2.90 Å have not been observed in other Cu_3Pz_3 crystals. This indicates that such a short Cu−Cu contact may be "undesirable", and the additional directed supramolecular forces in **Br-*α*** (i.e., the halogen−halogen interactions orthogonal with Cu−Cu interaction) impose the extreme short Cu−Cu contact. To further understand the nature of Cu−Cu interactions, topological analyses (Figure 7) based on electron density distribution were performed. Quantum theory of atoms in molecules (QTAIM) analyses suggested that intratrimer Cu−Cu interactions did not exist, and the intertrimer Cu−Cu interactions were typical closed-shell interactions (London dispersion force domination; Figure 7a). However, the blue-green reduced density gradient (RDG) isosurfaces indicated that the intertrimer Cu−Cu interactions in the chair dimer were remarkably stronger than normal vdW attractions (Figure 7b). In the case of the Br_4 tetrameric unit, Br−Br interactions were also confirmed as closed-shell interactions, and the green RDG isosurfaces between the Br atoms indicated common vdW attractions (Figure 7c).

Compared to homometallic CTCs, their heterometallic analogues are less investigated, even though the first heterometallic CTC was reported as early as 2005.[95] Only

https://dx.doi.org/10.1021/acs.chemrev.0c00011
Chem. Rev. 2020, 120, 9675−9742

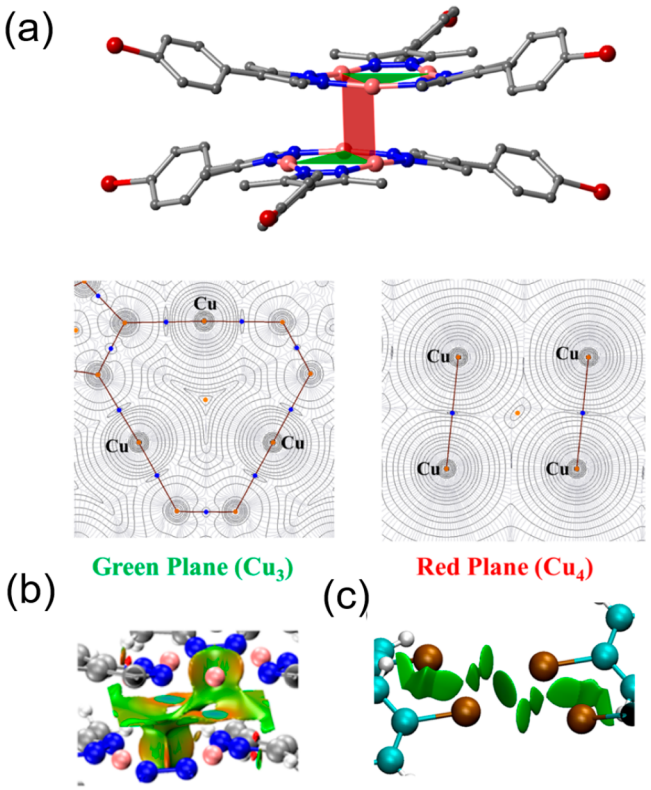

Figure 7. (a) QTAIM results in the planes containing intratrimer (Cu_3, shown in green) and intertrimer (Cu_4, shown in red) Cu(I)−Cu(I) interaction in the dimer of **Br-*α***. RDG isosurfaces of (b) the chair dimer connected by Cu(I)−Cu(I) interactions and (c) the tetramer connected by Br−Br interactions in **Br-*α***. The calculated models were taken from the X-ray data of **Br-*α*** determined at 100 K. [Reprinted with permission from ref 94. Copyright 2016, American Chemical Society, Washington, DC.]

three mixed-Au/Ag mixed-ligand CTCs have been documented with well-defined crystal structures. The shortest intertrimer Au−Ag distances are 3.082(2), 3.462(2), and 3.1423(8) Å for $AuCbAg_2Pz_2$, $(Au_2Cb_2AgPz)\cdot CH_2Cl_2$, and $AuImAg_2Pz_2$, respectively, where Cb = *p*-TolN═COEt, Pz = 3,5-Ph_2Pz, and Im = 1-BzIm (*p*-Tol = *p*-tolyl). The intertrimer Au−Ag distances 3.082(2) Å and 3.1423(8) Å are shorter than the intertrimer M−M contacts in most of the previously reported homometallic Au(I)/Ag(I) CTCs. However, these Au−Ag distances are still longer than 2.9786(11) Å, the intertrimer Ag−Ag distance in unsolvated crystalline $Ag_3(3,5\text{-}Ph_2Pz)_3$. The hybridization picture was reported to be suitable for intratrimer and intertrimer heterometallic metal−metal bonding. Muñiz and co-workers claimed that the intratrimer Au−Ag bonding involved the mixing of Au 5d and Ag 4d orbitals, by calculating a series of mixed-Au/Ag mixed-ligand CTCs, while the intertrimer Au−Ag bonding involved the mixing of Au 6s and Ag 5s orbitals.[96]

By replacing Ag with Cu, a mixed-Au/Cu mixed-ligand CTC can exhibit a much shorter intertrimer metal−metal contact. Recently, an extremely short ligand-unsupported Au−Cu contact of 2.8750(8) Å was observed by Omary and co-workers in the chairlike dimer of $Au_4Cu_2(1\text{-EtIm})_4[3,5\text{-}(CF_3)_2Pz]_2$.[20] This Au−Cu contact was noticeably shorter than not only the sum of vdW radii of Au and Cu but also other intratrimer and intertrimer Au−Ag distances in mixed-Au/Ag CTCs and Au−Au distances in Au CTCs. The binding energy was estimated to be 35−43 kcal/mol by DFT calculations, akin to typical M−M single-bond energies. In addition, nine Au−Cu strongly bonding molecular orbitals were found among the occupied orbitals. Computational results suggested that such ground-state ligand-unsupported Au−Cu interactions were polar-covalent bonds, further experimentally supported by the far-IR vibration mode in the FT-IR spectra. Nevertheless, it cannot be concluded that the Au−Cu bonding has a tendency to be stronger than the Au−Ag bonding in the heterometallic CTC family. By replacing the Et groups in $Au_4Cu_2(1\text{-EtIm})_4[3,5\text{-}(CF_3)_2Pz]_2$ with the bulkier benzyl (Bz) or less bulky Me groups, significantly longer Au−Cu contacts were observed with respective lengths of 3.317 and 3.055 Å.

Apart from heterometallic CTCs, sandwich-like Au_3−Ag−Au_3 clusters are newly developed heterometallic clusters in the CTC family, which have received much attention, because of their interesting luminescence and electron conductive behaviors.[5] Much shorter metal−metal contacts, compared to those in heterometallic CTCs, have been observed in these sandwiched clusters. The shortest intertrimer Au−Ag distances among all the reported crystals with Au_3−Ag−Au_3 clusters fall within the range 2.73−2.81 Å. Notably, apart from the CTC family, only 9 results for ligand-unsupported Au−Ag contacts shorter than 2.9 Å can be found in the Cambridge Structural Database (CSD).[97] The extremely short ligand-unsupported Au−Ag interactions in Au_3−Ag−Au_3 clusters are attributed to the synergism of heterometallic metal−metal bonding and Lewis-acid/π-base interaction (i.e., cation-π interaction). The orbital hybridization mechanism could be used to explain the heterometallic metal−metal bonding; however, extensive and in-depth electronic structural analysis to clarify the nature of such close metal−metal contacts has not been presented to date.

Despite that the intratrimer M(I)−M(I) interactions are often weak to absent in Au/Ag/Cu CTCs, intratrimer M(I)−M(I) bonding usually dominates the lowest-lying singlet and triplet excited states of Au/Ag/Cu CTC monomers. Furthermore, the extensive experimental and theoretical investigations performed before 2008 suggested that intertrimer M(I)−M(I) bonding is more essential in metal-centered phosphorescence than intratrimer interactions.[24,25]

Au(I) and Cu(I) CTCs are well-known metal−metal bonding phosphorescent coordination luminophores, while Ag CTCs with bright phosphorescence are quite rare. In this section, electronic insight into excited-state metal−metal bonds and their influence on the metal-centered phosphorescence of CTCs is discussed.

A series of important events demonstrated that intertrimer metal−metal bonding played a more important role than intratrimer metal−metal bonding in the bright phosphorescence of cyclic trinuclear Au(I)/Ag(I)/Cu(I) pyrazolate complexes. In 2003, Raptis and co-workers reported the bright rt red metal-centered phosphorescent unsubstituted Au_3Pz_3 and $Au_3(4\text{-}MePz)_3$, both exhibiting the shortest intertrimer Au−Au contacts below 3.20 Å.[98] In contrast, $Au_3(3\text{-Me-}5\text{-}PhPz)_3$ is nonemissive, because of its much longer intertrimer Au−Au contacts (>3.50 Å). Importantly, these three Au_3Pz_3 complexes display very similar intratrimer Au−Au distances, ranging from 3.30 Å to 3.40 Å.

In the same year, Dias, Omary, and co-workers reported a series of solid- and solution-state phosphorescence behaviors for $Cu_3[3,5\text{-}(CF_3)_2Pz]_3$, which exhibited infinite column stacking of CTC molecules (detailed structural and luminescence discussions in sections 4.2.2 and 5.1.1).[21] The spectral evidence

https://dx.doi.org/10.1021/acs.chemrev.0c00011
Chem. Rev. 2020, 120, 9675−9742

suggested that the bright room-temperature orange phosphorescence displayed by crystalline $Cu_3[3,5\text{-}(CF_3)_2Pz]_3$ was highly relevant to intertrimer Cu−Cu bonding rather than intratrimer Cu−Cu bonding, although the intertrimer Cu−Cu distances (>3.80 Å) were too long to observe ground-state Cu−Cu interactions. In 2005, Coppens and co-workers performed time-resolved single-crystal X-ray diffraction (SCXRD) on this Cu_3Pz_3 complex, and studied its phosphorescence emissive state (T_1 state) generated in the crystalline state at 17 K.[24] The X-ray structure analysis revealed a notable shortening of the intertrimer Cu−Cu distances from 4.018(1) Å at ground state to 3.46(1) Å at the T_1 state. Therefore, they confirmed that the phosphorescence was due to the formation of an intertrimer Cu−Cu bonding excimer rather than the shortening of the intratrimer Cu−Cu distances or the formation of a continuous chain of interacting CTC molecules. Theoretical calculations at the BLYP level of theory based on a ground-state dimer model revealed that the highest occupied molecular orbital (HOMO) and HOMO−1 consisted of large d-orbital contributions from the four Cu atoms that did not participate in excimer bonding, whereas the lowest unoccupied molecular orbital (LUMO) showed a pσ bonding orbital linked with the interacting Cu atoms, accompanied by additional contributions from the p-orbitals on the adjacent N atoms (Figure 8).

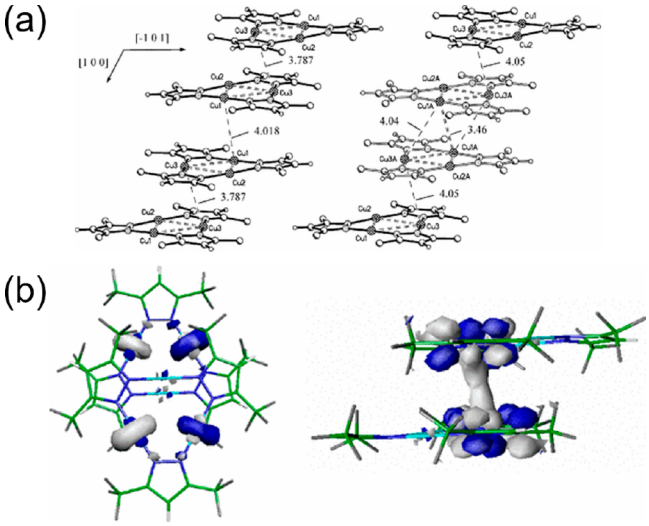

Figure 8. (a) Crystal structures of $Cu_3[3,5\text{-}(CF_3)_2Pz]_3$ at (left) ground state and (right) T_1 state at 17 K, and (b) the contours (isovalue = 0.03) of (left) HOMO and (right) LUMO for the ground-state dimer of $Cu_3[3,5\text{-}(CF_3)_2Pz]_3$. [Reprinted with permission from ref 24. Copyright 2005, American Physical Society.]

Further time-dependent density functional theory (TDDFT) calculations on $Cu_3[3,5\text{-}(CF_3)_2Pz]_3$ were performed by Zhang and co-workers in 2007, to investigate the influence of the related orientations and intertrimer distances of the dimer-of-trimer on the excitation and emission energies.[99] Their results suggested that longer intertrimer Cu−Cu distances favored higher excitation and emission energies.

The features of electronic structures and the relationship between the M−M distances and excited-state energies of the above-mentioned dimer-of-trimer were reproduced in the unsubstituted M_3Pz_3 complex, where M = Au(I), Ag(I), and Cu(I). In 2005, preliminary computational studies suggested the importance of excited-state metal−metal covalent bonding in the phosphorescence emissive states of CTCs.[23] The Kohn−Sham orbitals were calculated based on monomeric and dimeric models of Au(I)/Ag(I)/Cu(I) CTCs with unsubstituted Pz (Figure 9). The HOMO of monomeric Cu_3Pz_3 consists of Cu d-

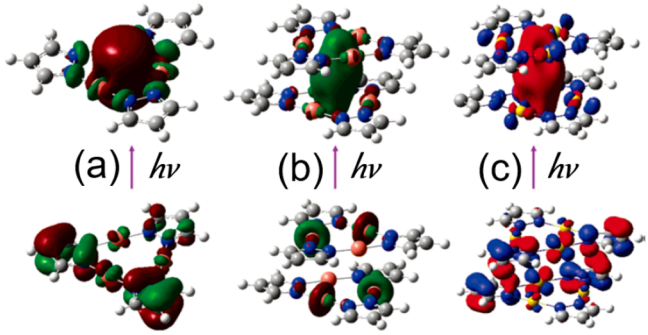

Figure 9. Contours of the two Kohn−Sham orbitals (HOMO and LUMO) involved in the lowest energy excitation of (a) the monomer and (b) the dimer of unsubstituted Cu_3Pz_3, as well as (c) the dimer of unsubstituted Au_3Pz_3. [Reprinted with permission from ref 23. Copyright 2005, American Chemical Society, Washington, DC.]

and Pz π^*-orbitals, and its LUMO is a typical intratrimer Cu−Cu bonding orbital. The dimeric model shows similar orbital populations, except that the HOMO is highly localized in the d-orbitals of Cu. Similar orbital features were presented for the Au and Ag models. Later, TDDFT calculations for these dimer models further confirmed the essential role of intertrimer metal−metal bonding in the phosphorescence of Au(I)/Ag(I)/Cu(I) CTCs.[25]

Therefore, the construction of an effective intertrimer metal−metal bonding excimeric triplet state is considered to be necessary to trigger the metal-centered phosphorescence of Au(I)/Ag(I)/Cu(I) CTCs, as well as CTU-based coordination cages and polymers. Related cases have been frequently reported to verify this mechanism.[36,90,100]

In 2019, Li's group reported a pair of room-temperature bright phosphorescent polymorphs (**Cl-*α*** and **Cl-*β***) of $Cu_3(4\text{-}ClPz)_3$.[36] TDDFT calculations at the PBE0 level of theory confirmed that the longer intertrimer Cu−Cu distances resulted in higher excitation and emission energies as both the lowest-lying singlet (S_1) and triplet (T_1) states were dominated by intertrimer Cu−Cu bonding (Figure 10). Such computational studies are consistent with the experimental observations. For instance, **Cl-*α***, with longer intertrimer Cu−Cu distances of 3.530 Å, afforded yellow emission (564 nm) triggered by high excitation (λ_{ex} = 270 or 290 nm), while **Cl-*β***, with shorter intertrimer Cu−Cu distances of 2.915 Å, produced orange emission (650 nm) triggered by a lower excitation (λ_{ex} = 330 nm).

2.2. Effects of the Electron Density Distribution

2.2.1. *π*-Acidity/Basicity. As a traditional concept in organic aromatic and supramolecular chemistry, π-acidity/basicity has been subject to extensive and in-depth investigation. The development of supramolecular chemistry shows that π-acidic/basic aromatic rings involve a series of supramolecular interactions, including $\pi-\pi$ stacking, cation/anion-π, π-acid/π-base packing, and C−H−π interactions. These π-acid/base-related rich and flexible supramolecular interactions render aromatics very promising candidates in many fields of applications, including gas and liquid adsorption and separation, optoelectronic materials, and catalysis. For most of the transition metal complexes, the π-acidity/basicity is usually dependent on

https://dx.doi.org/10.1021/acs.chemrev.0c00011
Chem. Rev. 2020, 120, 9675−9742

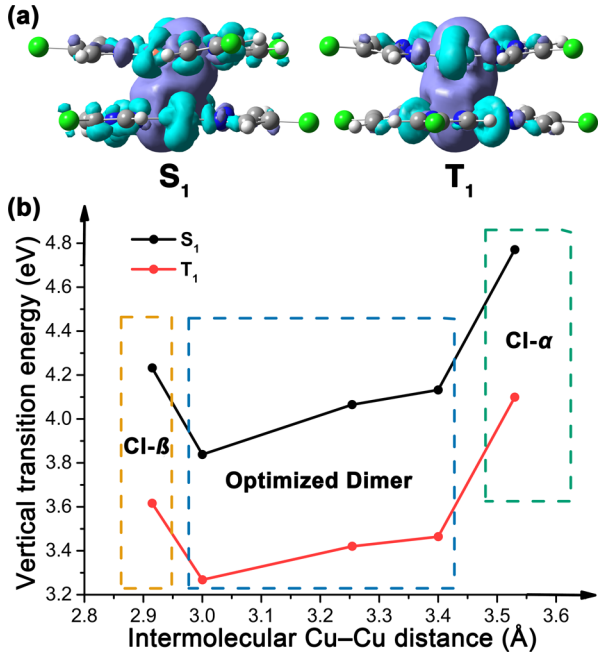

Figure 10. (a) Electron density difference (EDD) maps (isovalue = 5.0 × 10^{-4} a.u.) showing the intertrimer Cu−Cu bonding (left) S_1 and (right) T_1 states of optimized chair dimer of $Cu_3(4\text{-}ClPz)_3$. (b) Relationship between vertical transition energies of the S_1 and T_1 states and the intertrimer Cu−Cu distances of chair dimer models. The calculated models of **Cl-*α*** and **Cl-*β*** were taken from the corresponding single-crystal X-ray structures at 150 K. The optimized dimer referred to the optimized chair dimer with intertrimer Cu−Cu distances of 3.254 Å and the models were obtained by changing the Cu−Cu distances of this optimized geometry to 3.200 and 3.400 Å, respectively. Data were taken from ref 36.

their aromatic ligands, with small deviation from that of their proligands.

However, the unique metal−organic *π*-acidity/basicity of Au(I)/Ag(I)/Cu(I) CTCs is remarkably different from that of their respective proligands. The computational studies conducted by Omary, Cundari, Dias, and co-workers in 2005 and 2008 pioneered in the development of *π*-acidity/basicity for CTCs.[11,23] Positive charge attraction (PCA) energies and electrostatic potential (ESP) maps were adopted to quantify and visualize *π*-acidity/basicity and subsequently compare a series of CTCs and organic arenes. The following valuable deductions were made:

(i) The *π*-acidity/basicity of CTCs can be facilely modulated across a wide range by altering the chemical factors (metal, bridging ligand, and substituted groups). The relative *π*-acidity increases or *π*-basicity decreases in the following orders: Au → Cu → Ag for a given ligand, Im → Py → Cb → Pz → Trz for a given metal, and electron-donating substituents → electron-withdrawing substituents for a given M(I) CTC. To confirm their results, the ESP surfaces were reproduced (Figure 11) at the PBE0 level of theory[101,102] with the LanL2DZ basis set[103] for metals and the 6-31G(d,p) basis set[104] for nonmetals.

(ii) The *π*-basicity/*π*-acidity for trimetal nine-membered rings exceeds that of their corresponding ligands, despite these ligands being free or ligated.

(iii) Superior *π*-basicity and *π*-acidity can be achieved by rational design of the chemical compositions, compared to those of organic *π*-acids/bases.

The *π*-acidity/basicity is the most critical feature in predicting or explaining the binding strength between CTCs and other species, including inorganic Lewis bases (e.g., NH_3), inorganic Lewis acids (e.g., metal cations), and organic and metal−organic *π*-acids/*π*-bases.[4,5] Moreover, compared to those of organic *π*-acids/bases, the superior *π*-acidity/basicity of CTCs can provide

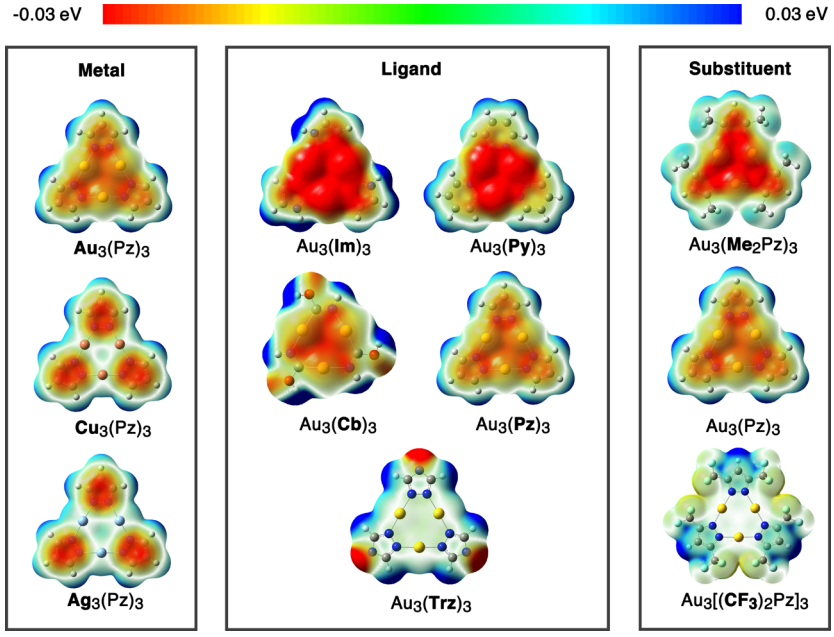

Figure 11. ESP surfaces showing the relative *π*-basicity of CTCs as a function of the metal, bridging ligand, and substituent. ESP surfaces are mapped on electron densities of the molecule (basicity increases in the direction of blue → green → yellow → orange → red in the ESP color scale). To compare the effects of substituent (R), the $Au_3[3,5\text{-}(R)_2Pz]_3$ models (simply denoted as $Au_3[(R)_2(Pz)]_3$) are selected with R = Me, H, and CF_3, respectively.

https://dx.doi.org/10.1021/acs.chemrev.0c00011
Chem. Rev. 2020, 120, 9675−9742

higher binding affinities.[11] A representative example was reported by Hahn, Esser, and co-workers in 2018.[27] By applying strong π-basic Au CTCs (i.e., Au_3Py_3, Au_3Im_3, and Au_3Cb_3), the π-acid/π-base adducts between Au CTCs with strong organic π-acceptors showed binding energies larger than those of many organic π-acid/π-base adducts. By replacing the organic π-acceptors with the stronger π-accepting $Ag_3[3,5\text{-}(CF_3)_2Pz]_3$, stronger binding with π-basic Au CTCs was achieved. The binding free energies between a series of π-basic Au_3Py_3 and $M_3[3,5\text{-}(CF_3)_2Pz]_3$ complexes increased with the increasing π-accepting abilities of $M_3[3,5\text{-}(CF_3)_2Pz]_3$ (Au < Cu < Ag).

Comparatively, the smaller rings *c*-$M_3(\mu\text{-}X)_3$ (*c* = *cyclo*), composed of Au(I), Ag(I), and Cu(I) cations and bridging halogen anions (i.e., F^-, Cl^-, Br^-, and I^-), are representative cases characterized as π-acids only by DFT calculations.[105,106] Positive ESP maps indicated that the M_3X_3 rings associated with the larger binding energies of π-basic benzene rather than those of π-acidic C_6F_6 (Figure 12).

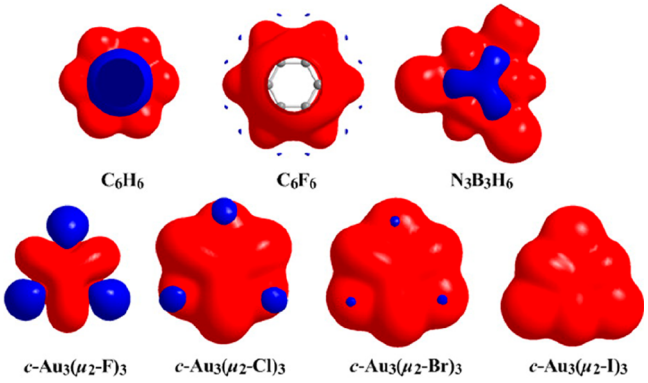

Figure 12. ESP isosurfaces (positive and negative regions shown in red and blue, respectively) of the *c*-$Au_3(\mu\text{-}X)_3$ (X = F, Cl, Br, I) CTCs and the benzene, hexafluorobenzene, and borazine molecules, calculated at the M05-2X/Def2-TZVPP level of theory (isovalue = 0.260 a.u.). [Reprinted with permission from ref 106. Copyright 2013, American Chemical Society, Washington, DC.]

On the other hand, for larger rings, the electron-deficient nature in the centroid of the ring allows the insertion of atoms or ions. One representative is the cyclic trinuclear Cu(II) pyrazolate unit, wherein a μ_3-bridging OH^- anion coordinates with three Cu ions, lying on the Cu_3 plane and along the C_3 axis.[107] For the Au(I)/Ag(I)/Cu(I) CTCs focused in this Review, experimental insertions of an atom or ion into the centroid of the ring without decomposition are still not documented. Interestingly, by selecting bulkier bridging ligands, this situation seems possible. The recent computational studies by Oliva-Enrich and co-workers showed that the cyclic trinuclear metal-carborane $[Au_3(\mu\text{-}1,2\text{-}C_2B_{10}H_{10})_3]^{3-}$ could host Be^{2+} and H^+ ions in the centroid of the Au_3 ring, lying on the Au_3 plane, while larger cations (e.g., Li^+ and Hg^{2+}) deviated from the Au_3 plane (Figure 13).[108] In addition, a carbon dioxide molecule could be inserted into the ring, where the C atom was located at the centroid of the Au_3 ring and the CO_2 molecule coincided with the C_3 axis of the CTCs. Notably, studies focusing on the π-acidity/basicity of coordination rings large enough to host an atom or ion in the ring plane are very scarce.

2.2.2. Aromaticity. Metalloaromaticity is one of the fundamental areas involved in cyclic trinuclear d^{10}-metal complexes.[11,17]

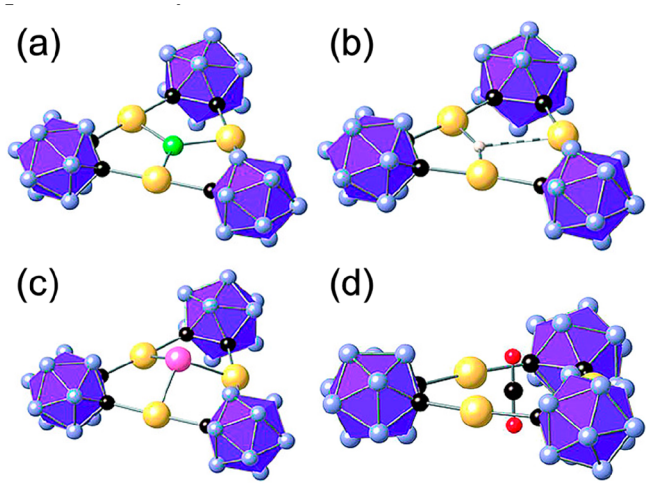

Figure 13. Optimized structures of $\{[Au_3(\mu\text{-}1,2\text{-}C_2B_{10}H_{10})_3]^{3-}\cdot G\}$ complexes, where G represents a guest and is (a) Be^{2+}, (b) H^+, (c) Li^+, and (d) CO_2, respectively. [Reprinted with permission from ref 108. Copyright 2019, Wiley−VCH Verlag GmbH & Co. KGaA, Weinheim, Germany.]

In 2006, the aromaticities of four Au CTCs with different ligands (MeN═COMe, $3,5\text{-}Me_2Pz$, 1-MeIm, and unsubstituted Py) were preliminarily studied by Sansores and co-workers, based on the index of the nucleus-independent chemical shift (NICS).[109] The negative NICSs in the centers of the nine-membered rings (NICS(0)) indicate their aromatic nature, while the more negative NICS values of the Pz and Im rings indicate a stronger aromaticity than that of the respective nine-membered rings. Of note, Py rings and the corresponding nine-membered Au_3Py_3 rings show close aromatic intensity.

In 2015, Caramori and co-workers conducted more comprehensive investigations on aromaticity. These included the anisotropy of the induced current density (AICD) and NICS (Figure 14) of Au(I)/Ag(I)/Cu(I) CTCs with five-/six-membered heterocyclic ditopic ligands, including the experimentally reported Pz and Py.[89] Although their results indicated that aromaticity only existed in the five- or six-membered rings of the ligands, they also noted that these data might be insufficient to determine the aromatic character of heavy-atom systems, using magnetic criteria.

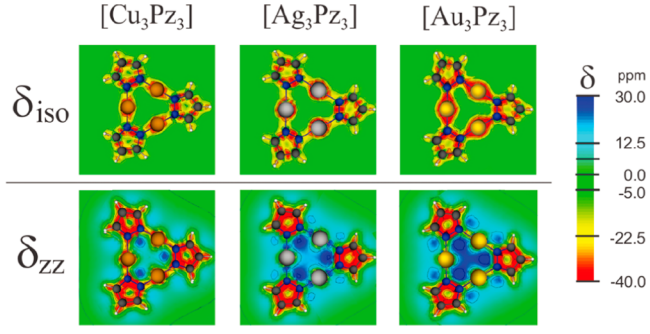

Figure 14. NICS over the molecular domain for unsubstituted Cu_3Pz_3, Ag_3Pz_3, and Au_3Pz_3. δ_{iso} and δ_{zz} represent isotropic values and along the *zz* directions, respectively. [Reprinted with permission from ref 89. Copyright 2015, Royal Society of Chemistry, London.]

Apart from those of Au(I)/Ag(I)/Cu(I) CTCs with nine-membered coordination rings, the metalloaromaticities of other

https://dx.doi.org/10.1021/acs.chemrev.0c00011
Chem. Rev. 2020, 120, 9675−9742

cyclic polynuclear Au(I)/Ag(I)/Cu(I) complexes with intra-trimer metal−metal interactions are also attractive. The review article by Tsipis in 2016 summarized numerous examples.[17] For instance, the above-mentioned π-acidic cyclic M_3X_3, where M represents d^{10} monovalent coinage metal ion and X represents bridging halogen anion, can interact with organic aromatics (e.g., benzene) to form binary stacks. NICS*zz*-scan analyses were conducted to evaluate the magnetotropicity of the binary stacks, and the results indicated that the diatropicity (magnetic aromaticity) of the M_3 rings increased upon interaction with aromatic arenes.[17,105,106] In this way, we are also expecting the stronger aromaticity of stacking CTCs, including binary adducts and dimers-of-trimers, is observed and confirmed, although Tsipis did not extend his conclusions to the CTC family.

Very recently, Kira, Li, and co-workers reported the synthesis of a cyclic $(R_2SnAu)_3$ anion (R_2Sn = 2,2,5,5-tetrakis-(trimethylsilyl)-1-stannacyclopentane-1,1-diyl), which was obtained as a stable blue salt with $K^+(THF)_6$, where THF is tetrahydrofuran (Figure 15).[110] The cyclic $(R_2SnAu)_3$ anion

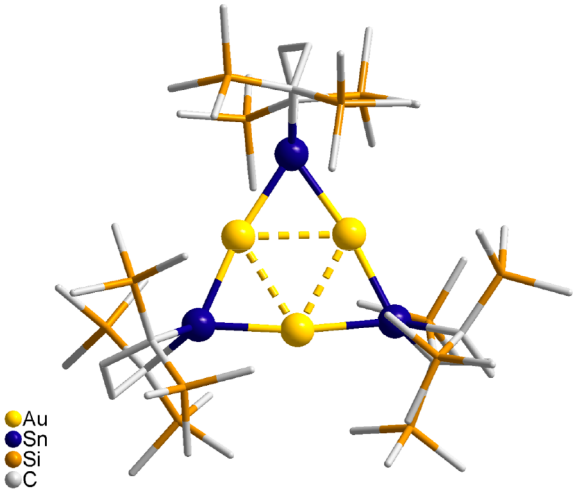

Figure 15. Molecular structure of $K^+[(R_2SnAu)_3]^-(THF)_6$, as determined by X-ray diffraction. [H atoms, solvent molecules, and the K^+ cation have been omitted from the figure for the sake of clarity.]

with three divalent tin ligands reported in ref 112 is not only the first example of a stable trigold anion but also a σ-Möbius aromatic molecule predicted by perturbation MO analyses at the CCSD level of theory.

3. SYNTHESIS AND REACTIVITY

3.1. Synthesis and Crystallization

Numerous cyclic trinuclear Au(I)/Ag(I)/Cu(I) complexes with the ligands Pz, Im, Trz, Py, and Cb, as well as a series of coordination cages and porous and nonporous coordination polymers adopting Au(I)/Ag(I)/Cu(I) CTUs as building blocks, have been obtained over the past decades. This section summarizes the synthetic approaches for CTCs and CTU-based coordination compounds and discusses several aspects that affect the formation of these compounds.

3.1.1. Electronic Effects: Ligands and Substituents. The electronic effects of ligands usually refer to their Brønsted acidity, which is the deprotonation ability of a ligand to afford the conjugated base. Experimental and calculated proton affinities have revealed that the energies of deprotonation of the ligands HIm, HPy, and HCb are considerably higher (>30 kcal/mol) than those of the HPz and HTrz ligands.[11] Such differences often result in a change in the reaction conditions required to prepare CTCs. Taking Au(I) CTCs as examples, Au_3Im_3, Au_3Py_3, and Au_3Cb_3 are usually obtained utilizing strong bases (e.g., *n*-butyllithium, KOH), while moderate or weak bases (e.g., triethylamine (Et_3N)) are considered for Au_3Pz_3 and Au_3Trz_3.

The stabilities of metal sources and their corresponding CTCs toward oxygen, temperature, and light are noteworthy. Most Au(I) CTCs are obtained by direct reactions between Au(Y)Cl (Y = reductive neutral weak donor, e.g., tetrahydrothiophene (THT), triphenyl phosphine (PPh_3), and dimethyl sulfide (Me_2S)) and the ligands. As an example, the weak electron-donating ability of THT allows ligand exchange with the strong μ-C,C/C,N/N,N-donating bridging ligands, and its reductivity stabilizes the easily oxidized Au(I) cation. Apart from the careful choice of Y, the thermal stability of Au(I) complexes must be considered during the synthesis of Au(I) CTCs. Thus, the syntheses and subsequent reactivity investigations of Au(I) CTCs are usually performed at room temperature or lower. Interestingly, the thermal stability of as-synthesized Au(I) CTCs is significantly better than that of the corresponding Au(I) sources.

The unsubstituted Au_3Py_3 complex was the first member of the Au/Ag/Cu CTC family, introduced by Vaughan in 1970.[8] By adding Au(Ph_3As)Cl to the dry THF solution of 2-pyridyllithium at −40 °C (Figure 16a), Au_3Py_3 was isolated as

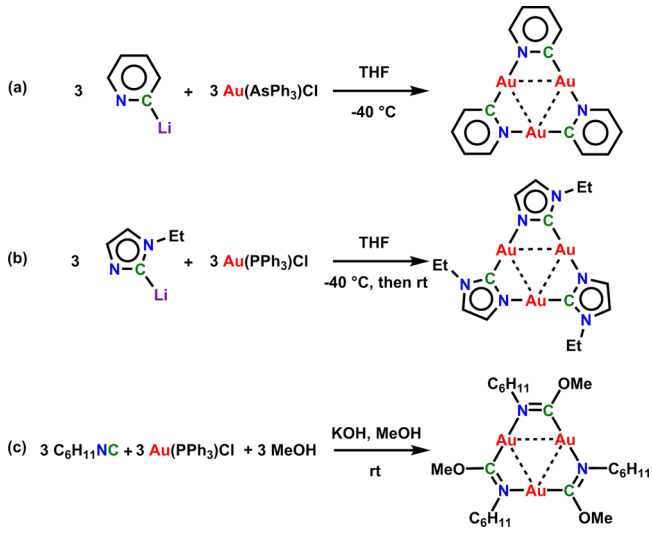

Figure 16. Typical synthetic approaches to Au(I) CTCs with μ-C,N-donor ligands, including (a) Au_3Py_3, (b) Au_3Im_3, and (c) Au_3Cb_3.

a powder in good yield and was insoluble in common organic solvents at rt (Box 1). After 30 years, single crystals suitable for X-ray diffraction (XRD) analysis were grown from hot pyridine solution, and their crystal structure was determined.[111] To date, a series of alkyl-substituted Au_3Py_3 have been synthesized using Vaughan's method; however, none of their corresponding X-ray crystal structural data have been reported.[8,26,27]

Au_3Py_3 is insoluble in most common organic solvents but can be recrystallized from high-boiling basic solvents such as pyridine (best), dimethyl sulfoxide (DMSO), and dimethylformamide (DMF). The pure compound is bright yellow crystalline solid, stable to air and water, but rather sensitive to light. When the compound is heated, decomposition is first

https://dx.doi.org/10.1021/acs.chemrev.0c00011
Chem. Rev. 2020, 120, 9675−9742

Box 1. Vaughan's Method to Synthesize Au_3Py_3.[8]

The compound is prepared by addition of solid $Au(Ph_3As)Cl$ to a THF (or ether) solution of 2-pyridyllithium at −40 °C. As the solution warms, the arsine complex dissolves (approximately −25 °C), followed by precipitation of the product (approximately −5 °C) in 90−100% yield. The reaction presumably proceeds through (2-pyridyl)$Au(AsPh_3)$ as an intermediate, followed by displacement of $AsPh_3$ by the unshared electron pair on nitrogen. $AsPh_3$ can be isolated from the solvent in the yields of 75−95%.

noted at ∼120 °C, followed by melting, with complete decomposition at 150 °C.

Sharing a similar C−Au−N coordination environment, Au_3Im_3 complexes were also obtained by Vaughan's method, affording $Au_3(1\text{-R-Im})_3$ with R = Me,[112] Et,[90] and Bz.[112] After adding $Au(Ph_3P)Cl$ to a dry THF solution of 1-R-2-lithiumimidazole at −40 °C (Figure 16b), crude brown solid powders were obtained, under rt conditions overnight, which could be extracted with CH_2Cl_2. Very recently, Ruiz et al. developed a new approach to Au_3Im_3 by producing a series of $Au_3(1\text{-R-5-MeIm})_3$ complexes with R = 2,6-xylyl, Ph, and 4-MeOPh.[113] The complexation of the mononuclear $[Au(CNR)_2]^+$ cations and $NH_2CH_2C{\equiv}CH$ in a molar ratio of 1:2 afforded the bis(diaminocarbene) derivative cations $[Au(C(NRH)(NHCH_2C{\equiv}CH))_2]^+$ and the mixture underwent a cyclization process to form dinuclear aggregates of Au(I) complexes with protic N-heterocyclic carbene (pNHC), following further treatment with NaH. $Au_3(1\text{-R-5-MeIm})_3$ could be obtained by treating the dinuclear Au(I)-pNHC aggregates with lithium bis(trimethylsilyl)amide (LiHMDS) and $Au(SMe_2)Cl$ or by directly heating them under vacuum at 150 °C (Scheme 1).

Cb ligands are also a class of μ-C,N-donors; however, Au_3Cb_3 is usually prepared under milder conditions than those adopted in Vaughan's method. The typical synthetic approach is illustrated in Figure 16c. By adding the Au(I) source before the corresponding isocyanide ($R_1{-}N{\equiv}C$) and KOH stoichiometrically in the R_2OH solution (R_1 and R_2 refer to a series of alkyl or aryl groups), insoluble Au_3Cb_3 complexes could be formed and crushed out. Since the first Au_3Cb_3 reported by Bonati and co-workers in 1972, this procedure has always been used to obtain Au_3Cb_3 complexes sharing the general formula $Au_3(R_1N{=}COR_2)_3$.[114] The only exception was $Au_3[2\text{-pyridyl-}N{=}CN(H)Me]_3$, which was prepared from the self-assembly of a mononuclear Au(I) carbene complex after deprotonation by KOH.[115]

Au_3Pz_3 and Au_3Trz_3 are constructed from μ-N,N-donor ligands, whereby the Au_3Pz_3 family has the most reported single crystal structures among the documented Au(I) CTCs. Since the first reported crystal structure of Au_3Pz_3 compounds ($Au_3[3,5\text{-}(CF_3)_2Pz]_3$[116]), most Au_3Pz_3 complexes and the only reported Au_3Trz_3 ($Au_3[3,5\text{-}(i\text{-Pr})_2Trz]_3$[100]) have been obtained via a typical approach described in Figure 17. Briefly, a mixture of the Au(I) source, pyrazole or triazole ligand, and base (e.g., KOH, NaH, or Et_3N) in THF or MeOH solution is stirred at rt to form colorless powders of the corresponding Au_3Pz_3 or Au_3Trz_3. For soluble Au_3Pz_3 and $Au_3[3,5\text{-}(i\text{-Pr})_2Trz]_3$, the single crystals are usually obtained by applying simple slow solvent evaporation or gas-phase diffusion of a poor solvent to their solution. Occasionally, if the evaporation and diffusion methods fail, the recrystallization approach is also employed for growing

Scheme 1. Brief Synthetic Routes for $Au(1\text{-R-5-MeIm})_3$ from $[Au(CNR)_2]^+$[a]

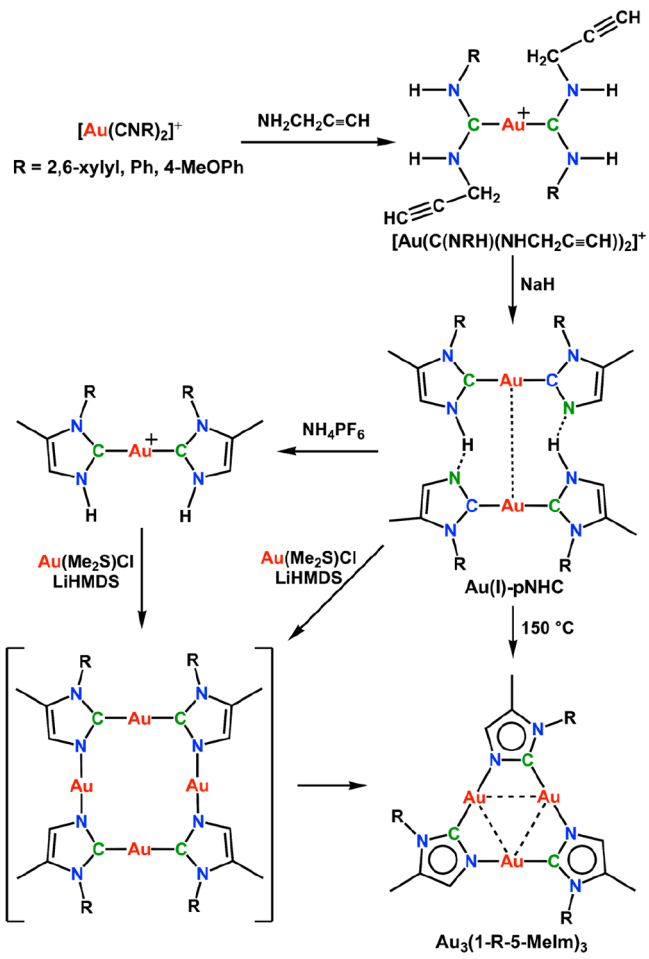

[a]See ref 113.

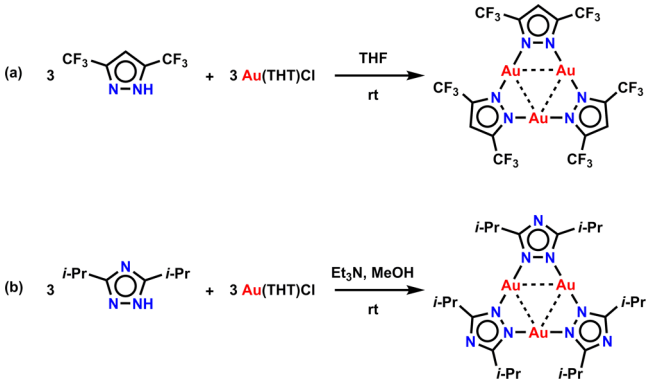

Figure 17. Typical synthetic approaches to Au(I) CTCs with μ-N,N-donor ligands, including (a) Au_3Pz_3 and (b) Au_3Trz_3.

single crystals of better quality. For example, suitable single crystals of $Au_3(Me_3Pz)_3$ were recrystallized from its fluorobenzene solution at 90 °C.[117] For the insoluble Au_3Pz_3 complexes, an alternative strategy for growing single crystals could be adopted by slow gas-phase diffusion of Et_3N, instead of direct addition into the reaction mixtures. The unsubstituted Au_3Pz_3 was synthesized by mixing Au(THT)Cl and pyrazole in the mixed MeOH/THF (v:v, 1:1) solvent, and the Et_3N vapor was then allowed to slowly diffuse into this clear solution, affording

https://dx.doi.org/10.1021/acs.chemrev.0c00011
Chem. Rev. 2020, 120, 9675−9742

colorless single crystals in 65% yield.[98] Notably, most of the Au_3Pz_3 and Au_3Trz_3 complexes were synthesized in organic solvents, some of which were dried before use.

Unlike Au(I) complexes, many Ag(I) compounds are photosensitive and, therefore, the syntheses of Ag(I) CTCs require special protection of the reaction mixture from light. In addition, Ag(I) sources and Ag(I) CTCs are usually less thermally stable than Cu(I) sources and Cu(I) CTCs, although their thermal stability is considerably better than that of Au(I) compounds. Furthermore, Cu(I) sources and many Cu(I) CTCs in solution display much higher sensitivities to oxygen and water than their Au(I) and Ag(I) analogues. Thus, an inert environment is often required during the preparation of Cu(I) CTCs. The families of Ag(I) and Cu(I) CTCs are mainly constructed from Pz ligands, with a few examples of M_3Trz_3 and Ag_3Cb_3 and only one example of Cu_3Py_3.

The synthetic methods for Ag and Cu CTCs are similar to those of their Au analogues and are highly dependent on the properties of their bridging ligands. For instance, in 1988, Fackler and co-workers reported the reaction of CuCl and Na[3,5-Ph_2Pz] in the presence of $AgNO_3$ to afford Ag_3(3,5-Ph_2Pz_3)$_3$, which could also be obtained by mixing Na(3,5-Ph_2Pz) and Ag(THT)NO_3.[92,118,119] The reaction of $AgNO_3$ with pyrazolate ion under neutral conditions or pyrazole under basic conditions afforded Ag_3[3,5-$(NO_2)_2$Pz]$_3$ and Ag_3(4-NO_2Pz_3)$_3$.[120,121] In addition, by replacing $AgNO_3$ with Ag(PhCOO), a similar synthetic strategy could produce Ag_3(3-Me-5-PhPz)$_3$, Ag_3(4-Br-3,5-Ph_2Pz)$_3$, Ag_3[3-(2′-Cl-Ph)-Pz]$_3$, Ag_3(4-Cl-3,5-Ph_2Pz)$_3$, and Ag_3(4-Me-3,5-Ph_2Pz)$_3$.[122,123] Moreover, Ag_3(PzIN)$_3$ was synthesized from the reaction of HPzIN (3-pyrazolyl imino nitroxide), $AgClO_4$, and 1,8-diazabicyclo[5.4.0]undec-7-ene in acetonitrile, as reported by Ishida et al.[124] Unsubstituted Ag_3Pz_3 was also obtained by oxidation of the dinuclear Ag pyrazolate, [Ag(Ph_3P)Pz]$_2$, with hydrogen peroxide. Notably, this was the first example that demonstrated that the crystal structure of CTCs could be determined ab initio by using powder XRD (PXRD) data and refined with the Rietveld technique.[125]

The first reported Cu_3Pz_3 was Cu_3(3,5-Ph_2Pz)$_3$, as a minor product in the synthesis of Ag_3(3,5-Ph_2Pz)$_3$, presented by Fackler and co-workers in 1988.[118] Later, the rt reactions of soluble Cu(I) salts with pyrazolate ligands afforded numerous Cu_3Pz_3 complexes under an oxygen-free environment. The most used Cu(I) salt was [Cu(CH_3CN)$_4$](BF_4), adopted in the syntheses of Cu_3[3,5-(*i*-Pr)$_2$Pz]$_3$,[22] Cu_3(4-NO_2Pz)$_3$,[121] Cu_3(3,5-Me_2Pz)$_3$,[22] and Cu_3(4-*R*-3,5-Me_2Pz)$_3$, where R = Ph, naphthyl (Nap), anthryl (An),[126] and NO_2.[127] By utilizing [Cu(CH_3CN)$_4$](PF_6), both Cu_3[3-(2′-pyridyl)-Pz]$_3$[128] and Cu_3[3-(2′-(6′′-Me)-pyridyl)-Pz]$_3$[129] were synthesized, and their single crystals isolated as co-crystals with pyridine solvent.

Over the past decades, the rt reactions by mixing metal(I) salts and pyrazolate derivatives were used to synthesize many M_3Pz_3 (M = Au(I)/Ag(I)/Cu(I)) CTCs, including most of the M_3Pz_3 complexes that exhibited liquid-crystal properties.[130−134] As a result of the superior thermal stabilities compared to those of Au(I) complexes, the syntheses of Ag(I) and Cu(I) azolate CTCs could also be achieved at higher temperatures. Dias's group introduced fluorinated pyrazolates to the Cu(I) and Ag(I) CTC families in 2000 and developed a convenient and useful synthetic method to afford Cu_3Pz_3 and Ag_3Pz_3, which can also be extended to their Trz analogues.[135] The reactions of Cu_2O and Ag_2O with substituted pyrazoles and triazoles in refluxing benzene or toluene under N_2 atmosphere afforded a series of fluorinated M_3Pz_3 and M_3Trz_3 complexes, including Cu_3(3-CF_3Pz)$_3$,[22] Cu_3(3-Me-5-CF_3Pz)$_3$,[22] Cu_3(3-CF_3-5-PhPz)$_3$,[22] M_3[4-X-3,5-$(CF_3)_2Pz$]$_3$ (X = Cl or Br),[136] M_3[3,5-$(CF_3)_2Pz$)]$_3$,[135] and M_3[3,5-(n-C_3F_7)$_2$Trz]$_3$[137] (M = Cu(I) or Ag(I), Figure 18a). In refluxing benzene/toluene solutions, the deprotonation for fluorinated pyrazoles and triazoles was effective in the presence of the metal(I) oxides.

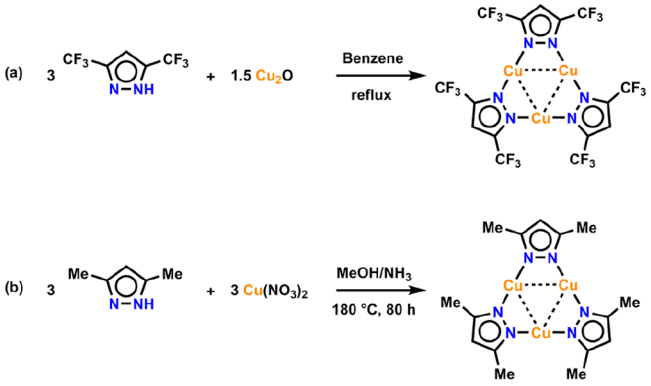

Figure 18. Typical synthetic approaches to Cu_3Pz_3 by (a) Dias's method and (b) the solvothermal method.

As another convenient and environmentally friendly synthetic approach, hydro(solvo)thermal synthesis features chemical reactions in a sealed reactor at elevated temperature and autogenous pressure, and has become a powerful technique for the fabrication of inorganic and metal−organic solid materials in recent decades.[138] This fascinating method was first introduced to the syntheses of the CTC family by Li's group in 2006 (Figure 18b, Box 2).[53] Since then, numerous CTCs and their corresponding single crystals were obtained, covering structural dimensions from zero-dimensional (0D) to three-dimensional (3D), and including discrete compounds, supramolecular oligomers/aggregates, coordination cages, and coordination polymers/metal−organic frameworks. The noticeable advantages of this method include: (i) special care (i.e., protection from light and removal of oxygen) is no longer necessary; (ii) the increasing solubilities under hydro(solvo)thermal conditions allow the usage of insoluble metal(I) sources or ligands and the slow crystallization of products that are insoluble at rt; and (iii) Cu(II) ions undergo spontaneous reduction to Cu(I) ions under solvothermal conditions (usually at temperatures ≥140 °C), thus CuO and Cu(II) salts can be used for the synthesis of Cu(I) CTCs.

Box 2. Solvothermal Synthesis of Cu_3(3,5-Me_2Pz)$_3$.[53]

A mixture of $Cu(NO_3)_2·3H_2O$ (0.241 g, 1.0 mmol), H(3,5-Me_2Pz) (0.096 g, 1.0 mmol), aqueous ammonia (25%, 5 mL) and MeOH (5 mL) was stirred for 10 min in air, then transferred to and sealed in a 23 mL Teflon-lined reactor, heated in an oven to 180 °C for 80 h. The resulting yellowish block crystals were filtered, washed, and dried in air; yield 0.10 g, ca. 65%.

The first report of Ag_3Cb_3 complexes dates back to 1973, where three Ag_3Cb_3 compounds sharing the general formula $Ag_3(R_1\text{-}N{=}COR_2)_3$, where R_1 = *p*-Tol and R_2 = Me, Et, *n*-Pr, were obtained (Figure 19a).[139,140] Since then, neither their X-ray crystal structures nor new Ag_3Cb_3 CTCs have been reported.

https://dx.doi.org/10.1021/acs.chemrev.0c00011
Chem. Rev. 2020, 120, 9675−9742

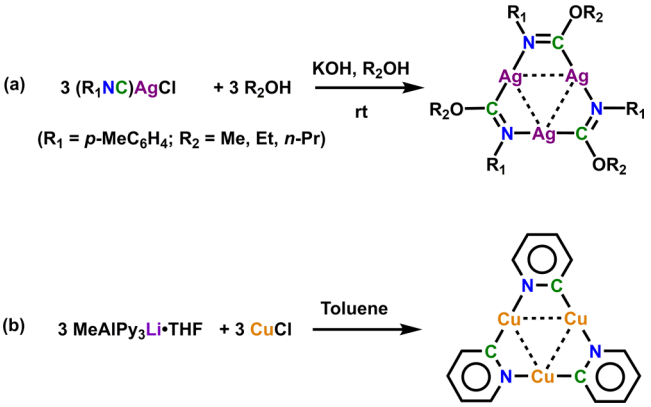

Figure 19. Typical synthetic approaches to (a) Ag_3Cb_3 and (b) Cu_3Py_3.

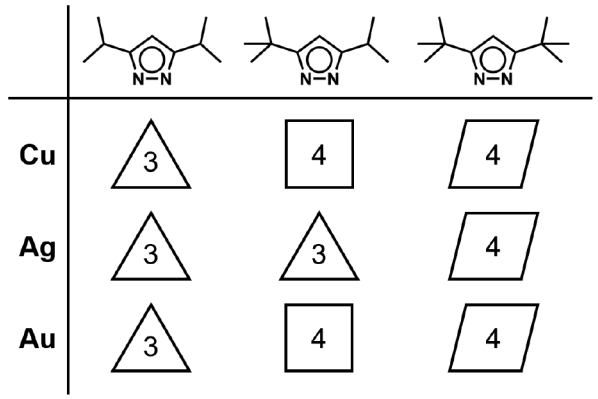

Figure 20. Synoptic geometry of the nuclearity of the complexes summarized in ref 145.

In the Cu_3Py_3 family, only the unsubstituted complex has been reported. In 2004, Hopkins, Wright, and co-workers demonstrated a rt reaction of CuCl with $MeAlPy_3Li{\cdot}THF$ in toluene, affording bright orange needle-like crystals in 64% yield (Figure 19b).[93] Their attempt to prepare Cu_3Py_3 by the direct reaction of CuCl with 2-pyridyllithium at −70 °C (Vaughan's method) led to the rapid decomposition of the Cu(I) source into metallic copper.

3.1.2. Steric Effect: Oligomeric Versus Polymeric Structures. In the self-assembly process between linear two-coordinated metal cations and angular ditopic bridging ligands, either the closed-ring oligomers or open-chain polymers can be formed. The former is more thermodynamically stable, because of the increase in global entropy, while the latter is more kinetically favorable.[7] In the complexations of d^{10} monovalent coinage metal cations with pyrazolate anions, consideration of the steric effect from substituents in the 3,5-positions of the Pz rings is essential to form coordination rings or chains.

The first notable example was $M_n(3,5\text{-}Ph_2Pz)_n$, where $Cu_3(3,5\text{-}Ph_2Pz)_3$ was reported in 1988 as a minor product from the reaction mixture of CuCl, $AgNO_3$, and $Na(3,5\text{-}Ph_2Pz)$.[118] Six years later, the *cyclo*-tetramer, $Cu_4(3,5\text{-}Ph_2Pz)_4$, was synthesized by mixing $[Cu(CH_3CN)_4](BF_4)$ and $H(3,5\text{-}Ph_2Pz)$ in the presence of Et_3N.[141] Similarly, two cyclic Au(I) pyrazolate complexes were obtained from different routes by Fackler et al. in 1988.[119] The reaction mixture of $Au(Me_2S)Cl$ and $Na(3,5\text{-}Ph_2Pz)$ afforded $Au_3(3,5\text{-}Ph_2Pz)_3$, while the reaction between $Au(Ph_3P)Cl$, Ag(PhCOO), and $Na(3,5\text{-}Ph_2Pz)$ yielded $Au_6(3,5\text{-}Ph_2Pz)_6$.[119] However, in stark contrast to the Cu(I)/Au(I) analogues, only the *cyclo*-trimer $Ag_3(3,5\text{-}Ph_2Pz)_3$ was reported, although multiple synthetic routes were applied.[92,118,119] By replacing the phenyl group with a bulkier *tert*-butyl (*t*-Bu) group, only cyclic tetrameric $M_4[3,5\text{-}(t\text{-}Bu)_2Pz]_4$ products were obtained, no matter which d^{10} metal was used.[142−144] In contrast, the adoption of less bulky *i*-Pr groups only resulted in cyclic trimeric $M_3[3,5\text{-}(i\text{-}Pr)_2Pz]_3$ products for all three metals.[145]

After investigating and comparing the above-mentioned studies, dating from 1988 to 2010, Fujisawa and co-workers suggested that, for the self-assembly of M(I)-pyrazolate complexes with bulky substituents at the 3- and 5-positions on the pyrazolates, the formation of larger coordination rings was more favorable than that of cyclic trinuclear complexes (Figure 20).[145] Moreover, the steric hindrance effects became less important with the increasing radii Cu(I) < Au(I) < Ag(I). For instance, the Cu_3Pz_3 could not be obtained when the large bulky pyrazolate ligand was employed, whereas the reaction proceeded with Ag_3Pz_3.

Oro, Serrano, and co-workers constructed Au_3Pz_3 with liquid-crystal phases using long alkyl chain-substituted 3,5-diaryl-pyrazolates in 1996 and 1998.[131,132] However, in 2010, when using the similarly long bulky Pz ligands, Elduque, Giménez, and co-workers obtained one-dimensional (1D) Ag(I) coordination polymers with columnar liquid-crystal phases instead of Ag(I) CTCs.[146] They attributed this result to the Ag−N bonds being more labile than Au−N bonds. This rendered the equilibrium exchange between silver and pyrazolate, so that their Ag(I) CTCs, if they existed, easily underwent ring-opening processes in solution. Generally, for a given 3- and 5-substituted bulky pyrazolate ligand, it is easier to afford Ag(I) CTC than Au(I) or Cu(I) CTC.

3.1.3. Solid-State Synthesis. Apart from the direct reactions of metal(I) sources and ligands, the reduction of cyclotrimeric mixed Au(I)/Au(III) pyrazolate complexes could produce Au(I) CTCs. In 1979, Bonati and co-workers reported the first case using $Au(I)_2Au(III)(3,5\text{-}Me_2Pz)_3I_2$, which is an Au CTC containing two Au(I) and one Au(III) cations. The thermal decomposition of its solid sample at temperatures of <100 °C resulted in the sublimation of iodine and afforded $Au_3(3,5\text{-}Me_2Pz)_3$.[147,148]

$Cu_3(3,5\text{-}Me_2Pz)_3$ and its crystal structure were first reported in 1990 using molten $H(3,5\text{-}Me_2Pz)$ with $Cu(OH)_2$ under nitrogen atmosphere at 130 °C for 10 days.[149] The crystals were then manually separated, under a microscope, from a reddish-brown powder, which was suspected to consist of Cu_nPz_n polymers. A similar method was adopted to synthesize $Cu_3(Me_3Pz)_3$ two years later.[150] The reaction of copper shot with molten HMe_3Pz in the presence of a limited amount of oxygen at 142 °C for 40 h afforded $Cu_3(Me_3Pz)_3$ and other unidentified Cu compounds. Manual separation was performed to afford pure crystals of $Cu_3(Me_3Pz)_3$.

The poor solubilities of $Cu_3(3,5\text{-}Me_2Pz)_3$ and $Cu_3(Me_3Pz)_3$ hampered their further purification by recrystallization from their solutions and thus, manual separation was necessary. However, Dias, Omary, and co-workers found that the pure form of $Cu_3(3,5\text{-}Me_2Pz)_3$ could be obtained by vacuum sublimation from the crude mixture.[21] In contrast, $Cu_3[3,5\text{-}(CF_3)_2Pz]_3$ could be purified via vacuum sublimation as well as recrystallization from its solution, because of its good solubility and stability in solution.[22]

3.1.4. Supramolecular Aggregations, Coordination Cages, and Polymers. The complexation between mono-Pz,

https://dx.doi.org/10.1021/acs.chemrev.0c00011
Chem. Rev. 2020, 120, 9675−9742

Im, Trz, Py, and Cb ligands and d^{10} coinage metal cations generally produces simple Au(I)/Ag(I)/Cu(I) CTCs as mentioned above. The coexistence of multiple interactions renders CTCs for exhibiting flexible and rich supramolecular aggregations with themselves and other molecules or ions. Single crystals can be considered as highly ordered solid-state supramolecular aggregates and molecular stackings, and structural parameters of CTCs in such aggregations can be analyzed by single-crystal X-ray crystallography. On the other hand, the assembly of CTCs in solution also produces supramolecular aggregations and can be investigated by solution techniques. In this section, two representative cases for studying the supramolecular aggregations of CTCs in solution will be discussed.

In the crystals of CTCs grown from CH_2Cl_2, hexane, or other alkanes, solvent molecules are usually absent or do not exhibit close contacts with CTC molecules. This is because the dispersion forces between CTCs and these solvent molecules are considerably weaker than the intertrimer metal−metal interactions between the CTC molecules (see discussion on typical crystal structures of CTCs in section 4.2). In contrast, the crystallization of CTCs from aromatic solvents often results in co-crystals, in which the CTC monomers or dimers are sandwiched by organic arenes. Such situations reflect that the π-acid/π-base electrostatic attractions (quadrupole−quadrupole interactions) between CTCs and solvent molecules are strong enough to compete with the intertrimer metal−metal interactions.

Dias's group probed the aggregation of Ag_3Pz_3 in solution using vapor pressure osmometry (VPO).[151] Their work unveiled the effects of substituents on the Pz ring, solvent, and concentration on the degrees of CTC aggregation. When Ag_3Pz_3 CTCs dissolved in heptane, $Ag_3[3,5\text{-}(CF_3)_2Pz]_3$, $Ag_3[3\text{-}(n\text{-}C_3F_7)\text{-}5\text{-}(t\text{-}Bu)Pz]_3$, and $Ag_3[3,5\text{-}(i\text{-}Pr)_2Pz]_3$ maintained trinuclear moieties at low concentrations; however, they formed dimers or polymers of CTC molecules at higher concentrations. Different situations were observed in toluene: $Ag_3[3,5\text{-}(i\text{-}Pr)_2Pz]_3$ was insoluble in toluene, while both fluorinated Ag_3Pz_3 complexes formed dimers or polymers of CTC molecules at high concentrations. However, $Ag_3[3,5\text{-}(CF_3)_2Pz]_3$ decomposed to mononuclear and dinuclear Ag(I) complexes at low concentrations while $Ag_3[3\text{-}(n\text{-}C_3F_7)\text{-}5\text{-}(t\text{-}Bu)Pz]_3$ remained intact. Recent studies have suggested that the π-acid/π-base interactions between $Ag_3[3,5\text{-}(CF_3)_2Pz]_3$ molecules and toluene are strong enough to break down the Ag−N coordination bonds and intratrimer Ag−Ag interactions, whereas the bulky and relatively more electron-rich pyrazolate $Ag_3[3\text{-}(n\text{-}C_3F_7)\text{-}5\text{-}(t\text{-}Bu)Pz]_3$ prevented such strong π-acid/π-base binding. Thus, the solubility and chemical stabilities of the above Ag_3Pz_3 complexes reflected the anticooperative effects or competition between multiple noncovalent interactions.[152]

In 2014, Li and co-workers presented an investigation on the assembly/disassembly behaviors of sandwich-like Au_3−Ag−Au_3 ($Au_3 = Au_3[3\text{-}(2'\text{-thienyl})\text{-}5\text{-PhPz})_3$] clusters in solution from molecular scale to nanoscale.[153] A series of characterization techniques, including transmission electron microscopy (TEM), confocal fluorescence microcopy, dynamic light scattering, UV−vis absorption, excitation, and emission spectroscopy were applied to monitor the assembly/disassembly processes during the formation/deformation of supramolecular aggregations (Figure 21). By adding CH_2Cl_2 solutions of $AgPF_6$ at concentrations of $>5 \times 10^{-4}$ M into the CH_2Cl_2 solution of Au_3Pz_3 (Pz = 3-(2′-thienyl)-5-PhPz; concentration = 1×10^{-3} M), a uniform nanoaggregate could be formed. Notably, the molar ratio (2:1) between the Au_3Pz_3 and Ag(I) ions in forming uniform nanoaggregates was inconsistent with that between Au_3Pz_3 and Ag(I) in the crystals of Au_3−Ag−Au_3 clusters (2:1).

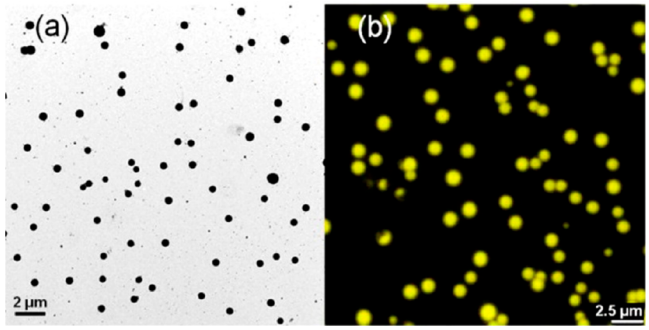

Figure 21. (a) TEM and (b) confocal fluorescence microscopy images of the nanoaggregates formed in the mixture solution of Au_3Pz_3 (1×10^{-3} M, Pz = 3-(2′-thienyl)-5-PhPz) and $AgPF_6$ (5×10^{-4} M) in CH_2Cl_2. [Reprinted with permission from ref 153. Copyright 2014, American Chemical Society, Washington, DC.]

In addition to CTC-based supramolecular aggregates, the construction of CTU-based coordination cages and polymers is also feasible to explore the chemistry of CTCs. Utilizing cyclic trinuclear Au(I)/Ag(I)/Cu(I) coordination units (Au(I)/Ag(I)/Cu(I) CTUs, mostly M_3Pz_3 units) as building blocks, a series of coordination cages, coordination polymers have also been synthesized.

The formation of hexanuclear Au(I)/Ag(I)/Cu(I) CTU-based coordination prism or antiprism cages by the direct reactions of metal sources with semirigid bis-pyrazole ligands (Figure 22) was reported.[43−50] The synthetic method for CTCs was also adopted for CTU-based coordination cages. The first Cu(I)/Ag(I)/Au(I) CTU-based cages were reported in 2011 by Thiel's group.[43] The complexation of chiral 2,2′-di(1,2-pyrazol-3-yl)-1,1′-binaphthyl with $[Cu(CH_3CN)_4](BF_4)$ in acetonitrile produced a chiral hexanuclear antiprism cage, and the use of Ag_2O or Au(THT)Cl instead of Cu(I) salts also produced a chiral Ag(I) or Au(I) cage. Although the above three isostructural hexanuclear cages were isolated as powders in high yields of 70%−80% and confirmed by FT-IR and NMR spectra, only the Cu(I) cage could be recrystallized in CH_2Cl_2 to afford single crystals suitable for X-ray structural analysis.

A series of hexanuclear Ag(I) and Cu(I) prism cages with semirigid bis-pyrazole ligands (Figure 22) was obtained under hydro(solvo)thermal conditions.[44−52] The one-pot hydro-(solvo)thermal reaction could give rise to the corresponding X-ray quality crystals of these cages as the final products.

The first Cu(I) prismatic cage was reported by Li's group in 2011.[44] It was obtained by heating a mixture of Cu_2O and H_2L (L = *m*-xylylene-bis(3,5-dimethyl)pyrazol-4-yl) in *n*-hexane and acetonitrile solution to 140 °C for 3 days in a sealed reactor, affording single crystals of the Cu(I) prism cage. As an extension of this work, by replacing the *m*-xylylene group of bis-pyrazole with the 2,6-dimethylpyridyl group, an isostructural Cu(I) cage was yielded under similar solvothermal conditions with a reaction temperature of 180 °C.[47] The uncoordinated N atoms of the pyridyl groups rendered the cage a metalloligand. Further solvothermal reaction of this cage with CuI in EtOH at 180 °C for 3 days produced crystals of a Cu_6−Cu_2−Cu_6 cluster (Cu_6 refers to a Cu(I) cage and Cu_2 refers to a Cu_2I_2 cluster), which

https://dx.doi.org/10.1021/acs.chemrev.0c00011
Chem. Rev. 2020, 120, 9675−9742

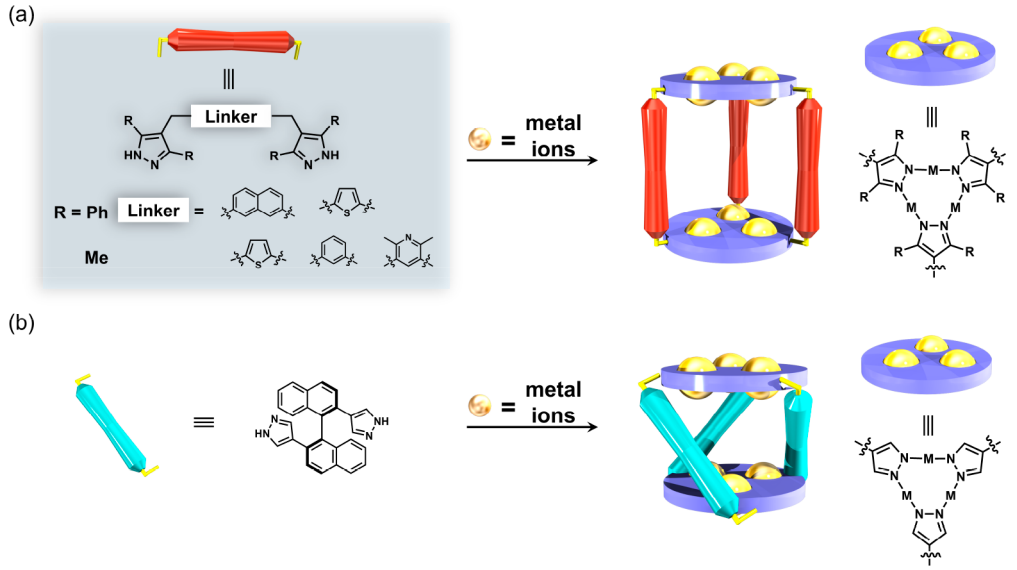

Figure 22. Semirigid bis-pyrazole ligand (H_2L) used for constructing Cu_6L_3 coordination (a) prismatic and (b) antiprismatic cages with CTUs.

could not be obtained by the direct reaction of CuI with the bis-pyrazole ligand.

Very recently, Li's group reported the first interlocked luminescent CTU-based heteroleptic Cu(I) metallocages.[51] By adopting a ligand replacement strategy, a solvothermal reaction of a homoleptic CTU-based prism and a new ligand (4,4′-(3,5-dimethyl-1*H*-pyrazol-4-ylthio)-diphenylthiol) afforded an edge-interlocked prismatic heteroleptic metallocage, which cannot be obtained by the direct one-pot reaction of copper salts with both ligands (Figure 23).

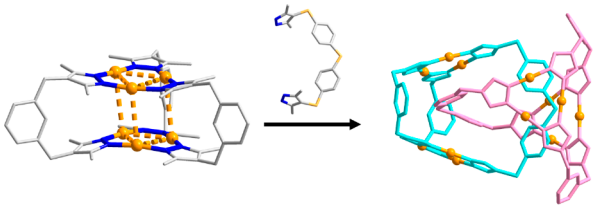

Figure 23. Preparation of the interlocked heteroleptic Cu(I) coordination cage through a ligand replacement reaction. [Color code: orange, Cu; blue, N; gray, C; light yellow, S. All H atoms have been omitted from the figure for the sake of clarity.]

Apart from organic linkers, it is also feasible to connect two M_3Pz_3 units (M = Ag(I) or Cu(I)) via organometallic linkers. By using the clip ligands (i.e., 1,1′-bis(pyrazol-3-yl)ferrocene with different substituents), Meyer and co-workers reported two coordination prisms with the ferrocene units as linkers in 2015 (Figure 24).[49] The reaction of the ferrocene-linked bis-pyrazole ligand with $[Cu(CH_3CN)_4](BF_4)$ and degassed Et_3N in dry MeOH afforded a Cu(I) cage as a powder, and the corresponding X-ray quality crystals were obtained by the vapor diffusion of diethyl ether into the DMF solution. By altering $[Cu(CH_3CN)_4](BF_4)$ to $AgBF_4$, an isostructural Ag(I) cage was obtained by a similar procedure. Notably, it is necessary to change the solvent from MeOH to acetonitrile or an acetonitrile/MeOH mixture to avoid oxidation of the ferrocene unit by the silver(I) salt. This is because the Ag/Ag^+ redox potential is much lower in acetonitrile than in other solvents.

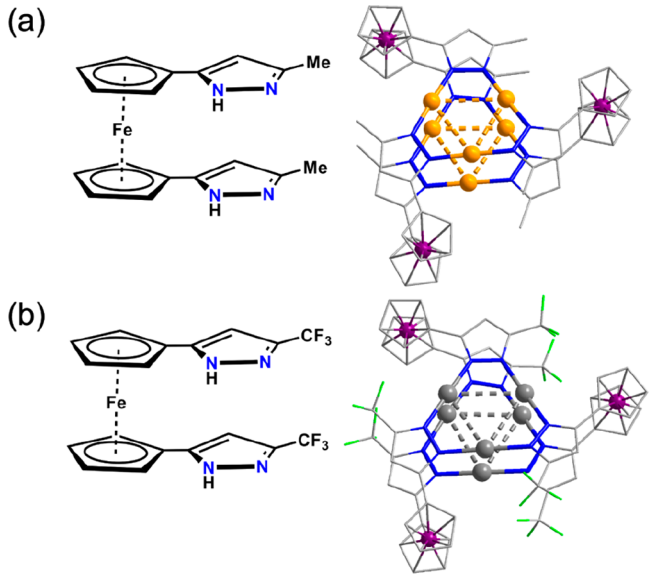

Figure 24. Chemical structures of 1,1′-bis(pyrazol-3-yl)ferrocene with (a, left) methyl group and (a, right) corresponding hexanuclear Cu(I) cage; and with (b, left) CF_3 and (b, right) corresponding hexanuclear Ag(I) cage. [Color code: orange, Cu; dark gray, Ag; blue, N; gray, C; green, F; purple, Fe. All H atoms have been omitted from the figure for the sake of clarity.]

Apart from prisms and antiprism cages, high symmetry polyhedra can also be constructed from CTUs. Presented by Lu and co-workers in 2010, the hydrothermal reaction of Ag(MeCOO), 1,2,4-triazole (Trz), and the trilacunary Keggin anion $[A\text{-}PW_9O_{34}]^{9-}$ in water yielded Ag(I) complexes with the formula $\{[Ag_2(Trz)_2][Ag_{24}(Trz)_{18}]\}(PW_{12}O_{40})_2$, where $Ag_{24}(Trz)_{18}$ refers to an adamantane-like nanocage.[42] During the reaction, the trivacant $[A\text{-}PW_9O_{34}]^{9-}$ species underwent a structure transformation to the saturated Keggin $[PW_{12}O_{40}]^{3-}$ motifs. The Keggin polyoxometalate anions acted as both counteranions and templates. The absence of the Keggin polyoxometalate led to the formation of a two-dimensional (2D) $[Ag(Trz)]_n$ network from the self-assembly of Ag(I) cations and 1,2,4-triazole.

https://dx.doi.org/10.1021/acs.chemrev.0c00011
Chem. Rev. 2020, 120, 9675−9742

In 2013, Volkmer and co-workers reported the synthesis of a metallosupramolecular Cu(I) octahedron cage by the reaction of $Cu(OAc)_2 \cdot H_2O$ with a rigid bis-pyrazole ligand (1,2-bis(3,5-dimethyl-1*H*-pyrazol-4-yl)benzene) in a dimethylacetamide (DMAc) solution with a small amount of Et_3N at 120 °C for 3 days.[45] Interestingly, they also found that the reaction time could be largely shortened from 3 days to ~15 min when a similar reaction mixture was irradiated with 200 W microwave at 140 °C instead of the conventional solvothermal conditions. This was the first time that microwave-assisted synthesis was introduced to the syntheses of the CTC family.

The direct self-assembly of the metal sources and bis-pyrazole ligands at rt were used to produce bulk samples of Ag(I) and Cu(I) CTU-based MOFs in powder form.[55] However, the highly insoluble nature of these MOFs does not allow their recrystallization from powder. Thus, liquid-phase diffusions, by carefully laying the EtOH (or acetonitrile) solution of the bis-pyrazole ligands on the aqueous ammonia solution of Ag_2O or Cu_2O, were adopted to afford single crystals of all the reported Ag(I) CTU-based MOFs and some Cu(I) CTU-based MOFs for X-ray crystal structural analysis.[54,55,60] Alternatively, other coordination polymers with Cu(I) CTUs were obtained as crystals by hydro(solvo)thermal syntheses.[53−59]

In the hydro(solvo)thermal syntheses for obtaining crystals of Cu(I) CTU-based coordination polymers, the reaction temperatures ranged from 85 °C to 180 °C, usually depending on the copper sources (Cu(I) or Cu(II) sources) and solubility of the reactants. In addition, during the synthesis of porous coordination polymers (PCPs) or MOFs, the interpenetration occurred at temperatures above 150 °C, resulting in a decrease in porosity.[53,55]

In most cases, for Cu(I) CTU-based MOFs constructed from rigid bis-pyrazole ligands, only Cu_3Pz_3 units served as SBUs.[53−55,60] One exception was presented by Li and co-workers in 2014.[63] In this case, the reaction of a cyclic trinuclear Cu(II) cluster ($[Cu_3(\mu_3\text{-}OH)(\mu\text{-}Pz)_3(MeCOO)_2(HPz)]$, HPz = unsubstituted pyrazole) with 3,3′,5,5′-tetraethyl-4,4′-bipyrazolate in DMF and MeOH at 100 °C led to a Cu(I) MOF with both Cu_3Pz_3 and Cu_4Pz_4 units as SBUs. Notably, the direct reaction of Cu salts with the same ligand afforded poorly crystalline products.

Using pyridyl-pyrazole ligands to react with CuX (X = Cl, Br, I), Li,[58,59,62,68] Song,[65] and Wang[57] presented a series of Cu(I) polymers with both Cu_3Pz_3 and Cu_nX_n units under solvothermal conditions at 140−180 °C. In this reaction, the pyridyl group acts as a soft base (N atom) donor to bind with Cu_nX_n clusters. Yin and co-workers provided an exceptional example.[56] They reported that the reaction of CuX (X = Cl, Br, I) with 4-(4′-pyridyl)-3,5-dimethylpyrazole in a mixed acetonitrile/aqueous ammonia solvent, under solvothermal conditions at 150 °C, led to the formation of a 4-fold interpenetration network with Cu_3Pz_3 units and CuCN chains. In this coordination polymer, CN^- anions resulted from the in situ thermal decomposition of acetonitrile.

With the replacement of pyridyl with carboxylic acid, the solvothermal reactions of pyrazolecarboxylic acids and Cu(II) or Zn(II) salts at 85−120 °C resulted in a series of MOFs with pyrazolate Cu(I) CTUs and Cu(II), Zn(II) paddlewheel, or other Zn(II)-based units.[61,67] In this reaction, the carboxylate group acts as a hard base (O atom) donor to bind with Cu(II) or Zn(II).

3.2. Stability and Reactivity

Among the Au(I)/Ag(I)/Cu(I) CTCs, Au(I) CTCs usually exhibit the best chemical stabilities and are less sensitive to light and oxygen compared to their Ag(I) and Cu(I) analogues. In addition, the thermal stability of Au(I) CTCs has been documented for many years.[8,41] Taking Au_3Py_3 as an example, a series of solid-state unsubstituted and alkyl-substituted Au_3Py_3 are thermally stable up to at least 100 °C, and single crystals of unsubstituted Au_3Py_3 were grown from its hot pyridine solution.[8,111] Conversely, Au(THT)Cl, a commonly used Au(I) source in synthesizing Au(I) CTCs, undergoes slow decomposition in air at rt. Ag(I) and Cu(I) CTCs often display remarkably better thermal stability than their Au(I) analogues, and the introduction of fluorinated groups (e.g., CF_3) to M_3Pz_3 or M_3Pz_3 units (M = Ag(I) or Cu(I)) as SBUs to construct coordination polymers usually further improves their thermal and chemical stabilities, as discussed in the subsequent sections.

Despite the frequently documented good stabilities of CTCs, Au(I)/Ag(I)/Cu(I) CTCs represent active chemical entities. As a unique class of metal−organic π-acids/bases, their π-acidity/π-basicity could be modulated across a wide range, achieving superior π-acidity/π-basicity compared to those of most organic π-acceptors/donors. In addition, the linear two-coordinate metal centers are unsaturated metal centers (UMCs; Lewis acidic sites) and Au(I)/Ag(I)/Cu(I) cations are potential closed-shell metal−metal interacting sites. Finally, the +1 state is the intermediate oxidation state for Au/Ag/Cu elements, allowing reduction or oxidation to other formal oxidation states. To date, the interactions of CTCs and CTU-based materials with Lewis and π-acids/bases have been well reviewed, demonstrating the formation of simple acid/base adducts or new compounds as well as the remarkable property changes (e.g., luminescence and CT behaviors) during adduction.[1−5,9,10,13] Indeed, new related cases are still being reported.

3.2.1. Lewis Acid/Base and π-Acid/Base Interactions.

3.2.1.1. Interaction with Metal Cations. Strong π-basic Au(I) CTCs can strongly attract metal cations to form cation-π type adducts. The first example was reported by Burini, Fackler, and co-workers in 1998.[154] By layering $AgBF_4$ acetonitrile solution over the CH_2Cl_2 solution of $Au_3(1\text{-}BzIm)_3$, single crystals of the sandwich-like $Au_3-Ag-Au_3$ cluster were isolated, displaying a 1D supramolecular column stacking structure. Two years later, they conducted a systematic investigation focusing on the interactions of Au_3Im_3 and Au_3Cb_3 with metal cations (Ag(I) and Tl(I)).[155] Similar liquid-phase diffusion methods were adopted to grow mixed Au/Ag and Au/Tl sandwich-like clusters, from Au_3Im_3 and Au_3Cb_3 (Im = 1-BzIm or 1-MeIm, Cb = *p*-TolN═COEt) with $AgPF_6$, $AgBF_4$, and $TlPF_6$ as precursors with 2:1 molar ratios. The crystal structure displayed discrete packing of sandwich-like $Au_3-Ag-Au_3$ or $Au_3-Tl-Au_3$ clusters (Figure 25). However, the reaction of $Au_3(1\text{-}BzIm)_3$ and $AgClO_4$ afforded $[Au_3]$ and Ag cations with respective molar ratios of 1:1 and 1:2 in the adducts. Therefore, they reported that the chemical analyses and IR spectral data suggested the existence of $Ag-Au_3-Au_3-Ag$ and $Ag-Au_3-Ag$ clusters. The corresponding X-ray crystal structures have not yet been obtained.[155] Moreover, when $Au_3[3,5\text{-}(CF_3)_2Pz]_3$ or $Au_3(3,5\text{-}Ph_2Pz)_3$ was used as the starting material, crystals of the parent Au(I) CTCs, rather than the mixed-Au/Ag clusters, were obtained.[155] This was attributed to the significantly lower π-basicity of Au_3Pz_3, compared to those of Au_3Im_3 and Au_3Cb_3 adopted in their work.[155]

https://dx.doi.org/10.1021/acs.chemrev.0c00011
Chem. Rev. 2020, 120, 9675−9742

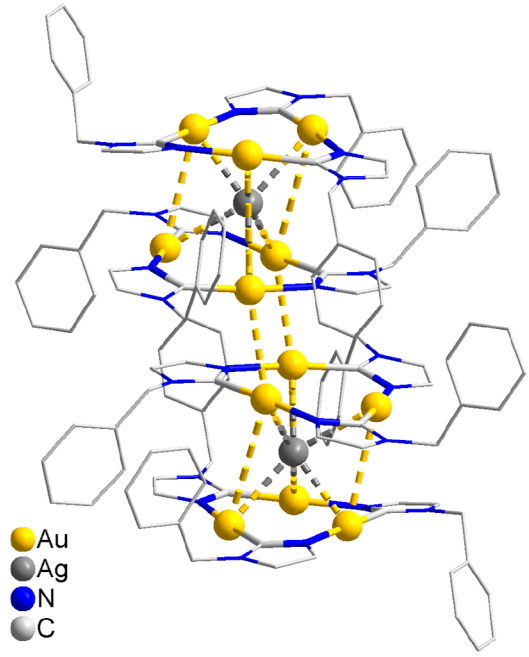

Figure 25. Crystal structure of $[Au_3(1\text{-BzIm})_3]_2Ag$, showing the column stacking of a sandwich-like Au_3−Ag−Au_3 cluster. [All H atoms have been omitted from the figure for the sake of clarity.]

In addition to $Au_3(1\text{-BzIm})_3$, two other Au_3Im_3 complexes have been reported to form sandwich-like mixed Au/Ag clusters, confirmed by single-crystal determinations. Thus, for $Au_3(1\text{-MeIm})_3$, the sandwich-like mixed-Au/Ag clusters could only be synthesized under the assistance of cagelike or tray-shaped complexes (works by Fujita and co-workers in section 3.2.1.4).[41,156−159] The second complex was the *N*-aryl Au_3Im_3, $Au_3(1\text{-xylyl-5-MeIm})_3$.[113] A THF solution of $Au_3(1\text{-xylyl-5-MeIm})_3$ was mixed with $AgBF_4$ THF solution in a 2:1 molar ratio, affording a crystalline powder and tiny crystals of the corresponding Au_3−Ag−Au_3 clusters after standing the solution overnight without stirring. Further slow diffusion of hexane into a dichloroethane solution of the crystalline powders produced large single crystals for X-ray structural analysis.

Grinding a solid mixture of Au_3Pz_3 (Pz = 3-(2′-thienyl)-5-PhPz) and $AgPF_6$ could also afford the heterometallic sandwich-like cluster, as reported by Li and co-workers in 2014.[153] This was the first time that the mechanical synthetic technique was introduced to the CTC family. They also reported the first X-ray crystal structure of a mixed-Au/Ag sandwich cluster based on Au_3Pz_3, displaying discrete packing of the Au_3−Ag−Au_3 clusters (Figure 26). Notably, this conventional synthetic method also worked by directly mixing Au_3Pz_3 and $AgPF_6$. The slow evaporation of the CH_2Cl_2 solution of the obtained yellow powder afforded the solvated crystal $[(Au_3Pz_3)_2Ag]PF_6\cdot 4CH_2Cl_2$.

3.2.1.2. Interaction with Organic Compounds. Apart from metal cations, strong π-basic Au(I) CTCs can interact with organic π-acidic aromatics to form face-to-face stacking π-base/π-acid adducts. The crystal structures of these adducts were first reported in 2001. Balch and co-workers mixed $Au_3(MeN{=}COR)_3$ (R = Me or Et) and four types of nitrofluorenone derivatives in CH_2Cl_2 after either evaporation or diffusion of diethyl ether or EtOH into the above-mentioned CH_2Cl_2 solutions.[160] The resulting four co-crystals exhibited the two supramolecular column stacking modes AB and ABB, where A

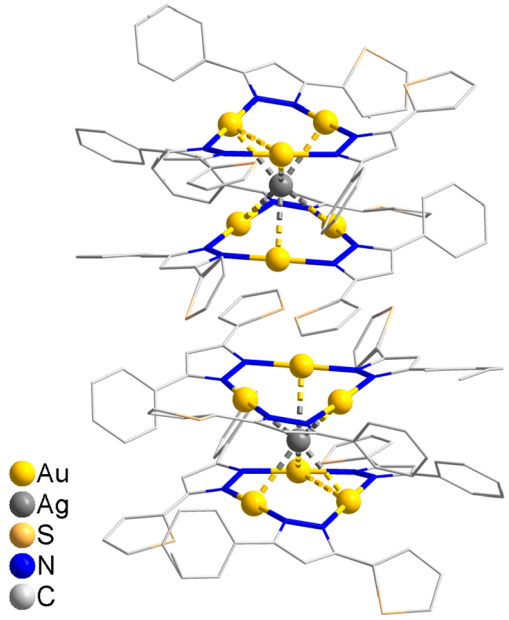

Figure 26. Crystal structure of $[Au_3(3\text{-}(2'\text{-thienyl})\text{-}5\text{-PhPz})_3]_2Ag$, showing discrete sandwich-like Au_3−Ag−Au_3 cluster. [All H atoms have been omitted from the figure for the sake of clarity.]

refers to π-acidic aromatics and B refers to π-basic Au(I) CTCs (Figure 27).

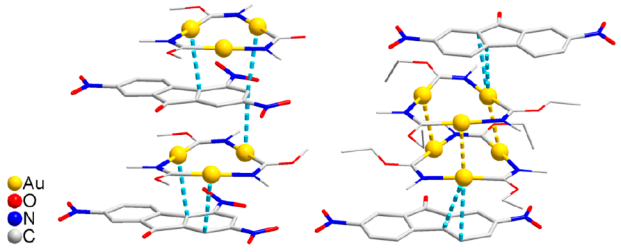

Figure 27. Crystal structures of (left) $Au_3(MeN{=}COMe)_3$ adducted 2,4,7-trinitro-9-fluorenone showing AB stacking column and (right) $Au_3(MeN{=}COEt)_3$ adducted 2,7-dinitro-9-fluorenone showing ABB stacking column. [All H atoms have been omitted from the figure for the sake of clarity.]

In the same year, Burini, Fackler, and co-workers reported the synthesis of an ABB stacking co-crystal of $Au_3(1\text{-BzIm})_3$ and TCNQ by adding ether to their CH_2Cl_2 solution, as well as an AB stacking co-crystal of $Au_3(p\text{-TolN}{=}COEt)_3$ and C_6F_6 by cooling their CH_2Cl_2 solution to 4 °C.[91] The presence of AB infinite column stacking indicates that the π-acid/π-base electrostatic attraction (quadrupole−quadrupole interaction) was strong enough to break the intertrimer Au−Au interactions. More remarkably, the AB-stacked $Au_3(p\text{-TolN}{=}COEt)_3/C_6F_6$ adduct could be prepared by exposing the $Au_3(p\text{-TolN}{=}COEt)_3$ crystals to C_6F_6 vapor. Notably, the intertrimer Au−Au distances in the $Au_3(p\text{-TolN}{=}COEt)_3$ structure is 3.244(1) Å, which is significantly shorter than the sum of the vdW radii of Au (3.32 Å), indicating strong Au−Au interactions.[161]

Strong intertrimer Au−Au interactions in crystalline π-basic Au(I) CTCs often result in bad solubility, and the breaking of Au−Au interactions usually requires strong organic π-acceptors. To date, Au(I) CTC/organic π-acidic aromatic adducts are still rarely reported and most of the documented acid/base adducts

https://dx.doi.org/10.1021/acs.chemrev.0c00011
Chem. Rev. 2020, 120, 9675−9742

resulted from the interactions between π-acidic CTCs and organic compounds of the CTC family. The combination of π-acidity and Lewis acidity in the nine-membered coordination rings of Ag(I) and Cu(I) CTCs endowed strong affinity toward organic π-acidity and Lewis donors, as well as organic compounds with both π-acid and Lewis-donating sites. Notably, $M_3[3,5\text{-}(CF_3)_2Pz]_3$ (M = Cu(I) or Ag(I)) complexes were frequently selected and well-studied in these adducts.[4,5]

The competition between intertrimer metal−metal interaction and π-acid/π-base attraction was also observed during the complexation between $Ag_3[3,5\text{-}(CF_3)_2Pz]_3$ and organic arenes, and the complexation patterns could be modulated by altering the affecting factors mentioned in section 3.2.1. Crystallization of $Ag_3[3,5\text{-}(CF_3)_2Pz]_3$ from benzene solution led to co-crystals with discrete BAB units (Figure 28a), where A = π-acidic $Ag_3[3,5\text{-}(CF_3)_2Pz]_3$ and B = π-basic organic arenes.[162] However, the addition of CH_2Cl_2 to a benzene solution of $Ag_3[3,5\text{-}(CF_3)_2Pz]_3$ afforded co-crystals of discrete BAAB units (Figure 28b). These observations indicated that the quadrupole−quadrupole interaction between benzene and $Ag_3[3,5\text{-}(CF_3)_2Pz]_3$ was strong enough to break down the Ag−Ag interaction in the crystalline $Ag_3[3,5\text{-}(CF_3)_2Pz]_3$, whose comprised a Ag−Ag distance (3.31 Å at 298 K) that was considerably shorter than the sum of the vdW radii of Ag (3.44 Å).[135]

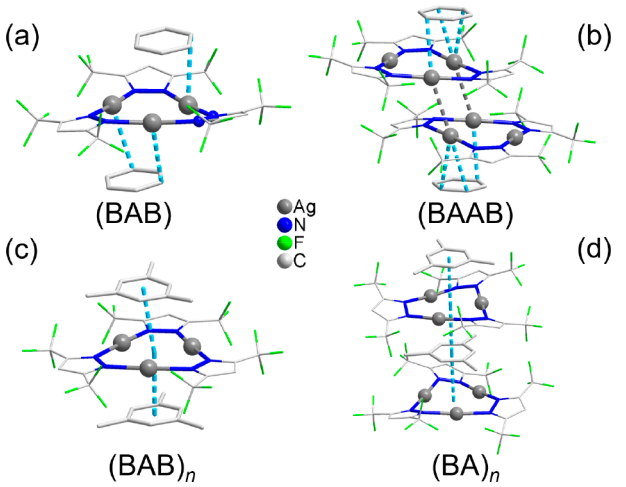

Figure 28. Crystal structure of $Ag_3[3,5\text{-}(CF_3)_2Pz]_3$/benzene adducts showing discrete (a) BAB and (b) BAAB units. The crystal structure of $Ag_3[3,5\text{-}(CF_3)_2Pz]_3$/mesitylene adducts showing face-to-face stacking with repeated (c) BAB and (d) BA units. A = $Ag_3[3,5\text{-}(CF_3)_2Pz]_3$ and B = organic arenes (benzene and mesitylene here). [All H atoms have been omitted from the figure for the sake of clarity.]

Replacing benzene with the more π-basic mesitylene resulted in stronger quadrupole−quadrupole interaction. Thus, co-crystals of the $Ag_3[3,5\text{-}(CF_3)_2Pz]_3$/mesitylene adduct with BAB 1D chains were isolated by crystallization of $Ag_3[3,5\text{-}(CF_3)_2Pz]_3$ from its mesitylene solution (Figure 28c), while diluting the mesitylene with CH_2Cl_2 afforded adduct co-crystals with 1D AB chains (Figure 28d).[162] In addition, by exposing the drop-cast film of $Ag_3[3,5\text{-}(CF_3)_2Pz]_3$ in benzene or mesitylene vapor, π-acid/π-base adducts formed readily and quickly and could be determined by the changes in photoluminescence.[39]

Compared to $Ag_3[3,5\text{-}(CF_3)_2Pz]_3$, the Au and Cu analogues are less π-acidic and their intertrimer metal−metal interactions are significantly weaker. This is indicated by the intertrimer Au−Au and Cu−Cu distances (>3.80 Å at approximately rt), which are much longer than the sum of the vdW radii (3.32 Å for Au and 2.80 Å for Cu).

Only the co-crystal of the 1D AAB chains was isolated by growing crystals of $Au_3[3,5\text{-}(CF_3)_2Pz]_3$ from its toluene solution or those of $Cu_3[3,5\text{-}(CF_3)_2Pz]_3$ from its benzene solution (A = π-acidic Au or Cu CTC and B = π-basic organic arenes).[23,163] Interestingly, the X-ray structures revealed that the Au−Au (3.298 or 3.542 Å) and Cu−Cu (3.031 or 3.091 Å) distances were considerably shorter than those in the arene-free crystalline CTCs, suggesting that the intertrimer metal−metal interactions were enhanced when the supramolecular aggregates formed. However, the significantly weaker π-acidity of $Cu_3[3,5\text{-}(CF_3)_2Pz]_3$, compared to that of its Ag analogue, rendered the extremely rapid decomposition of the $Cu_3[3,5\text{-}(CF_3)_2Pz]_3$/benzene adduct in air under ambient environment so that the fluorometer could not detect changes in its luminescence.[163] Moreover, $Ag_3[3,5\text{-}(CF_3)_2Pz]_3$ can also interact with *o*-terphenyl (*o*TP)and thiophene-derivatives, forming supramolecular columns with a face-to-face stacking mode.[164,165]

Recently, Omary's group reported a series of co-crystals consisting of $M_3[3,5\text{-}(CF_3)_2Pz]_3$ (M = Cu(I)/Ag(I)/Au(I)) and tetrathiafulvalene (TTF) derivatives.[166] TTF and its derivatives are well-known electron donors, while $M_3[3,5\text{-}(CF_3)_2Pz]_3$ species are electron-deficient. By forming π-acid/base binary adducts, the authors claimed the existence of ground-state CT behavior within the stacked materials and electronic communication in both solid state and solution.

$M_3[3,5\text{-}(n\text{-}C_3F_7)_2Trz]_3$ (M = Ag(I), Cu(I)) are stronger π-acids than $M_3[3,5\text{-}(CF_3)_2Pz]_3$ and display strong binding affinity toward toluene to form co-crystals featuring a 1D column with repeated BAB units.[137]

In the formation of face-to-face stacking π-acid/π-base adducts with organic arenes, Au(I)/Ag(I)/Cu(I) CTCs do not usually undergo serious molecular distortions and the nine-membered rings remain intact and planar. However, the interaction of CTCs with appropriate Lewis bases may result in their molecular rearrangement, thereby forming new compounds. In 2005, Dias and co-workers reported that the reactions of $Cu_3[3,5\text{-}(CF_3)_2Pz]_3$ with 2,4,6-collidine, benzo[*c*]-cinnoline, and pyridazine afforded neutral dinuclear, trinuclear, and tetranuclear complexes, respectively (Figure 29).[167]

Similarly, the reactions of $Ag_3[3,5\text{-}(CF_3)_2Pz]_3$ with 2,4,6-collidine and pyridazine resulted in neutral tetranuclear and dinuclear complexes, respectively (Figure 30).[167] Both dinuclear Cu(I) and Ag(I) complexes with 2,4,6-collidine are blue-emissive.

In 2011, Dias, Rawashdeh-Omary, and co-workers reported the reactions of $Ag_3[3,5\text{-}(CF_3)_2Pz]_3$ with 2-(*N*,*N*-diethylanilino-4-yl)-4,6-bis(3,5-dimethylpyrazol-1-yl)-1,3,5-triazine) (L), resulting in a coordination compound with both dinuclear cationic and pentanuclear anionic coordination units.[168] The dinuclear coordination unit was a clip-like luminophore, exhibiting high-energy (HE) green phosphorescence in form A and low-energy (LE) orange phosphorescence in form B (Figure 31a). Thus, this complex showed bright concentration-dependent tunable dual-emission in acetonitrile solution by modulating the transitions between form A, form B, and the aggregates (Figure 31b).

In 2018, Cundari, Omary, Dias, and co-workers reported the reactions of $Cu_3[3,5\text{-}(CF_3)_2Pz]_3$ with internal alkynes (MeC≡CMe and EtC≡CEt), and obtained three dinuclear/tetranuclear phosphorescent Cu(I) complexes.[169] In the tetranuclear

https://dx.doi.org/10.1021/acs.chemrev.0c00011
Chem. Rev. 2020, 120, 9675−9742

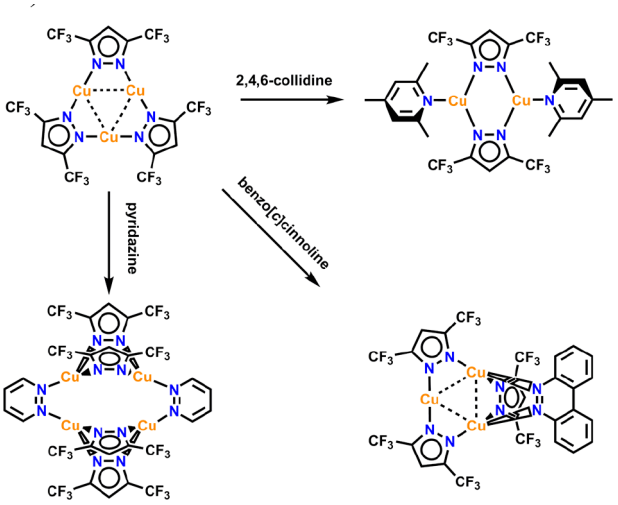

Figure 29. Reactions of $Cu_3[3,5\text{-}(CF_3)_2Pz]_3$ with neutral N-donor ligands.

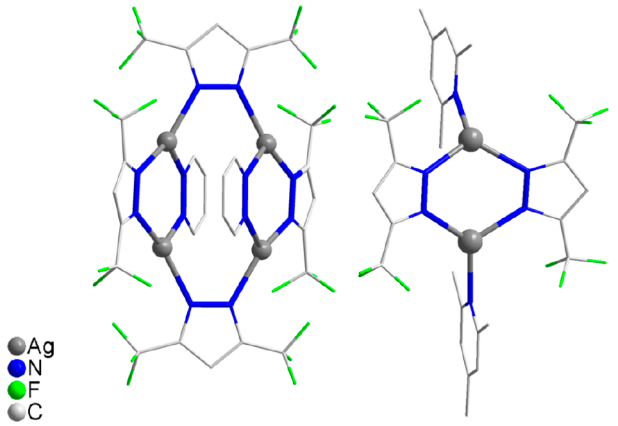

Figure 30. Neutral tetranuclear (left) and dinuclear (right) Ag(I) complexes. [All H atoms have been omitted from the figure for the sake of clarity.]

compounds, the internal alkynes adopted a $\mu\text{–}\eta^2,\eta^2$ bridging coordination mode, which was rare for the copper(I)–alkyne complexes reported in previous literature.

In the following year, by replacing the internal alkynes with terminal alkynes, Titov, Larionov, and co-workers unveiled the activation of the carbon–carbon triple bond by $Cu_3[3,5\text{-}(CF_3)_2Pz]_3$.[28] The coordination between this Cu_3Pz_3 and the C≡C of the alkyne (1-octyne and phenylacetylene) leads to active catalytic species in click reactions with *ortho*-fluorobenzyl azide. Therefore, 1,4-substituted 1,2,3-triazoles were obtained in good yields under mild reaction conditions without the presence of an inert gas atmosphere, base, and heating (Scheme 2). Single crystals of the active species were obtained from equimolar reagent mixtures of $Cu_3[3,5\text{-}(CF_3)_2Pz]_3$ and the alkyne in mixed CH_2Cl_2/hexane (v:v = 1:1) solutions in air. The single-crystal structure revealed that $Cu_3[3,5\text{-}(CF_3)_2Pz]_3$ was irreversibly transformed to $Cu(I)_2Cu(II)Pz_4(alkyne)_2$ during the reaction.

In the same year, Dias and co-workers further extended the reactions of fluorinated Cu_3Pz_3 with alkynes.[170] The reactions of $Cu_3[4\text{-R-}3,5\text{-}(CF_3)_2Pz]_3$ (R = H, Br, Cl) and HC≡CH or a terminal alkyne (phenylacetylene, 1,8-nonadiyne, 1,7-octadiyne) afforded a series of new dinuclear and tetranuclear Cu(I) complexes. In this work, they highlighted the role of

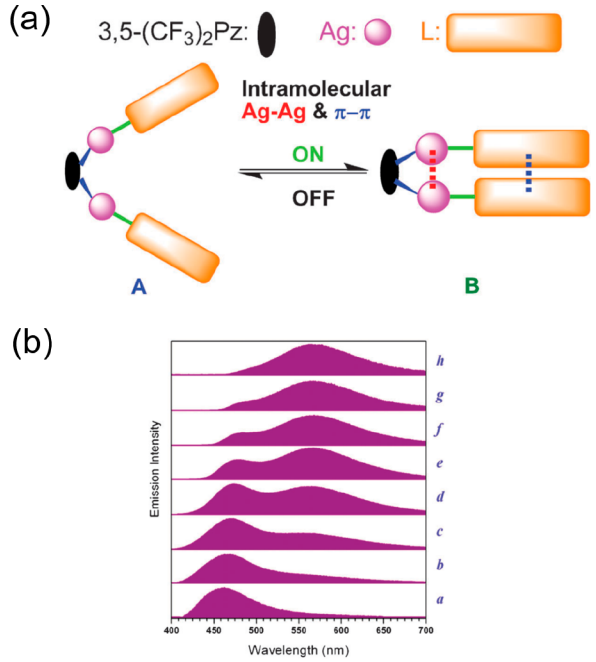

Figure 31. (a) Proposed conformational rearrangement of the binuclear cation. Toggling between form A and form B leads to on/off switching of intramolecular interactions and affects the luminescence signal, which can be further modified upon supramolecular association. (b) Concentration-dependent emission spectra in acetonitrile: trace *a*, 2.5×10^{-7}; trace *b*, 1.2×10^{-6}; trace *c*, 3.6×10^{-6}; trace *d*, 1.4×10^{-5}; trace *e*, 7.2×10^{-5}; trace *f*, 2.8×10^{-4}; trace *g*, 8.6×10^{-4}; and trace *h*, 2.6×10^{-3} M. [Reprinted with permission from ref 168. Copyright 2011, Royal Society of Chemistry, London.]

Scheme 2. Alkyne–Azide Cycloaddition Catalyzed by $Cu_3[3,5\text{-}(CF_3)_2Pz]_3$

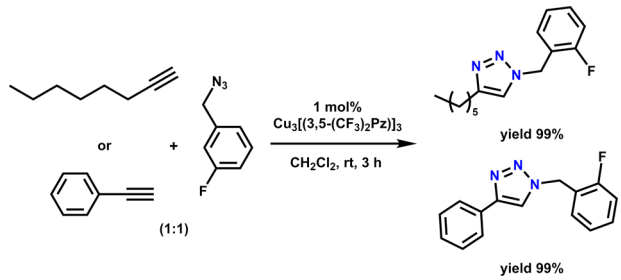

$Cu_3[3,5\text{-}(CF_3)_2Pz]_3$ as a very versatile and competent catalyst for alkyne transformations, including C(sp)–H bond carboxylation with CO_2, 1,2,3-triazoles arising from facile azide–alkyne cycloaddition related to rare chemistry involving acetylene itself, and S–H addition to an alkyne moiety leading to vinyl sulfides.

Very recently, Li's group reported an unexpected transformation of the commonly used $Ag_3[3,5\text{-}(CF_3)_2Pz]_3$ into noria-like Ag_{13} clusters by introducing the σ-donating phenylacetylene.[171] The metal cluster crystals would spontaneously grow from a benzene solution in the presence of mixed Et_3N/hexane vapors under ambient environment. Apart from pure $Ag_3[3,5\text{-}(CF_3)_2Pz]_3$, mixed $Ag_3[3,5\text{-}(CF_3)_2Pz]_3$ and $Cu_3[3,5\text{-}(CF_3)_2Pz]_3$ were also selected for the reactions and mixed-Ag/Cu cluster analogues in different ratios were obtained under the same synthetic conditions as those employed for the Ag_{13} cluster (Figure 32).

https://dx.doi.org/10.1021/acs.chemrev.0c00011
Chem. Rev. 2020, 120, 9675–9742

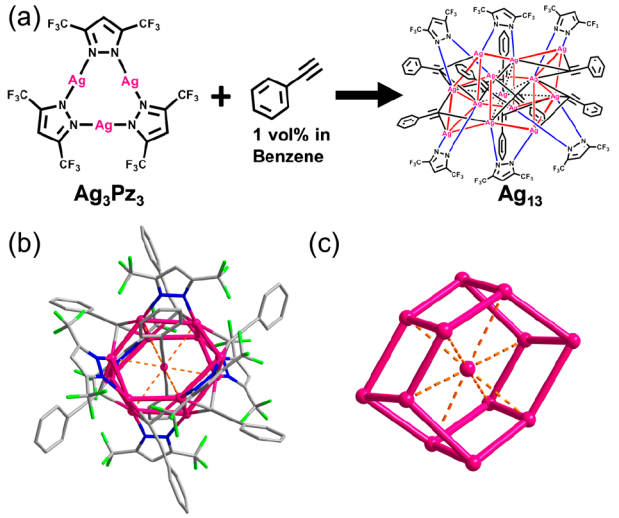

Figure 32. (a) Synthetic route from $Ag_3[3,5\text{-}(CF_3)_2Pz]_3$ to Ag_{13} cluster. (b) Crystal structure of Ag_{13} cluster and (c) simplified form of noria-like Ag_{13} kernel. [Color code: magenta, Ag; blue, N; gray, C; green, F. All hydrogen atoms and disordering phenyl rings are omitted from the figures for clarity. Adapted with permission from ref 171. Copyright 2020, Royal Society of Chemistry, London.]

Different from the simple σ- and π-donors, benzophenone (Ph_2CO) and tertiary diphosphine (dppm) represent a class of organic compounds with both Lewis base and π-donating abilities.[172,173] Mixing $Ag_3[3,5\text{-}(CF_3)_2Pz]_3$ and Ph_2CO in hexane in a 2:1 molar ratio results in a BAAB stacking column, while those with a 1:1 molar ratio led to the formation of an ABA stacking column, where A = $Ag_3[3,5\text{-}(CF_3)_2Pz]_3$ and B = Ph_2CO (Figure 33).[172] In the ABA stacking column, each O atom

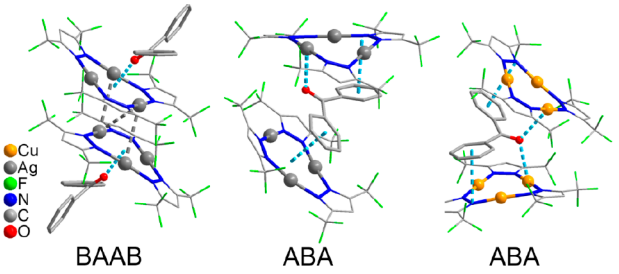

Figure 33. Molecular packing illustrations of co-crystals of $M_3[3,5\text{-}(CF_3)_2Pz]_3$ [M = (left and middle) Ag(I) and (right) Cu(I)] and Ph_2CO.

coordinates with all the Ag atoms in one Ag(I) CTC with the Ag−O distances ranging from 2.768 Å to 2.952 Å. On the other hand, in the BAAB stacking column, both the O atoms and phenyl groups interact with the Ag(I) CTCs. In the case of $Cu_3[3,5\text{-}(CF_3)_2Pz]_3$, only the ABA stacking mode could be found in the crystals (Figure 33).

Both $Ag_3[3,5\text{-}(CF_3)_2Pz]_3$ and $Cu_3[3,5\text{-}(CF_3)_2Pz]_3$ still maintained their near-planar geometries upon interacting with benzophenone. However, significant distortions were discovered in the co-crystals of these two CTCs and dppm with 1:1 molar ratios, because of the strong M−P coordination bonds.[173] Interestingly, the solutions of both adducts display intramolecular dynamics related to the "merry-go-round" movement of the diphosphine above the trinuclear metal core plane.

3.2.1.3. Interaction with Planar Metal Complexes. By mixing $Au_3(1\text{-BzIm})_3$ or $Au_3(MeN{=}COMe)_3$ with $Hg_3(o\text{-}C_6F_4)_3$ in CH_2Cl_2, Burini and co-workers reported the first π-acid/π-base adducts consisting of two different CTCs in 2000.[174] Both co-crystals exhibited BAB stacking columns, where A = π-acidic $Hg_3(o\text{-}C_6F_4)_3$ and B = π-basic Au(I) CTCs. Later, they confirmed the close stacking of $Au_3(1\text{-BzIm})_3$ and $Au_3(p\text{-TolN}{=}COEt)_3$ with $Hg_3(o\text{-}C_6F_4)_3$ in solution by ^{19}F, heteronuclear Overhauser effect spectroscopy (HOESY), and pulsed-field gradient spin−echo (PGSE) NMR techniques.[175] Both Au_3Hg_3 and $Au_3Hg_3Au_3$ aggregates were found in the mixture comprising $Au_3(1\text{-BzIm})_3$ and $Hg_3(o\text{-}C_6F_4)_3$ CH_2Cl_2 solution, while only the Au_3Hg_3 aggregates were observed in the mixture of $Au_3(p\text{-TolN}{=}COEt)_3$ and $Hg_3(o\text{-}C_6F_4)_3$, along with the free Au and Hg CTCs.

In 2005, Burini, Fackler, and co-workers further attempted to prepare π-acid/π-base adducts with Ag and Au CTCs by replacing the π-acidic $Hg_3(o\text{-}C_6F_4)_3$ with the π-acidic $Ag_3(3,5\text{-}Ph_2Pz)_3$.[95,176] However, the mixed-ligand and mixed-metal CTCs were obtained from the solution instead of the proposed π-acid/π-base adducts. Thus, they developed a synthetic method for obtaining atomically precise phosphorescent heterometallic clusters with controllable Au/Ag ratios by mixing Ag(I) and Au(I) CTCs in stoichiometric ratios.[95,176] In 2017, Omary's group revealed the formation of stacked complex between $Au_3(1\text{-BzIm})_3$ and $Cu_3[3,5\text{-}(CF_3)_2Pz]_3$. However, no crystals were obtained[20] and only mixed metal/ligand hexanuclear dimers-of-trimers were successfully isolated.

Interestingly, by substituting $Ag_3(3,5\text{-}Ph_2Pz)_3$ with the stronger π-acidic $Ag_3[3,5\text{-}(CF_3)_2Pz]_3$, the simple π-acid/π-base adducts, rather than the mixed-Au/Ag CTCs, could be formed in solution.[26,27] In 2018, Hahn, Esser, and co-workers presented a comprehensive and systematic quantitative investigation (e.g., UV-vis absorption and NMR titration) as well as high-level quantum chemical computations on complexation between strong π-basic Au(I) CTCs and $M_3[3,5\text{-}(CF_3)_2Pz]_3$ (M = Au(I)/Ag(I)/Cu(I)) in solution.[27] With increasing π-acidity of $M_3[3,5\text{-}(CF_3)_2Pz]_3$ (Au < Cu < Ag), the binding strengths between the π-basic Au(I) CTCs (a series of Au_3Py_3, Au_3Im_3, and Au_3Cb_3) with $M_3[3,5\text{-}(CF_3)_2Pz]_3$ also increased. For instance, the association constants of the 1:1 complexes could be as large as 2.34×10^7 L mol^{-1} between Au_3Py_3 and $Ag_3[3,5\text{-}(CF_3)_2Pz]_3$, with binding free energies of 10.1 kcal mol^{-1}. This indicated much stronger binding strengths than was previously reported for π-acid/π-base adducts (association constant = 2.60×10^4 L mol^{-1}) between two planar arenes without the assistance of other noncovalent interactions. High-level quantum chemical calculations clarified that the London dispersion interactions played a crucial role and accounted for 77%−93% of the total interaction energies.

Apart from the different CTCs, the complexations between CTCs and planar mononuclear complexes were also explored. In 2015, Yang, Omary, and co-workers designed $Ag_3[3,5\text{-}(n\text{-}C_3F_7)_2Trz]_3$ as a biphasic supramolecular octopus to host a free porphyrin and its Pt(II) complex via strong quadrupole−quadrupole and metal-π interactions.[177]

Li's group reported the formation of a $Cu_3Pz_3{-}Cu_2I_2{-}Cu_3Pz_3$ sandwiched cluster with face-to-face stacking in 2018, using a one-pot solvothermal reaction of CuI with 4-(1′-methyltetrazol-5′-ylthio)-3,5-dimethyl-1*H*-pyrazole in a cyclohexane, benzene, *i*-propanol, and $NH_3{\cdot}H_2O$ (25%) mixed solvent at 140 °C for 72 h (Figure 34).[178] In this co-crystal, a $Cu_2I_2(NH_3)_2$ cluster was sandwiched by two Cu_3Pz_3 units and the afforded adduct was stabilized by multiple noncovalent interactions (Figure 34). This is an example of cooperativity between

https://dx.doi.org/10.1021/acs.chemrev.0c00011
Chem. Rev. 2020, 120, 9675−9742

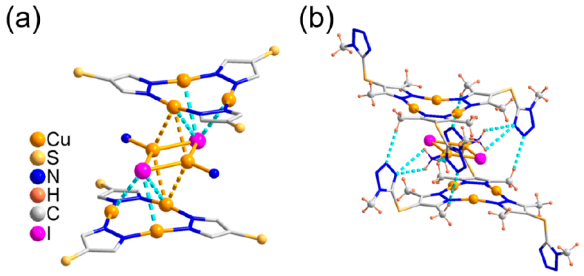

Figure 34. Crystal structure of the adduct with intermolecular Cu_3···I (π-acid−base) and (a) Cu−Cu interactions and (b) N−H hydrogen bonds highlighted with dashed lines.

intertrimer Cu−Cu interactions and π-acid/Lewis base interactions. Relative short Cu−Cu distances (3.085 and 3.165 Å) between the $Cu_2I_2(NH_3)_2$ and Cu_3Pz_3 clusters were observed in this adduct. In addition, other examples of Cu_nX_n clusters sandwiched by Cu_3Pz_3 units showed perpendicular orientations between these two classes of metal clusters, where X = Cl, Br, I, and SCN and n = 2 and 3. These results suggested that only the π-acid···base interactions between the Cu_3Pz_3 units and X anions contributed to the stabilization of these sandwiched clusters, while Cu−Cu contacts between the Cu_3Pz_3 units and Cu_nX_n clusters were absent.[57,58,65]

3.2.1.4. Interaction with Other Inorganic and Organometallic Compounds. Since 2010, Fujita and co-workers have developed a template-confined method for tailoring discrete 3D supramolecular polynuclear metal ion arrays (e.g., $(Au_3)_n$ clusters, where Au_3 refers to $Au_3(1\text{-MeIm})_3$ or $Au_3[3,5\text{-}(COOMe)_2Pz]_3$ and n is the sacking number; Figure 35).[41,156−159] The templates to obtain discrete $(Au_3)_n$ clusters were hexanuclear Pt(II) or Pd(II) trigonal prismatic coordination cages with strong π-acidic 2,4,6-tris(4-pyridyl)-1,3,5-triazine (TPT) ligands as roofs and floors. The host−guest complexes (denoted as $(Au_3)_n$@cage complexes herein) were synthesized by mixing Au CTCs with aqueous solutions of the cages or their components (i.e., Pd(II) or Pt(II) salts, TPT ligands, and pillar ligands) at 60 °C for 12 h. By altering the pillar ligands from the shortest one (pyrazine) to the longer 2,2′,6,6′-tetramethyl-4,4′-bipyridine and subsequently the longest one (1,4-di(4-pyridyl)benzene), $(Au_3)_n$@cage complexes with n = 1, 2, and 3, respectively, were obtained.[156]

Apart from discrete $(Au_3)_n$ clusters with defined stacking numbers, discrete sandwich-like Au_3/Ag clusters could also be tailored by the same approach used by Fujita et al.[41,156−159] When Au_3 represented $Au_3(1\text{-MeIm})_3$, the reaction of $(Au_3)_2$@cage with Ag(I) salts produced Au_3−Ag−Au_3@cage, while the reaction of $(Au_3)(TPT)(Au_3)$@cage with Ag(I) salts produced Au_3−Ag−Au_3−Ag−Au_3@cage. Notably, to date, Au_3−Ag−Au_3−Ag−Au_3 sandwich-like clusters have not been directly synthesized without a cage. As an extension of these works, Fujita's group found that both the host with confined space and the tray-shaped complexes can be used as the template. Indeed, by using tray-shaped Pd_3Au_3 complexes as scaffolds, Au_3Pz_3−Au_3Im_3−Ag−Au_3Im_3−Au_3Pz_3 (Pz = 3-(3′-pyridyl)Pz, Im = 1-MeIm herein) was obtained (Figure 36).[158]

The above elegant and interesting cases presented by Fujita and co-workers well-demonstrated the cooperative effects of noncovalent interactions. All these host−guest complexes were stabilized by the confinement effect of the host cages, the π-acid/π-base interactions between TPT and the Au CTCs, and the intermolecular M−M interactions. In the case of $(Au_3)_n$@cage

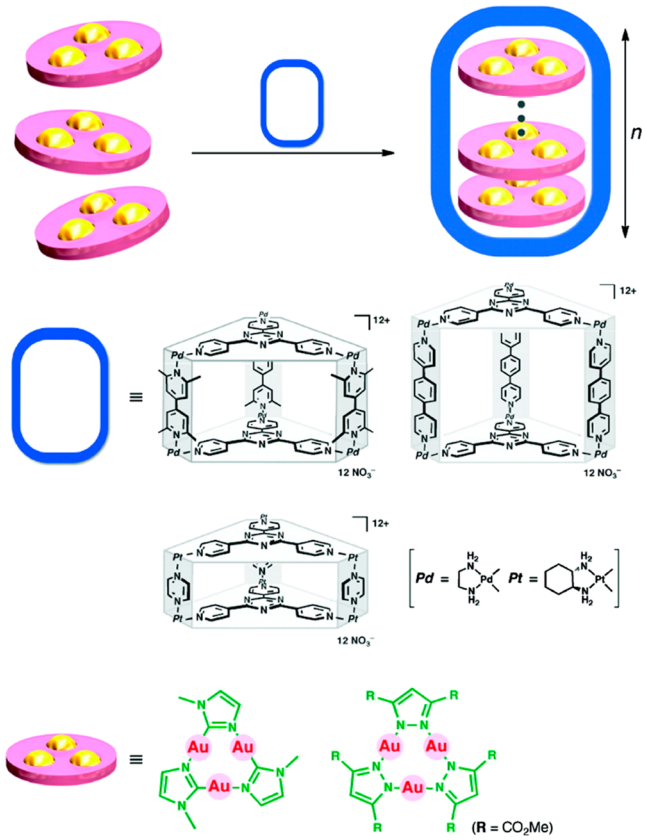

Figure 35. Cyclic trinuclear gold(I) complexes forming 3D supramolecular trigonal prismatic arrays with coordination cages (n = 1−3). [Reprinted with permission from ref 156. Copyright 2010, American Chemical Society, Washington, DC.]

complexes, the molecular stacking in the eclipsed, pseudo-D_{3h} symmetry for each Au CTC dimer or trimer was realized inside the cage, because of the cooperativity of the π-acid/π-base interactions, aurophilicity, and geometrical restriction from the trigonal prismatic host cages. Notably, such eclipsed stacking has not been observed in any Au(I)/Ag(I)/Cu(I) CTC crystals without enclosing CTC molecules in the cages, because of the strong electrostatic repulsion between the CTC molecules. The only exception is the hexagonal crystalline phase of $Au_3(MeN{=}COMe)_3$ (see detailed discussions given in section 4.2.1).

With the increase in length of the pillar ligands, the stacking number of Au_3 in the cage can be tuned from 1 to 3. Indeed, $(Au_3)_n$@cage complexes, where Au_3 = $Au_3(1\text{-MeIm})_3$ and n = 1 and 2, were obtained by respectively employing pyrazine and bipyridine as the pillar ligands. However, by employing the longest pillar ligand, the $(Au_3)(TPT)(Au_3)$@cage complex was obtained instead of the expected $(Au_3)_3$@cage complex. This was attributed to the strong electrostatic repulsion between the π-basic $Au_3(1\text{-MeIm})_3$, which prevents the formation of $(Au_3)_3$ within the cage. Thus, the stable $(Au_3)(TPT)(Au_3)$@cage complex formed with A-D-A-D-A stacking, where A = TPT panel or guest (electron acceptor) and D = $Au_3(1\text{-MeIm})_3$ (electron donor). By replacing the $Au_3(1\text{-MeIm})_3$ with the less π-basic $Au_3[3,5\text{-}(COOMe)_2Pz]_3$, the $(Au_3)_3$@cage complex could be obtained. However, the weak π-basicity of $Au_3[3,5\text{-}(COOMe)_2Pz]_3$ prevents its binding with Ag(I) cations, even with the aid of cages. As a result, cages with Au_3/Ag clusters could only been synthesized when Au_3 = $Au_3(1\text{-MeIm})_3$. In addition, since the above $(Au_3)_3$@cage complexes were

https://dx.doi.org/10.1021/acs.chemrev.0c00011
Chem. Rev. 2020, 120, 9675−9742

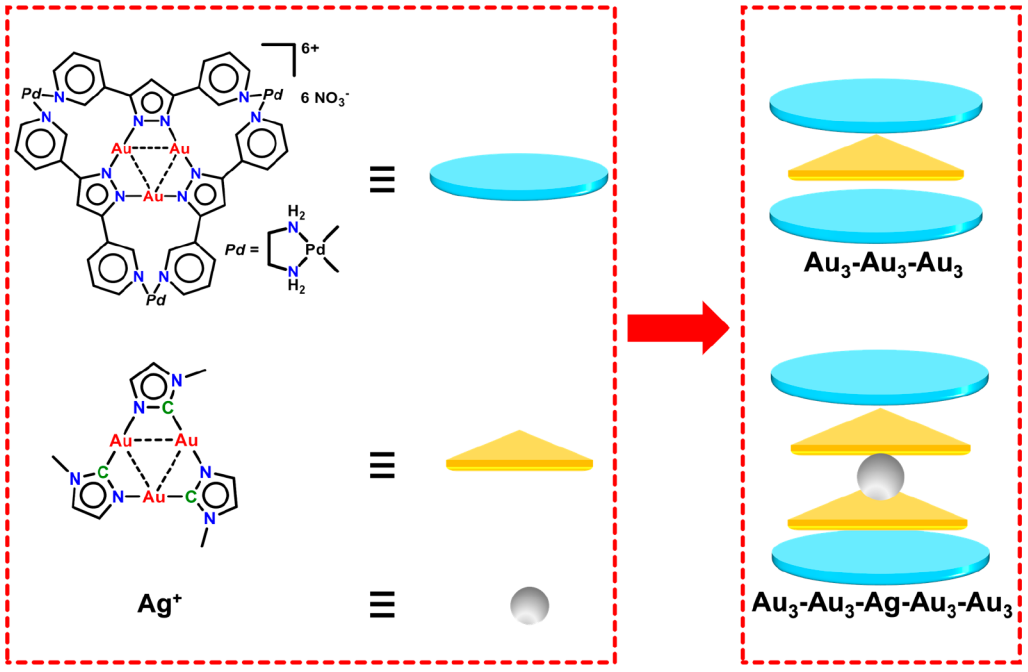

Figure 36. Stacking illustrations of the homometallic and heterometallic sandwich-like adducts constructing from the tray-shaped $Au_3Pd_3Pz_3$, Au_3Im_3, and/or Ag(I) ion.

obtained in the warm aqueous solutions, the remarkably higher thermal stabilities of the Au CTCs, compared to those of Au(Y)Cl, were highlighted.

Ferrocene (Fc) and its analogues are typical chemical entities that exhibit competition between the π-acid and Lewis acid donating sites in the interactions with π-acidic CTCs. The molecular stacking in the co-crystal of $Ag_3[3,5\text{-}(CF_3)_2Pz]_3$ and Fc can be roughly described as face-to-face stacking between each cyclopentadiene (Cp) anion in an Fc and $Ag_3[3,5\text{-}(CF_3)_2Pz]_3$ (Figure 37, left). Similar stacking modes were also found in the co-crystals of Fc-adducted $Cu_3[3,5\text{-}(CF_3)_2Pz]_3$ and $M_3[3,5\text{-}(CF_3)_2Pz]_3$ (M = Ag(I), Cu(I)) adducted with a series of ruthenium sandwich compounds.[179,180] However, in the case of the acetylferrocene ($FcC(O)CH_3$), its co-crystals exhibited the discrete packing of the BAB unit with O−M_3 interactions, where A = $M_3[3,5\text{-}(CF_3)_2Pz]_3$, B = $FcC(O)CH_3$, and M = Ag(I), Cu(I) (Figure 36, right).

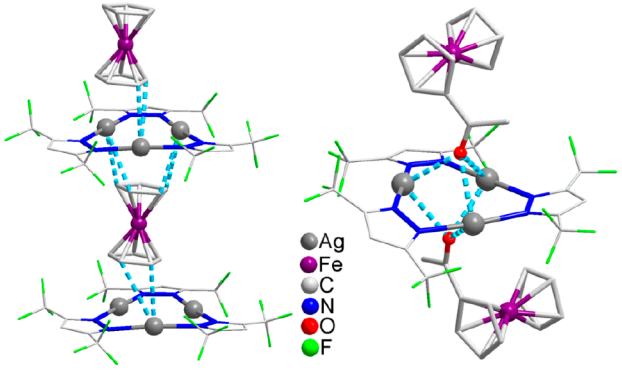

Figure 37. Molecular packing diagrams of co-crystals of $Ag_3[3,5\text{-}(CF_3)_2Pz]_3$ and (left) ferrocene and (right) acetylferrocene.

By replacing acetylferrocene with $FcC(O)CH_2Ph$, its co-crystal with $Ag_3[3,5\text{-}(CF_3)_2Pz]_3$ was stabilized by O−Ag_3 and π-acid/π-base interactions between $Ag_3[3,5\text{-}(CF_3)_2Pz]_3$ and the Ph group (Figure 38).[181] Thus, it seems that the Cp rings in Fc derivatives are weaker π-donors than the carbonyl groups.

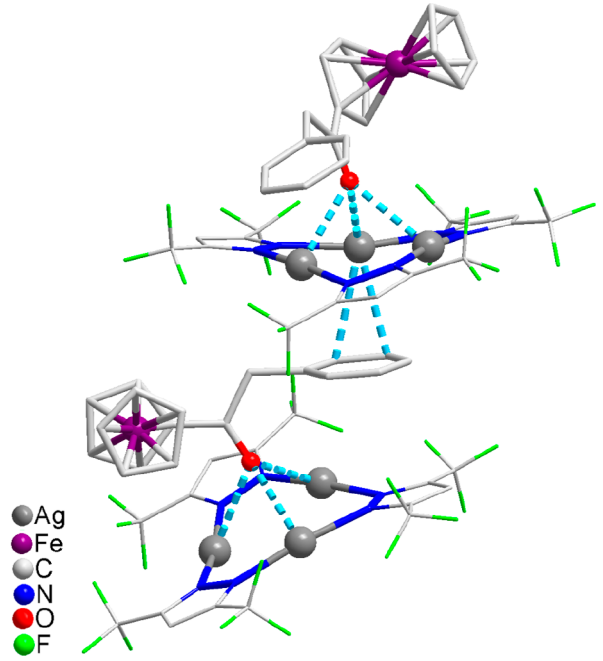

Figure 38. Molecular packing diagrams of co-crystals of $Ag_3[3,5\text{-}(CF_3)_2Pz]_3$ and $FcC(O)CH_2Ph$.

Interestingly, as an isomorphic species of Fc, pentaphosphaferrocene ($Fe(\eta^5\text{-}P_5)(Cp^*)$, where Cp* = pentamethylcyclopentadiene) represents a remarkably stronger π-donor than Fc.[182] The complexation between $Fe(\eta^5\text{-}P_5)(Cp^*)$ and $Cu_3[3,5\text{-}(CF_3)_2Pz]_3$ resulted in a noticeable coordination change between the *cyclo*-P_5 rings and two Cu(I) ions, revealed by the

https://dx.doi.org/10.1021/acs.chemrev.0c00011
Chem. Rev. 2020, 120, 9675−9742

almost perpendicular molecular conformation between a Pz plane and the trinuclear Cu plane of $Cu_3[3,5\text{-}(CF_3)_2Pz]_3$ (Figure 39a). In addition, a significant color change, from the green solution of Fe(η^5-P_5)(Cp*) in hexane to red-orange after the addition of $Cu_3[3,5\text{-}(CF_3)_2Pz]_3$, indicated the formation of a CT complex. EDA analysis suggested that the Cu−P coordination bonds were stronger than the Cu−N bonds, and natural orbitals for chemical valence (NOCV) analysis indicated that Cu atoms played the role of both Lewis acids and Lewis bases (Figure 39b).

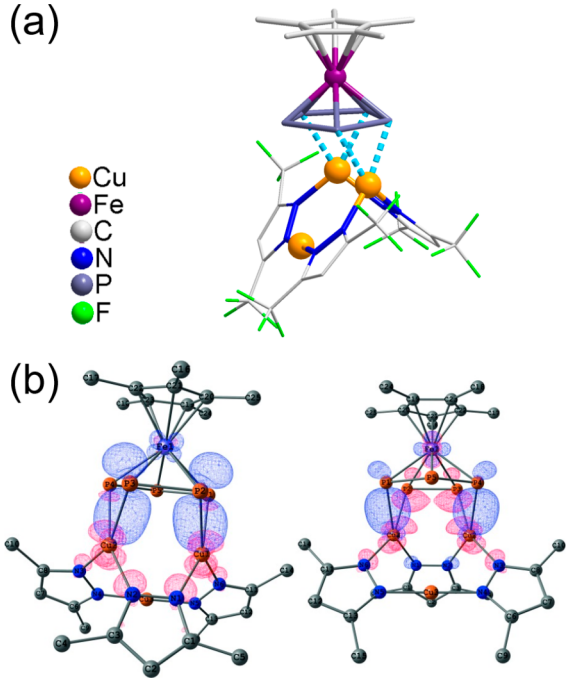

Figure 39. (a) Molecular structure of Fe(η^5-P_5)(Cp*)/$Cu_3[3,5\text{-}(CF_3)_2Pz]_3$ adduct. (b) NOCV deformation densities showing back-donation from $Cu_3[3,5\text{-}(CF_3)_2Pz]_3$ to Fe(η^5-P_5)(Cp*). Reprinted with permission from ref 182. Copyright 2015, Wiley−VCH Verlag GmbH & Co. KGaA, Weinheim, Germany.

The comprehensive and extensive review by Titov et al. in 2018 has summarized most of the simple acid/base adducts formed in solution and as crystals by the interactions between $M_3[3,5\text{-}(CF_3)_2Pz]_3$ (M = Ag(I), Cu(I)) and organic or inorganic bases, including the above-mentioned cases and the adducts with boron hydrides, triethylamine borane, and anionic polyhedral boron hydrides.[4] The study also discussed important design principles and a series of possible pathways of $M_3[3,5\text{-}(CF_3)_2Pz]_3$ (M = Ag(I), Cu(I)) as an acid in the formation of the above simple acid/base adducts (Scheme 3). Their design principles and the possible adducting pathways for acid/base adduct formation could be extended to other CTCs.

The spontaneous escape of organic arenes at rt indicated that the adducts formed by $Ag_3[3,5\text{-}(CF_3)_2Pz]_3$ and benzene, toluene, or mesitylene were not thermally stable in air,[39] even though these adducts are more stable than the $Cu_3[3,5\text{-}(CF_3)_2Pz]_3$/benzene adduct.[163] Dias and co-workers suggested that the convex-shaped molecular conformation of $M_3[3,5\text{-}(CF_3)_2Pz]_3$ (M = Au(I)/Ag(I)/Cu(I)) was suitable to host C_{60} rather than the planar arenes, to form sandwich-like host−guest adducts.[183] In their co-crystals, each C_{60} bound with four dimers of M_3Pz_3 (Figure 40a), each of which was sandwiched by two C_{60} molecules (Figure 40b). Interestingly, for the Au(I)/Cu(I) CTC/C_{60} adducts, the intertrimer M(I)−M(I) distances within the dimers were markedly shorter than those of the parent $M_3[3,5\text{-}(CF_3)_2Pz]_3$ (M = Au(I), Cu(I)). Thus, the intertrimer Au(I)−Au(I) and Cu(I)−Cu(I) distances decreased from 3.885 Å to 3.263 Å and from 3.813 Å to 3.150 Å, respectively. Conversely, the intertrimer Ag(I)−Ag(I) distances of $Ag_3[3,5\text{-}(CF_3)_2Pz]_3$ did not show any noticeable changes (~3.20 Å) before and after adduction with C_{60}. All these co-crystals showed much higher thermal stabilities than the previously reported $M_3[3,5\text{-}(CF_3)_2Pz]_3$ adducted arenes. The RDG and EDA calculations at the DFT-D3 level of theory performed by Muñoz-Castro and co-workers manifested that the interactions between $M_3[3,5\text{-}(CF_3)_2Pz]_3$ and C_{60} were dominated by strong vdW interactions (London dispersion forces) and supported by electrostatic interactions, while CT characteristics were negligible.[184] To date, C_{60} is still the largest molecule co-crystallized with CTCs reported in the literature.

Scheme 3. Possible Pathways of $M_3[3,5\text{-}(CF_3)_2Pz]_3$ (M = Ag(I) or Cu(I)) Supramolecular Aggregations[a]

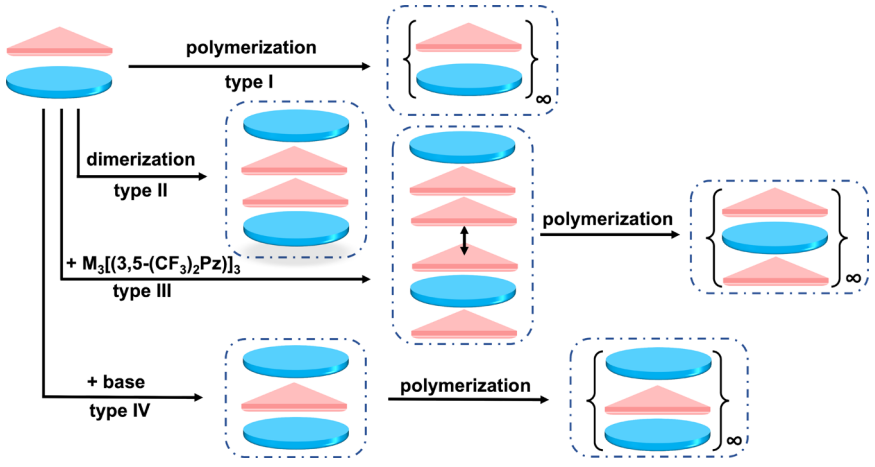

[a]Host CTCs $M_3[3,5\text{-}(CF_3)_2Pz]_3$ are depicted as triangles, guest bases−as ellipsoids. Reprinted with permission from ref 4. Copyright 2018, Elsevier, Amsterdam.

https://dx.doi.org/10.1021/acs.chemrev.0c00011
Chem. Rev. 2020, 120, 9675−9742

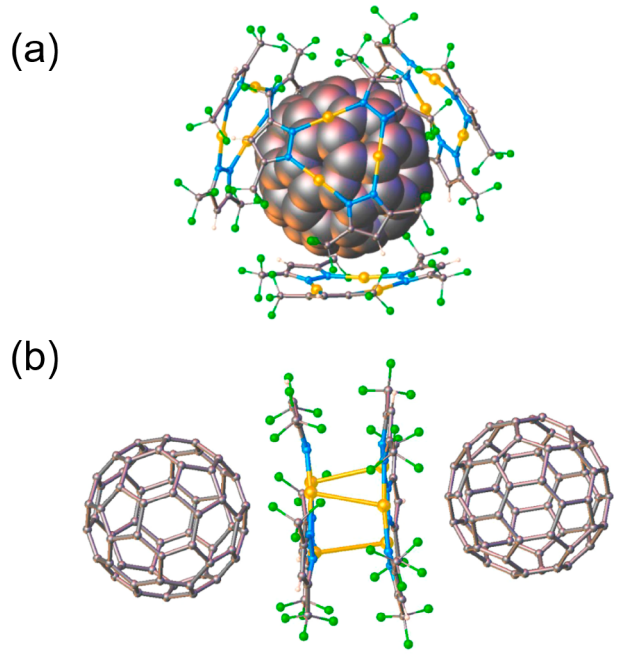

Figure 40. Crystal structure of $Au_3[3,5\text{-}(CF_3)_2Pz]_3$) adducted C_{60} showing (a) a C_{60} molecule surrounded by four Au_3Pz_3 molecules and (b) a dimer of Au_3Pz_3 sandwiched by two C_{60} molecules. Color code: golden, Au; blue, N; gray, C; and green, F. [All H atoms have been omitted from the figures for the sake if clarity. [Reprinted with permission from ref 183. Copyright 2016, American Chemical Society, Washington, DC.]

3.2.2. Metal Metathesis and Redox Reactions. The excessive addition of Au(Y)Cl into Ag(I) CTC solutions could produce Au(I) CTCs and AgCl precipitates. Such metal metathesis reactions afforded $Au_3(p\text{-TolN}{=}COEt)_3$ in 1975[140] and $Au_3[3,5\text{-}(4'\text{-F-Ph-thioethyl})_2Pz]_3$ in 2012.[185]

In 1977, Balch et al. reported the first case of oxidative addition in the family of CTCs, showing the stepwise oxidative addition of $Au_3(MeN{=}COMe)_3$ by I_2.[186] After 20 years, they reported the crystal structures of these higher-valence products during the stepwise oxidative addition (i.e., $Au_3(MeN{=}COMe)_3I_2$, $Au_3(MeN{=}COMe)_3I_4$, and $Au_3(MeN{=}COMe)_3I_6$).[187] In these mixed-valence or completely oxidized Au CTCs, the unsaturated Au(III) were satisfied by further coordinating I^- anions, resulting in a square planar AuN_2I_2 coordination environment. In addition, $Au_3(MeN{=}COMe)_3$ can be partially electrochemically oxidized to yield the needle-like crystals of $[Au_3(MeN{=}COMe)_3](ClO_4)_{0.34}$.[188] The reaction of $Au_3(3,5\text{-}Ph_2Pz)_3$ with aqua regia afforded the partially oxidized product $Au_3(3,5\text{-}Ph_2Pz)_3Cl_2$, in which one of the three Au(I) ions was oxidized to Au(III).[189] This mixed-valence $Au(I)_2Au(III)$ CTC can also be synthesized by the direct reaction of Au(pyridine)Cl_3 with $Na(3,5\text{-}Ph_2Pz)$ in a THF solution.[190] In 2002, Raptis et al. reported the X-ray crystal structures of $Au(I)Au(III)_2$ and $Au(III)_3$ species from the oxidation reactions of $Au_3(3,5\text{-}Me_2Pz)_3$ with aqua regia.[191]

Bovio, Burini, and co-workers discovered that $Au_3(1\text{-BzIm})_3$ could undergo partial oxidative addition to afford mixed-valence $Au(I)_2Au(III)$ and $Au(I)Au(III)_2$ CTCs and complete oxidative addition to afford Au(III) CTC.[192−194] However, unlike the stepwise oxidative addition of $Au_3(MeN{=}COMe)_3$ by a specified reagent (i.e., I_2), the transformation of $Au_3(1\text{-BzIm})_3$ to different oxidation products required the usage of different reagents capable of oxidative-addition, such as alkyl halides, acyl halides, Me_3SiI, and $SOCl_2$.

Apart from the oxidation of Au(I) CTCs in solution, a rare case of reduction within the crystal was reported. Exposing the crystals of unsubstituted Au_3Py_3 in air for months or immersing them in 4 M hydrochloric acid for a few days led to hourglass-shaped figures inside the crystals.[111]

Unlike Au(I) CTCs, the oxidative addition of Ag(I) and Cu(I) CTCs often resulted in the decomposition of nine-membered rings. Usually, the oxidation of Cu(I) CTCs resulted in unidentified Cu(II) or polynuclear Cu(II) compounds. For example, the solution of $Cu_3(3,5\text{-}Me_2Pz)_3$ in pyridine rapidly absorbed oxygen in the presence of water to form the blue complex $[Cu_8(3,5\text{-}Me_2Pz)_8(OH)_8]$.[195]

4. TYPICAL STRUCTURES WITH CYCLIC TRINUCLEAR UNITS (CTUs)

4.1. Simple Cyclic Trinuclear Complexes (CTCs)

In this section, the intramolecular structural parameters of neutral Au(I)/Ag(I)/Cu(I) CTCs will be discussed based on the available X-ray crystal data, including metal−metal distances, coordination bond lengths, and angles. In addition, the intertrimer metal−metal distances as well as stacking modes are included in section 4.2. The structures of CTU-based coordination cages and polymers are discussed in sections 4.3 and 4.4, respectively however, the detailed structural parameters are beyond the scope of this review and will not be discussed. Structural parameters, including intra/intertrimer M−M distances, coordination bond lengths, and angles of some selected representative CTCs, are listed in Table 1, while the full table of all of the published CTCs is included in Tables S1 and S2 in the Supporting Information.

The following discussion adopts the covalent radii of Au(I) (1.25 Å), Ag(I) (1.34 Å), and Cu(I) (1.11 Å) provided by Omary, Cundari, Dias, and co-workers for two-coordinate transition-metal ions in CTC molecules[23] and the covalent radii of C (0.77 Å) and N (0.75 Å) provided by Butler and Harrod.[196]

4.1.1. CTCs with μ-N,N-Donor Ligands. Most of the Au/Ag/Cu CTCs with μ-N,N-donor ligands are trimeric, featuring linear two-coordinate M(I) environments and planar or near-planar nine-membered M_3N_6 rings. Based on the CSD database, the M−N bond lengths vary in the ranges of 1.89−2.05 Å for Au_3Pz_3, 2.028−2.24 Å for Ag_3Pz_3, and 1.814−2.105 Å for Cu_3Pz_3 (see Table S1 in the Supporting Information).[97] Because of factors such as the steric effect, metal−metal interactions, and influences from the substituent, the N−M−N bond angles deviate, to some extent, from linearity (180°) in the order Ag > Cu > Au. According to the above ranges of intramolecular structural parameters for Au/Ag/Cu CTCs, both intratrimer M−M distances and M−N bond lengths roughly decrease in the order Ag > Au > Cu, which also follows the trends for both the vdW and covalent radii of these metals.

Careful analyses by scattering the differential values of the upper and lower limit of intratrimer distances (Δd) and the subtraction results of the lower limit and corresponding radii of the coordinated atoms (d − r) reveal hidden information (Figure 41). For intratrimer M−M distances, both the Au−Au and Ag−Ag distances are mainly close to or slightly shorter than the sum of the vdW radii of the metals. However, the intratrimer Cu−Cu distances are significantly longer than the sum of the vdW radii of two Cu atoms, indicated by subtraction results ≥0.3 Å (Figure 41a). This tendency also reveals that the ground-state

https://dx.doi.org/10.1021/acs.chemrev.0c00011
Chem. Rev. 2020, 120, 9675−9742

Table 1. Structural Parameters of Selected CTCs

complex	temperature, T (K)	d_{intra}(M−M)[a] (Å)	d_{inter}(M−M)[b] (Å)	d(M−N)[c] (Å)	d(M−C)[d] (Å)	angle (N/C−M−N)[e] (deg)	CCDC RefCode	ref
$Cu_3(3,5\text{-}Me_2Pz)_3$	298	3.1950(5)−3.2582(5)	2.9534(5), 2.9534(5)	1.850(2)−1.858(2)	NA[f]	173.79(10)−175.42(11)	LEPZAI	53
$Cu_3[3,5\text{-}(CF_3)_2Pz]_3$	298	3.221−3.242	3.879(1), 3.893(1)	1.853(4)−1.869(4)	NA[f]	178.7(2)−179.2(2)	XELXAN	135
$Cu_3(3,5\text{-}Ph_2Pz)_3$·0.5*n*-Hexane	295	3.280(1)−3.406(1)	>5.0	2.041(7)−2.105(7)	NA[f]	169.2(3)−178.6(3)	VADNAP	118
$Cu_3[3,5\text{-}(n\text{-}C_3F_7)_2Trz]_3$· 2Toluene	100	3.215(2)−3.264(2)	NA[f]	1.859(8)−1.887(7)	NA[f]	163.5(3)−176.7(4)	EFAWIS	137
Cu_3Py_3	180	3.127(9)−3.1632(6)	2.7624(6), 2.7624(6)	1.898(3)−1.901(3)	N/C disorder	168.01(12)−176.59(18)	NAHJIQ	93
Ag_3Pz_3	295	3.414(6) − 3.449(6)	3.431(4)	2.13(2) − 2.24(2)	NA[f]	172.1(7) − 177(1)	HESBUC	125
$Ag_3(3,5\text{-}Me_2Pz)_3$	298	3.318(9)−3.388(11)	3.230(13)	2.028(51)−2.049(46)	NA[f]	NG[g]		197
$Ag_3[3,5\text{-}(CF_3)_2Pz]_3$	298	3.4399(8)−3.5408(9)	3.3073(13), 3.3073(13), 3.830(1)	2.066(6)−2.097(6)	NA[f]	172.5(2)−178.6(3)	XELXER	135
$Ag_3(3,5\text{-}Ph_2Pz)_3$	110	3.3571(8)−3.525	2.9786(11)	2.073(4)−2.106(4)	NA[f]	171.17(17)−172.30(16)	FISDIV	92
$Ag_3[3,5\text{-}(n\text{-}C_3F_7)_2Trz]_3$· 2Toluene	100	3.4330(4)−3.5013(5)	NA[f]	2.102(3)−2.139(3)	NA[f]	161.50(12)−174.07(12)	EFAWOY	137
Au_3Pz_3	299	3.3723(5)−3.4014(5)	3.1596(1), 3.3128(5), 3.3128(5)	1.992(6)−2.014(6)	NA[f]	176.9(3)− 178.9(3)	MUTKUH	98
$Au_3[3,5\text{-}(CF_3)_2Pz]_3$	295	3.345(2)−3.355(2)	3.998(1), 3.998(1)	1.89(3)−1.96(2)	NA[f]	178(1)−180(1)	COHFIO	116
$Au_3(3,5\text{-}Ph_2Pz)_3$	295	3.368(1)	>5.0	1.978(9)	NA[f]	179.6(3)	FUWXOK	119
$Au_3[3,5\text{-}(i\text{-}Pr)_2Trz]_3$	293	3.3595(12)−3.400(1)	3.416(1), 3.416(1), 3.463(2)	1.963(13)−2.032(14)	NA[f]	172.9(6)−175.8(6)	HEMTID01	100
Au_3Py_3	140	3.309(2)−3.346(3)	3.077(2)−3.146(3)	2.01(2)−2.11(2) (disorder)	N/C disorder	174.3(18)−178.0(8)	EFOTIC	111
$Au_3(MeN{=}COMe)_3$ ($P6/m$)[h]	130	3.308	3.346	2.03	2.000	178.55, 180.0	RETDAV, RETDAV01	31
$Au_3(1\text{-}MeIm)_3$	100	3.4342(5)−3.5222(5)	3.6660(5)−3.7526(3)	2.034(5)−2.056(5)	1.974(6)−1.993(6)	172.9(2)−177.3(3)	VUQFEV	113

[a]Intratrimer metal−metal distance. [b]Intertrimer metal−metal distance. [c]Metal−nitrogen coordination bond length. [d]Metal−carbon coordination bond length. [e]Nitrogen/carbon−metal−nitrogen coordination bond angle. [f]NA = not applicable. [g]NG = not given. [h]Hexagonal phase.

https://dx.doi.org/10.1021/acs.chemrev.0c00011
Chem. Rev. 2020, 120, 9675−9742

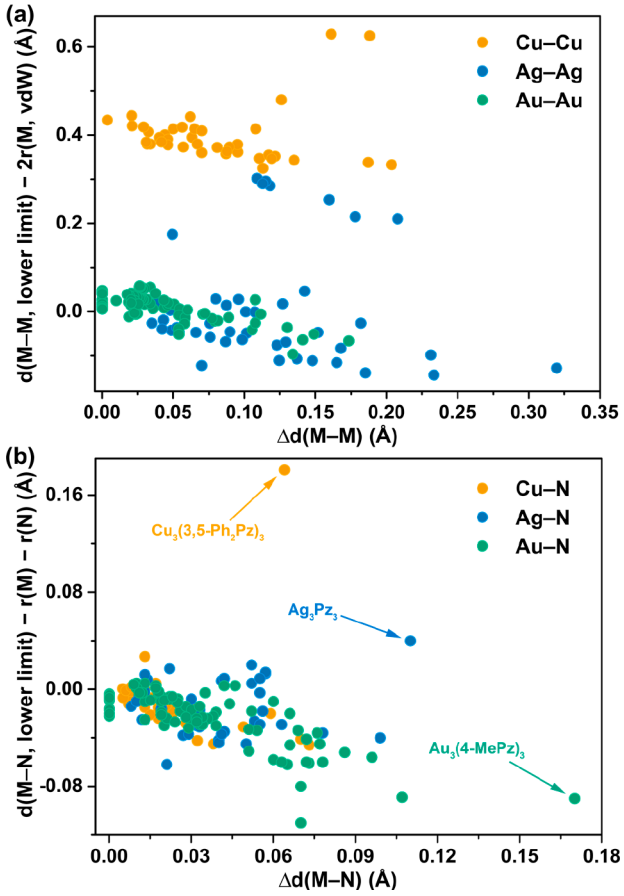

Figure 41. Scatter plots of (a) differences of upper and lower limits of intratrimer M−M distances (Δd(M−M)) versus values of lower limit subtracting the sum of vdW radii of corresponding metal atoms in one pyrazolate CTC; (b) differences of upper and lower limits of M−N coordination bond lengths (Δd(M−N)) versus of lower limit subtracting the sum of covalent radii of corresponding metal and N atom in one pyrazolate CTC.

intratrimer Cu−Cu interactions are quite weak or even absent compared to those observed in Au_3Pz_3 and Ag_3Pz_3. Moreover, relatively larger Δd(M−M) values always afford smaller subtraction results of the lower limit of intratrimer M−M distances and the sum of vdW radii of two metal atoms (d(M−M, lower limit) − 2r(M, vdW)), hinting that the distortion of the M_3N_6 nine-membered ring would lead to at least one pair of stronger intratrimer M−M interactions. The analyses of the M−N coordination bond lengths indicate that all M−N bond strengths are comparable, because of the subtraction results approaching zero (Figure 41b). Influenced by the ligands, some M−N bond lengths deviate from the majority.

The differences between electron-donating (e.g., Me, *i*-Pr) and electron-withdrawing (e.g., CF_3, NO_2) groups do not result in significant deviations in the M−N bond lengths and intratrimer M−M distances (see Table S1 in the Supporting Information). However, the bulkiness of the substituents on the 3,5-posittions of Pz may play an evident role, especially for Cu_3Pz_3. For instance, the Cu−N bond lengths of Cu_3(3,5-$Ph_2Pz)_3$ (295 K, 2.041(7)−2.105(7) Å) are significantly longer than those of other Cu_3Pz_3 complexes (Figure 41b).[118] Moreover, significant distortion of the nine-membered rings was observed for Cu_3(3,5-$Ph_2Pz)_3$ (Figure 42).

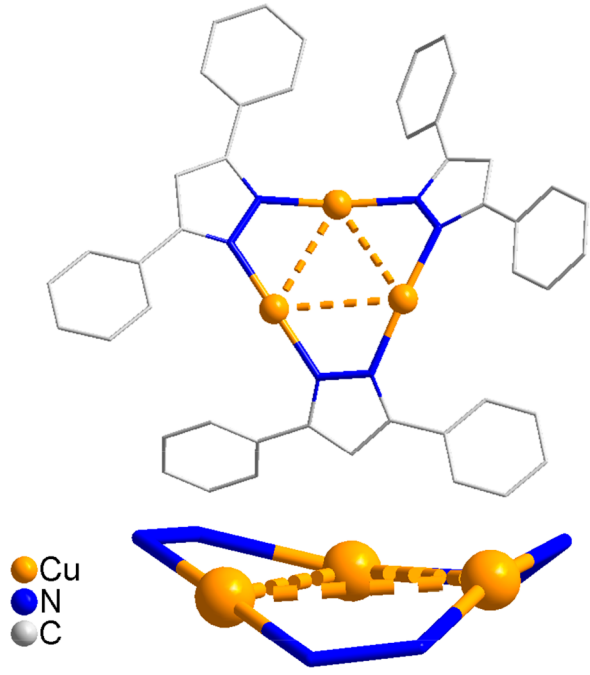

Figure 42. Crystal X-ray structure of Cu_3(3,5-$Ph_2Pz)_3$ at 295 K. [All H atoms have been omitted from the figure for the sake of clarity.]

For the Pz ligand with a 2-pyridyl group on the 3-position, the weak intramolecular coordination between the pyridyl nitrogen and metal center was observed for the corresponding Cu and Ag CTCs.[128,198−200] The N_{Pz}−M−N_{Pz} bond angles approached 160°, suggesting that the coordination between the metal ions and N atom in the pyridyl group (M−N_{Py}) is significantly weaker than that of M−N_{Pz}. Therefore, the coordination geometry of the metal ions should be "2 + 1" T-shaped coordinate rather than linear two-coordinate or triangular three-coordinate. The large deviations from 180° of the N_{Pz}−M−N_{Pz} bond angles, result in particularly long intratrimer M−M distances (3.425(3)−3.613(3) Å for Cu CTCs and 3.7301(5)−3.8429(6) Å for Ag CTCs). Similarly, the intertrimer Cu−Cu distance of the Cu_3[3-(2′-pyridyl)-Pz]$_3$ CTC is as short as 2.824(3) Å, shorter than most other Cu CTCs. Moreover, the intertrimer Ag−Ag distance (3.0639(3) Å) of the Ag_3[3-(2′-pyridyl)-Pz]$_3$ CTC is much shorter than that in the Ag_3Pz_3 CTC with one or two substituted CF_3 groups, although it is still longer than those of several Ag CTCs with saturated alkyl groups (e.g., Ag_3[3,5-(*i*-Pr)$_2$Pz]$_3$).[135,201] In addition, the Ag CTC with the radical ligand 3-pyrazolyl iminonitroxide displays both intramolecular weak coordination of the substituents and a rather short intertrimer Ag−Ag distance of 3.1792(8) Å.[124]

To date, only one example of Au_3Trz_3 and Cu_3Trz_3 (Au_3[3,5-(*i*-Pr)$_2$Trz]$_3$ and Cu_3[3,5-(*n*-C_3F_7)$_2$Trz]$_3$, respectively) and a few Ag_3Trz_3 complexes have been reported, some of which could only co-crystallize with strong organic Lewis/π-bases.[100,137,202,203] The crystal structure of Au_3[3,5-(*i*-Pr)$_2$Trz]$_3$ reveals Au−N bond lengths and N−Au−N bond angles in the ranges 1.963(13)−2.032(14) Å and 172.9(6)°−177.10(15)°, respectively.[100] In addition, intratrimer Au−Au distances fall within the range of 3.3527(7)−3.400(1) Å. All these structural parameters still follow the trends discovered in Au(I)-pyrazolate CTCs.

https://dx.doi.org/10.1021/acs.chemrev.0c00011
Chem. Rev. 2020, 120, 9675−9742

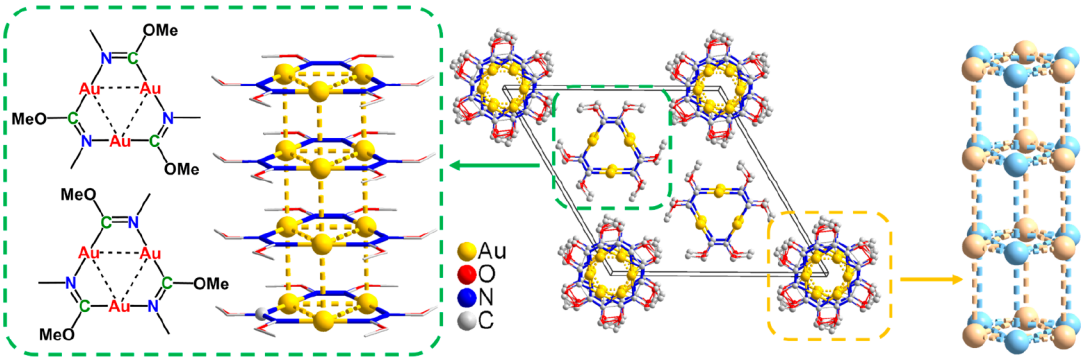

Figure 43. Crystal structure of (middle) the hexagonal phase of $Au_3(MeN{=}COMe)_3$, showing (left) the flip disorder that leads to two alternate positions for the methoxy-methyl groups and (right) rotation disordered supramolecular columns. [All H atoms have been omitted from the figure for the sake of clarity.]

4.1.2. CTCs with μ-C,N-Donor Ligands. For carbeniate Au(I) CTCs–$Au_3(R_1\text{-}N{=}COR_2)_3$, Au–N bond lengths, Au–C bond lengths, N–Au–C bond angles, and intratrimer Au–Au distances usually fall within the respective ranges of 1.98–2.16 Å, 1.78–2.07 Å, 173.1°–180.0°, and 3.224–3.363 Å (Table S2 in the Supporting Information).[31,34,91,115,155,161,204−207]

The syntheses and crystal structures of $Au_3(1\text{-}R\text{-}Im)_3$ (R = methyl, ethyl, and benzyl group) and $Au_3(1\text{-xylyl-}5\text{-}MeIm)_3$ have been reported.[90,113,208] The Au–N bond lengths, Au–C bond lengths, N–Au–C bond angles, and intratrimer Au–Au distances of the Au_3Im_3 complexes without co-crystal molecules fall within the respective ranges of 2.026–2.059 Å, 1.964–2.001 Å, 172.9°–177.3°, and 3.425–3.522 Å.

Only the crystal structure of unsubstituted Au_3Py_3 has been reported in the family of pyridinate Au(I) CTCs, and its coordination bond lengths and angles fall within the respective ranges of 2.01(2)–2.11(2) Å and 174.3(18)°–178.0(8)°.[111] Moreover, the only reported crystal structure of unsubstituted Cu_3Py_3 in the family of pyridinate Cu(I) CTCs displayed coordination band lengths and angles within the respective ranges 1.898(3)–1.901(3) Å and 168.01(12)°–176.59(18)°.[93] The ligated C and N atoms could not be distinguished because of disorder. The intratrimer Cu–Cu distances range from 3.1279 Å to 3.1632(6) Å for Cu CTC, while intratrimer Au–Au distances are in the range of 3.309(2)–3.346(3) Å for Au CTC.

4.2. Crystal Stacking Modes

Intertrimer metal–metal interactions were usually considered as the main driving force in the supramolecular aggregation and crystallization of CTCs, and steric hindrance from ligands could not be neglected. Other noncovalent interactions, especially the π-acidity/basicity, also play significant roles. To some extent, the CTC crystallization resulted from cooperative and anticooperative effects between the metal–metal interactions, π-acidity/basicity, and other noncovalent interactions.

4.2.1. Semiprismatic Stacking. When an organic arene forms a dimer, the eclipsed face-to-face stacking pattern is rare, because of the strong electrostatic repulsions between the same aromatics, especially when exhibiting strong π-acidity or π-basicity.[209] As is well-known for metal–organic π-acids/bases, the eclipsed face-to-face stacking pattern is also very rare in CTCs. The hexagonal phase of $Au_3(MeN{=}COMe)_3$ displays both trigonal prismatic 1D column arrays (eclipsed stacked conformation) and rotation disordered 1D column arrays (Figure 43).[205] Such a unique stacking pattern has not yet been observed in other CTCs. The following aspects are relevant to the trigonal prismatic column in the hexagonal phase of $Au_3(MeN{=}COMe)_3$:

(i) Au_3Cb_3 complexes display weaker π-basicity than Au_3Py_3 and Au_3Im_3 complexes;

(ii) the order of homometallic metal–metal bonding strength is Au > Ag > Cu;

(iii) the absence of aromatic rings in $Au_3(MeN{=}COMe)_3$ prevents electrostatic repulsion; and

(iv) the methyl group is the smallest substituent, resulting in the minimum steric hindrance.

However, the intertrimer electrostatic repulsion still renders a relatively long intertrimer Au–Au contact of 3.346(1) Å, which is longer than the sum of the vdW radii (3.32 Å) of Au.

Because of the lack of strong attractions between the metal ions and repulsions between the CTC planes, $Au_3(MeN{=}COMe)_3$ itself also crystallizes in the monoclinic space group and exhibits an uncommon stacking mode. In the monoclinic phase, the three closest CTC molecules form a trigonal prismatic stack with short Au–Au contacts of ~3.28 Å, and every two neighboring prismatic stacks are corner-linked with a long Au–Au contact of ~3.65 Å, which results in infinite supramolecular chains (Figure 44).[205] The above infinite and discrete trigonal prismatic stacks have not been observed in any other CTCs.

The semi- or distorted-prismatic stack was reported in other Au(I) CTCs. Indeed semiprismatic dimers and unequal intertrimer aurophilic distances (3.3464(4) and 3.5576(4) Å) were observed in the $Au_3(1\text{-}BzIm)_3$ crystals (recall Figure 5).[208] Similar semiprismatic dimers were also observed in the crystal

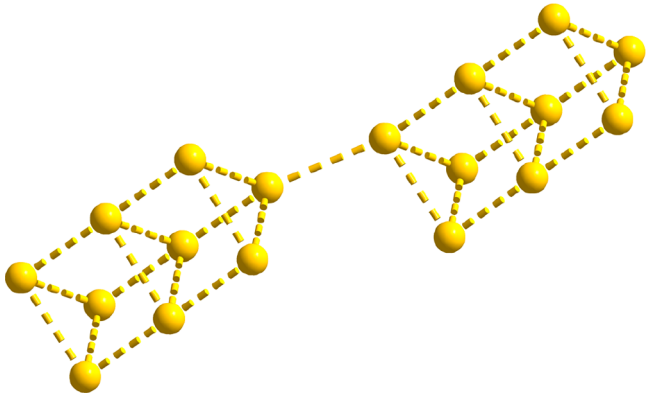

Figure 44. Crystal structure of $Au_3(MeN{=}COMe)_3$ in the monoclinic space group, showing molecular packing patterns. [The disordering Cb ligands have been omitted from the figure for the sake of clarity.]

https://dx.doi.org/10.1021/acs.chemrev.0c00011
Chem. Rev. 2020, 120, 9675–9742

structure of $Au_3[3,5\text{-}(i\text{-}Pr)_2Trz]_3$, which displayed C_2 effective symmetry with aurophilic distances of 3.1932(4), 3.5476(4), and 3.5476(4) Å at 95 K and D_3 effective symmetry with aurophilic distances of 3.463(2), 3.416(1), and 3.416(2) Å at rt.[100] The reversible interconversion between the dimers with C_2 and D_3 effective symmetries was achieved either in the crystal by changing the temperature or in solution by tuning the concentration (Figure 45).

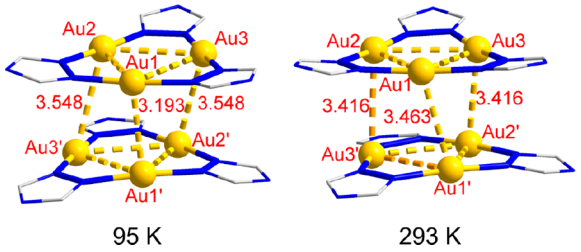

Figure 45. Crystal structure of dimer-of-trimer prismatic units of $Au_3[3,5\text{-}(i\text{-}Pr)_2Trz]_3$ at 95 K (left) and rt (right), showing intertrimer Au(I)−Au(I) distances. [All H atoms have been omitted from the figure for the sake of clarity. Numbers shown in red refer to intertrimer Au−Au distances (Å).]

4.2.2. Chair Dimer Stacking. Apart from the hexagonal and monoclinic phases, $Au_3(MeN{=}COMe)_3$ can also crystallize in the triclinic space group, exhibiting a chairlike structure. For example, two CTC molecules form a chair dimer with short Au−Au contacts of ∼3.22 Å, which are shorter than the Au−Au contacts observed in the hexagonal and monoclinic phases.[205] Each dimer in the triclinic phase further interacts with a neighboring dimer by long Au−Au contacts of ∼3.53 Å, producing infinite supramolecular chains (Figure 46). Such a stacking mode is commonly observed in the CTC family, especially for Cu_3Pz_3.

As the simplest Au_3Pz_3, unsubstituted Au_3Pz_3 displays a stacking mode with chair dimers as repeated units (Figure 47). In the crystal, two pairs of Au−Au contacts of 3.3128(5) Å bind two CTC molecules together to form a chair dimer, and each

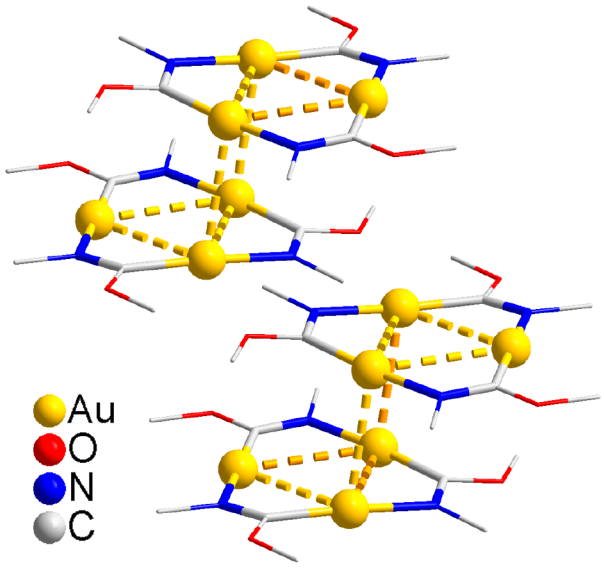

Figure 46. Crystal structure of $Au_3(MeN{=}COMe)_3$ in the triclinic space group, showing molecular packing patterns. [All H atoms have been omitted from the figure for the sake of clarity.]

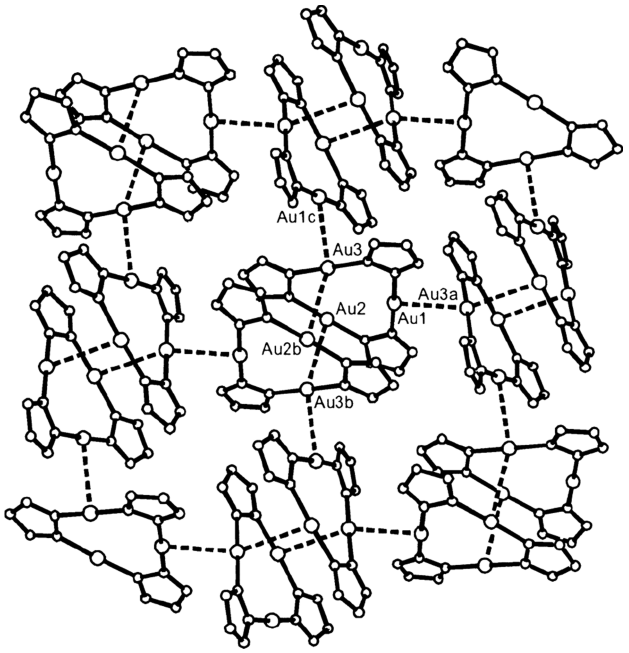

Figure 47. X-ray structure of unsubstituted Au_3Pz_3 showing the 2D supramolecular network. [The intertrimer Au−Au interactions with distances of <3.6 Å are shown as dashed lines. All H atoms have been omitted from the figure for the sake of clarity. Reprinted with permission from ref 98. Copyright 2003, American Chemical Society, Washington, DC.]

dimer links four dimers with a short Au−Au distance of 3.1596(1) Å, resulting in a 2D supramolecular network.[98] For the substituted M_3Pz_3 complexes (M = Au(I)/Ag(I)/Cu(I)), a dimer can interact with a maximum of two other CTC molecules.

Subsequently, several other stacking modes involving chair dimers were also documented. For example, the crystal of $Cu_3[3,5\text{-}(i\text{-}Pr)_2Pz]_3$ shows a discrete chair dimer with intertrimer Cu−Cu distances of 2.9889(3) Å (Figure 48a).[22]

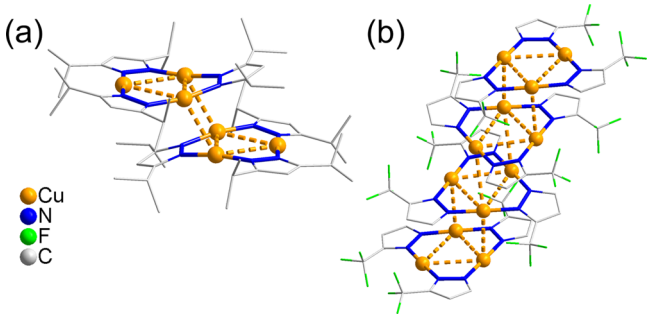

Figure 48. Crystal structures of (a) $Cu_3[3,5\text{-}(i\text{-}Pr)_2Pz]_3$ and (b) $Cu_3(3\text{-}CF_3Pz)_3$ showing molecular packing in the crystal. [All H atoms have been omitted from the figure for the sake of clarity.]

The complex $Cu_3(3,5\text{-}Me_2Pz)_3$ adopts a similar discrete chair dimer packing mode with intertrimer Cu−Cu distances of 2.944(2) Å.[149] In the case of $Cu_3(3\text{-}CF_3Pz)_3$, an infinite column packing was observed (Figure 48b).[22] In each column, two neighboring CTC molecules form a chair dimer with intertrimer Cu−Cu distances of 3.100 and 3.482 Å.

Each $Cu_3(3\text{-}CF_3Pz)_3$ molecule shows an asymmetrically oriented pyrazolyl group and the substituents at the 3- and 5-

https://dx.doi.org/10.1021/acs.chemrev.0c00011
Chem. Rev. 2020, 120, 9675−9742

positions of the pyrazolyl group (H and CF_3) do not show a regular alternating pattern (Figure 48).[22] Similar structural features were also reported for Cu_3(3-Me-5-CF_3Pz)$_3$ (Figure 49a).[22] However, Ag_3(3-Me-5-CF_3Pz)$_3$ exhibits pseudo C_3

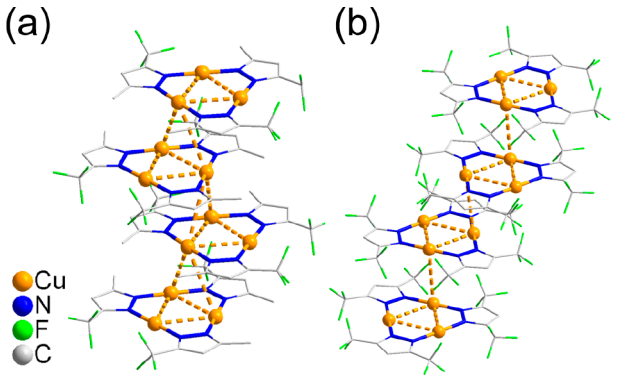

Figure 49. Crystal structure of (a) Cu_3(3-Me-5-CF_3Pz)$_3$ and (b) Cu_3[3,5-(CF_3)$_2$Pz]$_3$ showing molecular packing mode. [All H atoms have been omitted from the figure for the sake of clarity.]

symmetry with both hydrogen and CF_3 groups oriented in the same direction.[210] In addition, although their crystal structures exhibit an infinite column packing structure, the packing mode in the Cu_3(3-Me-5-CF_3Pz)$_3$ crystal is significantly different from those observed in the Ag_3(3-Me-5-CF_3Pz)$_3$ and Cu_3(3-CF_3Pz)$_3$ crystals. Thus, in each infinite column of Ag_3(3-Me-5-CF_3Pz)$_3$, two equal and relatively short Ag···Ag contacts (3.3553(4) Å) exist within a chair dimer and another two equal and relatively long Ag···Ag contacts (3.4263(5) Å) exist between two neighboring chair dimers. The crystal structure of Cu_3(3-CF_3Pz)$_3$ displays a similar structure packing mode to that of Ag_3(3-Me-5-CF_3Pz)$_3$. However, Cu_3(3-Me-5-CF_3Pz)$_3$ does not comprise chair dimers and the intertrimer Cu−Cu contacts range from 3.704 Å to 3.915 Å.

Similar to Cu_3(3-CF_3Pz)$_3$, asymmetrically oriented pyrazolyl groups were observed in Cu_3(3-CF_3-5-PhPz)$_3$; however, this complex adopted a similar infinite column packing to that of Cu_3[3,5-(CF_3)$_2$Pz]$_3$ and each two neighboring CTC molecules in a column linked each other by only one Cu−Cu contact that did not show a chairlike dimer conformation (Figure 49b).[22] Their shortest intertrimer Cu−Cu distances are too long (3.8482(4) Å for Cu_3(3-CF_3-5-PhPz)$_3$ and 3.8132(6) Å for Cu_3[3,5-(CF_3)$_2$Pz]$_3$, respectively) to be considered as intertrimer Cu−Cu interactions at the ground state, as suggested by Dias, Omary, and co-workers.[22] Since the CF_3 and *i*-Pr groups are sterically comparable, the considerable differences in the intertrimer Cu−Cu distances (2.9889(3) Å for Cu_3[3,5-(*i*-Pr)$_2$Pz]$_3$ and 3.8132(6) Å for Cu_3[3,5-(CF_3)$_2$Pz]$_3$) should be rationalized as the differences in the electronic structures. It was concluded that Cu(I)-CTCs with electron-withdrawing substituents (e.g., CF_3 and NO_2) favored 1D column stacking with long intertrimer Cu−Cu distances for Cu_3Pz_3, while those with electron-donating substituents favored dimers with short intertrimer Cu−Cu distances. This structure−property relationship between the electronic structures of the substituents and intertrimer M−M distances has been supported by numerous Cu_3Pz_3 X-ray data and is usually also suitable for Au_3Pz_3 and Ag_3Pz_3.

For the aromatic substituents, steric effects often display a more important role than electronic effects in affecting the intertrimer M−M distances. Cu_3(3,5-Ph_2Pz)$_3$ is a representative of this. The phenyl groups on both the 3- and 5-positions of each Pz ring renders significant distortion of the planar nine-membered rings (Figure 42) and a much longer Cu−Cu distance (5.40 Å), when compared to other fluorinated Cu_3Pz_3 complexes.[118] Similar discrete monomer packing with a severely distorted nine-membered coordination ring was reported for Ag_3[3-(*n*-C_3F_7)-5-(*t*-Bu)Pz]$_3$, showing an intertrimer Ag−Ag distance of 5.376 Å.[210] Moreover, Au_3(3,5-Ph_2Pz)$_3$ exhibits intratrimer Au−Au distances of 3.368(1) Å, which are longer than those for saturated alkyl group-substituted Au(I)-CTCs.[119] These examples disclose that bulky substituents in both the 3- and 5-positions of Pz and Trz could lead to a severely distorted coordination ring and prevent the formation of intertrimer metal−metal interactions.

Chairlike dimers are commonly observed in the stacking modes of Au(I)/Ag(I)/Cu(I) CTCs, because of the existence of two pairs of intertrimer metal−metal interactions and a lack of strong frontal electrostatic repulsions between the aromatic ligands. Instead, M−N or M···aromatic ring (cation-π) electrostatic attraction between the CTC molecules is observed, which is believed to incline to a chairlike dimer. Although intertrimer Au−Au distances that are shorter than the sum of the vdW radii for Au (3.32 Å) could be seen in prismatic and semiprismatic stacking crystals, the shortest Au−Au distances among the Au CTCs exist in the chairlike dimers of Au_3(1-BzIm)$_3$ and unsubstituted Au_3Py_3.[111,208] Compared to the intertrimer Au−Au and Ag−Ag interactions, the Cu−Cu interaction is noticeably weaker. As a result, all Cu CTCs show short Cu−Cu contacts (<3.2 Å) in the chairlike dimers. A representative case is **Br-*α*** (a polymorph of Cu_3[4-(4′-Br-Ph)-3,5-Me_2Pz]$_3$ in ref 94) with the shortest Cu−Cu distances (2.8622(15) Å at 293 K and 2.8174(9) Å at 100 K) among all the reported Cu_3Pz_3 complexes.[94] The unsubstituted Cu_3Py_3 exhibits Cu−Cu distances of 2.7624(6) Å at 180 K, which is the only example with Cu−Cu distances shorter than the sum of the vdW radii of Cu (2.80 Å) reported to date.[93]

For M_3Pz_3 with halogen atoms in the 4-positions of the Pz rings, noncovalent interactions related to halogen atoms play important roles in stabilizing the crystals. For example, each chair dimer of Ag_3[3-(*t*-Bu)-4-BrPz]$_3$ participates in the formation of two distorted trigonal pyramid-like structures by Ag_3−I interactions, resulting in 1D supramolecular chains (Figure 50).[121] Because the intertrimer Ag−Ag distances within a chairlike dimer are relatively long (>3.62 Å), suggesting rather weak intertrimer Ag−Ag interactions, the Ag_3−I interactions might be comparable to the intertrimer Ag−Ag interactions during crystallization.

Cu_3(4-ClPz)$_3$ is a rare case in the Cu CTC family that shows significantly different Cu−Cu distances in a pair of polymorphs (**Cl-*α*** and **Cl-*β***) stacking in two chairlike conformations (Figure 51).[36] The multiple noncovalent interactions involving Cl atoms (Cu−Cl and Cl−H) are believed to contribute to the distinct different Cu−Cu separations in these polymorphs.

Strong electron-withdrawing CF_3 and NO_2 groups can effectively weaken the Cu−Cu bonding, resulting in long intertrimer Cu−Cu distances.[22] Compared to M_3[3,5-(CF_3)$_2$Pz]$_3$ (M = Cu(I) or Ag(I)), M_3[4-X-3,5-(CF_3)$_2$Pz]$_3$ (X = Br or Cl) complexes are stronger π-acids and the intertrimer metal−metal distances in their crystals exceed 5.0 Å, values that are too long to show intertrimer metal−metal interactions at both the ground and excited states.[136] Instead, the intertrimer M_3−X interactions are crucial in stabilizing the crystals. For instance, in Ag_3[4-X-3,5-(CF_3)$_2$Pz]$_3$, each Ag_3 ring participates

https://dx.doi.org/10.1021/acs.chemrev.0c00011
Chem. Rev. 2020, 120, 9675−9742

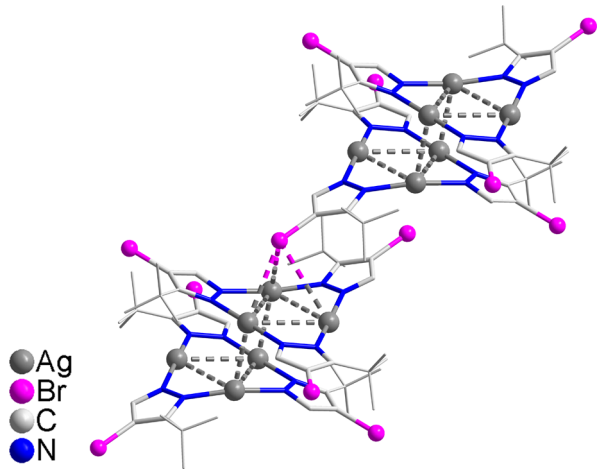

Figure 50. Crystal structure of $Ag_3[3\text{-}(t\text{-Bu})\text{-}4\text{-BrPz}]_3$ showing molecular packing mode. [All hydrogen atoms have been omitted from the figure for the sake of clarity.]

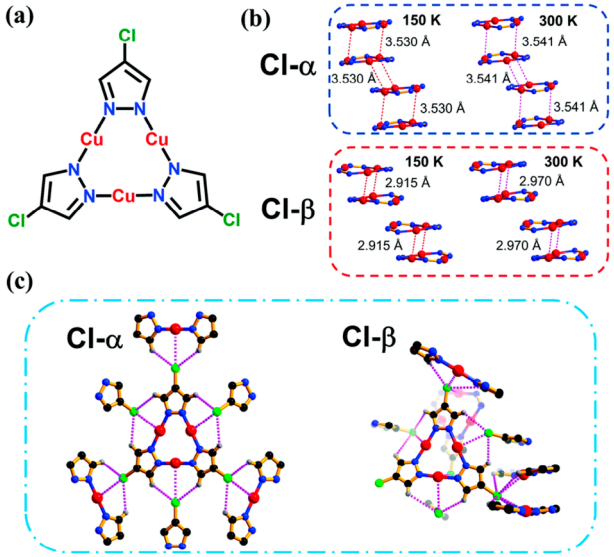

Figure 51. (a) Molecular structure of $Cu_3(4\text{-ClPz})_3$, (b) two polymorphs in chairlike conformations showing Cu−Cu contacts between nine-membered rings at 150 and 300 K, and (c) Cl-involved multiple noncovalent interactions at 300 K. [Color code: red, Cu; blue, N; black, C; green, Cl; gray, H; red dashed line, intertrimer Cu−Cu contact; purple dashed line, Cl-involved noncovalent interactions. Reprinted with permission from ref 36. Copyright 2019, Royal Society of Chemistry, London.]

in two Ag_3−X pyramids with two X atoms above and below the Ag_3 plane (Figure 52a). For $Cu_3[4\text{-X-}3,5\text{-}(CF_3)_2Pz]_3$, each Cu_3 ring participates in only one Cu_3−X pyramid, similar to the stacking mode of $Ag_3(4\text{-X-}3,5\text{-}Ph_2Pz)_3$ (Figure 52b).[123]

4.3. Supramolecular Cages with CTUs

4.3.1. Prisms and Antiprisms. In 2011, Thiel's group reported the first example of a supramolecular antiprism cage containing an M_3Pz_3-type (M = Cu(I)/Ag(I)/Au(I)) CTU from the self-assembly of the enantiomerically pure (*S*)-2,2′-di(1,2-pyrazol-3-yl)-1,1′-binaphthyl ligands (L) and a metal source.[43] However, only the crystal structure of Cu_6L_3 was characterized, namely, a hexanuclear Pelton-wheel-like shape with two tricopper planes linked by two parallel bis-pyrazolate ligands (Figure 53a). In addition, the intratrimer Cu−Cu

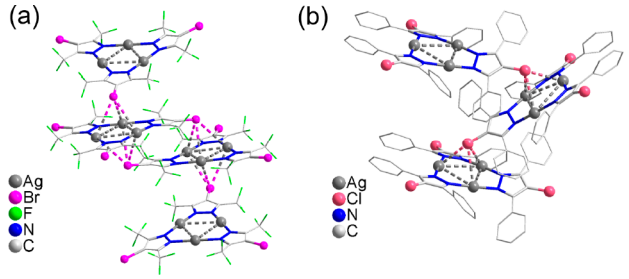

Figure 52. Crystal structure of (a) $Ag_3[4\text{-Br-}3,5\text{-}(CF_3)_2Pz]_3$ and (b) $Ag_3(4\text{-Cl-}3,5\text{-}Ph_2Pz)_3$ showing molecular packing mode. [All H atoms have been omitted from the figure for the sake of clarity.]

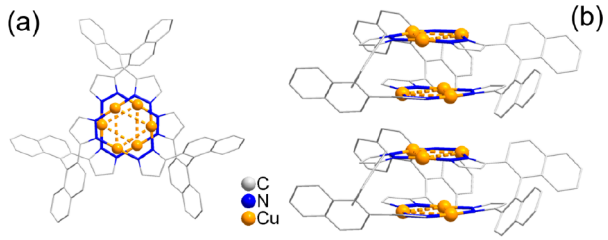

Figure 53. (a) Crystal structure of hexanuclear Pelton-wheel-like Cu_6L_3 (L = (*S*)-2,2′-di(1,2-pyrazol-3-yl)-1,1′-binaphthyl) cage; (b) Stacking mode of Cu_6L_3 cage in the crystal. [All H atoms have been omitted from the figure for the sake of clarity.]

distances (3.2275(10) Å) are ∼10% longer than those discussed in the previous literature, and the intertrimer Cu−Cu distances are 5.2002(7), 4.0298(7), and 4.1270(7) Å, respectively.[211−213] Because of the large steric hindrance of the naphthyl group, the interantiprism Cu−Cu distances are 5.3488(7), 4.2198(7), and 4.3128(7) Å, which are much longer than those in the stocked simple Cu_3Pz_3 CTCs (Figure 53b).

In the same year, Li's group reported the first example of a Cu_6L_3 (L = *m*-xylylene-bis(3,5-dimethyl)pyrazol-4-yl) prismatic cage based on Cu_3Pz_3 CTUs.[44] The Cu_6L_3 coordination prismatic cage displayed two planar nine-membered Cu_3N_6 rings with two coordinate Cu(I) sites as two triangle facets, linked by three xylylene groups as edges perpendicular to the Cu_3N_6 rings. The intratrimer Cu(I)−Cu(I) distances are 3.174, 3.195, 3.199, 3.203, 3.212, and 3.217 Å, respectively, while the intertrimer Cu(I)−Cu(I) distances are 3.696, 3.868, and 3.946 Å, respectively, values that are significantly shorter than those reported by Thiel.[43] Notably, this is the first example of uncommon Cu_3−Cu_3 frontal mode arrangement. The frontal mode of Cu_3−Cu_3 is unfavorable for the dimer-of-trimer of Cu(I) CTCs due to the weak Cu−Cu interactions and strong electrostatic repulsion between the CTC molecules; thus, it has not been reported until the publication of this Review. Parallel to organic linkers, Meyer and co-workers reported a successful trial for connecting two M_3Pz_3 units (M = Ag(I), Cu(I)) by three ferrocene units (recall Figure 22).[49] In the crystal structure of the Ag_6 cage, the Ag ions adopted a frontal mode arrangement, and the intratrimer and intertrimer Ag(I)−Ag(I) distances fell within the respective ranges 3.40−3.49 Å and 3.28−3.30 Å. Such Ag(I)−Ag(I) distances are shorter than the sum of the vdW radii of Ag atoms (3.44 Å), indicating weak intertrimer closed-shell d^{10}−d^{10} interactions, while the interprism Ag(I)−Ag(I) distances are longer than 4.5 Å. In addition, the Cu_6 cage exhibited a structure similar to that of the Ag_6 cage, also adopting a frontal mode arrangement. The intratrimer and intertrimer Cu(I)−Cu(I) distances ranged from 3.13 Å to 3.26 Å and from

https://dx.doi.org/10.1021/acs.chemrev.0c00011
Chem. Rev. 2020, 120, 9675−9742

3.44 Å to 3.51 Å, respectively, and were slightly longer than the sum of the vdW radii of Cu atoms. The Cu_6 cage crystallizes as an infinite chain of hexanuclear entities showing short (<4 Å) interprism Cu−Cu contacts. Interestingly, the introduction of a metal−organic moiety (i.e., ferrocene motif) may pave the way to mediate the intramolecular distance of two M_3N_6 decks by oxidation of the ferrocene units.

Although several coordination prismatic cages with CTUs have been reported, the encapsulation of guest molecules into their cavity has been unsuccessful, because of the short intratrimer M−M distances between the two trimers and small intrinsic cavity. Raptis and co-workers reported a trigonal prismatic Cu(I) and Ag(I) pyrazolato nanocage host with a cavity volume of ∼230 $Å^3$ by elongation of the bridge moiety (from xylylene to naphthalene) between the two pyrazolyl groups.[44,46] From the single crystallography analyses, the average intertrimer M···M distances for Cu_6L_3 and Ag_6L_3 (L = 2,7-bis[(3′,5′-diphenyl-pyrazol-4′-yl)methyl]naphthlene) are 7.581 and 7.651 Å, respectively, while their intratrimer M···M distances are in the respective ranges 3.18−3.28 Å and 3.39−3.53 Å. A guest, *cyclo*-octasulfur (S_8), can be encapsulated within the cavity of the Ag_6L_3 cage host and the crystals of the host−guest adducts could be prepared by diffusion of cyclohexane into $CHCl_3$ solutions containing Ag_6L_3 and S_8 (Figure 54).[46]

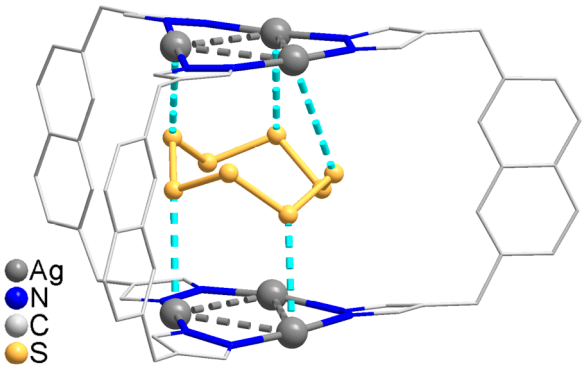

Figure 54. Crystal structure of Ag_6L_3 (L = 2,7-bis[(3′,5′-diphenyl-pyrazol-4′-yl)methyl]naphthlene) cage host encapsulating one S_8 guest within its cavity. [All H atoms and phenyl groups have been omitted from the figure for the sake of clarity.]

Notably, the reaction of $Ag_3(3,5\text{-}Ph_2Pz)_3$ with S_8 under similar conditions resulted in black Ag_2S. Thus, they highlighted the role of the confined space of the Ag_6L_3 cage in stabilizing the host−guest complex.

Inspired by this strategy, Yang's group designed a trigonal prismatic copper(I)-bis-pyrazolato cage from the self-assembly of 2,5-bis(4′-methylene-1*H*-3′,5′-diphenylpyrazole)thiophene and $Cu(OAc)_2$ under hydrothermal conditions.[48] During the synthesis, one THF guest molecule was accommodated within the cavity of the prismatic cage. In 2019, Li's group constructed a very similar trigonal prismatic Cu_6L_3 (L = 2,5-bis(4′-methylene-3′,5′-dimethylpyrazolate)thiophene) coordination cage.[50] Interestingly, this Cu_6L_3 cage can act as a host to encapsulate one toluene molecule, resulting in the guest-induced luminescence-thermochromic phenomenon. Because of the poor solubility of this cage, the encapsulation of other guests failed. To overcome this problem, an isostructural coordination prismatic cage was prepared by replacing the Me group on the pyrazolate ligand with an Et group.[52] This Et-modified cage host can accommodate a series of benzene derivates with π-acidity (e.g., nitrobenzene) or basicity (e.g., *o*-, *m*-, and *p*-xylene) within a wide range, because of the confined cavity and the moderate π-acidity of the Cu_3Pz_3 units among Au(I)/Ag(I)/Cu(I) CTUs.

Apart from the construction of single prism and antiprism cages with CTUs, Li's group have developed an interesting approach to connect two trigonal prismatic Cu_6L_3 cages with a Cu_2I_2 linker (Figure 55).[47] Because of its well-defined C_3

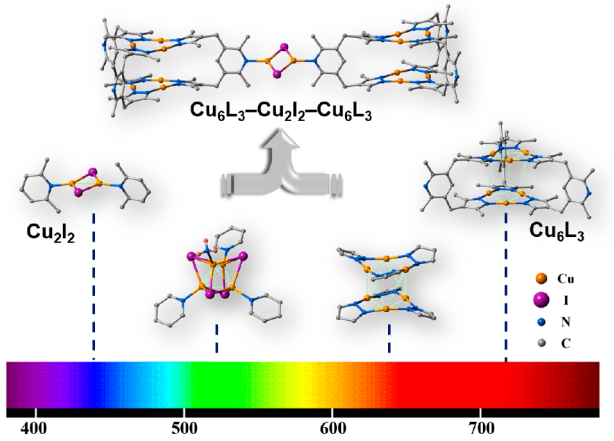

Figure 55. Emission color profiles of four copper(I) cluster-based phosphors, Cu_2I_2, Cu_4I_4, $[Cu_3Pz_3]_2$, and Cu_6Pz_6 (from left to right) in the visual spectrum, and the binary compound (upper) uniting the Cu_2I_2 and Cu_6Pz_6 clusters. [All H atoms have been omitted from the figure for the sake of clarity. Reprinted with permission from ref 47. Copyright 2014, Royal Society of Chemistry, London.]

symmetry, they envisioned that the crystalline Cu_6L_3 cage can be used as a building block to construct Cu_2I_2 clusters by introducing a pyridine group between the two pyrazolyl groups. Indeed, the tetradecanuclear copper(I) cluster compound Cu_6L_3−Cu_2I_2−Cu_6L_3 (L = 3′,5′-bis((3,5-dimethyl-pyrazol-4′-yl)methyl)-2,6-dimethyl-pyridine), synthesized through a step-wise reaction, exhibited well-resolved blue/red dual emissions and two-way luminescent thermochromism.

4.3.2. High-Symmetry Polyhedron. There are still experimental challenges in synthesizing high-symmetry polyhedrons utilizing CTUs as building blocks. Such difficulties arise because M(I) pyrazolate complexes often form complex impure mixtures of several oligomers in solution or intermediately precipitate unknown products. In 2010, Lu and co-workers reported the synthesis of a Ag(I) CTU-based adamantane-like cage, which contains an adamantane-like nanocage with the molecular formula $Ag_{24}(Trz)_{18}$, with intratrimer Ag−Ag distances of 3.58 Å (Figure 56).[42] Interestingly, each octahedral nanocage is catenated by six others through all its six of the vertices to form sextuple polycatenation, resulting in an unprecedented 3D extended polycatenated polyhedral architecture.

Volkmer's group reported the only example of an octahedron $Cu_{12}L_6$ (L = 4,4-(1,2-phenylene)bis(3,5-dimethylpyrazol-1-ide)) supramolecular cage (Figure 57).[45] This cage crystallized in the space group $I4_1/amd$ and six pyrazolate ligands and four triangular tricopper units form a coordination cage of tetragonal bipyramidal shape. The Cu ions are bridged by three pyrazolate rings forming almost planar metallacyclic triangles, and within each CTU the Cu(I) ions are almost linearly coordinated. In addition, the intratrimer Cu−Cu distances are 3.1499(4) and 3.2728(8) Å, and intermolecular Cu−Cu interactions between two neighboring metallamacrocycles are equal at 3.103(5) Å.

https://dx.doi.org/10.1021/acs.chemrev.0c00011
Chem. Rev. 2020, 120, 9675−9742

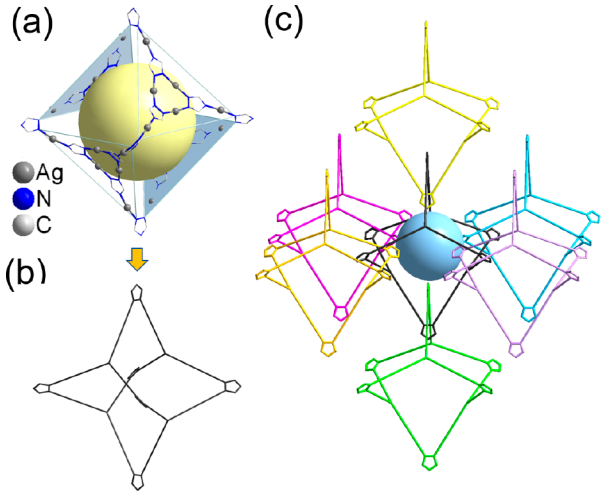

Figure 56. Schematic representation of the overall structure of the polycatenanes from a discrete $[Ag_{24}(Trz)_{18}]^{6+}$ nanocage to sextuple polycatenation. (a) Discrete $[Ag_{24}(Trz)_{18}]^{6+}$ nanocage [all H atoms have been omitted from the figure for the sake of clarity]; (b) simplified structure of the $[Ag_{24}(Trz)_{18}]^{6+}$ nanocage; and (c) view of a $[Ag_{24}(Trz)_{18}]^{6+}$ nanocage (black) catenated by six others through its vertices.

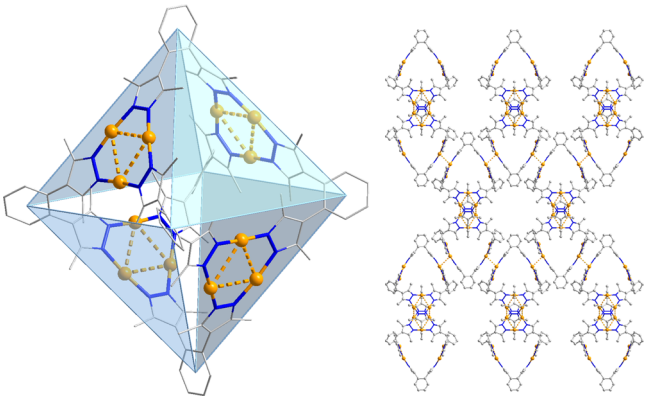

Figure 57. (left) The (pseudo)octahedral structure of $[Cu_{12}L_6]$ cage, and (right) crystal packing of $[Cu_{12}L_6]$ cage along the *b*-axis showing the porosity. [All H atoms and solvent molecules are omitted from the figure for sake of clarity.]

There are two different types of micropores in the crystal structure, resulting in a surface area of 680 $m^2\ g^{-1}$ (Brunauer–Emmett–Teller (BET) analysis).

4.4. Coordination Polymers with CTUs

When semirigid bis-pyrazole ligands were employed, a discrete cage with CTUs could be obtained as mentioned above, revealing that the rational design of pyrazole ligands is important for preparing supramolecular coordination compounds. In this section, a series of coordination polymers containing CTUs have been reported so far, which will now be divided into three separately discussed categories (i.e., 1D, 2D, and 3D coordination polymers.

4.4.1. One-Dimensional Structures. One-dimensional coordination polymers with coinage metal CTUs were synthesized by introducing a second coordination moiety into the pyrazole ligand.[57,68] For instance, in 2011, Li's group introduced a pyridyl group in the 3-position of the pyrazole ring to include an additional coordination site. Two isomeric 1D coordination polymers (denoted as **1D-1** and **1D-2** herein) were obtained from the reaction of CuI and the ligand 3-(4-pyridyl)-5-isobutyl-1*H*-pyrazole under solvothermal conditions.[58] Both **1D-1** and **1D-2** contained Cu_3Pz_3-type CTUs and Cu_3I_3 units connected via $Cu–N_{pyridyl}$ bonds. The Cu_3Pz_3-type CTUs in both compounds slightly deviated from the planar arrangement. In compound **1D-1**, two adjacent 1D chains were linked to each other through an intertrimer Cu–Cu interaction with a distance of 2.99 Å. On the other hand, no perpendicular intertrimer Cu–Cu interactions were found in **1D-2**, because of the distortion of the CTUs, which prevented its planarity and occupied one Cu site (Figure 58). The structure differences gave rise to their distinct phosphorescence properties with bright yellow and orange emissions, respectively.

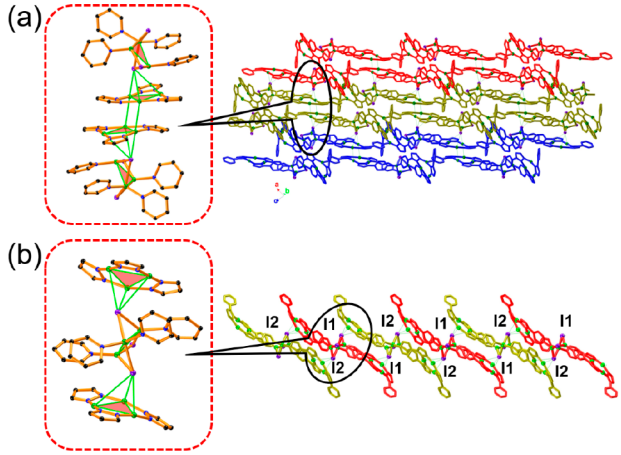

Figure 58. Partial views of the structures of (a) **1D-1** and (b) **1D-2**, showing the distinction intertrimer Cu–Cu interaction.

4.4.2. Two-Dimensional Structures. A 2D coordination polymer **2D-1** with Cu_3Pz_3-type CTUs was prepared from the self-assembly of copper(I) iodide and 3-(4′-pyridyl)-5-*p*-tolyl-pyrazolate ligand under solvothermal conditions.[62] Interestingly, **2D-1** consisted of two classical coordination luminophores, Cu_4I_4 and Cu_3Pz_3, linked and stabilized via coordination bonds and cuprophilic interactions to form an extended 2D lamellar structure. Although the Cu_3Pz_3 CTUs were slightly twisted, intratrimer and intertrimer Cu–Cu distances lay within the normal ranges (3.2104(6)–3.6459(7) Å). Because of the incorporation of two Cu(I) cluster-based luminophores, this 2D coordination polymer exhibits tunable thermochromic photoluminescence due to the dual emissions from both luminophores. This model compound was further used to develop a *Chemopalette* strategy. This strategy allowed the regulation of the photoluminescence properties of these 2D coordination polymers by adjusting the supramolecular microenvironments as a result of the fine-tuning of intermolecular Cu–Cu distances between two neighboring layers (Figure 59).[62] Yang's group have also reported 2D coordination polymers containing Cu(I) CTUs via a reaction between 1,4-bis((3,5-diphenyl-1*H*-pyrazol-4-yl)methyl)benzene and $CuCl_2$ under hydrothermal conditions. However, only the X-ray structures were reported and no photoluminescence properties were investigated.[64]

4.4.3. Three-Dimensional Structures. Although the introduction of secondary coordination motifs into the 3- or 5-position of pyrazole ring has led to the successful construction of 1D and 2D supramolecular networks with CTUs, high-porosity 3D CTU-based MOFs still remain unexplored. In their pioneering work Yin, Li, and co-workers designed a new method

https://dx.doi.org/10.1021/acs.chemrev.0c00011
Chem. Rev. 2020, 120, 9675–9742

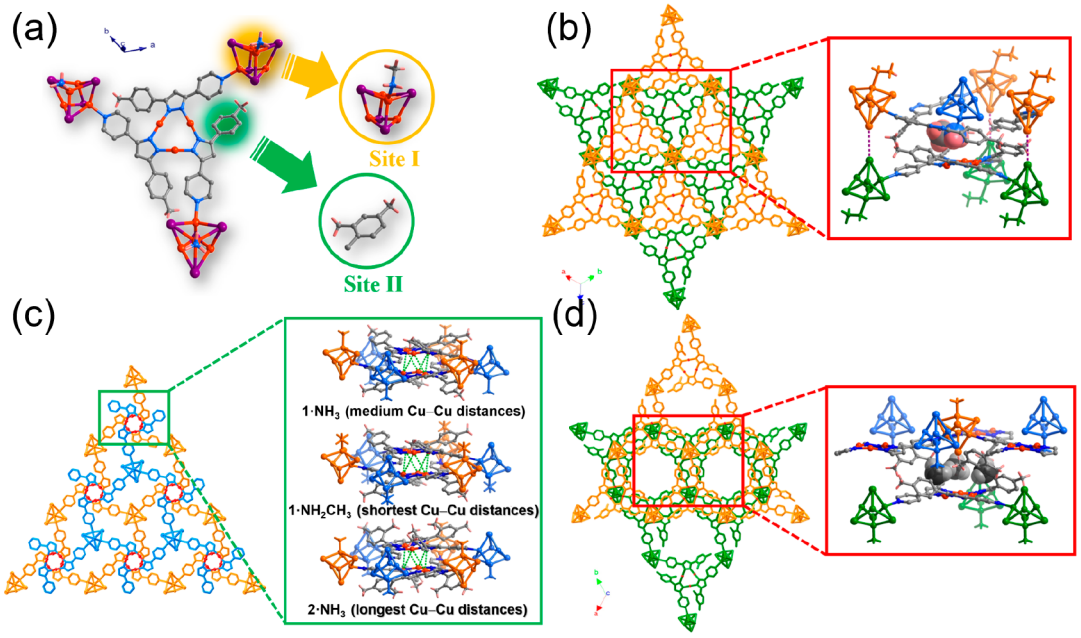

Figure 59. (a) Schematic representation of the *chemopalette* strategy in the supramolecular system of **2D-1·NH$_3$**; (b-d) the supramolecular microenvironments of Cu_3Pz_3 and Cu_4I_4 coordination luminophores. Reprinted with permission from ref 62. Copyright 2013, John Wiley & Sons.

to construct CTU-based MOFs with an extended bipyrazole ligand by introducing a secondary pyrazole motif into the 4-position of the pyrazole ring.[53] The self-assembly of 3,3′,5,5′-tetramethyl-4,4′-bipyrazole and $Cu(NO_3)_2$ afforded a Cu(I) CTU-based MOF in the binodal topology $(6^2{\cdot}10)(6{\cdot}10^2)$ (**nof**) with a large pore size of 35 Å, which exhibited an 8-fold interpenetrated net structure. In 2007 and 2008, Kitagawa's group reported a series of CTU-based porous coordination polymers utilizing the same bipyrazole ligand.[54,55] For instance, a 3D Ag(I) CTU-based MOF was obtained as colorless polyhedral crystals from the reaction of Ag(I) salt and bipyrazole ligand. The structure has a highly distorted (10,3)—a (**srs**) topology with the Ag_3Pz_3 units behaving as three-connected nodes and the C−C single bonds as linkers—while the adjacent Ag_3Pz_3 units staggered in an unusual fashion by triple argentophilic interactions with intertrimer Ag−Ag distances of 3.319 Å (Figure 60). The N_2 adsorption isotherm analysis indicated a BET surface area of 240 $m^2\ g^{-1}$, and inclusion of guest molecules (e.g., benzene and toluene) was achieved in a single-crystal-to-single-crystal fashion.

In 2014, Li's group prepared an exceptionally stable and water-resistant Cu(I) CTU-based MOF by slightly modifying the bis-pyrazole ligand (replacement of methyl with an ethyl group).[63] This MOF, containing Cu_3Pz_3 and Cu_4Pz_4 motifs with a high BET surface area of 576 $m^2{\cdot}g^{-1}$, is capable of efficient removal of trace organic wastes (e.g., benzene, toluene, xylene, and mixtures thereof) from contaminated water. It also allows the first nonhysteretic MOF-based heterogeneous lyophobic system as a molecular spring with exceptional properties, including mechanical and thermal energetic characteristics and stability.[214] Moreover, its highly ordered cylindrical pores prevent nanotriboelectrification during reversible water intrusion into the nanopores.[215] Such topology prevents double layer separation during the intrusion−extrusion process, eliminating electrification and, hence, maximizing the mechanical and thermal energy storage performance. Finally, the combination of exceptional stability and high framework flexibility allowed the development of a smart pressure-transmitting fluid capable of dissipating undesirable high-frequency vibrations. In view of their promising performance, CTU-based MOFs may provide more suitable avenues for practical environment and energy applications.

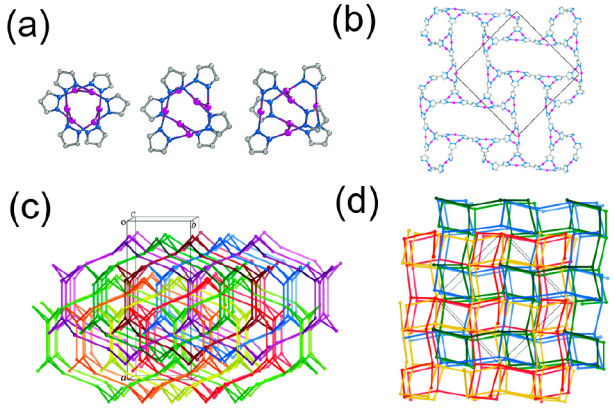

Figure 60. (a) Three different dimer conformations of Ag_3Pz_3 SBUs, and (b) a single coordination network in Ag(I) MOF with 4-fold interpenetrated **srs** topology, methyl groups are omitted for clarity. [Color code: magenta, Ag; blue, N; gray, C.] (c) 8-fold interpenetrated **nof** and (d) 4-fold interpenetrated **srs** topologies for Ag(I)/Cu(I) CTU-based MOFs. [Reprinted with permission from ref 55. Copyright 2008, American Chemical Society, Washington, DC.]

Apart from the bis-pyrazole ligand, some other ligands have also been synthesized and used for constructing 3D CTU-based MOFs. For example, the incorporation of a carboxyl functional group into the pyrazole ligand can be used to prepare new types of 3D CTU-based MOFs.[61,67] In 2013, Wei et al. reported the synthesis of a Cu CTU-based MOF, PCN-91, from the reaction of 4-(3′,5′-dimethyl-1*H*-pyrazol-4′-yl)-benzoic acid and $Cu(NO_3)_2$ under solvothermal conditions.[61] In the crystals, the intratrimer Cu−Cu distance (3.185 Å) approaches those of Cu CTUs, and the Cu CTUs are linked by Cu_2 paddlewheel SBUs, leading to a porous 3D framework with a high BET surface area of 644 $m^2\ g^{-1}$.

https://dx.doi.org/10.1021/acs.chemrev.0c00011
Chem. Rev. 2020, 120, 9675−9742

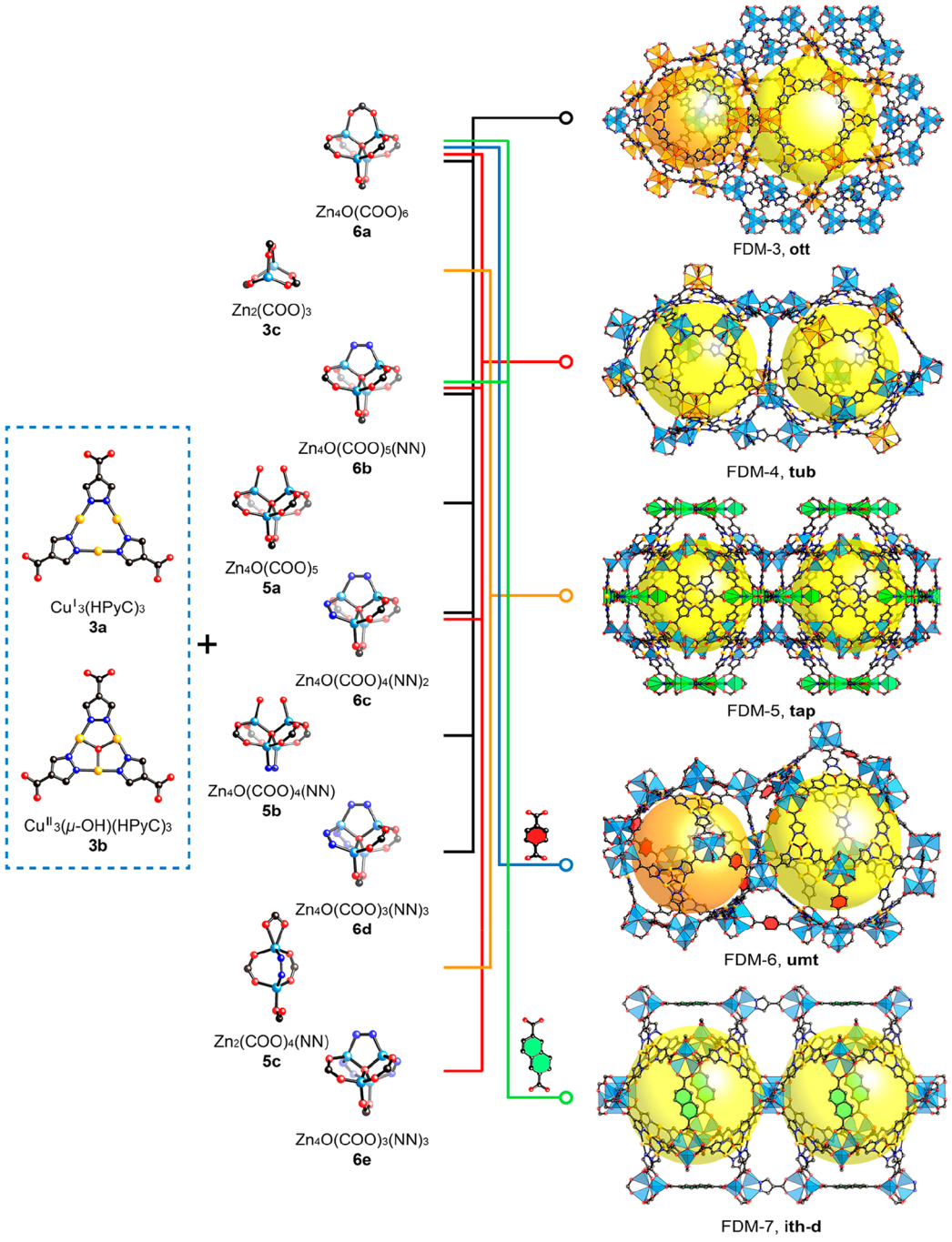

Figure 61. Reticular chemistry of Cu(I) CTU-based MOFs (FDM-3−7). [Reprinted with permission from ref 67. Copyright 2017, American Chemical Society, Washington, DC.]

In 2017, Tu et al. further developed the reticular chemistry of Cu(I) CTU-based MOFs, and five reversible redox active mesoporous MOFs with BET surface areas in the range of 1067−3393 m^2 g^{-1} were constructed (FDM-3−FDM-7; see Figure 61).[67] They confirmed the catalytic performance of these redox-active MOFs by the oxidation of CO and aromatic alcohols and the decomposition of H_2O_2. Moreover, the incorporation of a pyridyl functional group into the pyrazole ligand could be used to construct 3D CTU-based MOFs. For instance, Zhang et al. and Kivi et al. have synthesized a Cu_3Pz_3-type CTU-based MOF via the reaction of 4-(pyrid-4′-yl)-3,5-dimethylpyrazole and CuBr under solvothermal conditions.[56,65] The crystal structure of this MOF showed a binodal $(6^2{\cdot}10)_2(6{\cdot}10^2)$ topologized network. The large voids in the framework result in 4-fold interpenetration and the intratrimer Cu−Cu distances are 3.249 and 3.128 Å.

5. LUMINESCENCE PROPERTIES

Photoluminescence is one of the most important and intriguing properties in closed-shell coinage-metal-based systems and bridges ground and excited states, which could provide detailed comprehension of the excited-state properties. In principle, photoluminescence of a closed-shell system includes (i) fluorescence from a singlet excited state and (ii) phosphorescence from a triplet excited state, and generally follows Kasha's rule.[216] Because of the heavy-atom effect and perturbation from

https://dx.doi.org/10.1021/acs.chemrev.0c00011
Chem. Rev. 2020, 120, 9675−9742

spin−orbit coupling (SOC), radiative transitions from triplet excited states are not strictly forbidden and are sometimes favorable in CTCs, as reflected by some cases of high QYs. Based on the origins and insights of emissive excited states, this section is divided into two main parts, namely, photophysical progresses in typical luminescence and luminescence chromism behaviors discovered in CTCs and CTU-based materials to date.

5.1. Photophysical Processes of Luminescence

5.1.1. Metal-to-Metal Charge Transfer (MMCT)-Based Phosphorescence. Cyclic trinuclear Au(I) and Cu(I) pyrazolate complexes often exhibit bright phosphorescence at rt, while their Ag(I) analogues may display bright phosphorescence at low temperatures but are often nonemissive at rt. Pioneering work performed by Omary,[21−25] Dias,[22,23] Cundari,[23,25] Li,[53] Raptis,[98] and Zhang[99] between 2003 and 2007 has manifested and emphasized the underlying roles of excited-state intratrimer/intertrimer metal−metal bonding in the phosphorescence of Au(I)/Ag(I)/Cu(I) CTCs. Their studies revealed that the phosphorescence of pyrazolate-based Au(I)/Ag(I)/Cu(I) CTCs arose from the intertrimer metal−metal bonding triplet states, especially for those without aromatic substituents. In most cases, the MMCT- and ligand-to-metal−metal charge transfer (LMMCT)-based phosphorescence of Au(I)/Ag(I)/Cu(I) CTCs is considered to stem from the intertrimer metal−metal bonding excited dimers or excimers.

Nonaryl-substituted Cu_3Pz_3 complexes usually exhibit bright phosphorescence at rt, featuring LE emissions (yellow-to-red color), large Stokes shifts, and emission decay times ranging from 15 μs to 50 μs. Dias, Omary, and co-workers reported a series of representative cases in 2005, including $Cu_3(3\text{-}CF_3Pz)_3$, $Cu_3(3,5\text{-}Me_2Pz)_3$, $Cu_3(3\text{-}Me\text{-}5\text{-}CF_3Pz)_3$, $Cu_3[3,5\text{-}(CF_3)_2Pz]_3$, and $Cu_3[3,5\text{-}(i\text{-}Pr)_2Pz]_3$ (Figure 62).[22] The detailed photoluminescence properties at both rt and cryogenic temperature have been well-determined. All five Cu_3Pz_3 complexes show unstructured broad bands at rt and their emission maxima range from 634 nm for $Cu_3(3\text{-}Me\text{-}5\text{-}CF_3Pz)_3$ to 662 nm for $Cu_3[3,5\text{-}(i\text{-}Pr)_2Pz]_3$. In addition, their emission lifetimes and Stokes shifts range from 28 μs for $Cu_3[3,5\text{-}(i\text{-}Pr)_2Pz]_3$ to 53 μs for $Cu_3[3,5\text{-}(CF_3)_2Pz]_3$ and from 16 000 cm^{-1} for $Cu_3(3\text{-}Me\text{-}5\text{-}CF_3Pz)_3$ to 17 700 cm^{-1} for $Cu_3(3,5\text{-}Me_2Pz)_3$, respectively. Lowering the temperature to 77 K reduces their nonradiative transitions and slightly prolongs their emission decay times.

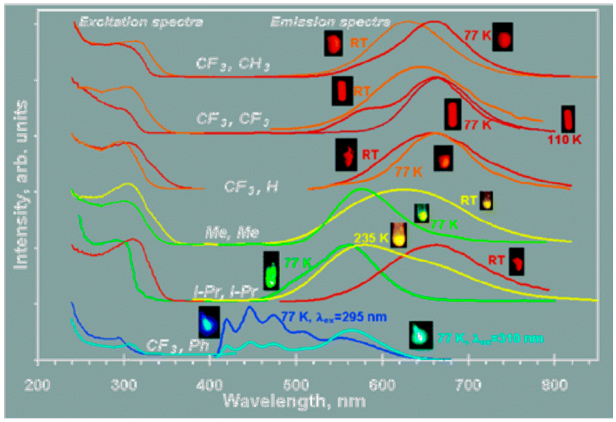

Figure 62. Room- and cryogenic-temperature excitation and emission spectra of $Cu_3(3\text{-}R_1\text{-}5\text{-}R_2\text{-}Pz)_3$ in ref 22 of corresponding R_1 and R_2 denoted above the curves. [Reprinted with permission from ref 22. Copyright 2005, American Chemical Society, Washington, DC.]

Thus, $Cu_3(3,5\text{-}Me_2Pz)_3$ exhibits the longest lifetime (69 μs) at 77 K among all the reported crystalline nonaryl-substituted Cu_3Pz_3 complexes reported to date. Furthermore, cooling of these Cu_3Pz_3 complexes could induce the remarkable luminescence thermochromism related to the multiple intertrimer Cu−Cu bonding emissive states, which is described in detail in section 5.2.1.

The relationship of ground-state intertrimer Cu−Cu distances and Cu−Cu bonding phosphorescence has been debatable when discussing the formation of intertrimer Cu−Cu excimers in Cu_3Pz_3. It is absolutely clear that Cu−Cu separation approaching the sum of the vdW radii benefits MMCT, while the phosphorescence of $Cu_3[4\text{-}(4'\text{-}Br\text{-}Ph)\text{-}3,5\text{-}Me_2Pz]_3$, with the shortest recorded intertrimer Cu−Cu distance (2.817 Å) to date, originates from ligand-centered (LC) emission accompanied with metal-to-ligand charge transfer (MLCT).[94] On the other hand, although intertrimer Cu−Cu separations exceed 3.80 Å, $Cu_3[3,5\text{-}(CF_3)_2Pz]_3$ still features ^{3}MMCT phosphorescence. In this case, by comparing its excitation profile in the crystalline state with the UV-vis absorption spectrum in solution, Dias, Omary, Cundari, Coppens, and co-workers claimed that effective excitation for triggering the bright phosphorescence of $Cu_3[3,5\text{-}(CF_3)_2Pz]_3$ corresponded to the singlet−triplet spin-forbidden transition of its monomer-of-trimer, followed by excimer formation and subsequently, Cu−Cu bonding phosphorescence.[23,24] This result further emphasized the essence of excited-state intertrimer Cu−Cu distances/bonding, rather than the ground-state intertrimer distances. Recently, Li's group proposed another approach to estimate the upper threshold of excimer formation and developed a new strategy to confine the unfavorable face-to-face stacking between CTUs by using the semirigid bis-pyrazolate bridging ligands *m*-xylylene-bis(3,5-dimethyl)pyrazol-4-yl (Figure 63).[44] In this case, the restricted intertrimer Cu−Cu distances do not fall below 3.696 Å. Moreover, because of the metal−metal bound emissive states, the excimeric phosphorescence is expected to be LE (716 nm) and long-lived (18.84 ± 0.04 at rt to 24.66 ± 0.03 μs at 10 K). These results push the upper threshold of the excimeric Cu−Cu bonding distance to ~4.0 Å for ground-state structures. These examples highlight the strong tendency of excited-state metal−metal bonding and excimer formation of

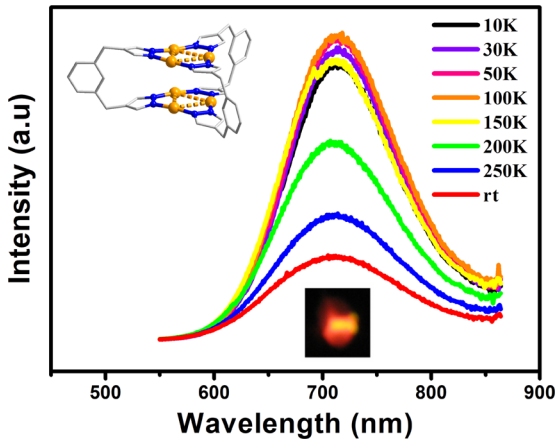

Figure 63. Simplified structure of hexanuclear Cu(I) coordination prism, along with the temperature-dependent emission spectra. The inserted picture below the emission spectra showed the bright intense red phosphorescence of the crystalline sample. Data are taken from ref 44.

https://dx.doi.org/10.1021/acs.chemrev.0c00011
Chem. Rev. 2020, 120, 9675−9742

the Cu_3Pz_3 monomer, attributed to its lowest-lying ^{3}LMMCT state and planar molecular conformation.

Apart from Cu_3Pz_3, Au(I) and Ag(I) analogues could also exhibit bright metal−metal bonding phosphorescence (Figure 64),[23] and the phosphorescence of Au_3Pz_3 and Ag_3Pz_3 also

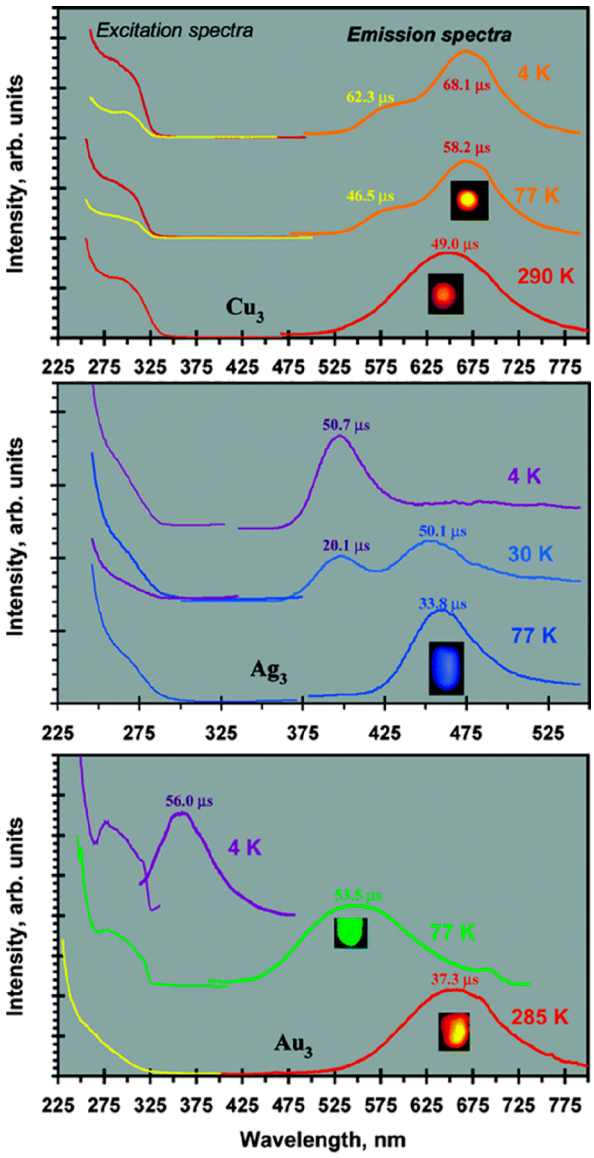

Figure 64. Photoluminescence spectra of $M_3[3,5\text{-}(CF_3)_2Pz]_3$ (M = Cu(I), Ag(I), and Au(I)) versus temperature in the crystalline state. Lifetimes are noted for each band with errors of <5%. Photographs are shown for colorless crystals packed in Suprasil quartz tubes while being exposed to UV light at room temperature or immediately after removal from a liquid-nitrogen bath (77 K). [Reprinted, with permission, from ref 23. Copyright 2005, American Chemical Society, Washington, DC.]

originated from the intertrimer metal−metal bonding emissive, rather than intratrimer, states. In addition, similar to Cu_3Pz_3, Au_3Pz_3 also shows a strong tendency toward excimer formation from the monomer. Omary's group presented a comprehensive investigation of fluorinated M_3Pz_3 (M = Cu(I)/Ag(I)/Au(I)) by combining X-ray crystallographic analysis, UV-vis absorption, excitation and emission spectra, and theoretical calculations.[23] Notably, $Ag_3[3,5\text{-}(CF_3)_2Pz]_3$ only emits the MMCT-based phosphorescence at ∼470 nm under cryogenic temperatures, while the two Cu(I) and Au(I) analogues exhibit bright LE phosphorescence, of MMCT origin, at ∼650 nm under rt (Figure 64). Yang et al.[98] and Ovejero et al.[217] considered that an Au−Au distance of >3.6 Å was too long to produce Au−Au bonding phosphorescence. However, Omary and co-workers have found that, similar to $Cu_3[3,5\text{-}(CF_3)_2Pz]_3$, the Au(I) analogue still displayed bright orange phosphorescence, even though its intertrimer Au−Au distance (3.8853(3) Å) is significantly longer than the sum of the vdW radii of Au (3.32 Å).[23] Furthermore, the intertrimer Ag−Ag distance (3.2037(4) Å) is much shorter than the sum of vdW radii of Ag (3.44 Å), indicating that the ground-state intertrimer Ag−Ag interactions are considerably stronger than those of its Au(I) and Cu(I) analogues. These three $M_3[3,5\text{-}(CF_3)_2Pz]_3$ complexes show a decrease in emission decay times in the order Cu > Ag > Au, at the same temperature, influenced by the strengths of the heavy-atom effects.

Despite $Cu_3[3,5\text{-}(CF_3)_2Pz]_3$ and its Au analogue having long intertrimer M(I)−M(I) distances at rt, their bright phosphorescence still suggests that the intertrimer M(I)−M(I) distances might not be solely responsible for the nonemissive nature of aryl-substituted M_3Pz_3 complexes. For example, although $Au_3(3\text{-Me-}5\text{-PhPz})_3$ exhibits intertrimer Au(I)−Au(I) distances of ∼3.70 Å, which are shorter than those observed in $Au_3[3,5\text{-}(CF_3)_2Pz]_3$ (3.8853(3) Å), it is nonemissive at rt.[98] This is because excimer formation is prevented by the bulky Ph substituents. In this case, the steric effect of the substituents is more significant than the intertrimer Au(I)−Au(I) contacts. The intertrimer metal−metal bonding emissive state also triggers the bright phosphorescence of $Ag_3[3,5\text{-}(CF_3)_2Pz]_3$, although it only shows emission at low temperatures.[23]

In addition to studies of pyrazolate CTCs, extensive investigations on CTCs have suggested that excited-state intertrimer metal−metal bonding is necessary for triggering the metal-centered phosphorescence of CTCs with other ligands. As a representative case of Au_3Im_3, $Au_3(1\text{-EtIm})_3$, reported by Omary's group in 2017, exhibits the shortest intertrimer Au−Au distances within a dimer (3.0662(3) Å) documented to date and bright solid-state phosphorescence centered at 700 nm at rt.[90] Such photoluminescence cannot be detected in its dilute solution or polymer matrix, at either ambient or cryogenic temperatures, because of the absence of intertrimer metal−metal bonding. As the only known Au_3Trz_3, $Au_3[3,5\text{-}(i\text{-Pr})_2Trz]_3$, reported by Coppens, Omary, and co-workers in 2006, shows bright room-temperature phosphorescence centered at 750 nm in both its crystals and concentrated CH_2Cl_2 solution, which disappears in its diluted solution or upon the addition of acids.[100] Detailed discussions on the temperature-dependent and/or pH-responsive emission behaviors of $Au_3(1\text{-EtIm})_3$ and $Au_3[3,5\text{-}(i\text{-Pr})_2Trz]_3$ are presented in the subsequent sections. These two reports provide an alternative scenario to confirm the MMCT-based phosphorescence by determining its existence in the crystalline phase, concentrated solutions, and dilute solutions.

As mentioned above, a short intertrimer M(I)−M(I) distance is required to trigger the intertrimer metal−metal bonding excimeric phosphorescence, even though the ground-state intertrimer M(I)−M(I) distance could be considerably longer than the sum of the vdW radii of the metals. In addition, the emission energies are expected to be modulated by altering the intertrimer M(I)−M(I) distances. For alkyl-substituted Au_3Cb_3, Cundari, Gnade, Omary, and co-workers conducted DFT calculations.[34] They attributed the different emission profiles

https://dx.doi.org/10.1021/acs.chemrev.0c00011
Chem. Rev. 2020, 120, 9675−9742

to the varied intertrimer aurophilic interactions and assigned them as MMCT-based phosphorescence, supported by the metal-centered FMOs.[34] The respective shortest intertrimer Au−Au separations in $Au_3[(n\text{-Bu})N{=}COMe]_3$ and $Au_3[(c\text{-Pen})N{=}COMe]_3$ are 3.517 and 3.466 Å, with the only phosphorescence peaks for these two Au_3Cb_3 complexes being centered at 686 and 679 nm with respective Stokes shifts of 17 681 and 16 918 cm^{-1}. This correlation of the M(I)−M(I) distance and emission energy could also be found in $Cu_3(4\text{-ClPz})_3$, supported by experimental and theoretical evidence in different polymorphs (vide supra).[36]

Apart from homometallic CTCs, their heterometallic analogues exhibit greater tendencies to metal-centered phosphorescence. A recent report from Galassi et al. reveals the high quantum efficient MMCT emission from an Au−Cu bonded mixed-ligand CTC.[20] A short intertrimer Au−Cu distance of 2.8750(8) Å in $Au_4Cu_2(1\text{-EtIm})_4[3,5\text{-}(CF_3)_2Pz]_2$ proves the presence of ground-state Au−Cu polar covalent bonds. The effective symmetry in the dimer-of-trimer is lowered from D_{3h} (homometallic) to C_{2v} (heterometallic), leading to enhancement of the transition dipole moment and extinction coefficients. Steady-state room-temperature photoluminescence spectra reveal a maximum emission peak of ∼510 nm, with a near-unity quantum efficiency of 90.31% ± 0.70%.

Another representative series of heterometallic complexes in the CTC family that shows MMCT phosphorescence is the sandwich-like Au_3−M−Au_3 (M = Ag(I), Tl(I)) cluster, presented by Burini and Fackler,[154,155] Fujita,[156,157] Li,[153] and Ruiz.[113] Because of the π-basicity of Au(I) CTCs with electron-donating groups, metal cations that behave as Lewis acids are spontaneously sandwiched by two Au(I) CTCs. Remarkable luminescence color changes during the formation of such sandwich-like heterometallic clusters have been well-documented.[153] The greatest advantage of this sandwich-like Au_3−M−Au_3 cluster phosphorescence is that the emission center is highly localized in the heptanuclear metal core and fully protected by the peripheral ligands. This advantage allows bright phosphorescence not to be affected by ambient environment, such as the solvent, oxygen, and/or molecular collisions. Because of the heptanuclear metal phosphorescent centers, the emission of solid-state Au(I) CTCs could be turned on by forming the sandwich-like mixed Au/Ag cluster. $[Au_3Im_3$−Ag(I)−$Au_3Im_3](BF_4)$ (Im = 1-xylyl-5-MeIm) clusters are strongly white-emissive in the crystalline state, while the crystals of $Au_3(1\text{-xylyl-5-MeIm})_3$ are nonemissive, lacking intertrimer Au−Au bonding.[113]

Although much attention has been paid to the intriguing luminescence behaviors of sandwich-like Au_3−Ag−Au_3 clusters, theoretical insights of their excited states and main photophysical processes remain less explored. The preliminary DFT and TDDFT calculations presented by Li's group elucidated the differences in the electronic structures of the ground and excited states between the parent $Au_3[3\text{-}(2'\text{-thienyl})\text{-5-PhPz}]_3$ and its Au_3−Ag−Au_3 cluster (Figure 65a).[153] For the parent Au_3Pz_3, the ligand π^*-orbitals dominated the LUMOs of both monomer and dimer, over the d-orbitals of the Au atoms (Figure 65a). On the other hand, in the sandwich-like Au_3−Ag−Au_3 cluster, the LUMO was composed of Ag 5s/5p and Au 5d orbitals, without noticeable contributions from the ligands. TDDFT results revealed that the LUMO of the Au_3−Ag−Au_3 cluster was involved in major absorption transitions and, thus, the lowest excited states were highly localized in the heptanuclear metal core and protected by outer-shell ligands. Indeed, these

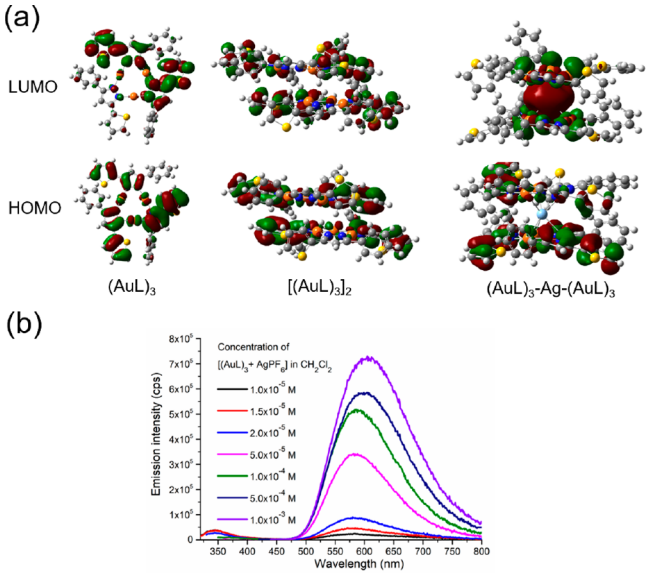

Figure 65. (a) Contours of FMOs (isovalue = 0.02) for the monomer and dimer of Au_3Pz_3 and the cationic $[Au_3Pz_3$−Ag−$Au_3Pz_3]$ cluster (Pz = 3-(2′-thienyl)-5-PhPz). (b) Emission spectra characterizing the dynamic aggregation upon varying concentrations in aerated CH_2Cl_2 solution.

sandwich-like $[Au_3Pz_3$−Ag−$Au_3Pz_3](PF_6)$ clusters show bright yellow phosphorescence (∼600 nm) in both aerated and degassed CH_2Cl_2 solutions (Figure 65b), while the parent Au_3Pz_3 complex is faintly emissive in aerated CH_2Cl_2 solution, although it exhibits bright green phosphorescence in the solid state.[153]

5.1.2. Metal-to-Ligand/Ligand-to-Metal Charge Transfer (ML/LMCT)-Based Phosphorescence. ML/LMCT transitions are commonly observed in four-coordinated square-planar d^8 and tetrahedral d^{10} metal complexes, including Pt(II), Pd(II), Au(III), and Cu(I).[16] For low-coordinate d^{10} complexes and two- and linear-coordinated CTCs, MLCT events are associated with large reorganization energies, which are attributed to excited-state Jahn−Teller distortions in the nd^9 electron configurations, and vibronic coupling through $S_n \rightarrow T_m$ and $T_m \rightarrow S_0$ intersystem crossing (ISC) progresses ($n, m \geq 1$ and are integers). Such an effect will not only decrease the photoluminescence quantum efficiency by energy loss and vibrational relaxation but also increase the nonradiative rate constant, both of which are unfavorable for CTC radiative transitions.

Few CTCs with appropriate ligands show MLCT-dominated luminescence. One representative example is unsubstituted Au_3Py_3, reported by Balch et al. in 2002.[111] The shortest intertrimer Au−Au distance in this Au_3Py_3 complex (3.077(2) Å) is shorter than those observed for Au(I) CTCs, except for $Au_3(1\text{-EtIm})_3$. The only sharp emission peak is located at 490 nm and assigned as MLCT. Theoretical studies have revealed that the major contribution to HOMOs is from the Au 5d orbitals, while the LUMO is mainly located on the Py rings.[218]

$[Hg(o\text{-}C_6F_4)]_3$ is another example, exhibiting emission centered at 440 nm with a shoulder at 530 nm.[219] The photoluminescence of $[Hg(o\text{-}C_6F_4)]_3$ could only be observed in the solid state and was quenched in solution. Compared to the absorption spectra in CH_2Cl_2 solution, the maximum absorption peak shifted bathochromically from 275 nm to 355 nm in the solid state, suggesting the aggregation by intertrimer interactions

https://dx.doi.org/10.1021/acs.chemrev.0c00011
Chem. Rev. 2020, 120, 9675−9742

in the solid state. Theoretical studies were also conducted on the staggered dimer-of-trimer, revealing that LMCT contributed to both the absorption and emission profiles.[220] The intertrimer centroid−centroid distance was shortened from 3.277 Å at the ground state to 3.004 Å at the lowest triplet excited state, as revealed by the optimized dimer-of-trimer structure. Moreover, the lowest unoccupied molecular spinors (LUMS) showed the excited-state metal−metal bonding nature and increased bonding interactions between the stacked dimer.

5.1.3. Ligand-Centered (LC) Photoluminescence. The easy modification of Pz ligands allows the introduction of a series of organic chromophores (usually aromatic groups) to cyclic trinuclear Au(I)/Ag(I)/Cu(I) pyrazolates. Bulky aromatic substituents could produce large steric hindrance between CTC molecules, preventing the formation of intertrimer metal−metal bonding excimers. In addition, the direct linkage between organic chromophores and Pz rings could stabilize the LC excited states below the low-lying metal−metal bonding emissive states of the CTCs, leading to LC photoluminescence. The only problem here is that the lowering of the ligand-based excited state restricts the substituent diversity attached to the pyrazolate ligands and prohibits intriguing metal−metal interactions/bonding from participating into the emissive states. Most LC luminescent behaviors show unsatisfied quantum efficiencies and options of nonaryl-substituents are limited. One possible alternative is to use long and saturated bridging chains to connect the pyrazolates and organic chromophores to avoid electronic coupling between the CTCs and unsaturated systems.

LC fluorescence is commonly observed in M_3Pz_3 complexes with organic chromophores. In 2010, Li, Yang, and co-workers reported the luminescence properties of Cu_3(4-R-3,5-$Me_2Pz)_3$ (Figure 66).[126] When R is a Ph group, only excimeric orange

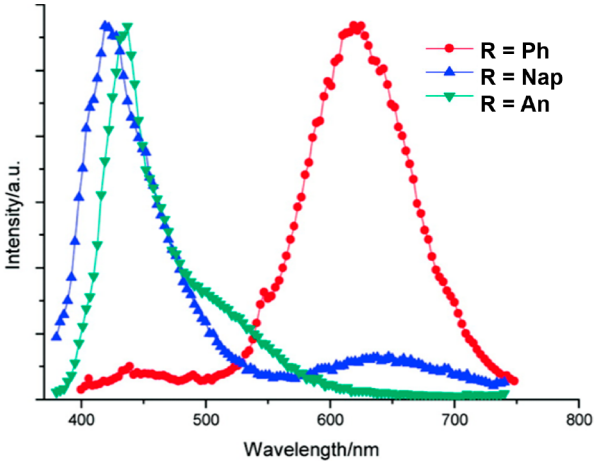

Figure 66. Room-temperature solid-state emission spectra for Cu_3(4-*R*3,5-$Me_2Pz)_3$ (R = Ph, Nap, and An). [Reprinted, with permission, from ref 126. Copyright 2010, American Chemical Society, Washington, DC.]

phosphorescence with an emission decay time of 18.2 μs is observed. If Nap or An groups are attached, the emission peaks centered at ~450 nm with an emission decay time of ~4.0 ns are attributed to LC fluorescence. The changes in luminescence result from the non-negligible steric hindrance from the Nap and An groups, which further prevent effective excimer formation. Even when an external pressure of ≤3.0 GPa is applied, the emission profiles of the Nap- and An-substituted CTCs are still dominated by LC fluorescence bands, despite the shortening intertrimer Cu−Cu distances.

The structure−property (luminescence) relationship of Cu_3[4-(4′-esteryl-Ph)-3,5-$Me_2Pz]_3$, reported by Li's group in 2014, presented a different picture.[221] Much stronger ligand-based fluorescence was observed for this series of crystalline Cu_3Pz_3 complexes with esteryl substituents, compared to the excimeric LE phosphorescence. Technically, *para*-esteryl-Ph groups provide limited steric hindrance in the excimer formation of the chairlike dimer packing of Cu_3Pz_3, because the bulkier groups are spatially away from the metal cores. In fact, the intertrimer Cu−Cu distances (~3.08 Å) of these *para*-esteryl-Ph substituted Cu_3Pz_3 complexes are noticeably shorter than those of Cu_3(4-Ph-3,5-$Me_2Pz)_3$ (~3.58 Å) in the same chairlike dimer conformations.[126] TDDFT calculations at the PBE0 level of theory for the Cu_3[4-(4′-esteryl-Ph)-3,5-$Me_2Pz]_3$ dimer manifest that the low-lying singlet excited states (S_n) are mainly dominated by ligands, while the first intertrimer metal−metal bonding S_n rises to S_{36}, resulting in a slow ISC event (Figure 67).

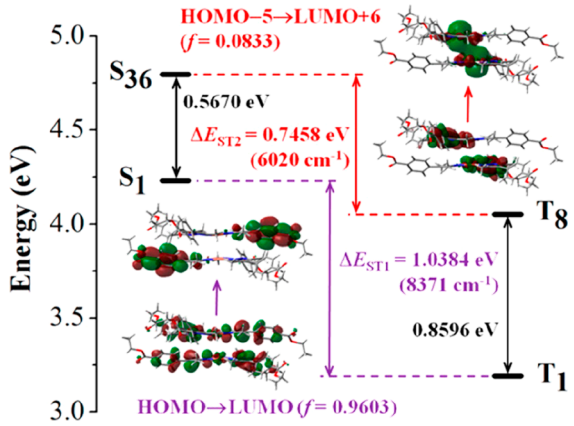

Figure 67. Energy levels and ordering of the singlet and triplet excited states related to the HE (S_1 and T_1) and LE (S_{36} and T_8) bands for the dimer of Cu_3[4-(4′-esteryl-Ph)-3,5-$Me_2Pz]_3$. The inserted molecular orbitals are from the major transitions responsible for the HE (marked in purple) and LE (marked in red) bands, respectively (f = oscillator strength). [Reprinted with permission from ref 221. Copyright 2014, American Chemical Society, Washington, DC.]

As a result, low-energy LE excimeric phosphorescence occurs after the preferred internal conversion rather than ISC between the high-lying metal-centered excited states. This work further emphasized that the electronic features (i.e., π-conjugation) of aromatic groups prevent the formation of metal−metal bonding excimers for Cu_3Pz_3 complexes.

The correlation between the origin of luminescence and conjugation length was not well established until the work by Wolf's group in 2014.[222] A series of Au(I) CTCs comprising thienyl-pyrazolate ligands (Figure 68a) were systematically investigated. By tuning the conjugated numbers of the thienyl groups and orientations of the peripheral ligand moiety, these Au(I) CTCs showed distinct luminescence behaviors. Detailed photoluminescence and computation studies were conducted to reveal assignments of the ligand-based emissions. The monothienyl-substituted complexes of Au_3[4-(2′-thienyl)$Pz]_3$ and Au_3[4-(2′-thienyl)-3,5-$Me_2Pz]_3$ exhibit similar fluorescence profiles as those of their proligands at rt. Fine structured emissions under an excitation of 375 nm are observed upon cooling to 77 K. Excited by 315 nm, these two Au(I) CTCs are

https://dx.doi.org/10.1021/acs.chemrev.0c00011
Chem. Rev. 2020, 120, 9675−9742

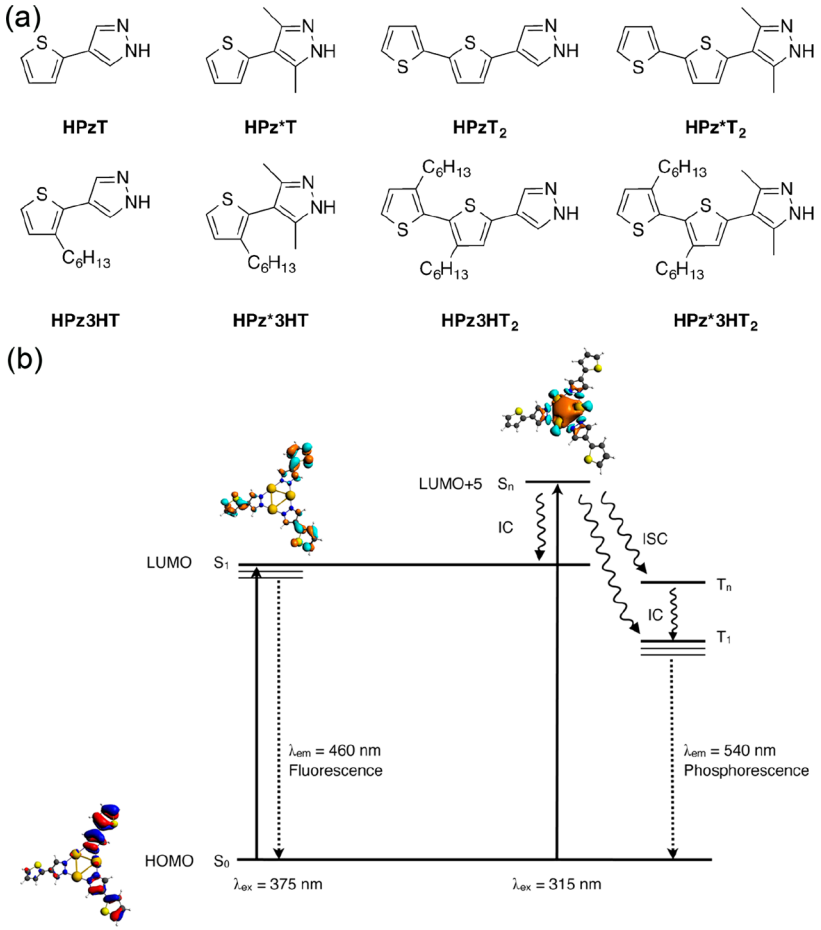

Figure 68. (a) Monothienyl and bithienyl Pz for constructing Au_3Pz_3 in ref 222. (b) Jablonski diagram for Au_3[4-(2′-thienyl)-Pz]$_3$. [Reprinted, with permission, from ref 222. Copyright 2014, American Chemical Society, Washington, DC.]

nonluminescent under ambient temperature but generate broad, weakly structured emission peaks with lifetimes of 2 ms centered at 540 and 520 nm at 77 K, respectively. The large Stokes shift (12 000−13 000 cm^{-1}) and long-lived emission lifetimes suggest metal-sensitized ligand-localized phosphorescence of these Au(I) CTCs, accompanied with average spacing in the range 1400−1500 cm^{-1} for the thienyl and/or pyrazolate groups in the cryogenic emission profiles. However, the bithienyl-substituted complexes of Au_3[4-(5-(3,3′-dihexyl-2,2′-bithienyl))Pz)]$_3$ and Au_3[4-(5-(3,3′-dihexyl-2,2′-bithienyl))-3,5-Me_2Pz)]$_3$ both show LE structured emission bands at cryogenic temperature, but the Stokes shifts for these bands are relatively smaller (∼7000 and 3200 cm^{-1}, respectively) than those of the monothienyl analogues. These results suggest that the ligand-based phosphorescence of bithienyl Au(I) CTCs are directly excited to the lowest-lying ligand-localized excited states.

DFT calculations clearly reveal that the metal-centered unoccupied orbital rose to LUMO+5, while the energy levels of the ligand-localized LUMOs were significantly lower, with respect to the increase in conjugation length (Figure 68b).[222] To construct effective ISC pathways between the singlet and triplet excited states, the involvement of metal-contributing excited states is required for metal complexes. Consequently, it is postulated that ISC occurs between the electronic states involving metal-centered unoccupied orbitals, followed by efficient population of the lowest and ligand-localized phosphorescent state. This leads to observed emission for monothienyl-substituted Au(I) CTCs. Further introduction of unsaturated thienyl groups results in more significant ligand contributions to frontier molecular orbitals and low-lying excited states, and subsequently pushes metal-centered unoccupied orbitals to higher energy levels.

Very recently, Wang, Zang, Li, and co-workers combined the M_3Pz_3 units with a well-known aggregation-induced emission (AIE) luminophore (ligand = 3,5-dimethyl-4-(4-(1,2,2-triphenylvinyl)benzyl)-1*H*-pyrazole) (Figures 69a and 69b).[223] The resulting Cu/Ag/Au CTCs show AIE fluorescent behaviors in solution and noticeably enhanced fluorescent QYs in the solid state, compared to those of the proligands. The intense blue-green emission profiles of these M_3Pz_3 complexes, such as the emission peak centered at 490 nm and nanosecond-scale emissive lifetimes, are highly similar to those of the ligand (Figure 69c). Thus, their emissions are assigned as ligand-based fluorescence. The solid-state room-temperature QYs were determined as 6.92% for Au_3Pz_3, 12.01% for Ag_3Pz_3, and 9.82% for Cu_3Pz_3, which are all higher than those of the proligand (1.59%). The authors attributed the high QYs of these M_3Pz_3 complexes to two factors:

(i) the structural rigidity resulting from the stack between planes can effectively restrict nonradiative decay, and

(ii) the ordered stack of the interlayer can form a stable internal complex architecture.

Nevertheless, much effort has been made to acquire highly emissive CTCs, with limited progress achieved. To ensure

https://dx.doi.org/10.1021/acs.chemrev.0c00011
Chem. Rev. 2020, 120, 9675−9742

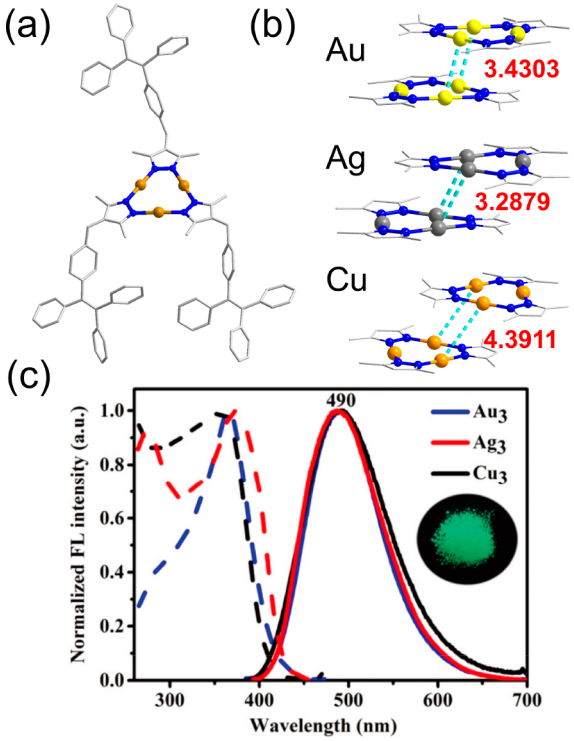

Figure 69. (a) Molecular structure and (b) interlayer stacking structure of this series of M_3Pz_3 (M = Au(I), Ag(I), and Cu(I); Pz = 3,5-dimethyl-4-(4-(1,2,2-triphenylvinyl)benzyl)-pyrazolate). (c) (Dotted line) Excitation and (solid line, excited by 366 nm) fluorescence spectra of (blue) Au_3Pz_3, (red) Ag_3Pz_3, and (black) Cu_3Pz_3 in the solid state at rt. Inset photograph shows the fluorescence image of Ag_3Pz_3 under 365 nm UV light. [Reprinted, with permission, from ref 223. Copyright 2019, Royal Society of Chemistry, London.]

efficient phosphorescence via ISC, a substantial involvement of the metals is required in the related singlet and triplet excited states to promote the SOC effect. Conversely, the aforementioned MLCT for d^{10} metal centers would bring significant excited-state Jahn−Teller distortion and large reorganization energy, especially for low-coordinate species (Scheme 4b).[224−232] Such difficulties in the field of d^{10} metal CTCs could be overcome by MMCT/metal-centered (MC)-based phosphorescence to avoid excited-state Jahn−Teller distortions in the metal−metal bonding triplet states. $Cu_3[3,5\text{-}(CF_3)_2Pz]_3$ is a representative example, with relatively high photoluminescence quantum efficiency with $S_0 \leftrightarrow T_1$ spin-forbidden transitions (Scheme 4a).[23−25] On the other hand, by pushing unfavorable MLCT states into higher energies and enforcing high-lying ISC, LC-dominated excited states are stabilized as efficient emissive states to harvest both higher-energy ^{3}LC emission and lower-energy excimer emission through thermal equilibrium (Scheme 4c). This strategy was proven effective in a recent report by Li and co-workers.[200]

Li created three Cu(I)/Ag(I) pyrazolate CTCs with pyridyl substituents that showed distinct photophysical behaviors (Figure 70a).[200] $Cu_3[3\text{-}(4'\text{-pyridyl})Pz]_3$ (**Cu-4** in ref 200) and $Ag_3[3\text{-}(2'\text{-pyridyl})Pz]_3$ (**Ag-2** in ref 200) exhibit emission maxima located at 650 and 570 nm with long lifetimes (27.9 and 5833.7 μs, respectively) and high QY values (65% and 25%, respectively), under ambient conditions. On the other hand, the copper analogue $Cu_3[3\text{-}(2'\text{-pyridyl})Pz]_3$ (**Cu-2** in ref 200) shows weak emission centered at 655 nm with a relative shorter lifetime of 5.8 μs and significantly lower QY of 1.3% (see Figures

Scheme 4. Proposed Jablonski Diagrams for Cyclic Trinuclear Complexes (a) $Cu_3[3,5\text{-}(CF_3)_2Pz]_3$, (b) Cu-2, and (c) Ag-2 and Cu-4[a]

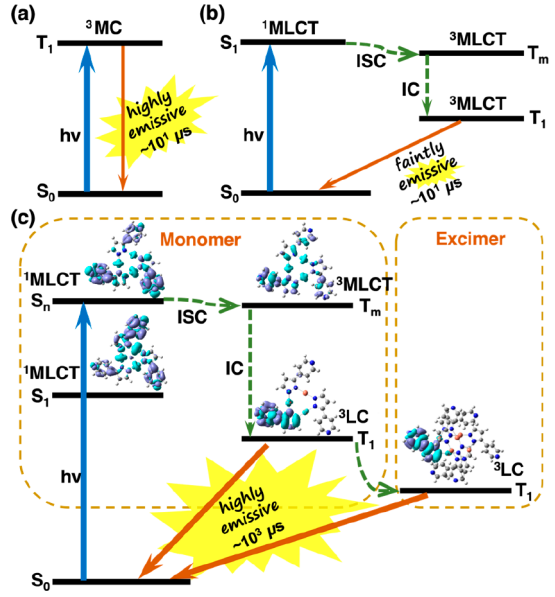

[a]Reprinted, with permission, from ref 200. Copyright 2020, American Chemical Society, Washington, DC.

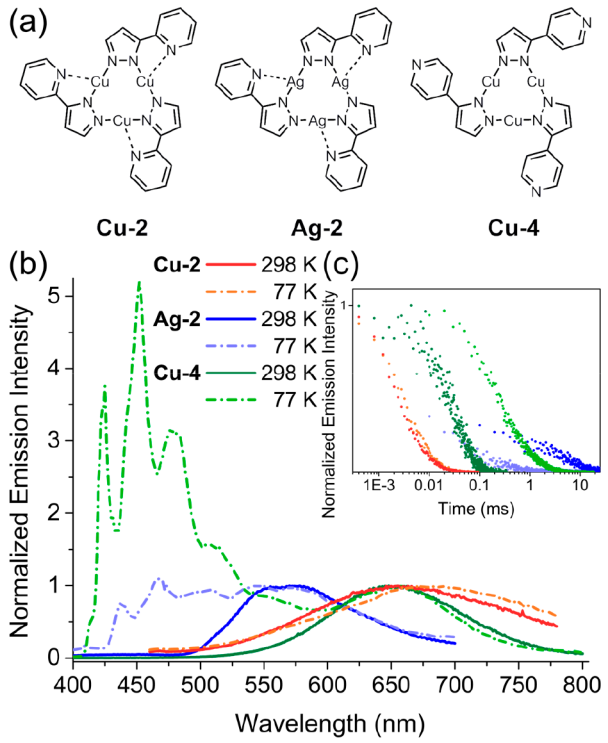

Figure 70. (a) Structures of $Cu_3[3\text{-}(2'\text{-pyridyl})Pz]_3$ (**Cu-2**), $Ag_3[3\text{-}(2'\text{-pyridyl})Pz]_3$ (**Ag-2**), and $Cu_3[3\text{-}(4'\text{-pyridyl})Pz]_3$ (**Cu-4**). (b) Solid-state emission spectra at 298 and 77 K. The emission intensities are normalized, with respect to the low-energy bands. (c) Corresponding decay lifetime semilog profiles of the three complexes at 298 and 77 K. [Reprinted, with permission, from ref 200. Copyright 2020, American Chemistry Society, Washington, DC.]

70b and 70c). Upon cooling to 77 K, the **Cu-4** and **Ag-2** emission spectra exhibit drastically different behaviors and

https://dx.doi.org/10.1021/acs.chemrev.0c00011
Chem. Rev. 2020, 120, 9675−9742

include high-energy structured bands in the range of 420−550 nm. A bathochromic shift (∼30 nm) and vanishingly decreasing emission intensity are observed for **Cu-2**. In view of the metal, ligand, and supramolecular effects, **Cu-2**, with the shortest intertrimer Cu−Cu distance and d−π conjugation through weak Cu−N_{py} coordination, was initially expected to be the best emitter. However, **Cu-4** and **Ag-2** show higher photoluminescence quantum efficiencies. Detailed DFT and TDDFT calculations at different levels of theory were conducted to elucidate the intricate photophysical process. Thus, the hidden high-lying ISC paths are proposed to explain the differences. By comparing the corresponding *f*, adiabatic singlet−triplet energy differences ($\Delta E_{S\text{-}T}$), and SOC matrix element values, the MLCT-based ISC channels S_7, $S_8 \rightarrow T_{17}$, T_{18} for **Ag-2-*m*** (***m*** = theoretical monomer model) and S_6, S_7, and $S_8 \rightarrow T_{22}$, T_{23}, and T_{24} for **Cu-4-*m*** are revealed, while low-lying $S_1 \rightarrow T_4/T_5$ transitions are proposed as the major ISC process for **Cu-2** (Scheme 4b).

5.1.4. Luminescence of π-Acid/π-Base Adducts. The superior π-acidity/basicity of Au(I)/Ag(I)/Cu(I) CTCs endows them with a strong tendency for adducting organic aromatics (arenes), usually resulting in noteworthy alterations in their luminescence behaviors.[5] For emissive π-acid/π-base adducts, the luminescence can be assigned as fluorescence or phosphorescence from the arene monomers or the phosphorescence from exciplexes and CT complexes.

Luminescent organic aromatics usually only exhibit fluorescence at rt but may exhibit ultralong-lived vibronic-structured phosphorescence at cryogenic temperature (e.g., 77 K). After adducting with Au(I)/Ag(I)/Cu(I) CTCs, the phosphorescence of the aromatic monomer could be triggered at rt by the external heavy-atom effect. Such luminescence, termed "metal-sensitized phosphorescence", shows emission profiles similar to the phosphorescence profiles of the corresponding free organic arenes under cryogenic temperature, but with much shorter emission decay times. Both singlet and triplet CT excited states are thought to be formed, between which promoting ISC channels lie, and the organic arene-dominating T_1 state remains the contributor to the phosphorescence.[3]

Usually, the complexation of organic π-acceptors and Au(I) CTC leads to nonemissive adducts.[5] One exception is perfluoronaphthalene ($C_{10}F_8$), which represents a rare organic aromatic π-acceptor with rt phosphorescence that could be triggered after interaction with Au(I) CTCs. The insertion of $C_{10}F_8$ between the Au(I) CTC molecules quenches intertrimer Au−Au bonding phosphorescence (blue light for Au_3(*p*-TolN═COEt)$_3$[233] and green light for Au_3(1-BzIm)$_3$[208]). On the other hand, it turns on the bright yellow metal-sensitized phosphorescence of the $C_{10}F_8$ monomer at rt, which has lifetimes (3.5 and 1.8 ms after adduction with Au_3(*p*-TolN═COEt)$_3$[233] and Au_3(1-BzIm)$_3$,[208] respectively) that are 2 orders of magnitude shorter than those (0.25−0.38 s) of $C_{10}F_8$ phosphorescence in frozen solution.[233]

Other representative examples of metal-sensitized phosphorescence are mainly based on π-acidic CTCs, such as Ag_3[3,5-$(CF_3)_2$Pz]$_3$ and Cu_3[3,5-$(CF_3)_2$Pz]$_3$. The frozen CH_2Cl_2 solution of Ag_3[3,5-$(CF_3)_2$Pz]$_3$ and naphthalene, in a 1:1 molar ratio, exhibits green phosphorescence with structured emission peaks, which are also observed for the crystals of the binary adduct (Ag_3[3,5-$(CF_3)_2$Pz]$_3$/naphthalene) at 298, 77, and 4 K.[234] The heavy-atom effect from Ag_3[3,5-$(CF_3)_2$Pz]$_3$ renders the metal-sensitized rt phosphorescence of naphthalene with a lifetime (830 μs) that is much shorter than that of naphthalene in a frozen CH_2Cl_2 matrix (2.4 s). Similar green phosphorescence from the T_1 state of the naphthalene monomer can also be induced by forming binary adducts with Cu_3[3,5-$(CF_3)_2$Pz]$_3$.

Usually, the interaction of organic chromophores with Ag(I) and Cu(I) CTCs results in the fluorescence quenching of these organic arenes by forming phosphorescent π-acid/π-base adducts. Promoted by the external heavy-atom effect or low-lying CT excited states, the ISC rate constant competes with the internal conversion and fluorescence radiative decay. Recently, Zhan, Li, and co-workers reported a unique π-acid/π-base adduct that exhibited dual emission comprising both blue fluorescence and yellow phosphorescence at 77 K.[164] By mixing Ag_3[3,5-$(CF_3)_2$Pz]$_3$ with *o*TP in solution, the 1:1 binary adduct was isolated in a co-crystal conformation. Each *o*TP molecule binds with the two closest Ag_3Pz_3 molecules through its central phenyl and one peripheral phenyl ring, while each Ag_3Pz_3 molecule binds with two adjacent *o*TP molecules through its nine-membered ring. This leads to a binary column in (Ag_3)-*o*TP-(Ag_3)-*o*TP stacking mode (Figure 71a). TDDFT results revealed that the HE fluorescence and LE phosphorescence bands respectively originated from the lowest-lying singlet and triplet excited monomer of *o*TP, compared with the emission spectra of the free *o*TP and its adduct (Figure 71b). This is the first example wherein the fluorescence of arenes is maintained

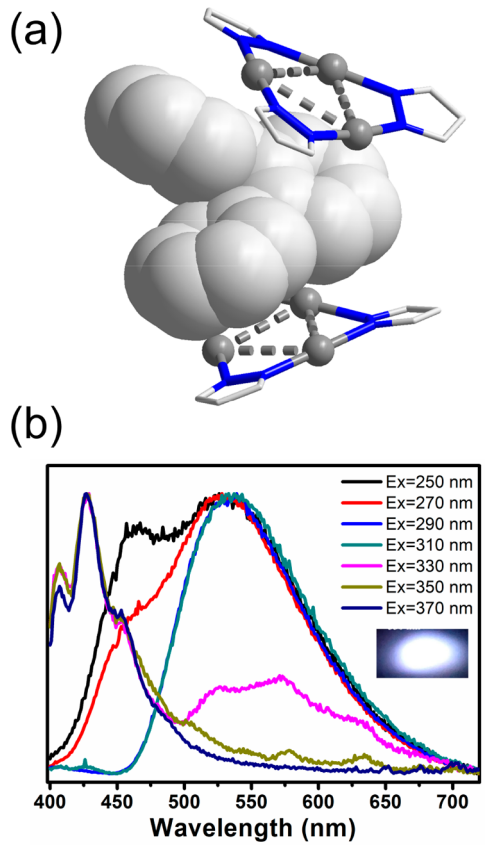

Figure 71. (a) Crystal structure of the Ag_3[3,5-$(CF_3)_2$Pz]$_3$/*o*TP adduct, showing Ag_3···π interactions. [Color code: gray, Ag; blue, N; light gray, C. All CF_3 groups and H atoms have been omitted from the figure for the sake of clarity.] (b) Normalized solid-state photoluminescence spectra of the adduct under 77 K upon excitation from 250 nm to 370 nm (inset is a photograph showing white light of the adduct with 330 nm excitation under 77 K).

https://dx.doi.org/10.1021/acs.chemrev.0c00011
Chem. Rev. 2020, 120, 9675−9742

after adduction with Ag_3Pz_3. Although its photophysical progress remains unclear, several conclusions could be drawn by thorough comparison with $Ag_3[3,5\text{-}(CF_3)_2Pz]_3$/planar arene adducts (e.g., benzene, toluene, mesitylene, and naphthalene).[39,234] In the crystal structure of $Ag_3[3,5\text{-}(CF_3)_2Pz]_3$/*o*TP, the centroid−centroid distances between the Ag_3N_6 nine-membered rings and phenyl rings of *o*TP range from 3.33 Å to 3.90 Å, which are much longer than those of the $Ag_3[3,5\text{-}(CF_3)_2Pz]_3$/planar arene adducts. Moreover, in *o*TP, only two of the three phenyl rings interact with one $Ag_3[3,5\text{-}(CF_3)_2Pz]_3$ molecule due to steric hindrance. In contrast, the planar arene molecules are sandwiched by two $Ag_3[3,5\text{-}(CF_3)_2Pz]_3$ units. Thus, the external heavy-atom effect of $Ag_3[3,5\text{-}(CF_3)_2Pz]_3$ may be insignificant in the lowest-lying excited states of $Ag_3[3,5\text{-}(CF_3)_2Pz]_3$/*o*TP. As a supplementary note, it is more difficult to experimentally trigger phosphorescence in *o*TP than in naphthalene, because, at 77 K, naphthalene shows phosphorescence while free *o*TP only exhibits fluorescence. In this work, the authors proposed an alternative simple solution to attain aromatic phosphorescence in the area of lighting.

Apart from metal-sensitized phosphorescence, the adductions between CTCs and arenes may result in phosphorescence with colors that are different from those of both the parent CTCs and free arenes, which are often assigned from the triplet exciplexes, spin-forbidden intermolecular CT, or the cooperation of these two mechanisms. For example, the adducts of $Ag_3[3,5\text{-}(CF_3)_2Pz]_3$ and benzene, toluene, or mesitylene show bright rt green or blue phosphorescence,[39] while the adduct of $Cu_3[3,5\text{-}(CF_3)_2Pz]_3$ and mesitylene shows bright room-temperature green phosphorescence.[163]

The luminescence behaviors of π-acid/π-base adducts and exciplexes derived from CTCs and organic aromatics are rich and interesting, leading to their potential application in solid-state lighting, displays, and chemical sensors, which are described in detail in section 6. However, both the experimental and computational investigations of the excited-state nature of such adducts have been less explored. The lack of efficient strategies for forming stable CTCs/arene adducts hampers the systematic study of luminescence properties of such adducts. On the other hand, computational studies focusing on the excited-state nature of these adducts are also immature. If possible, research should focus on the syntheses and detailed (and maybe time-resolved) photophysical studies of stable 1:1 binary and 2:1 sandwich-like π-acid/π-base adducts that can be well-separated into dilute glassy solutions. Such prospects could bring other points of view and shed light on the theoretical studies of CT, exciplex formation, and photophysical progress.

Because of the confined well-ordered cavities and pores, coordination cages and MOFs/PCPs have become good platforms for the systematic investigation of guest-induced chemical and physical property changes. By introducing Cu_3Pz_3 units into coordination cages and MOFs/PCPs, researchers have further enriched the investigation of the luminescence behaviors of CTCs, following adduction with organic aromatics. Li's group constructed a hexanuclear Cu(I) trigonal coordination prism, which displayed emission maxima shifts as large as 35 nm after the inclusion of toluene molecules.[50] Later, a hexanuclear Cu(I) trigonal coordination prism with a nanocavity was prepared, which accommodates a series of aromatic guests (Figure 72).[52] These resulting host−guest inclusion complexes show guest-dependent phosphorescence behaviors. For instance, the QY values of inclusion complexes decrease as the guest ionization potential increases. Notably, for the organic

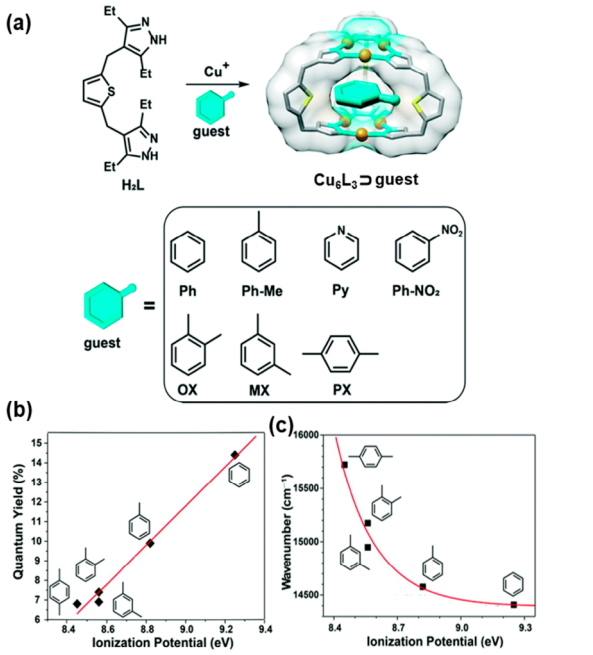

Figure 72. (a) Structural representation of the synthesis of inclusion complexes from Cu_6L_3 cage (L = 2,5-bis(4′-methylene-3′,5′-diethylpyrazolate)thiophene) host and various aromatic guests (Et groups on pyrazole rings are omitted for clarity). Linear or nonlinear correlation between the (b) quantum yield (QY, %) or (c) emission maximum (cm^{-1}) and ionization potential (eV) of inclusion complexes with the chemical structures of their corresponding guests. [Adapted with permission from ref 52. Copyright 2020, Royal Society of Chemistry, London.]

arenes, strong π-acidity results in a low ionization potential, while strong π-basicity results in a high ionization potential. The confined cavity and moderate π-acidity of the Cu_3Pz_3 units among the Au(I)/Ag(I)/Cu(I) CTUs provide an opportunity to systematically investigate the luminescence behaviors of π-acid/π-base adducts when the changes in the guest π-acidity/basicity span over a wide range.

5.1.5. Solvoluminescence (Solvent-Stimulated Luminescence). The phenomenon of solvoluminescence was first and solely reported for an Au_3Cb_3 complex−hexagonal $Au_3(MeN{=}COMe)_3$ in 1997, by Balch's group.[30,31,235] Upon irradiation of its crystalline sample by UV lamp (λ = 365 nm), the prompt HE structured (422 nm) emission band with a short-lived lifetime ($\tau \approx 1$ ms) and LE (552 nm) luminescence with long-lived lifetime (triexponential, $\tau \approx 1.4$, 4.4, 31 s) were observed at rt. Subsequently, after removing the UV light irradiation and the long-lived emission decayed, a drop of $CHCl_3$ on its crystalline samples triggered yellow emission peaking at 552 nm.[31] In addition, sequential addition of $CHCl_3$ drops to the above-mentioned photoirradiated solid samples could produce respective bursts of yellow emissions.[9] Apart from $CHCl_3$, other solvents, including CH_2Cl_2, toluene, MeOH, hexane, and water, are also able to trigger such luminescence. Qualitatively, the intensity of solvoluminescence is related to the solubility of this Au_3Cb_3, because it shows great solubility in $CHCl_3$ and CH_2Cl_2 and the visually strongest triggered emission change upon contact with these two solvents. Thus, until the sample maintains its solid-state form, the previously photo-irradiated powder exhibits solvoluminescence properties. The authors further claimed that this unique phenomenon differs from triboluminescence,[236] crystalloluminescence,[237] and lyo-

https://dx.doi.org/10.1021/acs.chemrev.0c00011
Chem. Rev. 2020, 120, 9675−9742

luminescence,[238] which have been defined as the special luminescence triggered by mechanical manipulation, crystallization, and dissolution of the solid sample, respectively. Notably, the triclinic and monoclinic polymorphs of the hexagonal $Au_3(MeN{=}COMe)_3$ complex do not exhibit solvoluminescence, even though their intertrimer Au−Au distances are shorter than those of the hexagonal phase.

To interpret this unique phenomenon, researchers have questioned how the energy is stored in the crystalline powder and how the solvent helps release the stored energy.[9] It was initially assumed that the dissolution of photoirradiated monomers-of-trimer led to energy release from the excited states. However, this was ruled out because a higher-energy emission (~442 nm) was observed for Au(I) CTC $CHCl_3$ solution, which was attributed to monomer emission, while the solvoluminescence peaked at ~552 nm. Taking further insight into the structure−property (luminescence) relationship, it was claimed that both eclipsed and disordered stacking modes contributed to the energy storage and trap, as well as the multiple aurophilic interactions shown in the hexagonal structures.[9,188] McDougald et al. and Zhu et al. studied the aurophilic interaction in 1D stacking and the influences brought by the different stacking directions. They concluded that this unique eclipsed stacking mode would benefit both the electron and hole transport confined along the stacking directions of the gold trimers.[34,239] The detailed transportation properties are discussed in section 6.4.

Recently, Rabaâ, Sundholm, and co-workers conducted detailed calculations on the stacking modes, directions, and excited states of Au_3Cb_3, to elucidate how the energy was stored in the crystals.[240] Their results suggested that the dimers-of-trimer contributed toward storage and exciton release during charging and solvent stimulation. The electron density of the exciton within the dimers increases the binding energies of the excited dimers and stabilizes them. In addition, the least bulky methyl substituents might assist the formation of stable excited dimers-of-trimer in solution. Alternatively, the disordered infinite chain plays a crucial role in energy trapping and energy transfer from the eclipsed dimers-of-trimers. Therefore, solvent contact results in surface dissolution of the dimers-of-trimer at high concentrations, and the energy is therefore released.

Greiner et al. further emphasized the significant role of dimers-of-trimer in comprehending solvoluminescence.[241] The detailed photophysical progresses of the $Au_3(MeN{=}COMe)_3$ monomer and dimer were calculated at the high level of theory, and rate constants of the vertical transitions, internal conversion, and ISC were estimated. The calculated slow phosphorescence rate constant for the $Au_3(HN{=}COH)_3$ (k_{phos} = 5 s^{-1}) dimer, accompanied by a large Stokes Shift (2.3 eV) and unity QY (100%), which were observed in $Au_3(MeN{=}COMe)_3$ dropped in good solvents after irradiation with UV light, suggest the existence of long-lived triggered phosphorescence.

Solvoluminescence was first discovered 20 years ago and documented in 1997; hexagonal $Au_3(MeN{=}COMe)_3$ is still the only reported molecule that shows this special phenomenon among all types of CTCs and organic/inorganic materials. The above-mentioned literature attempts to explain this phenomenon from both molecular and solid-state levels. Unfortunately, these interpretations do not explain the origin and mechanism of solvoluminescence satisfactorily. The core question of how excited states are preserved and maintained for some time remains unanswered. The unique eclipsed stacking mode may benefit energy storage; however, experimental reproduction of the stacking mode or solvoluminescence in other CTCs or materials must also be demonstrated.

5.2. Luminescence Chromism

5.2.1. Thermochromism. Luminescence thermochromism is the change in emission color with changing temperature. It arises from two main situations: the competition of two emissive states in thermal equilibrium and the change in the intensity and energy of an emission band that shows limited color differences at multiple temperatures. The concept of "luminescence thermochromism" was initially introduced to describe the temperature-dependent emission color change behavior of copper−iodine clusters by Hardt in 1973 and 1977.[242,243] Photoluminescence properties of multinuclear Cu(I) complexes with temperature-dependent emission color changes were subsequently well reviewed by Ford and co-workers.[244] The luminescence thermochromism of these copper−iodine clusters follows the first situation and usually consists of an HE halide/metal−ligand charge transfer (XLCT/MLCT) emissive state and an LE cluster-centered (CC; halide-metal charge transfer, XMCT) phosphorescent state. The decrease in temperature rigidifies the metal centers, enhances the excited-state Cu−Cu bonding, and subsequently destabilizes the CC excited state and decreases the intensity of the LE band. The HE band is also prominent, because of the excited-state thermal population and decrement of the nonradiative progress.[245,246] By controlling the temperature, it is possible to tune the emission colors of these thermochromic metal complexes.

Unlike copper−iodine clusters that have multiple types of emissive states, the thermochromism in CTCs usually arises from the thermal equilibrium of multiple intertrimer metal−metal bonding excited dimers or excimers. Among the multinuclear metal complexes, it is common to observe bathochromic shifts of the emission bands upon cooling, because of the shortening of the metal−metal distances after lattice contraction and energy lowering of the triplet metal−metal emissive state. Although multiple low-lying metal−metal bonding excited states exist in these multinuclear metal complexes, the strong coupling among these states leads to fast internal conversion to the lowest-lying emissive state and only one emissive band preserves in these systems. For CTCs, the coupling of metal−metal bonding excited states is poor enough to allow multiple emissive states to undergo radiative transitions back to the ground state. As a result, multiple metal−metal-interaction-dominated phosphorescence could be observed that would be influenced by temperature alteration.

$Cu_3[3,5\text{-}(CF_3)_2Pz]_3$ is an important representative and exhibits only a broad LE phosphorescence band (λ_{em} ~ 645 nm) at rt with an additional HE shoulder peak (λ_{em} ≈ 590 nm) at temperatures of ≤77 K (Figure 62, vide supra).[21,22] As a result, a drastic emission color change from red to orange is observed upon cooling, which is different from the well-documented bathochromic shift of other metal−metal bonding phosphorescence in multinuclear coinage-metal complexes. Extensive experimental and theoretical investigations have clarified that the main LE band and HE shoulder peak correspond to two respective excimers with short and separated intertrimer Cu−Cu contacts. This mechanism could be applied to interpret multiple excimer emissions that are composed of multiple intertrimer Cu−Cu interactions.

Compared to the crystalline fluorinated Cu_3Pz_3, $Cu_3[3,5\text{-}(i\text{-}Pr)_2Pz]_3$ shows more significant luminescence thermochromism, from red to green, when cooling the crystalline sample from

https://dx.doi.org/10.1021/acs.chemrev.0c00011
Chem. Rev. 2020, 120, 9675−9742

rt to 77 K (Figure 62, vide supra), contributed by two well-separated phosphorescence bands (a red band with λ_{em} = 662 nm and a green band with λ_{em} = 562 nm).[22] Moreover, at 235 K, the combination of these two bands gives a broad yellow phosphorescence band. In stark contrast to the limited difference in the HE-LE wavelengths of fluorinated Cu_3Pz_3, the ~100 nm separation in $Cu_3[3,5\text{-}(i\text{-}Pr)_2Pz]_3$ leads to a prominent color change under different temperatures and distinct luminescence thermochromism. In addition, the crystal structure of $Cu_3[3,5\text{-}(i\text{-}Pr)_2Pz]_3$ exhibits the discrete packing of a chair dimer with intertrimer Cu−Cu distances of 2.989 Å within the dimer and >7.52 Å between neighboring dimers. Thus, two or more excited dimers or excimers with different Cu−Cu distances are not expected. In this case, the well-separated phosphorescence bands are attributed to the radiative transitions from the first and second triplet excited states (i.e., T_1 and T_2, respectively). The mechanism of the luminescence thermochromism of $Cu_3(3,5\text{-}Me_2Pz)_3$ could be also described in this way (Figure 62, vide supra).

Recently, a similar phenomenon discovered in $Au_3(1\text{-}EtIm)_3$ has shown unprecedented remarkable photoluminescence thermochromism, from violet to red, attributed to the internal conversion between the higher-energy ($T_2 \rightarrow S_0$; $\lambda_{max} \approx 409$ nm) and lower-energy ($T_1 \rightarrow S_0$; $\lambda_{max} \approx 700$ nm) phosphorescent bands below and above 200 K, respectively, probably representing an excited-state phase change (Figure 73).[90]

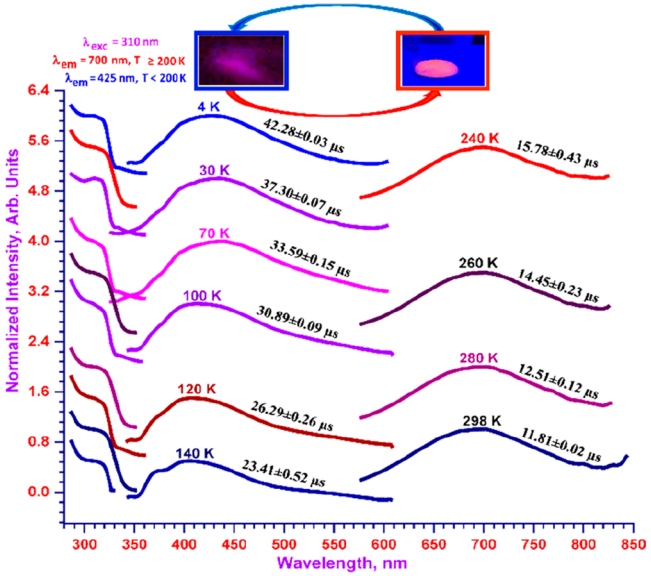

Figure 73. Photoluminescence (left) excitation and (middle and right) emission spectra of solid $Au_3(1\text{-}EtIm)_3$ versus temperature. The inset shows photographs of the luminescence of $Au_3(1\text{-}EtIm)_3$ taken while the solid is being irradiated with a hand-held UV lamp (short wavelength) at (left) 77 K and (right) 298 K. [Reprinted with permission from ref 90. Copyright 2017, American Chemical Society, Washington, DC.]

Unlike the above mechanisms, which are related to the thermal equilibrium of multiple intertrimer metal−metal bonding excited states, the very recently reported **Cl-*α*** (a polymorph of $Cu_3(4\text{-}ClPz)_3$ in ref 36) represents a unique case of photoluminescence thermochromism corresponding to the thermal equilibrium between an intratrimer Cu−Cu bonding monomer and an intertrimer Cu−Cu bonding excimer.[36] Upon excitation at 310 nm at rt, **Cl-*α*** exhibits white phosphorescence consisting of an HE monomeric band at 480 nm and a slightly weaker LE excimeric band at 564 nm. Cooling the crystalline sample to 77 K results in a remarkable emission color change, from white to green, because of the marked HE band (Figure 74a). When excited at 290 nm, **Cl-*α*** shows yellow light

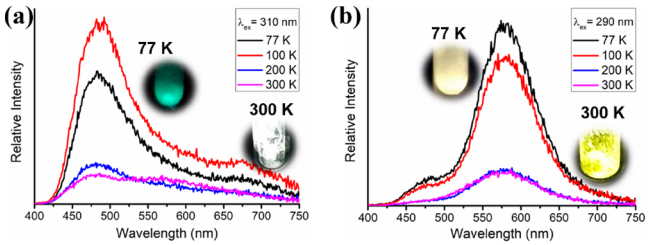

Figure 74. Solid-state emission spectra of **Cl-*α*** under the excitation of (a) 310 nm and (b) 290 nm at different temperatures. Inset photographs are crystals packed in suprasil quartz tubes under the corresponding UV-light excitations at 300 and 77 K, respectively.

consisting of a main LE band and a weaker but non-negligible HE shoulder peak, and the LE band turns much stronger upon cooling (Figure 74b). Such distinct luminescence responses to temperatures below the difference excitation energies are relevant to complex photophysical processes. The 310 nm excited LE band mainly arises from excimer formation, requiring vibration coupling (unfavorable at low temperature) between an excited and adjacent ground-state monomer. In contrast, under higher-energy excitation (e.g., 290 nm), the excited dimer could be mainly populated by direct excitation from a loosely bound ground-state dimer, rather than undergoing excimer formation after exciting a monomer. Furthermore, no noticeable red- or blue-shifts of the monomeric or excimeric band are observed for **Cl-*α***.

In addition to thermal equilibrium between different metal−metal bound excited states, the ligand-dominated emissive states would compete with the metal-centered excited states against temperature. In 2006, Coppens, Omary, and co-workers reported the thermochromism of $Au_3[3,5\text{-}(i\text{-}Pr)_2Trz]_3$ with the change in molecular symmetry (C_2 and D_3 symmetries; see Figure 75).[100] For temperatures >180 K, only an LE_1 band (~750 nm) dominates the luminescence. However, upon cooling to <180 K, an HE structured band at ~370 nm, with an average spacing of 1350 ± 40 cm^{-1}, and an LE_2 band (near 650 nm) appear. Both LE bands are assigned as metal−metal bonding exemeric states from the dimer-of-trimer, with varying intertrimer metal−metal distances within the temperature-dependent structural changes, and the HE structured band is still considered as the ligand-centered emission.

Another polymorph of $Cu_3(4\text{-}ClPz)_3$ (**Cl-*β*** in ref 36) is formed as a discrete chairlike dimer of shorter intertrimer Cu−Cu contacts and thus, only displays one single LE band originating from a triplet excited dimer.[36] Compared to those of **Cl-*α*** and other above-mentioned Cu_3Pz_3 complexes, the thermochromism of **Cl-*β*** is more commonly observed among coinage-metal bonding phosphorescent complexes and follows the second situation of luminescence thermochromism. Upon cooling from 300 K to 77 K, the emission color of the **Cl-*β*** changes from orange to red, with narrowing of the phosphorescence band and an increase in the intensity (Figure 76).

The Au_3−M−Au_3 sandwich-like clusters were also found to display luminescence thermochromism, as reported by Burini

https://dx.doi.org/10.1021/acs.chemrev.0c00011
Chem. Rev. 2020, 120, 9675−9742

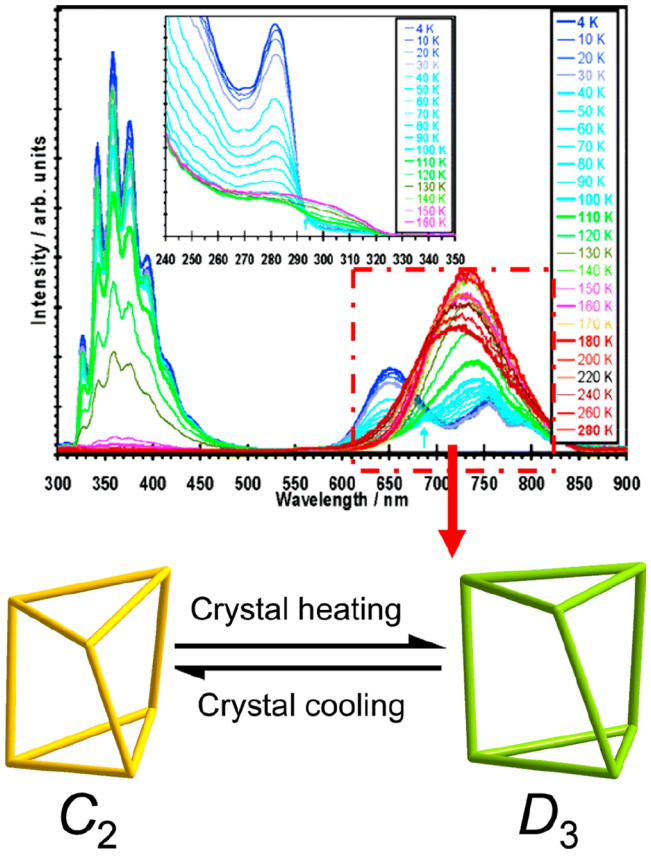

Figure 75. Photoluminescence spectra for crystals of $Au_3[3,5\text{-}(i\text{-}Pr)_2Trz]_3$ excited at 280 nm versus temperature. The inset shows excitation spectra monitoring at emission wavelength of 650 nm. Sky-blue arrows in the emission and excitation spectra illustrate isoemissive and isosbestic points, respectively, as indicated by the arrows. [Adapted with permission from ref 100. Copyright 2006, American Chemical Society, Washington, DC.]

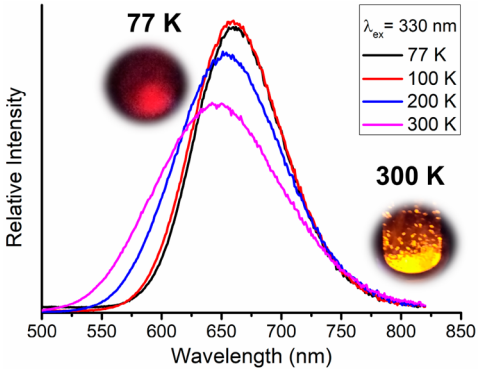

Figure 76. Solid-state emission spectra of **Cl-*β*** excited at 330 nm at different temperatures. Inset photographs are crystals packed in suprasil quartz tubes under the corresponding UV-light excitations.

and Fackler et al.[155] Three sandwich-like complexes, $[Au_3Im_3{-}Ag(I){-}Au_3Im_3](BF_4)$, $[Au_3Im_3{-}Tl(I){-}Au_3Im_3](PF_6)$, and $[Au_3Cb_3{-}Tl(I){-}Au_3Cb_3](PF_6)$ (Im = 1-BzIm and Cb = *p*-TolN═COEt), presented LE emissions at ambient temperature (425−535 nm) and red-shifted upon cooling. This consistent phenomenon is assigned to the shrinkage of the metal−metal distances and subsequent reduction of the band gap energy. Similar examples of mixed-Au/Ag CTCs, $AuCbAg_2Pz_2$, and Au_2Cb_2AgPz (Cb = *p*-TolN═COEt, Pz = 3,5-Ph_2Pz), were also reported.[95] Their emission bands exhibit a bathochromic shift, from green to yellow, upon cooling down from rt to 77 K.

5.2.2. Vapochromism. Generally, a significant change in the emissive behavior of a luminescent compound upon contact with chemical vapors is considered as luminescence vapochromism. Herein, this change includes luminescence enhancement or triggering, quenching (turn-on and turn-off), and emission color transformation.[247,248] The main mechanisms of luminescence vapochromism include the formations of emissive/nonemissive complexes and adducts or mixtures of different emission colors upon contact with chemical vapors. Because of the weak interactions between the vapor and host molecules, most vapochromic adducts or mixtures can be recovered upon removal of the vapor molecules by heat and/or vacuum. It is apparent that the degree or alteration of luminescence vapochromism will be highly dependent on the contact time with the chemical vapor. Therefore, in this section, we mainly focus our discussion on "true or false" questions qualitatively, while a further quantitative discussion is presented in section 6.3.1.

Rawashdeh-Omary et al. reported the luminescence quenching for a *π*-basic Au(I) CTC exposed in C_6F_6 vapor in 2001.[91] $Au_3(p\text{-TolN}{=}COEt)_3$ exhibits blue photoluminescence in the solid state at rt, while the co-crystal of $Au_3(p\text{-TolN}{=}COEt)_3$ and C_6F_6 in a 1:1 molar ratio is nonemissive at ambient temperature. When solid samples of the Au(I) CTC are placed in a closed chamber, together with a beaker of C_6F_6, the characteristic blue emission slowly disappears with increasing exposure time (Figure 77). However, lowering the crystallinity

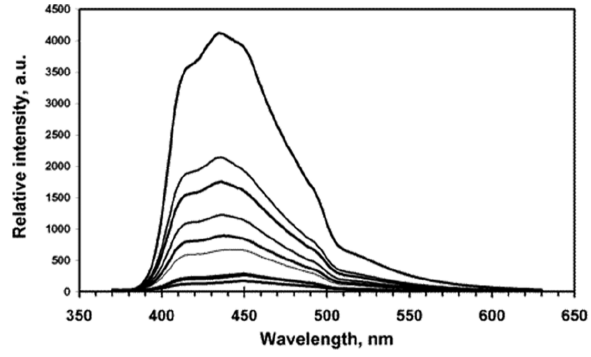

Figure 77. Emission spectra of $Au_3(p\text{-TolN}{=}COEt)_3$ versus exposure time to C_6F_6 vapor at ambient temperature and pressure. The exposure time was (top to bottom) 0, 51, 65, 98, 148, 208, 1322, 1439, and 1462 min, respectively. [Reprinted with permission from ref 91. Copyright 2001, American Chemical Society, Washington, DC.]

of the co-crystals by immersing them in a poor solvent (e.g., diethyl ether) triggers back the blue photoluminescence, which is similar to that of Au(I) CTC itself. This observation promotes the discovery of the interactions between the *π*-basic Au_3Cb_3 and *π*-acidic C_6F_6 molecules.

The turn-on type vapochromism was first reported by Rawashdeh-Omary, Dias, and co-workers in 2011 for $Ag_3[3,5\text{-}(CF_3)_2Pz]_3$ and *π*-basic benzene, toluene, and mesitylene.[39] Solid samples of $Ag_3[3,5\text{-}(CF_3)_2Pz]_3$ transform from non-luminescent to blue or green emitters under UV light, when exposed to a saturated vapor of *π*-basic benzene, toluene, or mesitylene for a short time of ∼30 min. The "switch-on" vapochromism could also be reverted to nonluminescence upon drying or heating the sample to remove the solvent molecules.

https://dx.doi.org/10.1021/acs.chemrev.0c00011
Chem. Rev. 2020, 120, 9675−9742

Emission color change, rather than turn-on type vapochromism, was observed for $Cu_3[4\text{-X-}3,5\text{-}(CF_3)_2Pz]_3$ (X = Cl, Br) upon contact with benzene or toluene.[136] The solid samples of both Cu_3Pz_3 complexes exhibit vapochromism from bright yellow to green phosphorescence in the presence of benzene or toluene. However, noticeable turn-off type vapochromism was observed for these Cu_3Pz_3 complexes after contacting with mesitylene vapors. Real-time luminescence switching could be monitored for benzene, toluene, and mesitylene based on the drop-cast films of these $Cu_3[4\text{-X-}3,5\text{-}(CF_3)_2Pz]_3$ complexes (Figure 78).

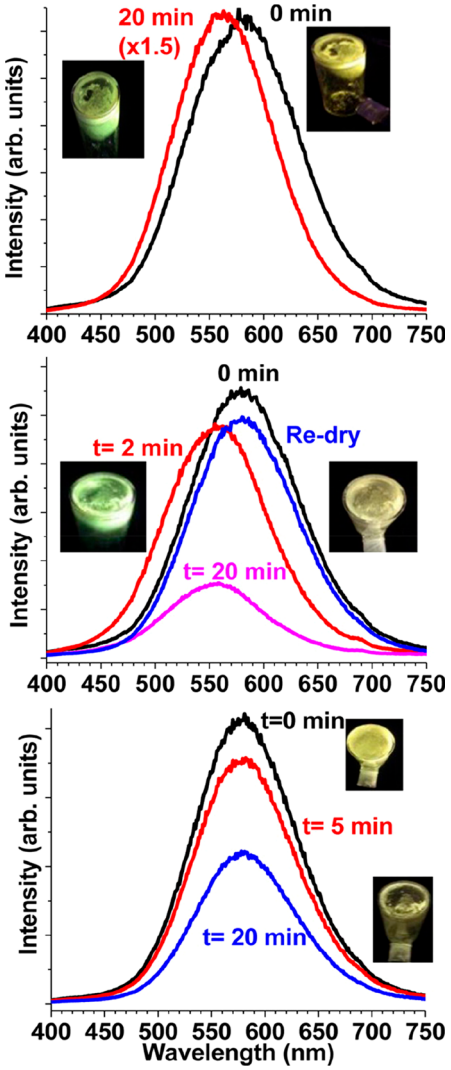

Figure 78. Photoluminescence spectral changes for a drop-cast thin film of $Cu_3[4\text{-Cl-}3,5\text{-}(CF_3)_2Pz]_3$ at rt (deposited from CH_2Cl_2 solution) upon introduction or removal of vapors of (top) benzene, (middle) toluene, or (bottom) mesitylene. [Reprinted with permission from ref 136. Copyright 2013, American Chemical Society, Washington, DC.]

5.2.3. Solvatochromism and Concentration Luminochromism. Molecules in excited states usually have high reactivities and polarities attributed to their unpaired electrons. Solvatochromism, known as the emission color change for CTCs in different solvents, is related to the excited-state properties of CTCs and electronic properties of solvents. Limited by their poor solubility and sensitivity to oxygen, solution-state luminescence studies have been restricted to a small number of CTCs. Dias, Omary, and co-workers reported that the frozen solutions of $Cu_3[3,5\text{-}(CF_3)_2Pz]_3$ exhibited various emission colors from deep blue to red (Figure 79).[22]

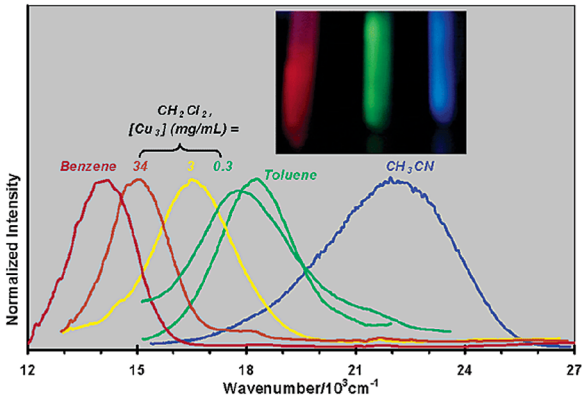

Figure 79. Representative emission spectra of rigid frozen solutions (77 K) of $Cu_3[3,5\text{-}(CF_3)_2Pz]_3$ versus solvent and concentration. The photograph shows selected CH_2Cl_2, toluene, and acetonitrile frozen solutions in supracell quartz tubes exposed to UV light immediately after removal from a liquid nitrogen bath. [Reprinted with permission from ref 21. Copyright 2003, American Chemical Society, Washington, DC.]

Even in solvents with similar properties (e.g., benzene and toluene), a dramatic difference in emission color could be observed in the glassy solution. Two hypotheses have been proposed to interpret this unique phenomenon. One suggests that the solvent molecules could approach to form exciplexes with the $[Cu_3]$ oligomeric excimers and solvent, because of the high reactivities of the excited molecules. Enhanced intermolecular interactions would further stabilize the occupied molecular orbitals of the exciplexes and subsequently lower the emission energy, which may produce a longer-wavelength emission than that in solid state. The second hypothesis speculates that the solvent would influence the formation and degree of aggregated $[Cu_3]$ and further affect the excited-state Cu−Cu bonding.[22]

A change in emission color with changing concentration (concentration luminochromism) was also observed when the concentration of the fluid or frozen solution was varied. One example for concentration luminochromism is $Cu_3[3,5\text{-}(CF_3)_2Pz]_3$, in which the emission color at high concentration approaches solid-state behavior (Figure 79).[21,22] Strong color changes occur in its CH_2Cl_2 solution under liquid nitrogen temperature, varying from blue to red with increasing concentration. It was suspected that, even in solution, the emission profile originated from excited $[Cu_3]_n$ excimers and exciplexes of varied numbers (n) and/or intertrimer Cu−Cu interactions within the adjacent trimers.

$Au_3[3,5\text{-}(i\text{-Pr})_2Trz]_3$ is another representative case of concentration luminochromism, observed in fluid solution at rt.[100] The transformation between C_2 and D_3 dimers in CH_2Cl_2 solution could be achieved by modulating the concentration of $Au_3[3,5\text{-}(i\text{-Pr})_2Trz]_3$. Thus, concentration luminochromism is realized by changing the ratio of these two dimers spontaneously (Figure 80). The symmetry change is confirmed by the apparent isoemissive point at 686 nm, reminiscent of the temperature-dependent solid-state emission with a symmetry change in the crystals (Figure 75).

https://dx.doi.org/10.1021/acs.chemrev.0c00011
Chem. Rev. 2020, 120, 9675−9742

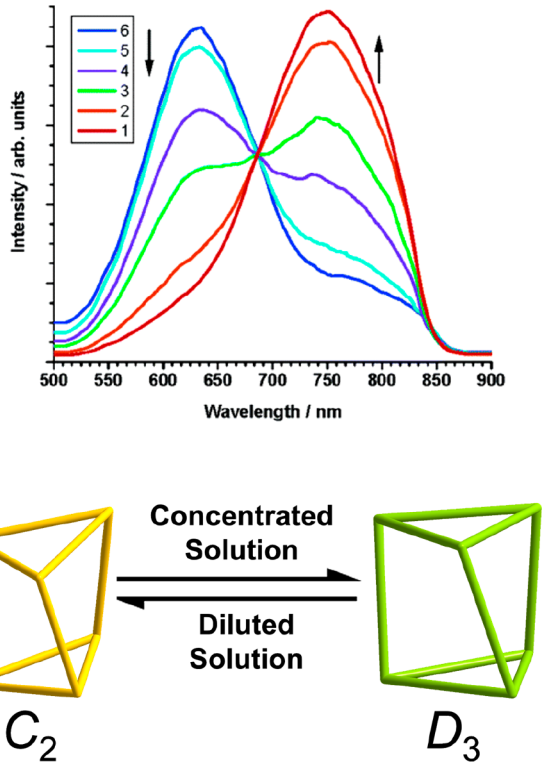

Figure 80. Area-normalized emission spectra of $Au_3[3,5\text{-}(i\text{-}Pr)_2Trz]_3$ in CH_2Cl_2 at rt. Concentrations ($\times 10^{-4}$ M) are 88, 44, 11, 2.8, 0.68, and 0.16 for traces 1−6, respectively (λ_{ex} = 270 nm). [Adapted with permission from ref 100. Copyright 2006, American Chemical Society, Washington, DC.]

5.2.4. Mechanochromism. Luminescence mechanochromism is defined as an emission color change that is stimulated by external forces, including isotropic and anisotropic factors. It usually occurs in a system that contains supramolecular interacting sites and requires a change in the excited-state ordering, lowest emissive state energy, or crystalline orientation. In the CTC family, intertrimer metal−metal interactions (especially homometallic), along with the interacting sites provided by the ligand substituents, are expected to show luminescence mechanochromism. In 2014, Li and coworkers presented a family of $Cu_3[4\text{-}(4'\text{-}COOR\text{-}Ph)\text{-}3,5\text{-}Me_2Pz]_3$ (R = Me, Et) complexes exhibiting reversible mechanically induced luminescence variation between bluish violet and red (Figure 81).[221] The as-synthesized solid samples exhibited bluish violet emission and gave a reddish emission color after being thoroughly ground. However, the violet emission color could be recovered back by treating the ground powder with drops of EtOH. Such high-contrast luminescence mechanochromism is achieved by modulating the ratio of an HE monomeric fluorescence band and LE excimeric phosphorescence band. The emission spectra of all these crystalline samples are dominated by the HE fluorescence bands located at ∼390 nm, similar to the emission peaks of the proligand ethyl-4′-benzoate-3,5-dimethylpyrazole. The ester group attached to the phenyl group serves as an auxochrome to enhance the absorbency and, thus, lower the energy of the ligand-based excited states. After grinding (under anisotropic stress), the intensity of the LE phosphorescence band overpowers the HE band, accompanied by a bathochromic shift of the emission maximum from ∼620 nm to 710 nm. Upon EtOH addition to the ground samples, the HE emission could be restored due to the recovery of the crystallinity. The supposed Cu−Cu distance shortening of the ground samples and the decrease in crystallinity were confirmed by TDDFT calculations and PXRD patterns. Excimer formation and the change in excited-state ordering were proposed to explain the switching of ligand-based fluorescence and metal-centered phosphorescence. Notably, an emission maximum >700 nm of the ground samples is the only example of near-infrared emission for all reported CTCs until the publication of this Review.

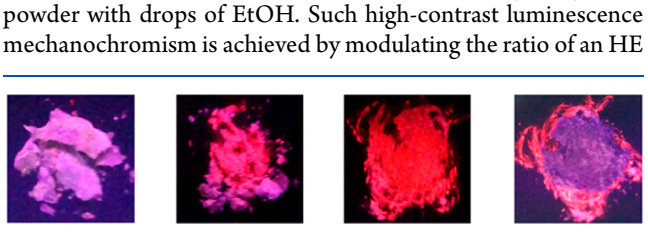

Figure 81. Photographs of samples of $Cu_3[4\text{-}(4'\text{-}COOEt\text{-}Ph)\text{-}3,5\text{-}Me_2Pz]_3$ under a 254 nm UV lamp. From left to right: crystalline sample; partially ground sample; thoroughly ground sample; sample treated with EtOH after grinding. [Reprinted with permission from ref 221. Copyright 2014, American Chemical Society, Washington, DC.]

$Au_3[3\text{-}(2'\text{-thienyl})\text{-}5\text{-}PhPz]_3$ was also reported to exhibit luminescence chromism, from green to yellow, upon grinding with $AgPF_6$.[153] After treating the ground mixtures with drops of acetone, the luminescence color reverted back to the green of the gold trimer, while regrinding changed the color back to yellow. This reversible behavior is believed to occur because of the formation of the sandwich-like complex $[Au_3{-}Ag(I){-}Au_3](PF_6)$, further confirmed by matrix-assisted laser desorption ionization time-of-flight mass spectrometry (MALDI-TOF MS).

5.3. Concluding Remarks

CTCs are well-known metal-containing luminophores with abundant luminescence behaviors, as summarized in this section. Intratrimer metal−metal bonding and heavy-atom effects play significant roles in the excited states, promoting ISC progress and efficient ^{3}MMCT-based phosphorescence, especially for alkyl-substituted CTCs. ^{3}LC emission and phosphorescence from π-acid/π-base adducts are often observed in aryl-substituted CTCs and CTC/arene adducts, respectively, and are also influenced by heavy-atoms effects. However, ^{3}MLCT/^{3}LMCT phosphorescence is unfavorable in low-coordinated d^{10} metal complexes (CTCs herein), because of excited-state Jahn−Teller distortion and unwanted vibronic coupling. In addition to triplet phosphorescence, CTC fluorescence could be triggered by the introduction of large π-conjugated substituents and quenching of metal-centered phosphorescence.

The extensive investigations on the luminescence behaviors of CTCs have been disclosed in section 5.2, revealing the responses of emissive states to external factors including temperature, chemical vapor, solvent, and pressure. The intertrimer metal−metal-bonding excited states are highlighted in relation to the formation of excimers and excited dimers that could be affected by external stimuli. Moreover, the luminescence vapochromism toward the formation and binding of π-acid/π-base adducts is remarkable.

However, more work is needed to elucidate the structure−property (luminescence) relationships and clarify the photophysical processes of CTCs and CTU-based materials. Indeed, at this stage, the design and synthesis of CTCs and CTU-based materials with tailored luminescence properties, high efficiency,

https://dx.doi.org/10.1021/acs.chemrev.0c00011
Chem. Rev. 2020, 120, 9675−9742

and/or luminescence chromism remains challenging. Thus, the development of time-resolved photospectrometric/crystallographic techniques, high-level quantum chemical calculations, and many other experimental/theoretical tools is predicted.

6. POTENTIAL APPLICATIONS

6.1. Thin-Film Fabrication

A series of techniques has been developed to fabricate CTCs into thin-films, including physical/chemical vapor deposition (PVD/CVD),[20,249] spin-coating,[34] dip-coating,[36] and even drop-casting.[20,136,250] Notably, thin-film fabrication is the first step toward practical optoelectronic applications as homogeneous layers.

Metallic silver shows excellent electrical conductivity and its thin film has low residual stress.[249] To fabricate silver thin films for application in conducting and semiconducting devices by the CVD method, silver sources that are stable toward air, moisture, and heat are required. To determine the suitable CVD source reagent for fabricating silver films, Chi, Carty, and co-workers presented their systematic investigation in 2005.[249] A series of Ag(I) pyrazolate complexes were selected in their study, including a mononuclear Ag compound and Ag(I) CTCs with 3,5-$(CF_3)_2$Pz, 3-(*t*-Bu)-5-CF_3Pz, and 3,5-(*t*-Bu)$_2$Pz ligands. Among them, $Ag_3[3,5\text{-}(CF_3)_2Pz]_3$ exhibited the best performance as a CVD source reagent, because of its high volatility and thermal stability and H_2-induced reduction. For efficient deposition of the Ag(I) CTC on a Si(100) wafer, high-temperature (~350 °C) and argon as the carrier gas are required to obtain the best composition, comprising 84% silver element, with good resistivity (3.81 $\mu\Omega$ cm).

In the field of corrosive protection, $Cu_3[3,5\text{-}(CF_3)_2Pz]_3$ can be drop-cast on an Al alloy 3003 surface, which is widely used for its moderate strength and good processability.[250] The high hydrophobic characteristics from six CF_3 substituents per molecule protect substrates from water and oxygen, which is crucial in anticorrosion application. Strong binding interactions between $Cu_3[3,5\text{-}(CF_3)_2Pz]_3$ and the Al substrate were also observed and computationally confirmed. Potentiodynamic polarization tests further verified the decrease in corrosion rate (1.00×10^{-2} mpy versus 4.50×10^{-3} mpy) and increase in resistance (1.80×10^3 versus 1.34×10^6 Ω cm^{-2}) after coating Cu(I) CTC on an Al alloy 3003 surface. In addition, orange phosphorescence from the Cu(I) CTC-coated Al alloy was maintained even after exposure to corrosive a 3.5% NaCl air-saturated aqueous environment.

6.2. Solid-State Lighting and Devices

The field of CTCs has attracted much attention, because of their great potential in next-generation optoelectronic devices, including OLEDs and organic photovoltaic devices (OPVs). Promising results for fabricating well-functional devices are presented in this section. As discussed in section 6.1, the introduction of CF_3 groups into CTCs has been proven an efficient strategy in thin-film fabrication, an essential progress in device fabrication, by improving the solubility and sublimability and enhancing the thermal and oxidative stabilities. Because $Cu_3[3,5\text{-}(CF_3)_2Pz]_3$ displays room-temperature orange phosphorescence with a high QY of 82.17% ± 0.16% mediated by excited-state intertrimer Cu−Cu bonding, it has been chosen to validate the possibility and processability of LEDs and OLEDs. The pioneer work performed by Galassi et al. has successfully introduced $Cu_3[3,5\text{-}(CF_3)_2Pz]_3$ into an OLED functional thin film by thermal evaporation (vacuum sublimation) and/or solution drop-casting.[20] This OLED functional thin film shows a higher crystalline orientation in small-angle diffraction ([*hkl* = 011]) than the neat solid powder, as confirmed by PXRD analysis. This is believed to benefit intertrimer excited-state metal−metal bonding and present better electron/hole mobility along a specific orientation. In addition, they also reported the preparation of an OLED functional thin film with mixed-metal CTC $Au_2Cu(1\text{-MeIm})_2[3,5\text{-}(CF_3)_2Pz]$ (**3a** in ref 20). The QY of $Au_2Cu(1\text{-MeIm})_2[3,5\text{-}(CF_3)_2Pz]$ approaches 97.13% ± 0.80% and the photoluminescence profiles fall between those of the OLED functional thin-film and its single crystals. The overall similarity illustrated in PXRD also confirms the sustainability of polymorphic forms in single crystals and thin films.

In the field of solid-state lighting, the development of single-phase white-light emitters, which could help avoid phase separation and color variation problems, is an important practical topic.[35] Specifically, lighting and display devices will face fading and decomposition of their organic and metal−organic emission layers so that different compounds have distinguished thermal stabilities during their operation lifetimes. Single-phase white-light emitters would avoid this disadvantage to ensure uniformity and color purity, because of the same fading rate and period of the single component. About 20 years after the discovery of the solvoluminescence of the hexagonal polymorph,[31] $Au_3(MeN{=}COMe)_3$ was further reported to exhibit solid-state cold-white-light emission with a color rendering index (CRI) of 95, correlated color temperature (CCT) of 8104 K, and CIE-1931 coordinates of (0.30, 0.30).[34] Broad dual-emission is composed of blue-turquoise direct band gap emission with a small Stokes shift (~3000 cm^{-1}) and an orange-red component with a larger Stokes shift (~8000 cm^{-1}) attributed to self-trapped excitons within the rotation disordered column-like stacks (Figures 43 and 82). To validate the

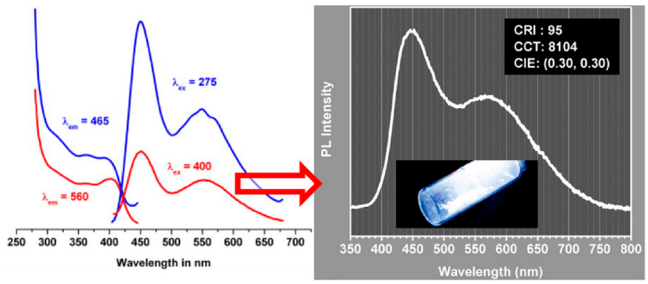

Figure 82. (Left) Solid-state photoluminescence spectra for the hexagonal polymorph of $Au_3(MeN{=}COMe)_3$ at 298 K. (Right) Inserted photograph shows the white emission color rendered upon irradiation with 365 nm irradiation from a hand-held UV lamp. [Reprinted with permission from ref 34. Copyright 2014, American Chemical Society, Washington, DC.]

preliminary device, an OFET was fabricated and a dramatic enhancement in electrical conductivity was observed upon *p*-doping with hexagonal $Au_3(MeN{=}COMe)_3$, further confirming its *p*-type semiconducting property. Moreover, by altering the substituted groups of Au_3Cb_3, the authors successfully modulated the intertrimer Au−Au distances, resulting in the tuning of the emission maxima of Au_3Cb_3 from 450 nm to 686 nm.

Intertrimer metal−metal excimeric phosphorescence of Au_3Pz_3 and Cu_3Pz_3 is restricted in the LE visible region (from yellow to red) at rt, and Ag_3Pz_3 complexes are usually

https://dx.doi.org/10.1021/acs.chemrev.0c00011
Chem. Rev. 2020, 120, 9675−9742

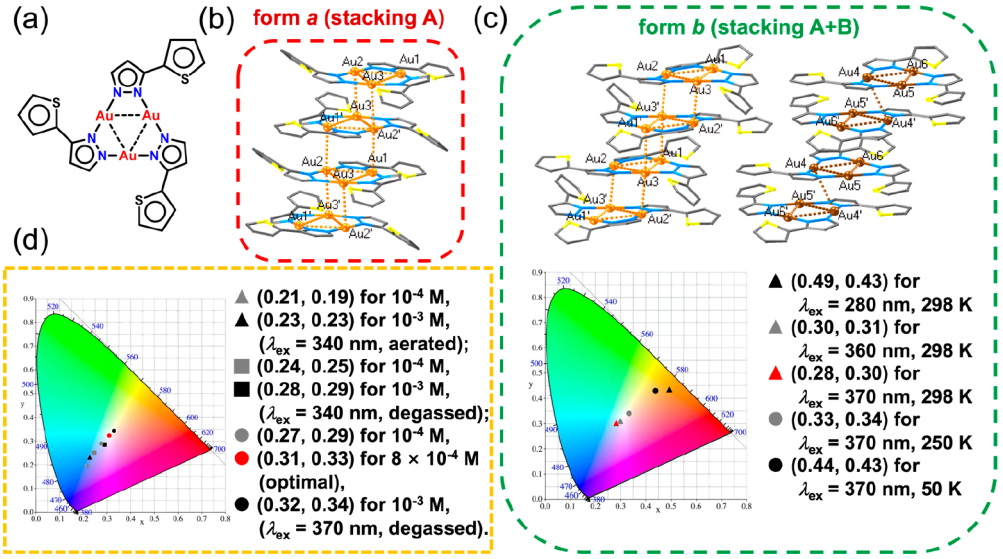

Figure 83. (a) Molecular structure formula of $Au_3[3\text{-}(2'\text{-thienyl})Pz]_3$. (b) The stacking pattern of ***a***. (c) The stacking pattern of ***b*** and its emission color profiles in CIE-1931 chromaticity diagram by varying excitation energy and temperature. (d) Corresponding emission color profiles of $Au_3[3\text{-}(2'\text{-thienyl})Pz]_3$ CH_2Cl_2 solutions in CIE-1931 chromaticity diagram. Note that natural white light at (0.33, 0.33). [Reprinted with permission from ref 35. Copyright 2013, John Wiley & Sons.]

nonemissive at this temperature. This limitation hinders the application of pyrazolate-CTCs as single-phase white-light emitters.

To overcome the above problems, Li's group proposed the *chemopalette* strategy.[35,36,47,58,59,62,66,68,153,164,178,221] The integration of two or more organic or inorganic luminophores leads to a supramolecular entity, in which different luminophores are weakly or even not coupled in their emissive states. This *chemopalette* strategy allows the modulation of dual emissions/multiemissions via internal structural modification of the luminophores (e.g., coordination environment, substituent, and guest) or the alteration of external stimuli (e.g., temperature, concentration, and excitation wavelength).

As a demonstrating example, Li and co-workers presented the only white-light emitting Au_3Pz_3 reported to date by modulating the monomer−excimer equilibrium and tuning the aurophilic interactions in $Au_3[3\text{-}(2'\text{-thienyl})Pz]_3$.[35] Two distinct packing patterns were observed in a pair of polymorphs (***a*** and ***b*** in ref 35; see Figures 83a−c): one is an extended stairlike chain with all the shortest intertrimer Au(I)−Au(I) distance of 3.161 Å (stacking A, Figure 83b), while the other is also composed of monomeric CTCs but with weak intertrimer Au(I)−Au(I) interactions (3.450 Å, stacking B, Figure 83c). Thus, by combining the HE ^{3}LC emission peak and LE excimeric emission band contributed by the ^{3}MM state, white-light emission with the CIE-1931 coordinates (0.30, 0.31) at rt could be achieved upon excitation at 360 nm (Figure 83c). The introduction of the organic chromophore−thienyl group lowers the LC excited states and then competes with the MMCT states in both the HE and LE bands. In addition, the lowest-lying ligand-based excited state exhibits a significantly lower tendency toward excimer formation, compared with the intratrimer Au−Au bonding excited state. Notably, it also shows white-light emission in the 8×10^{-4} M degassed CH_2Cl_2 solution (CIE-1931 coordinates: 0.31, 0.33) with a high QY of 41.3% upon excitation at 370 nm.

Very recently, Li's group reported the first white-phosphorescent copper trimer, the polymorph **Cl-*α*** of $Cu_3(4\text{-ClPz})_3$ in ref 36, exhibiting room-temperature emission color changes from blue, to white, and yellow with the synchronous lowering of the excitation energy from 330 nm, to 310 nm, and 270 nm, respectively.[36] Upon excitation at 310 nm, the **Cl-*α*** powder displays a broad emission band with a QY of 35.6% and CIE-1931 coordinates of (0.33, 0.37). Based on further spectroscopic studies of the low-concentration solid-state solution and TDDFT calculations, it is assumed that both the HE intratrimer Cu(I)−Cu(I) bonding monomeric species and LE intertrimer Cu(I)−Cu(I) excimeric bonding features contributed to the broad white phosphorescence. The polymorph **Cl-*β*** of $Cu_3(4\text{-ClPz})_3$ that exhibited bright room-temperature orange phosphorescence was also obtained. Moreover, the QYs approach 80% for the yellow phosphorescence of **Cl-*α*** and orange phosphorescence of **Cl-*β***, and both emission colors can be well reproduced after simply dip-coating these polymorphs onto commercially available UV-LED lamps (λ_{ex} = 260−280 nm; Figure 84).

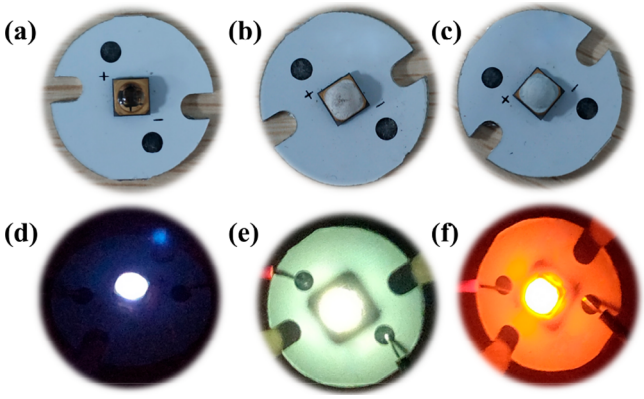

Figure 84. Photographs of (a) 260 nm reference UV LED (commercially available), (b) **Cl-*α*** and (c) **Cl-*β*** coated LEDs in off modes, the illuminating (d) reference LED in purple light, the (e) **Cl-*α*** and (f) **Cl-*β*** coated LEDs in respective bright yellow and orange light. [Reprinted with permission from ref 36. Copyright 2019, Royal Society of Chemistry, London.]

https://dx.doi.org/10.1021/acs.chemrev.0c00011
Chem. Rev. 2020, 120, 9675−9742

Another CTC-based white-light emissive complex comprising $Ag_3[3,5\text{-}(CF_3)_2Pz]_3$ and *o*TP was reported by Li's group (Figure 71).[164] Under 77 K and 326 nm excitation, this adduct shows a structured 460 nm band and broad 540 nm emission band and displays white color with the CIE-1931 coordinates (0.32, 0.34). Dual complementary emissions originate simultaneously; thus, the phosphorescence of *o*TP is sensitized by the perturbation of Ag_3 and the relative HE fluorescence of *o*TP could be maintained, because of the lack of strong interaction with Ag_3.

$Au_3[3\text{-}(2'\text{-thienyl})Pz]_3$, $Cu_3(4\text{-}ClPz)_3$ (**Cl-*α***), and the $Ag_3[3,5\text{-}(CF_3)_2Pz]_3$/*o*TP adduct presented by Li's group are representative examples of single-phase white-light-emitting and photoluminescence-color-tuning supramolecular assemblies based on pyrazolate CTCs.[35,36,164] Of interest, their dual emission band origins to approach white light are different, representing three different types of *chemopalette*. First, $Au_3[3\text{-}(2'\text{-thienyl})Pz]_3$ belongs to the most common type of *chemopalette*, which is realized by combining the M_3Pz_3 core with another luminophore. Its dual-phosphorescence bands consist of an LC monomeric peak and an Au−Au bonding excimeric peak. In the second type of *chemopalette*, both HE and LE phosphorescence bands of $Cu_3(4\text{-}ClPz)_3$ (**Cl-*α***) are relevant to the Cu−Cu bonding emissive states, arising from the excited monomer and excimer of Cu_3Pz_3. Finally, in the $Ag_3[3,5\text{-}(CF_3)_2Pz]_3$/*o*TP adduct, the white light is achieved by the combination of HE fluorescence and LE metal-sensitized phosphorescence of the *o*TP monomer.

Other efforts were made to push the CTC systems toward OLED applications. A representative strategy is phosphorescence sensitization of organic arenes via the heavy-atom effect from CTCs, proposed and developed by Rawashdeh-Omary and Omary.[2,3] For example, the phosphorescence of naphthalene is triggered at rt after adduction with $M_3[3,5\text{-}(CF_3)_2Pz]_3$ (M = Ag(I)/Cu(I)), and the adducts exhibit a much shorter emission decay time than the phosphorescence lifetime of naphthalene in the frozen solution or crystal at cryogenic temperature. Compared to fluorescent materials, phosphorescent emitters harvest 3-fold more excitons after electrical excitation and reduce energy loss, making them more promising OLED emitters. However, the shortest rt metal-sensitized phosphorescence lifetime of CTC/organic fluorophore adducts is still >700 μs, which is too long-lived for solid displays. Although Hg(II) CTCs, especially $Hg_3(o\text{-}C_6F_4)_3$, could trigger the phosphorescence of numerous organic π-electron-rich arenes to realize whole-color-region emissions at rt with considerably shorter lifetimes, their applications in lighting and display materials are highly limited, because of the high toxicity of mercury compounds.[2,5]

In 2015, Yang, Omary, and co-workers put forward another strategy related to π-acid/π-base adducts.[177] They designed a strong π-acidic Ag(I) CTC, $Ag_3[3,5\text{-}(n\text{-}C_3F_7)_2Trz]_3$, and prepared a $[Ag_3]$−PtOEP−$[Ag_3]$ adduct (PtOEP = Pt(II)-octaethyl-porphyrin). This adduct displays the strong phosphorescence of PtOEP at rt, with a relatively short lifetime of 55 μs. It is well-known that pure PtOEP is almost nonemissive in air, because of its extreme sensitivity to oxygen and concentration quenching through a strong bimolecular annihilation process.

6.3. Sensing and Detection

6.3.1. Organic Compounds. Some CTCs can easily form π-acid/π-base adducts by interacting with organic compounds in solution or contacting their vapors. Section 5.2.2 discussed the luminescence vapochromism of CTCs, while this section focuses on luminescence changes with changes in quantitative parameters including concentration and contacting time.

Omary, Gabbaï, and co-workers reported the "turn-off" luminescence sensing phenomenon of naphthalene ($C_{10}H_8$) in CH_2Cl_2 solution with increasing $Hg_3(o\text{-}C_6F_4)_3$.[251] The observed luminescence quenching is speculated to result from the spin−orbit perturbation provided from the Hg(II) CTC to the arene, suggesting the strong interaction between Hg(II) CTC and naphthalene. Based on a titration experiment, the calculated associated constant (K_{sv}) derived from Stern−Volmer analysis is 159 ± 6 M^{-1}. A similar case has been described in section 5.1.4, showing the fluorescence quenching of naphthalene in solution after the addition of the π-acidic $Ag_3[3,5\text{-}(CF_3)_2Pz]_3$.[234] The intermolecular deactivation of the bright S_1 state results from the enhanced ISC by the external heavy-atom effect of silver. The kinetic study of the Stern−Volmer analysis also yields a K_{sv} value of 94 ± 5 M^{-1} during the complexation of Ag(I) CTC and a π-basic aromatic compound. This K_{sv} value is remarkably smaller than that of the fluorescence quenching of naphthalene by the Hg(II) CTC, consistent with the smaller atomic number and thus, smaller spin−orbit constant of Ag (ξ_{4d} = 1830 cm^{-1}) vs Hg (ξ_{5d} = 4270 cm^{-1}).[234,252] The same idea was also successfully applied to the π-basic $Au_3(1\text{-}BzIm)_3$ quenching of the fluorescence of perfluoronaphthalene ($C_{10}F_8$) in solution.[208] The $C_{10}F_8$ luminescence is gradually quenched upon titration of $Au_3(1\text{-}BzIm)_3$ and Stern−Volmer analysis yields the K_{sv} value of 374 ± 5 M^{-1}. In addition, because of the constant emission decay times during the titration of all the above-mentioned cases, static quenching progresses are confirmed, along with the Stern−Volmer analyses, suggesting the formation of ground-state adducts rather than exciplexes.

The above Stern−Volmer analyses in solutions construct the relationships between the luminescence behaviors and quencher concentrations; however, such quantitative relationships are difficult to elucidate in sensing organic vapors. As a result, some qualitative studies were conducted to show luminescence changes, in terms of the contact time with organic vapors.

The luminescence vapochromism of $Ag_3[3,5\text{-}(CF_3)_2Pz]_3$ toward benzene, toluene, and mesitylene led to its potential application in sensing these organic arenes. For this propose, Rawashdeh-Omary, Dias, and co-workers fabricated a drop-cast film of this Ag_3Pz_3 on quartz plates.[39] After exposing the nonemissive dry film in organic vapors, bright luminescence was observed within minutes, exhibiting green phosphorescence with benzene and toluene and blue phosphorescence with mesitylene. By heating this luminescent film or exposing it to air at rt, the nonemissive dry film could be recovered. The reversible on/off processes could be repeated for more than 20 times without decomposition or compromise. Moreover, such real-time luminescence switching could only be observed for benzene, toluene, and mesitylene rather than the electron-deficient small organic molecule and nonaromatic solvents. Thus, Hettiarachchi, Rawashdeh-Omary, Dias, and co-workers prepared drop-cast thin films of Cu CTCs with the ligand 4-X-3,5-$(CF_3)_2Pz$ (X = Cl or Br), which exhibited emission color changes or a decrease in intensity upon exposure to π-basic aromatic molecules (recall Figure 78, *vide supra*).[136]

Apart from the kinetic study of π-acid/π-base adduct formation, CTU-based materials are also capable of sensing and detecting organic vapors. By incorporating CTCs into MOFs or PCPs, sensing for both aromatic and nonaromatic organic compounds became possible. In 2016, Song and co-

https://dx.doi.org/10.1021/acs.chemrev.0c00011
Chem. Rev. 2020, 120, 9675−9742

workers reported that a luminescent cationic MOF with $[Cu_3Pz_3][Cu_2Br_2][Cu_3Pz_3]$ (Pz = 4-(4-(3,5-dimethyl-pyrazol-4-yl)phenyl)pyridine) repeating units exhibited luminescence responses toward many volatile organic compounds (VOCs).[65] The water-treated MOF displayed noticeable luminescence turn-on behavior toward ethyl acetate, benzene, and *n*-pentane and noticeable luminescence turn-off behavior toward diethyl ether and $CHCl_3$ (Figure 85).

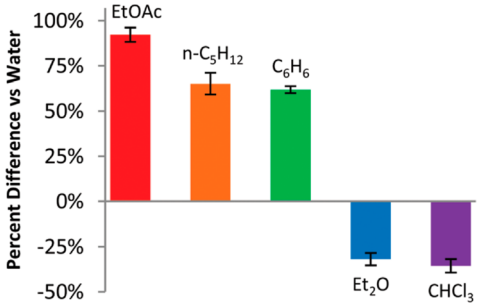

Figure 85. Selected VOC sensing results based on the solvent-treated luminescent cationic MOF in ref 63. An excitation wavelength of 469 nm was used and the luminescence response was measured at the emission maximum for each solvent treated sample. [Reprinted with permission from ref 65. Copyright 2016, Royal Society of Chemistry, London.]

6.3.2. Metal Cations. The fast binding of π-basic Au(I) CTCs with Ag(I) cations results in remarkable luminescence changes, making Au(I) CTCs promising candidates for sensing Ag(I) cations.

Recently, Marpu and Omary's group reported a phosphorescent Au CTC, Au_3(3-Me-5-COOH-Pz)$_3$, exhibiting unique selectivity and sensitivity to Ag cations in aqueous chitosan-stabilized solution (Figure 86a).[40] This chemosensor displays a new emission peak maximum in the range of 475−515 nm and 4-fold photoluminescence enhancement (19% ± 2%, compared to 5% ± 1% for sole Au CTC) upon titration with Ag cations, accompanied by an elongated lifetime. To avoid the influence brought from other metal cations, sequential additions of 15 different metal cation solutions into low-concentrated Au CTC in chitosan polymer media (≤5 μM) were conducted and a new emission only turned up after the addition of a silver salt solution. The detection limit was in the range of 6.4−72 ppb, depending on the chitosan concentration. Apart from Ag cations, Au_3(3-Me-5-COOH-Pz)$_3$ also shows sensing ability toward Tl^+, Pb^{2+}, and Gd^{3+} by changing the emission color from red to blue, cyan, and dark cyan/brighter red (different excitation wavelength), respectively, under significantly higher concentrations.

To further study the sensing behavior of Au_3(3-Me-5-COOH-Pz)$_3$, Omary's group employed Au_3(3-Me-5-COOH-Pz)$_3$ in chitosan media to differentially detect the free Ag ions (+1 valence) from the silver nanoparticles (AgNPs, zero valence).[253] The results clearly show that significant changes in the Au CTC luminescence (new intense emission peak at 475 nm) only occurred in the presence of free Ag cations, even in the presence of AgNPs. Since AgNPs will slowly decompose under ambient light and leach the Ag(I) cations in solution, the Au trimer still exhibits remarkable sensitivity toward AgNPs. In addition, the responding signal could be monitored and quantified by measuring the I/I_0 changes of the characteristic emission peak.

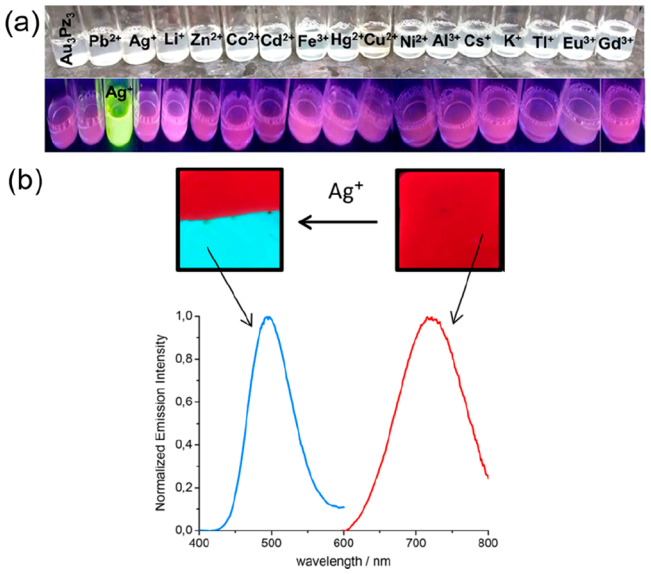

Figure 86. (a) Luminescent pictures for parent Au_3(3-Me-5-COOH-Pz)$_3$ and its mixtures with a series of metal cations in rt chitosan polymer aqueous media at pH ~6.5. [Reprinted with permission from ref 40. Copyright 2018, American Chemical Society, Washington, DC.] (b) Emission spectra (λ_{ex} = 295 nm) and photographs of a PMMA film (λ_{ex} = 254 nm) of Au_3(4-*n*-hexyl-3,5-Me_2Pz)$_3$ before and after dipping the lower half in a silver nitrate solution in MeOH. [Reprinted with permission from ref 38. Copyright 2018, American Chemical Society, Washington, DC.]

The research group of Elduque and Giménez demonstrated the response of Au_3(4-*n*-hexyl-3,5-Me_2Pz)$_3$ to Ag ions in aqueous solution.[38] Indeed, by simply dipping poly(methyl methacrylate) (PMMA) films of Au CTC into silver nitrate solution, the red luminescence (λ_{ex} = 709 nm) quickly changed into a turquoise color (λ_{ex} = 495 nm, Figure 86b). All the above-mentioned reported cases prove the specificity and selectivity of Au(I) CTCs toward Ag(I) cations in solution; however, the expense of gold materials limits the potential of these CTCs for industrial application. Because the interactions between the Au(I) CTCs and Ag(I) cations are dominated by electrostatic interactions and metallophilicity, π-basic and heterometallic Cu(I) CTCs could potentially replace their Au(I) analogues. Notably, more work on sensing and metal ion detection for CTCs and CTU-based materials is necessary.

6.3.3. pH. Omary's group studied $Au_3[3,5\text{-}(i\text{-}Pr)_2Trz]_3$ for its sensing capability toward proton concentration in solution. This is because the uncoordinated 4-position-N can be protonated in the presence of a Brønsted acid and the Au(I)−Au(I) bonded excimer would dissociate in solution, which serves as the origin of phosphorescence.[100] By adding acetic acid or trifluoroacetic acid into the Au CTC solution, the luminescence would be quenched by a loss in excitation energy or the dissociation of the dimer to two monomers in solution (Figure 87). The titration of Et_3N into the above mixture would gradually deprotonate the trimer or prevent protonation of the uncoordinated 4-position-N and recover the luminescence of the Au CTC. This reversible luminescence behavior suggests that protonation would increase the repulsion between two Au CTCs, leading to dissociation into monomers. However, the quenching by π-molecules, i.e., benzene and resorcinol, could not be recovered due to π intercalation between the two CTC monomers, in addition to the weak Brønsted acidity of resorcinol.

https://dx.doi.org/10.1021/acs.chemrev.0c00011
Chem. Rev. 2020, 120, 9675−9742

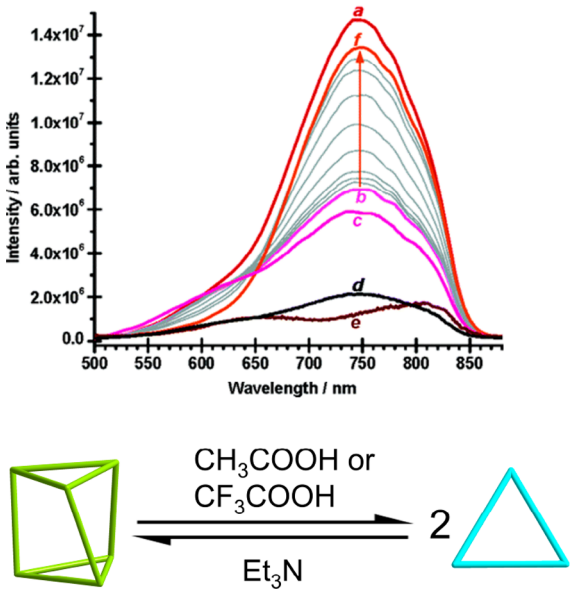

Figure 87. Change in the emission spectrum of 3.0 mL of a 5.0×10^{-3} M CH_2Cl_2 solution of $Au_3[3,5\text{-}(i\text{-}Pr)_2Trz]_3$ (trace a) upon the addition of 0.20 mL of CH_3COOH (trace b), 0.23 mL of benzene (trace c), 0.3 mg of resorcinol (trace d), or 7.0 μL of CF_3COOH (trace e). (f) Gray traces show the recovery of the quenched emission in trace b by successive additions of aliquots of Et_3N to a total of 0.21 mL. The added reagents represent 3.5, 2.6, 0.0027, 0.094, and 1.49 mmol for traces b–f, respectively. [Adapted with permission from ref 100. Copyright 2006, American Chemical Society, Washington, DC.]

6.3.4. Temperature and Pressure. In 2018, Zhan, Li, and co-workers reported a phosphorescent temperature sensor based on a sandwiched ternary adduct formulated as (Cu_3Pz_3)-$[Cu_2I_2(NH_3)_2](Cu_3Pz_3)$ (Pz = 1-methyl-tetrazol-5-ylthio)-3,5-dimethyl-pyrazolate).[178] The adduct shows potential for application as a temperature sensor, because its emission intensity exhibits a strong temperature-dependent effect with a relative sensitivity of -0.685% K^{-1} in a wide temperature range spanning from 50 K to 340 K (Figure 88).

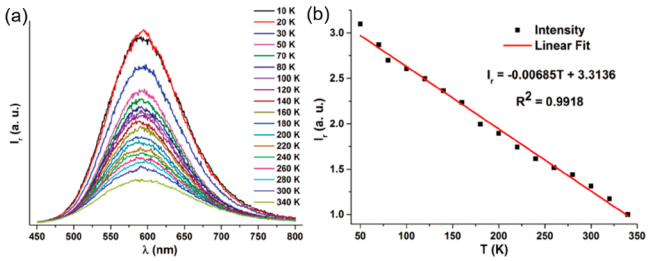

Figure 88. (a) Temperature-dependent photoluminescence spectra in the solid state upon 345 nm excitation from 10 K to 340 K, and (b) a linear fitted plot of intensity–temperature for the 50–340 K interval (I_r denotes the relative intensity). [Reprinted with permission from ref 178. Copyright 2018, Royal Society of Chemistry, London.]

Previously, Li's group reported a self-calibrated, wide-range luminescent molecular thermometer by connecting hexanuclear cages of Cu(I) CTUs (ligand = 3,5-bis((3,5-dimethyl-pyrazol-4-yl)methyl)-2,6-dimethylpyridine) with a Cu_2I_2 cluster.[47] The dual emission of such Cu_6–Cu_2-Cu_6 compounds consists of an HE ^{3}XLCT/^{3}MLCT phosphorescence band from the Cu_2I_2(pyridyl)$_2$ unit and an LE phosphorescence band from the intertrimer Cu–Cu bonding excimeric unit.

Raithby and co-workers systemically investigated the luminescence change of Au_3Pz_3 with a change in pressure by adopting a diamond-anvil cell and immersing solid samples in nujol.[117] The substituted Au_3Pz_3 (i.e., $Au_3(Me_3Pz)_3$ and Au_3(3-Me-5-PhPz)$_3$) displayed a red-shifted emission peak upon an increase in pressure and synchronous shorter Au–Au distances, indicating that the origin of luminescence is highly related to the metal–metal interactions. On the other hand, the unsubstituted Au_3Pz_3 exhibits two distinct emission peaks under high pressure, and the HE emission is relatively insensitive to pressure compared to its LE band. It is suspected that the emergence of the LE band is accompanied by a change in the electronic structure and leads to a different emitting state as the Au–Au distances decrease.

6.4. Semiconductors and Molecular Conducting Wires

In the CTC family, the first report of the semiconducting behavior was demonstrated by Rawashdeh-Omary et al. in 2001,[91] just after the report of CT complexes composed of Au_3(MeN = COR)$_3$ (R = Me, Et) and nitro-9-fluorenone derivatives including 2,7-dinitro-9-fluorenone, 2,4,7-trinitro-9-fluorenone, and 2,4,5,7-tetranitro-9-fluorenone by Balch and co-workers.[160] Their organic and metal–organic semiconducting properties were highly related to the ground-state CT, as was observed for the well-known purely organic conductor tetrathiafulvalene-tetracyanoquinodimethane (TTF-TCNQ) complex showing electrical conductance.[254] The CT adduct reported by Rawashdeh-Omary et al. shows the face-to-face stacking modes of TCNQ and the dimer-of-trimer Au_3(1-BzIm)$_3$.[91] The semiconducting property is revealed by a clear scanning electron microscope (SEM) micrograph without the conducting material coating and an apparent optical band gap (~1.4 eV) falling in the range of semiconductors rather than those of insulators and conductors. However, in the original report, they did thoroughly investigate the semiconducting properties of this unique CT complex.

Fujita and co-workers noted that CT could also be enhanced in π-acid/π-base adducts.[157] As described in Figure 35 in section 3.2.1.4, they synthesized a series of $(Au_3)_n$@cage complexes by encapsulating Au CTCs in self-assembled Pt(II) and Pd(II) coordination cages.[156,157] For $[Au_3(1\text{-}MeIm)_3]_2$@cage, the noticeable CT from Au_3(1-MeIm)$_3$ to the strong π-acidic/electron-deficient triazine panels quenches the emission of Au_3(1-MeIm)$_3$, while usually Au CTC dimers exhibit bright phosphorescence. The UV-vis spectra of $[Au_3(1\text{-}MeIm)_3]_2$@cage clearly show a strong CT band (ε = 3000 M^{-1} cm^{-1}) in solution, which diminishes after the insertion of the Ag(I) cation into $[Au_3(1\text{-}MeIm_3)]_2$, because of the significant decrease in electron density of the Pd_6 cage. With the further study of this host–guest complex, Fujita, Kiguchi, and co-workers found that inserting Ag ions into a $[3 \times 2]$ Au(I) ion cluster decreased the conductance through molecular wires by ~10-fold, from $>10^{-2}$ G_0 for the Au_3 enclosed in the cages to 3.3×10^{-4} G_0 and 0.9×10^{-4} G_0 for the Au–Ag double-decker and triple-decker sandwich complex@cages, respectively, using scanning tunneling microscope break-junction (STM-BJ) techniques (Figure 89).[41] These results further revealed that the electron transport was influenced by π-acid/π-base interaction and introduction of the Ag ions could tune the electronic properties of these host–guest complexes.

Apart from their π-acid/π-base adducts, the CTCs themselves are also suggested to display remarkable semiconducting properties, as proposed by Cundari, Omary, and co-workers in

https://dx.doi.org/10.1021/acs.chemrev.0c00011
Chem. Rev. 2020, 120, 9675–9742

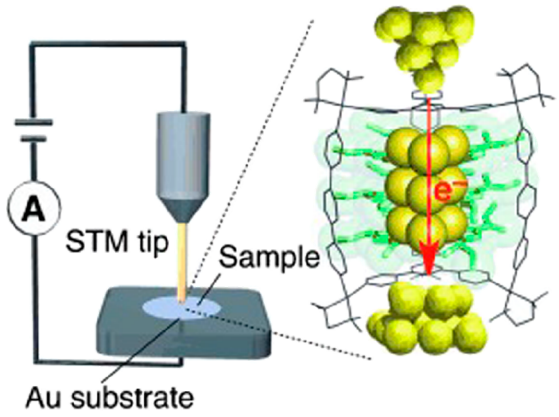

Figure 89. Schematic illustration of the experimental setup of the STM-BJ. [Reprinted with permission from ref 41. Copyright 2013, John Wiley & Sons.]

2008.[11] Their comprehensive computational studies highlight the superior π-acidity/π-basicity for CTCs, compared to the those of the well-known pure-organic semiconductors pentacene and perfluoropentacene. Because the CTC π-acidity/π-basicity can be mediated through the modification of the metal, ligand, and substituents, the energy levels of the FMOs of CTCs are highly adjustable. Strong π-acidity results in HOMOs and LUMOs with lower energies and is favorable for *n*-type semiconductors, represented by $Hg_3(o\text{-}C_6F_4)_3$, $Ag_3[3,5\text{-}(CF_3)_2Pz]_3$, and the proposed $Ag_3[3,5\text{-}(CF_3)_2Trz]_3$, which could also serve as hole blockers, because of the deep energetic HOMOs. Conversely, the strong π-basic/*p*-type semiconducting CTC $Au_3(1,4\text{-}Me_2Im)_3$, is considered to be a good candidate for exciton blocker materials in optoelectronic devices. Furthermore, besides their role as hole/exciton blockers, π-acidic/π-basic CTCs also show great potential for application as electron/hole transporting materials in OLED devices, allowing the construction of simpler device structures with fewer layers without sacrificing undue barriers.

The follow-up investigations (detailed discussion in section 5.1.5) have revealed that the solvoluminescent $Au_3(MeN{=}COMe)_3$ can act as molecular conducting wires and exhibit remarkable *p*-type field effects in OFET devices.[34] The DFT calculations conducted by Brédas and co-workers revealed a very small hole effective mass (0.21 m_0) for this CTC, along with the stacking directions of the $[Au_3]$ species.[239] Thus, the small hole effective mass would allow efficient hole transfer within the 1D confined column anisotropically. In addition, 5- to 6-fold larger electron effective masses (~1 m_0), comparable to the highest value reported in organic molecular semiconductors (i.e., pentacene), should allow the isotropic character of electron transfer. Based on these findings, the hexagonal polymorph of $Au_3(MeN{=}COMe)_3$ is suggested as a promising ambipolar material in the field of optoelectronic devices.

6.5. Soft Materials

6.5.1. Liquid Crystals. Because of the easy introduction of mesophases and wide tunability of mesoscopic materials, the synthesis of mesogenic coordination complexes from non-mesogenic ligands has been an emerging topic in the field of soft materials. The first series of liquid crystal trials in the field of CTCs was approached by Barberá et al. in 1996 and 1998 and Kim et al. in 1998.[131−133] Barberá and co-workers succeeded in preparing the Au CTC with multiple *n*-decyloxyl ($n\text{-}C_{10}H_{21}O$)-substituted phenyl groups attached to the pyrazolate ligand, which showed stable columnar mesophases and liquid crystal properties.[131,132] Characteristic fan-shaped and pseudofocal-conic textures were observed under polarized light by optical microscopy, further confirming the formation of hexagonal columnar mesophases. Kim and co-workers employed a different molecular design strategy by introducing long-chain alkyl groups to the 4-positions of the pyrazolate ligands, and two Au_3Pz_3 complexes with monotropic mesophases were obtained.[133] One of them, $Au_3[4\text{-}(n\text{-}C_8H_{17})\text{-}3,5\text{-}Me_2Pz]_3$, can form single crystals for X-ray analysis by slow diffusion of THF into its EtOH solution. Thus far, this is the only case of CTC that can exist in both single-crystalline and liquid crystalline forms.

The idea of preparing the CTCs with $n\text{-}C_{10}H_{21}O$-substituted phenyl groups attached to pyrazolate ligands was adopted by Cano and co-workers in 2004.[134] Only Au(I) and Ag(I) CTCs with nonmesogenic asymmetric pyrazolate ligands (3-(4′-$C_{12}H_{25}O$)PhPz) exhibit liquid crystal properties in the presence of columnar mesophases. On the other hand, those of the parent 3,5-position symmetric pyrazolate ligands behave as non-mesogenic materials, because of the absence of periphery alkyl chains. They also reported the liquid crystal properties of Ag(I) CTCs bearing mesomorphic and nonmesomorphic pyridyl-pyrazolate.[255] $Ag_3[3\text{-}(2'\text{-pyridyl})\text{-}5\text{-}(PhOC_nH_{2n+1})Pz]_3$ (n = 12, 16, and 18) shows crystalline polymorphism enantiotropic smectic A (SmA) mesophases when heated to ~100 °C and partial decompositions are observed at temperatures approaching isotropization. Moreover, focal conic and fanlike domains are observed under polarized optical microscope cooling from the isotropic liquid.

Although Kim et al. have proven that a CTC with liquid crystal properties could be constructed by only introducing three aliphatic side chains,[133] all the other CTCs exhibiting liquid crystalline states were constructed with $n\text{-}C_nH_{2n+1}O$-substituted phenyl groups attached to the pyrazolate ligands[131,132,134,255,256] or pyrazole-anchored poly(benzyl ether) dendrons (Aida et al.,[130] vide infra). Although some of them show good crystallinities, the efforts in obtaining single crystals failed, except for $Au_3[4\text{-}(n\text{-}C_8H_{17})\text{-}3,5\text{-}Me_2Pz]_3$. As alternatives, to elucidate the molecular stacking of some CTCs with liquid crystal properties, single crystals of their analogues with short-chain substituents were produced to compare the diffraction patterns, even though they did not show liquid crystalline character. Therefore, the importance of long-chain substituents in obtaining CTCs with liquid crystal properties have been demonstrated. Furthermore, it was found that the mesophase temperature ranges could be controlled by tuning the chain substitution (i.e., altering the long-chain substituents with different lengths).[133,256]

6.5.2. Dendrons/Dendrimers. Dendrimers are molecules with repetitively branched components and are usually highly symmetric. Typically, dendrimers contain a chemically addressable group, namely, the focal point, which can be accessible by branched substitutes. The focal point is composed of a spherically symmetric node, while in the CTC family, the metallotriangles serve as the focal point, and substituents on the coordinated ligands are considered as branched points. In 2001, Aida's group reported a family of Cu(I)/Ag(I)/Au(I) CTCs comprising pyrazole-anchored poly(benzyl ether) dendron ligands and expanded the generation number from two to four.[130] For their reported CTCs with a generation number of two, a white fibrous precipitate with a helical structure was formed upon cooling to rt, even though the CTC itself is devoid of chiral centers (Figure 90). The SEM micrographs clearly

https://dx.doi.org/10.1021/acs.chemrev.0c00011
Chem. Rev. 2020, 120, 9675−9742

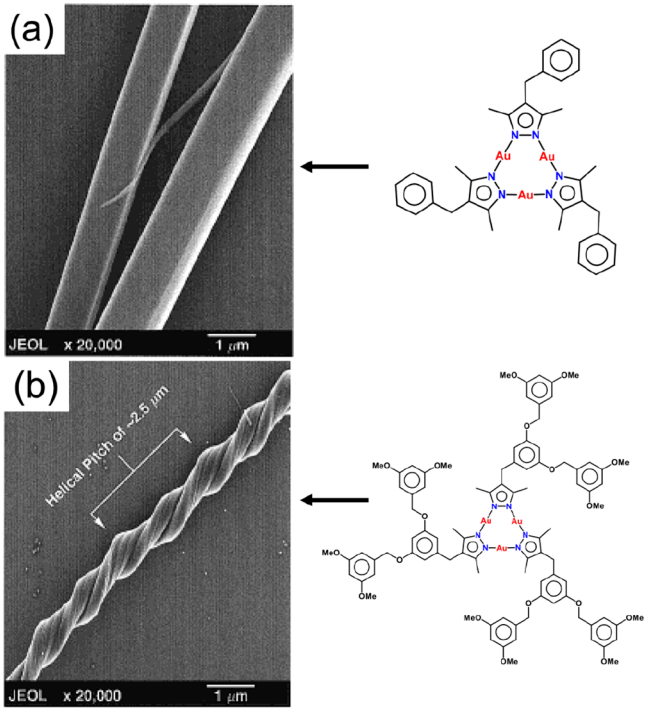

Figure 90. SEM images of self-organized structures formed upon heating paraffin suspensions of (a) $Au_3(4\text{-Bz-}3,5\text{-}Me_2Pz)_3$ and (b) a Au_3Pz_3 anchoring poly(benzyl ether) dendrons at 200 °C, followed by cooling to rt. [Adapted with permission from ref 130. Copyright 2001, American Chemical Society, Washington, DC.]

show superhelical fibers twisted by a bundle of elementary fibrils (~0.2 μm in diameter) with a helical pitch of ~2.5 μm. However, higher generation numbers (three and four) of dendritic CTCs only give nonfibers, and it is postulated that the formation of superhelical fibers requires the balance between reduced steric repulsion by edge-to-edge stacking and vdW interactions among the dendritic wedges.

Aida's group presented a phosphorescent organogel showing reversible RGB color switching based on a dendritic Au(I) pyrazolate CTC (ligand = 4-(3,5-dioctadecyloxybenzyl)-3,5-dimethylpyrazolate).[32] The red-emissive organogel displayed blue luminescence after a small amount of Ag(I) ion was dropped on it, attributed to the formation of a Au_3–Ag sandwich-like adduct without disrupting the gel. Recovery was attained by removing the Ag(I) ions by precipitation (Figure 91). Upon heating, the organogels undergo a gel-to-sol transition and dissociation of the metal–metal interactions/bonding, resulting in weak luminescence for the non-Ag(I)-doped system and green phosphorescence for the Ag(I)-doped solution. Both solutions without or with Ag(I) ions would also undergo sol-to-gel transition with the respective emission color changes hardly detectable to red and green to blue.

Aida's group also demonstrated the formation of a rewritable phosphorescent paper, by utilizing the temperature-sensitive self-assembly of dendritic Cu(I) pyrazolate CTCs (ligands in Figure 92) and blue-emissive polyethylene terephthalate (PET)

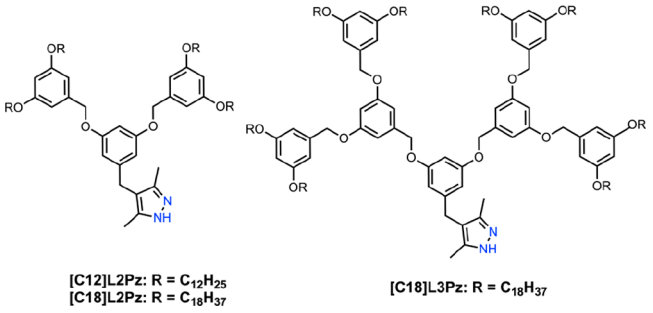

Figure 92. Molecular structures of dendritic pyrazoles in ref 257. ([C*n*]L*m*Pz; *n* = 12, 18; *m* = 2, 3). L*m* = the number (m) of dendritic layers, Pz = pyrazolate.

paper.[257] The naturally cooled $Cu_3([C18]L2Pz)_3$ melt emits a weak red phosphorescence centered at 650 nm, while slow-cooling of the hot melt leads to an intense yellow phosphorescence centered at 615 nm. The red and yellow luminescence observed for $Cu_3([C18]L2Pz)_3$ could be thermally switched. Thus, after coating PET paper with Cu(I) CTC containing a polymer support, the rewritable phosphorescent paper behaves as follows: predominant emission is blue, from the polymer paper (background), since the red phosphorescence of Cu(I) CTC is rather weak. After printing with a thermal facsimile-type printer, the emission of Cu(I) CTC changes to intense yellow luminescence and combines with the blue background. This results in pink emission and thus, a stark contrast in emission color between the intact and printed

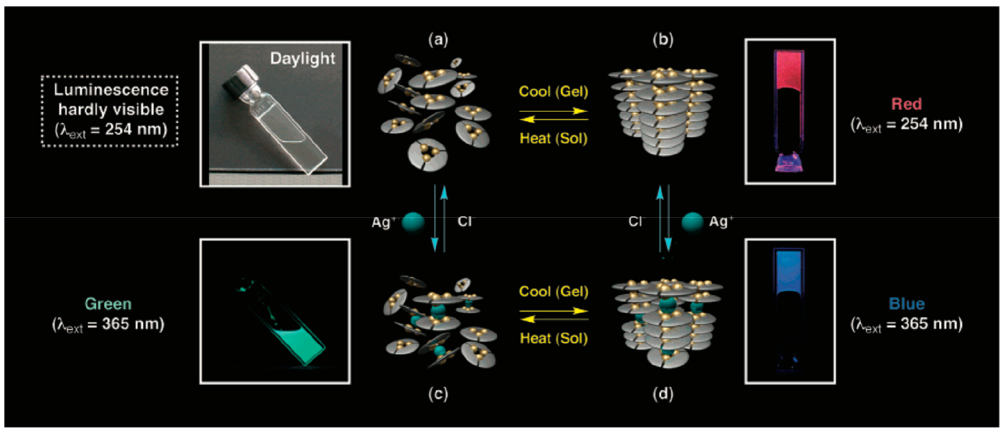

Figure 91. Luminescence profiles of the Au_3Pz_3 in hexane. Photographs and schematic self-assembling structures of (a) sol, (b) gel, (c) sol containing AgOTf (OTf = trifluoromethanesulfonate) (0.01 equiv), and (d) gel containing AgOTf (0.01 equiv). [Reprinted with permission from ref 32. Copyright 2005, American Chemical Society, Washington, DC.]

https://dx.doi.org/10.1021/acs.chemrev.0c00011
Chem. Rev. 2020, 120, 9675–9742

domains is observed. When the paper is heated to 40−50 °C, the printed domains age and spontaneously retrieve the pink emission. Thus, the paper reverts to its blue luminescence, identical to the original, and is ready for reuse.

Kinbara, Aida, and co-workers realized a self-healing/repairing material by confining cyclic trinuclear Au(I) complexes in 1D hexagonal silicate channels (Figure 93).[258]

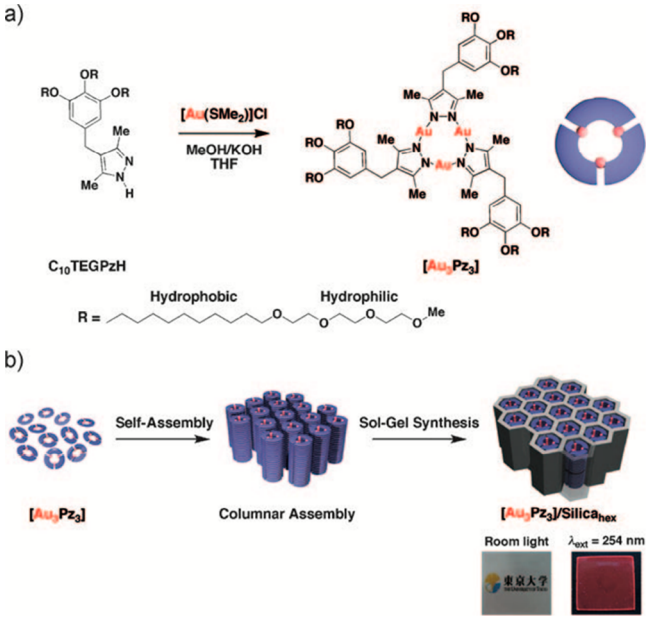

Figure 93. (a) Synthesis and molecular structure of Au_3Pz_3. (b) Sol−gel synthesis of $[Au_3Pz_3]$/silicahex, a mesostructured silica with a hexagonal geometry templated by columnarly assembled $[Au_3Pz_3]$. Photographs were taken at room temperature (lower left) under room light and upon exposure to UV light at 254 nm (lower right). [Reprinted with permission from ref 258. Copyright 2010, John Wiley & Sons.]

Without the protection of mesoporous silica, the red phosphorescent dendritic Au(I) CTC undergoes a sol-to-gel transition upon heating from 20 °C to 140 °C, followed by a dramatic drop in luminescence intensity, and neither gel structure nor phosphorescence could be recovered completely by cooling. However, by confining the dendritic Au(I) CTC into the hexagonal nanoscopic channels of mesoporous silica, because of the nanoscopic template effect, both the gel structure and emission intensity of the sample could be fully self-healed by cooling to 20 °C for 5 h after heating to 140 °C. Nevertheless, the negative effect on the self-healing/repairing of the luminescence and gel structure is observed when the lamellar structures are formed in the confined silicate layers.

6.6. Interfacial Supramolecular Assemblies

The study of the liquid/solid interface has grown into an emerging field of nanoscience and nanotechnology, as spontaneous assembly behaviors will provide us with a great insight into the dynamic processes, such as morphologic control, diffusion, and adsorption/desorption. In 2013, Swager's group described the first report of cyclic trinuclear Au(I) pyrazolate complexes on the graphite/1-octanoic acid interface at the molecular level.[259] Two Au(I) CTCs containing long alkyl chains (ligand = 3,5-$(C_nH_{2n+1})_2$Pz, n = 12, 18) form ordered layers after dropping on the graphite surface under both low and high concentrations (1×10^{-6} M to 1×10^{-3} M). However, the packing modes (monomeric or dimeric) are highly dependent on the ligand lengths and concentration, as confirmed by scanning tunneling microscopy (STM) technology. Moreover, the dimeric packing of Au(I) CTC bearing a $C_{18}H_{37}$-functionalized pyrazolate ligand is chiral and two enantiomeric domains exist, even in this achiral molecule.

In 2015, more self-assembly surface behaviors were discovered in the CTC family, including $Au_3[3,5\text{-}(COOEt)_2Pz)]_3$ and $Au_3[MeN{=}CO(n\text{-}Pr)]_3$, by Chilukuri, Omary, Hipps, and co-workers (Figure 94).[207] Both Au CTCs

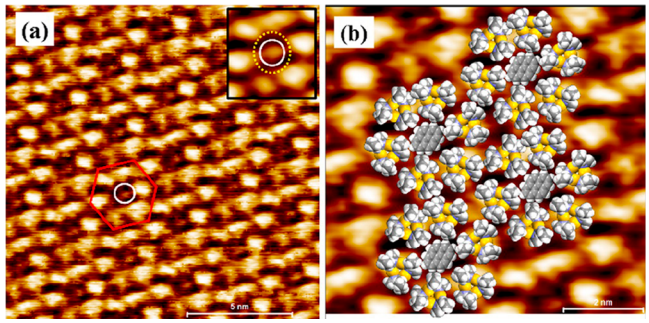

Figure 94. (a) STM image (−0.4 V and 60 pA set point) of a closed structure (CS) Au_3Cb_3 monolayer on HOPG with pyrene molecules at the center of CS. The red hexagon represents the unit cell; the inset at the top right corner represents a high-resolution image of each CS. The dotted yellow circle represents a nanopore, and the solid white circle represents a pyrene molecule. (b) Correlation-averaged CS STM image with proposed models of $Au_3[MeN{=}CO(n\text{-}Pr)]_3$ and pyrene laid on top. Pyrene molecules can be clearly seen at the center of each CS. [Reprinted with permission from ref 207. Copyright 2015, American Chemical Society, Washington, DC.]

form a monolayer on the highly oriented pyrolytic graphite (HOPG) (0001) substrate and lie flat on the surface, which suggests that the strong binding energy between Au and HOPG prevents the formation of Au(I)−Au(I) interactions. Au_3Pz_3 only displayed a uniform binding structure with HOPG, while Au_3Cb_3 assembles into a less-dense kinetically favored open structure (OS) and a denser thermodynamically favored closed structure (CS) on the interface. A porous network forms in the hexagonal closed structure and the pore is present at the center of six Au_3Cb_3 units with a diameter of ∼9.5 Å, where the pyrene molecules lie flat at the center of a pore without a detectable lattice change.

Taking advantage of the HOPG substrate in supporting Au CTCs, Esser and co-workers studied surface coadsorption using HOPG/Au_3Py_3 composites.[26] The functionalized HOPG is used to sense and detect the π-acidic $M_3[3,5\text{-}(CF_3)_2Pz]_3$ by donor−acceptor interactions between the π-electron systems. NMR titration experiments revealed that the binding energies of HOPG/Au_3Py_3 and π-acidic CTCs fell between −6.1 kcal/mol and −7.5 kcal/mol, which is recognized to be dominated by London dispersion forces, as suggested by high-level quantum calculations. This work also facilitates the further rational design of sensitive carbon nanotube (CNT)- or graphene-based sensors for π-acidic analytes.

To attain further insight into the binding modes and energies of aromatic donor−acceptor interaction, Esser's group also reported studies of reaction between a Au(I) Py/Im/Cb CTC and π-acidic $M_3[3,5\text{-}(CF_3)_2Pz]_3$ (M = Au(I), Ag(I), or Cu(I)) or organic π-acceptors.[27] NMR and UV-vis titration studies reveal binding free energies down to −10.1 kcal/mol and

https://dx.doi.org/10.1021/acs.chemrev.0c00011
Chem. Rev. 2020, 120, 9675−9742

association constants up to 2.34×10^7 M^{-1}, which are three orders of magnitude larger than those of known π-donor/π-acceptor adducts. In addition, by rational design of the acceptors, the molar ratio in the adducts could be fixed at a 1:2 (donor/acceptor) model to quantify the type and strength of interactions, also described by the London dispersion force.

6.7. Gas or Liquid Adsorption

In 2013, Galassi, Burini, Omary, and co-workers reported the remarkable tendency of $Ag_3[3,5\text{-}(NO_2)_2Pz]_3$ to form adducts with acetone, acetylacetone, ammonia, pyridine, acetonitrile, Et_3N, and Me_2S at rt and atmospheric pressure.[120] In addition, the interactions between $Ag_3[3,5\text{-}(NO_2)_2Pz]_3$ and ammonia led to the formation of $[Ag(NH_3)_2][Ag_3(3,5\text{-}(NO_2)_2Pz)_4]$ crystals with both cationic and anionic coordination units, thus representing an irreversible chemisorption toward ammonia gas. In contrast, the less π-acidic $Ag_3[3,5\text{-}(CF_3)_2Pz]_3$ does not adsorb the above-mentioned guest molecules, because of the significantly less polarizable ESP and strong Ag−Ag bonding, the energy of which is even higher than the quadrupole−dipole adduct bond energy.

Very recently, Chen, Yang, and co-workers discovered the potential application of $Ag_3[3,5\text{-}(CF_3)_2Pz]_3$ in the desulfurization of fossil fuels.[165] This Au_3Pz_3 complex could form binary adducts with heterocyclic aromatic sulfur compounds by multiple noncovalent interactions (e.g., π-acid/π-base, Ag−S, and Ag−C contacts; see Figure 95a). The high solubility of

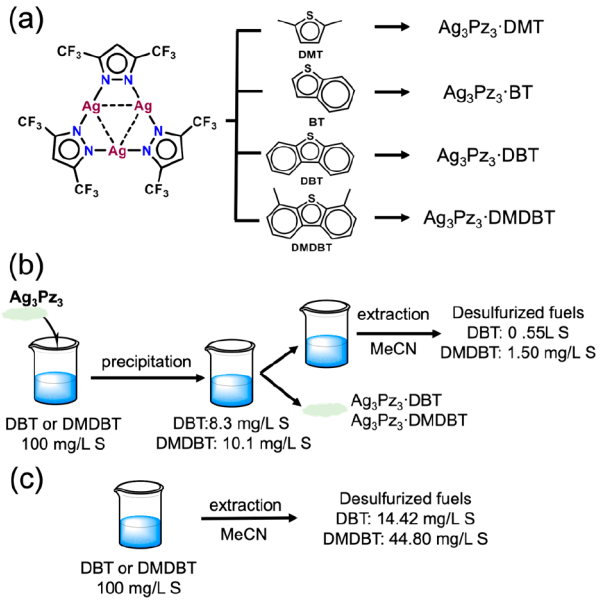

Figure 95. (a) $Ag_3[3,5\text{-}(CF_3)_2Pz]_3$ and its binary adducts with heterocyclic aromatic sulfur compounds. Also shown are schematic diagrams of (b) precipitation−extraction and (c) acetonitrile extraction schemes. [Reprinted with permission from ref 165. Copyright 2019, Royal Society of Chemistry, London.]

$Ag_3[3,5\text{-}(CF_3)_2Pz]_3$ and low solubilities of its adducts with dibenzothiophene (DBT) and 4,6-dimethyldibenzothiophene (DMDBT) in many organic solvents allows the precipitation−extraction process for the removal of these heterocyclic aromatic sulfur compounds from model oils (see Figures 95b and 95c). Notably, DBT and DMDBT are two of the most difficult molecules to remove from liquid fuels by the widely used hydrodesulfurization (HDS) technology. In addition, the relatively weak π-acidity of $Ag_3[3,5\text{-}(CF_3)_2Pz]_3$ facilitates its recycling after forming an adduct with heterocyclic aromatic sulfur compounds. However, the less expensive Cu CTCs may be more promising in the practical application of fossil fuel desulfurization than their Ag analogues. Therefore, more efforts toward enhancing the binding of Cu CTCs with heterocyclic aromatic sulfur compounds are predicted.

In 2018, Cowan, Dias, and co-workers presented the reversible chemisorption/desorption of ethylene gas by an unusual reversible rearrangement between Cu_3Pz_3 and $Cu_2Pz_2(C_2H_4)_2$ in the solid state (Pz = $(CF_3)_3Pz$; see Figure 96).[28] The overall heat of adsorption (13 ± 1 kJ mol^{-1} per Cu−

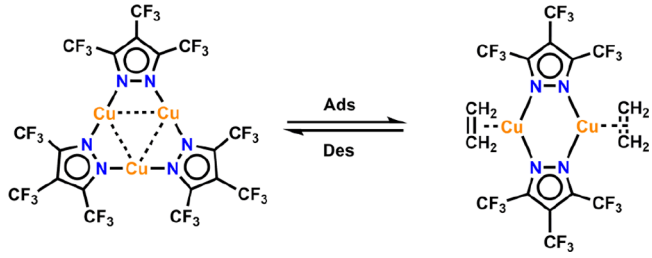

Figure 96. Reversible molecular rearrangement of $Cu_3[(CF_3)_3Pz]_3$ during the adsorption (Ads)/desorption (Des) process toward ethylene.

C_2H_4 interaction) is noticeably lower than that of the Cu−C_2H_4 interactions (24 kJ mol^{-1}). The low overall heat of adsorption, "step" isotherms, high ethylene capacity (2.76 mmol g^{-1}; 7.6 wt % at 293 K), and high ethylene/ethane selectivity (136:1 at 293 K) make $Cu_3[(CF_3)_3Pz]_3$ an interesting substance for the rational design of materials for LE ethylene/ethane separations.

The above-mentioned two cases as well as those discussed in section 3.2.1.2 have highlighted the remarkable binding tendency of strong π-acidic Ag(I) and Cu(I) CTCs toward organic σ- and π-donors in the gas phase and in solution. This strong binding tendency results from the incorporation of strong π-acidity and coordinated UMCs. By taking Ag_3Pz_3 or Cu_3Pz_3 units as SBUs, a series of binary,[54,55,60,63] ternary,[61] and quaternary[67] PCPs and MOFs with excellent performances in gas and liquid adsorption has been constructed, as demonstrated in section 4.4.3. Moreover, the thermal and/or chemical stabilities could be remarkably enhanced, compared to those of the parent CTCs, after constructing 3D CTU-based frames.

Kitagawa's group subsequently investigated the syntheses, supramolecular isomerism, and properties of four highly flexible isomorphous/isomeric Ag(I) and Cu(I) frameworks based on CTUs,[54,55] two of which are M(I) MOFs with a less-porous 8-fold interpenetrated **nof** topology and two of which are M(I) MOFs with a more-porous 4-fold interpenetrated **srs** topology. The strong coordination bonds and multiple interpenetration render these materials with exceptionally high thermal and chemical stabilities. For example, the Cu(I) framework with **srs** topology presents thermal stabilities of ≤500 °C, and only the Cu(I) cations on the crystal surface are oxidized after exposing the sample to air for a month.[55] With respect to gas absorption, the Ag(I) framework with **srs** topology exhibits a single-crystal-to-single-crystal transformation after readily adsorbing small aromatic molecules (e.g., benzene, toluene). The SCXRD analysis shows that arene monomers, dimers, or trimers are sandwiched by two Ag_3 planes. In addition, the **srs** M(I) frameworks exhibit higher affinities for C_2H_2 than for CO_2, compared with the less-porous **nof** M(I) frameworks. Similar high affinities for unsaturated hydrocarbons are also observed in

https://dx.doi.org/10.1021/acs.chemrev.0c00011
Chem. Rev. 2020, 120, 9675−9742

an exceptionally stable and water-resistant MOF bearing both Cu_3Pz_3 and Cu_4Pz_4 (Pz = 3,3′,5,5′-tetraethyl-4,4′-bipyrazolate) units, which was reported in 2014 by the Li group.[63]

The remarkably high thermal and chemical stabilities also favor the usage of Cu(I) CTU-based MOFs as redox catalysts. A recent case comprises the five quaternary mixed-Cu(I)/Zn(II) mixed-ligand MOFs reported by Li in 2017.[67] Significant catalytic activities are observed in the oxidation of CO and aromatic alcohols and decomposition of H_2O_2. Although the Cu(I) CTUs of these MOFs easily undergo partial oxidation in wet air, heating the partially oxidized samples to 200 °C under vacuum or 160 °C in *N*-methyl-2-pyrrolidone (NMP) results in the recovery of the Cu(I) CTUs. To the best of our knowledge, such Cu(II) CTC to Cu(I) CTC reductions have not yet been reported.

6.8. Concluding Remarks

Coinage-metal-based CTCs are open to a vast area of applications from the past decades to the future, with combinations of multiple advantages in chemical and physical aspects. Most CTC applications to date are related to their superior metal−organic or organometallic π-acid/π-base properties. As discussed herein, Ag(I) CTCs are inherently much more π-acidic than their Cu(I) and Au(I) analogues. The strong π-acidity/basicity as well as metallophilicity and other noncovalent interactions endow CTCs with good performances in a series of applications, including but not limited to (i) fast and selective luminescence responses toward metal cations in organic solvents and/or aqueous solutions or the vapors of arenes and their derivatives; (ii) the removal of air/water pollutants (e.g., NH_3, heterocyclic aromatic sulfur compounds); and (iii) *p*-type semiconductors in OFET devices and molecular wires.

In addition to their π properties, the feasible extensions and modifications of CTCs cannot be neglected as ligand substituents play essential roles in the field of soft materials. It is in prospect that more designed ligands applied to CTCs and new application scenarios would broaden requirements and possibilities.

Unfortunately, drawbacks including stability, toxicity, and expense issues still exist. The catalytic abilities of Cu(I) CTCs have been demonstrated in click reactions and alkyne transformations; however, these CTCs cannot retain nine-membered conformations. Although Hg(II) CTCs are also proven efficient in catalyzing phase-transfer nitration of aromatic substrates,[260,261] the toxicity of Hg complexes should be carefully treated. For coinage-metal-based complexes, the expense is a problem that cannot be bypassed. To satisfy this requirement, Cu(I) CTCs and Cu(I)-CTU-based materials should be considered as replacements for their Au(I) and Ag(I) analogues to reach identical or similar performances and functions.

7. CONCLUSION AND OUTLOOK

Research in the field of coinage-metal-based CTCs has been underway for over half a century. In the nonage of this area, before the 2000s, limited researchers and groups mainly focused on syntheses and structural characterizations, during which some interesting findings, including reactivities and solvoluminescence, were discovered. During the next stage, achievements in photophysical properties, metallophicity, and π-acid/base properties were gained. The discovery and comprehension of metal−metal bonding/interaction-dominated phosphorescence were considered as huge steps, because of the links between molecule design, electronic structures, and luminescent properties. Later in 2008, guidelines for modulating the π-acidity/basicity of CTCs were put forward by theoretical studies and further confirmed by fruitful experimental results, including π-acid/π-base adducts and sandwich-like mixed-metal clusters. The recent decade witnessed the rise of CTU-based coordination cages and polymers and more attempts to applications, some of which, such as semiconductors, chemiadsorbents, and luminescent *chemopalettes*, exhibit down-to-earth practicality.

As an emerging class of metal−organic optoelectronic materials, the combination of metal−metal interactions and highly adjustable π-acidity/basicity provide great potential for coinage-metal-based CTCs to exhibit a better performance than those of organic optoelectronic materials. Maximizing the π-acidity/basicity, such as attaching electron-withdrawing groups to Ag(I)-Trz CTCs and electron-donating groups to Au(I)-Im/Py CTCs, will benefit their hole/electron mobilities, CT abilities, and donor−acceptor interactions. The strategy could also be adopted to develop new electronic devices or simplify device structures by combining two or more layers into one multifunctional layer. More work is needed to optimize the CTC performance, in relation to optoelectronic devices and fabrications.

The combination of Lewis acidity and superior π-acidity/basicity has opened a vast area of functional acid/base adducts and novel products. Apart from π-acidity/basicity, because of the unsaturated metal centers of intermediate oxidation state, the CTCs display high reactivities, implying that CTCs can be good candidates for catalytic applications. Recent studies have highlighted the catalytic activities of π-acidic Cu_3Pz_3 complexes in many reactions; however, Cu_3Pz_3 complexes are sensitive toward oxygen, moisture, and light and might undergo irreversible molecular rearrangement and oxidation, resulting in difficulties in the identification of catalytic species. Therefore, catalytic mechanism studies are highly challenging and remain unexplored. Because of improvements in chemical and thermal stabilities and the restrictions of irreversible molecular rearrangement, CTU-based MOFs with high catalytic activities might address these issues. The design and synthesis of CTU-based reticular materials for catalytic application and further elucidation of the mechanism would be an emerging area.

The cooperation and competition of metallophilicity and other noncovalent interactions, inherency and inheritance of π-acidity/basicity and aromaticity, concordance and contradiction of electronic structures in the excited states, and chance and challenge of higher-nuclearity and higher-dimension complexes are enclosed and discussed in this Review, with the hope to bring new dimensions and opportunities in multidisciplinary research. More prospects of investigations in fundamental physical and chemical principles, performance optimization, and practical applications remain flourishing and are expanding.

ASSOCIATED CONTENT

Supporting Information

The Supporting Information is available free of charge at https://pubs.acs.org/doi/10.1021/acs.chemrev.0c00011.

Summaries of X-ray crystal structures of the Au(I)/Ag(I)/Cu(I) CTCs and their co-crystals, as well as luminescence properties of Au(I)/Ag(I)/Cu(I) CTCs and CTU-based materials (PDF)

https://dx.doi.org/10.1021/acs.chemrev.0c00011
Chem. Rev. 2020, 120, 9675−9742

AUTHOR INFORMATION

Corresponding Authors

Guo-Hong Ning − *College of Chemistry and Materials Science, Guangdong Provincial Key Laboratory of Functional Supramolecular Coordination Materials and Applications, Jinan University, Guangzhou 510632, People's Republic of China;* orcid.org/0000-0002-5640-9062; Email: guohongning@jnu.edu.cn

Dan Li − *College of Chemistry and Materials Science, Guangdong Provincial Key Laboratory of Functional Supramolecular Coordination Materials and Applications, Jinan University, Guangzhou 510632, People's Republic of China;* orcid.org/0000-0002-4936-4599; Email: danli@jnu.edu.cn

Authors

Ji Zheng − *College of Chemistry and Materials Science, Guangdong Provincial Key Laboratory of Functional Supramolecular Coordination Materials and Applications, Jinan University, Guangzhou 510632, People's Republic of China*

Zhou Lu − *College of Chemistry and Materials Science, Guangdong Provincial Key Laboratory of Functional Supramolecular Coordination Materials and Applications, Jinan University, Guangzhou 510632, People's Republic of China;* orcid.org/0000-0002-6447-4905

Kun Wu − *College of Chemistry and Materials Science, Guangdong Provincial Key Laboratory of Functional Supramolecular Coordination Materials and Applications, Jinan University, Guangzhou 510632, People's Republic of China;* orcid.org/0000-0002-2357-3288

Complete contact information is available at: https://pubs.acs.org/10.1021/acs.chemrev.0c00011

Author Contributions

The manuscript was written through contributions of all authors. All authors have given approval to the final version of the manuscript.

Notes

The authors declare no competing financial interest.

Biographies

Ji Zheng was born in Guangdong, China. He received his B.Sc. degree in 2009, M.Sc. degree in 2012, and Ph.D. degree in 2016 from Shantou University, under the supervision of Prof. Dan Li. After working with Prof. Dan Li as a postdoctoral fellow at Jinan University, he became a Lecturer from July 2020 in the College of Chemistry and Materials Science at the university. His current research interest includes the cooperation and competition of multiple noncovalent interactions in the ground and excited states of d^{10} coinage-metal-based cyclic trinuclear complexes and the related optoelectronic properties.

Zhou Lu was born in Jiangsu, China, in 1994. After receiving his B.Sc. in Chemistry under the supervision of Prof. Dan Li in Shantou University in 2016, he served as a research assistant in the same group in Shantou University and Jinan University successively in the following two years. Currently, he is a postgraduate student in University of North Texas, in the United States, and his research interests focus on the electronic structures, metal−metal bonding, aromaticity, and excited-state properties of d^{10} metal complexes and related applications.

Kun Wu was born in Henan, China. He received his B.Sc. degree from Zhengzhou Normal University at Henan in 2018. Currently, he is a M.Sc. student in Prof. Dan Li's laboratory at Jinan University. As a graduate student, Kun Wu is focusing on the investigations of photoluminescent metal−organic frameworks (MOFs) and related potential applications (e.g., chemical sensing, solid-state lighting and display).

Guo-Hong Ning is currently a Professor in the College of Chemistry and Materials Science at Jinan University. He obtained his B.Sc. degree from Hunan Normal University in 2007, and he received his M.Sc. degree from Renmin University of China and his Ph.D. degree from The University of Tokyo, under the supervision of Prof. Makoto Fujita. During the period of 2013−2015, he held a JSPS postdoctoral fellowship at The University of Tokyo, working with Prof. Makoto Fujita. Prior to joining Jinan University, he worked as a postdoctoral associate with Prof. Loh Kain Ping at National University of Singapore (2015−2017) and with Prof. Andrew I. Cooper (FRS) at The University of Liverpool (2017−2018). His primary research interests focus on function-led porous crystalline materials.

Dan Li received his B.Sc. degree from Sun Yat-Sen University in 1984 and then worked at Shantou University. He pursued his Ph.D. at The University of Hong Kong with Professor Chi-Ming Che during the period of 1988−1993. He then returned to Shantou University and became Professor in 2001. He moved to Jinan University in Guangzhou in 2016. He was a recipient of the National Science Found for Distinguished Young Scholars of China in 2008 and was a Fellow of The Royal Society of Chemistry (FRSC) in 2014. He has been working in the field of supramolecular coordination chemistry and focuses his research interest on the design and fabrication of supramolecular coordination assemblies and their functions, including photoluminescence, porosity, and chirality.

ACKNOWLEDGMENTS

This work was financially supported by the National Natural Science Foundation of China (Nos. 21731002 and 21975104), the Guangdong Major Project of Basic and Applied Research (No. 2019B030302009). G.-H. Ning thanks for the financial support from Guangdong Basic and Applied Basic Research Foundation (No. 2019B151502024), Guangdong Province Pearl River Scholar Funded Scheme (2019), and the Fundamental Research Funds for the Central Universities (No. 21619315).

ABBREVIATIONS

AICD	anisotropy of the induced current density
AIE	aggregation-induced emission
An	anthryl
BET	Brunauer−Emmett−Teller theory
Bz	benzyl
Cb	carbeniate
CC	cluster-centered
CNT	carbon nanotube
Cp	cyclopentadienyl
Cp*	1,2,3,4,5-pentamethylcyclopentadienyl
CT	charge transfer
CTC	cyclic trinuclear complex
CTU	cyclic trinuclear unit
CSD	Cambridge Structural Database
CVD	chemical vapor deposition
DFT	density functional theory
DMF	dimethylformamide
DMSO	dimethyl sulfoxide
dppm	bis(diphenylphosphino)methane
EDA	energy decomposition analysis
EHT	extended Hückel theory
ESP	electrostatic potential

https://dx.doi.org/10.1021/acs.chemrev.0c00011
Chem. Rev. 2020, 120, 9675−9742

Et_3N	triethyl amine
f	oscillator strength
Fc	ferrocene
FMO	frontier molecular orbital
HE	high-energy
HOESY	heteronuclear Overhauser effect spectroscopy
HOMO	highest occupied molecular orbital
HOPG	highly oriented pyrolytic graphite
HPzIN	3-pyrazolyl imino nitroxide
IC	internal conversion
Im	imidazolate
ISC	intersystem crossing
IR	infrared
K_{SV}	Stern−Volmer constant
λ	wavelength
LC	ligand-centered
LE	low-energy
LED	light-emitting diode
LMCT	ligand-to-metal charge transfer
LUMO	lowest unoccupied molecular orbital
LUMS	lowest unoccupied molecular spinors
LMMCT	ligand-to-metal−metal charge transfer
MALDI-TOF MS	matrix-assisted laser desorption ionization time-of-flight mass spectrometry
MC	metal-centered
Me_2S	dimethyl sulfide
MLCT	metal-to-ligand charge transfer
MOF	metal−organic framework
MO	molecular orbital
MP2	second-order Møller−Plesset perturbation method
MTP(H)	H_2CPH_2S anion
Nap	naphthyl
NHC	*N*-heterocyclic carbene
NICS	nucleus independent chemical shift
NP	nanoparticle
OFET	organic field-effect transistor
OLED	organic light-emitting diode/device
OPV	organic photovoltaic device
*o*TP	*ortho*-terphenyl
PCA	positive charge attraction
PCP	porous coordination polymer
PET	polyethylene terephthalate
PGSE-NMR	pulsed field gradient spin−echo nuclear magnetic resonance
Ph	phenyl
PMMA	poly(methyl methacrylate)
PPh_3	triphenyl phosphine
p-Tol	*para*-tolyl
PVD	physical vapor deposition
PXRD	powder X-ray diffraction
Py	pyridinate
Pz	pyrazolate
QTAIM	quantum theory of atom-in-molecule
QY	quantum yield
RDG	reduced density gradient
RGB	red-green-blue
rt	room temperature
SBU	secondary building unit
SCXRD	single-crystal X-ray diffraction
SEM	scanning electron microscope
STM	scanning tunneling microscope
SmA	smectic A
SOC	spin−orbit coupling
TADF	thermally activated delayed fluorescence
τ	lifetime
t-Bu	*tert*-butyl
TCNQ	7,7,8,8-tetracyanoquinodimethane
TDDFT	time-dependent density functional theory
TEM	transmission electron microscopy
THF	tetrahydrofuran
THT	tetrahydrothiophene
Trz	triazolate
TTF	tetrathiafulvalene
UMC	unsaturated metal center
UV	ultraviolet
UV-vis	ultraviolet−visible light
vdW	van der Waals
VOC	volatile organic compound
XLCT	halide-to-ligand charge transfer
XMCT	halide-to-metal charge transfer
XRD	X-ray diffraction

REFERENCES

(1) Omary, M. A.; Mohamed, A. A.; Rawashdeh-Omary, M. A.; Fackler, J. P., Jr. Photophysics of Supramolecular Binary Stacks Consisting of Electron-Rich Trinuclear Au(I) Complexes and Organic Electrophiles. *Coord. Chem. Rev.* **2005**, *249*, 1372−1381.

(2) Elbjeirami, O.; Rawashdeh-Omary, M. A.; Omary, M. A. Phosphorescence Sensitization via Heavy-Atom Effects in d^{10} Complexes. *Res. Chem. Intermed.* **2011**, *37*, 691−703.

(3) Rawashdeh-Omary, M. A. Remarkable Alteration of Photophysical Properties of Cyclic Trinuclear Complexes of Monovalent Coinage Metals Upon Interactions with Small Organic Molecules. *Comments Inorg. Chem.* **2012**, *33*, 88−101.

(4) Titov, A. A.; Filippov, O. A.; Epstein, L. M.; Belkova, N. V.; Shubina, E. S. Macrocyclic Copper(I) and Silver(I) Pyrazolates: Principles of Supramolecular Assemblies with Lewis Bases. *Inorg. Chim. Acta* **2018**, *470*, 22−35.

(5) Zheng, J.; Yang, H.; Xie, M.; Li, D. The π-Acidity/Basicity of Cyclic Trinuclear Units (CTUs): From a Theoretical Perspective to Potential Applications. *Chem. Commun.* **2019**, *55*, 7134−7146.

(6) Galassi, R.; Rawashdeh-Omary, M. A.; Dias, H. V. R.; Omary, M. A. Homoleptic Cyclic Trinuclear d^{10} Complexes: From Self-Association via Metallophilic and Excimeric Bonding to the Breakage Thereof via Oxidative Addition, Dative Bonding, Quadrupolar, and Heterometal Bonding Interactions. *Comments Inorg. Chem.* **2019**, *39*, 287−348.

(7) Zhang, J.-P.; Zhang, Y.-B.; Lin, J.-B.; Chen, X.-M. Metal Azolate Frameworks: From Crystal Engineering to Functional Materials. *Chem. Rev.* **2012**, *112*, 1001−1033.

(8) Vaughan, L. G. Organogold Chemistry. III. 2-Pyridylgold(I). *J. Am. Chem. Soc.* **1970**, *92*, 730−731.

(9) Fung, E. Y.; Olmstead, M. M.; Vickery, J. C.; Balch, A. L. Glowing Gold Rings: Solvoluminescence From Planar Trigold(I) Complexes. *Coord. Chem. Rev.* **1998**, *171*, 151−159.

(10) Fackler, J. P., Jr Forty-Five Years of Chemical Discovery Including a Golden Quarter-Century. *Inorg. Chem.* **2002**, *41*, 6959−6972.

(11) Tekarli, S. M.; Cundari, T. R.; Omary, M. A. Rational Design of Macrometallocyclic Trinuclear Complexes with Superior π-Acidity and π-Basicity. *J. Am. Chem. Soc.* **2008**, *130*, 1669−1675.

(12) Schmidbaur, H.; Schier, A. A Briefing on Aurophilicity. *Chem. Soc. Rev.* **2008**, *37*, 1931−1951.

(13) Abdou, H. E.; Mohamed, A. A.; Fackler, J. P., Jr.; Burini, A.; Galassi, R.; López-de-Luzuriaga, J. M.; Olmos, M. E. Structures and Properties of Gold(I) Complexes of Interest in Biochemical Applications. *Coord. Chem. Rev.* **2009**, *253*, 1661−1669.

https://dx.doi.org/10.1021/acs.chemrev.0c00011
Chem. Rev. 2020, 120, 9675−9742

(14) Schmidbaur, H.; Schier, A. Aurophilic Interactions as a Subject of Current Research: an Up-Date. *Chem. Soc. Rev.* **2012**, *41*, 370−412.
(15) Schmidbaur, H.; Schier, A. Argentophilic Interactions. *Angew. Chem., Int. Ed.* **2015**, *54*, 746−784.
(16) Yam, V. W.-W.; Au, V. K.-M.; Leung, S. Y.-L. Light-Emitting Self-Assembled Materials Based on d^8 and d^{10} Transition Metal Complexes. *Chem. Rev.* **2015**, *115*, 7589−7728.
(17) Tsipis, A. C. DFT Challenge of Intermetallic Interactions: From Metallophilicity and Metallaromaticity to Sextuple Bonding. *Coord. Chem. Rev.* **2017**, *345*, 229−262.
(18) Tsai, Y.-C.; Harisomayajula, N. V. S.; Makovetskyi, S. Cuprophilic Interactions in and Between Molecular Entities. *Chem. - Eur. J.* **2019**, *25*, 8936−8954.
(19) Schmidbaur, H.; Raubenheimer, H. G. Excimer and Exciplex Formation in Gold(I) Complexes Preconditioned by Aurophilic Interactions. *Angew. Chem., Int. Ed.* **2020**, DOI: 10.1002/anie.201916255.
(20) Galassi, R.; Ghimire, M. M.; Otten, B. M.; Ricci, S.; McDougald, R. N., Jr.; Almotawa, R. M.; Alhmoud, D.; Ivy, J. F.; Rawashdeh, A.-M. M.; Nesterov, V. N.; Reinheimer, E. W.; Daniels, L. M.; Burini, A.; Omary, M. A. Cupriphication of Gold to Sensitize d^{10}−d^{10} Metal−Metal Bonds and Near-Unity Phosphorescence Quantum Yields. *Proc. Natl. Acad. Sci. U. S. A.* **2017**, *114*, E5042−E5051.
(21) Dias, H. V. R.; Diyabalanage, H. V. K.; Rawashdeh-Omary, M. A.; Franzman, M. A.; Omary, M. A. Bright Phosphorescence of a Trinuclear Copper(I) Complex: Luminescence Thermochromism, Solvatochromism, and "Concentration Luminochromism. *J. Am. Chem. Soc.* **2003**, *125*, 12072−12073.
(22) Dias, H. V. R.; Diyabalanage, H. V. K.; Eldabaja, M. G.; Elbjeirami, O.; Rawashdeh-Omary, M. A.; Omary, M. A. Brightly Phosphorescent Trinuclear Copper(I) Complexes of Pyrazolates: Substituent Effects on the Supramolecular Structure and Photophysics. *J. Am. Chem. Soc.* **2005**, *127*, 7489−7501.
(23) Omary, M. A.; Rawashdeh-Omary, M. A.; Gonser, M. W. A.; Elbjeirami, O.; Grimes, T.; Cundari, T. R.; Diyabalanage, H. V. K.; Gamage, C. S. P.; Dias, H. V. R. Metal Effect on the Supramolecular Structure, Photophysics, and Acid−Base Character of Trinuclear Pyrazolato Coinage Metal Complexes. *Inorg. Chem.* **2005**, *44*, 8200−8210.
(24) Vorontsov, I. I.; Kovalevsky, A. Y.; Chen, Y.-S.; Graber, T.; Gembicky, M.; Novozhilova, I. V.; Omary, M. A.; Coppens, P. Shedding Light on the Structure of a Photoinduced Transient Excimer by Time-Resolved Diffraction. *Phys. Rev. Lett.* **2005**, *94*, 193003.
(25) Grimes, T.; Omary, M. A.; Dias, H. V. R.; Cundari, T. R. Intertrimer and Intratrimer Metallophilic and Excimeric Bonding in the Ground and Phosphorescent States of Trinuclear Coinage Metal Pyrazolates: a Computational Study. *J. Phys. Chem. A* **2006**, *110*, 5823−5830.
(26) Hahn, R.; Bohle, F.; Kotte, S.; Keller, T. J.; Jester, S.-S.; Hansen, A.; Grimme, S.; Esser, B. Donor−Acceptor Interactions Between Cyclic Trinuclear Pyridinate Gold(I)-Complexes and Electron-Poor Guests: Nature and Energetics of Guest-Binding and Templating on Graphite. *Chem. Sci.* **2018**, *9* (14), 3477−3483.
(27) Hahn, R.; Bohle, F.; Fang, W.; Walther, A.; Grimme, S.; Esser, B. Raising the Bar in Aromatic Donor−Acceptor Interactions with Cyclic Trinuclear Gold(I) Complexes as Strong π-Donors. *J. Am. Chem. Soc.* **2018**, *140*, 17932−17944.
(28) Jayaratna, N. B.; Cowan, M. G.; Parasar, D.; Funke, H. H.; Reibenspies, J.; Mykhailiuk, P. K.; Artamonov, O.; Noble, R. D.; Dias, H. V. R. Low Heat of Adsorption of Ethylene Achieved by Major Solid-State Structural Rearrangement of a Discrete Copper(I) Complex. *Angew. Chem., Int. Ed.* **2018**, *57*, 16442−16446.
(29) Titov, A. A.; Larionov, V. A.; Smol'yakov, A. F.; Godovikova, M. I.; Titova, E. M.; Maleev, V. I.; Shubina, E. S. Interaction of the Trinuclear Copper(I) Pyrazolate with Alkynes and Carbon-Carbon Triple Bond Activation. *Chem. Commun.* **2019**, *55*, 290−293.
(30) Gade, L. H. Hyt Was of Gold, and Shon So Bryghte···": Luminescent Gold(I) Compounds. *Angew. Chem., Int. Ed. Engl.* **1997**, *36*, 1171−1173.
(31) Vickery, J. C.; Olmstead, M. M.; Fung, E. Y.; Balch, A. L. Solvent-Stimulated Luminescence from the Supramolecular Aggregation of a Trinuclear Gold(I) Complex That Displays Extensive Intermolecular Au···Au Interactions. *Angew. Chem., Int. Ed. Engl.* **1997**, *36*, 1179−1181.
(32) Kishimura, A.; Yamashita, T.; Aida, T. Phosphorescent Organogels via "Metallophilic" Interactions for Reversible RGB−Color Switching. *J. Am. Chem. Soc.* **2005**, *127*, 179−183.
(33) Pan, M.; Liao, W.-M.; Yin, S.-Y.; Sun, S.-S.; Su, C.-Y. Single-Phase White-Light-Emitting and Photoluminescent Color- Tuning Coordination Assemblies. *Chem. Rev.* **2018**, *118*, 8889−8935.
(34) McDougald, R. N., Jr.; Chilukuri, B.; Jia, H.; Perez, M. R.; Rabaâ, H.; Wang, X.; Nesterov, V. N.; Cundari, T. R.; Gnade, B. E.; Omary, M. A. Molecular and Electronic Structure of Cyclic Trinuclear Gold(I) Carbeniate Complexes: Insights for Structure/Luminescence/Conductivity Relationships. *Inorg. Chem.* **2014**, *53*, 7485−7499.
(35) Ni, W.-X.; Li, M.; Zheng, J.; Zhan, S.-Z.; Qiu, Y.-M.; Ng, S. W.; Li, D. Approaching White-Light Emission from a Phosphorescent Trinuclear Gold(I) Cluster by Modulating Its Aggregation Behavior. *Angew. Chem., Int. Ed.* **2013**, *52*, 13472−13476.
(36) Yang, H.; Zheng, J.; Peng, S.-K.; Zhu, X.-W.; Wan, M.-Y.; Lu, W.; Li, D. A Chemopalette Strategy for White Light by Modulating Monomeric and Excimeric Phosphorescence of a Simple Cu(I) Cyclic Trinuclear Unit. *Chem. Commun.* **2019**, *55*, 4635−4638.
(37) Otten, B. M.; Melançon, K. M.; Omary, M. A. All That Glitters Is Not Gold: a Computational Study of Covalent vs Metallophilic Bonding in Bimetallic Complexes of d^{10} Metal Centers − a Tribute to Al Cotton on the 10th Anniversary of His Passing. *Comments Inorg. Chem.* **2018**, *38*, 1−35.
(38) Cored, J.; Crespo, O.; Serrano, J. L.; Elduque, A.; Giménez, R. Decisive Influence of the Metal in Multifunctional Gold, Silver, and Copper Metallacycles: High Quantum Yield Phosphorescence, Color Switching, and Liquid Crystalline Behavior. *Inorg. Chem.* **2018**, *57*, 12632−12640.
(39) Rawashdeh-Omary, M. A.; Rashdan, M. D.; Dharanipathi, S.; Elbjeirami, O.; Ramesh, P.; Dias, H. V. R. On/Off Luminescence Vapochromic Selective Sensing of Benzene and Its Methylated Derivatives by a Trinuclear Silver(I) Pyrazolate Sensor. *Chem. Commun.* **2011**, *47*, 1160−1162.
(40) Upadhyay, P. K.; Marpu, S. B.; Benton, E. N.; Williams, C. L.; Telang, A.; Omary, M. A. A Phosphorescent Trinuclear Gold(I) Pyrazolate Chemosensor for Silver Ion Detection and Remediation in Aqueous Media. *Anal. Chem.* **2018**, *90*, 4999−5006.
(41) Kiguchi, M.; Inatomi, J.; Takahashi, Y.; Tanaka, R.; Osuga, T.; Murase, T.; Fujita, M.; Tada, T.; Watanabe, S. Highly Conductive [3 × *n*] Gold-Ion Clusters Enclosed Within Self-Assembled Cages. *Angew. Chem., Int. Ed.* **2013**, *52*, 6202−6205.
(42) Kuang, X.; Wu, X.; Yu, R.; Donahue, J. P.; Huang, J.; Lu, C.-Z. Assembly of a Metal-Organic Framework by Sextuple Intercatenation of Discrete Adamantane-Like Cages. *Nat. Chem.* **2010**, *2*, 461−465.
(43) Jozak, T.; Sun, Y.; Schmitt, Y.; Lebedkin, S.; Kappes, M.; Gerhards, M.; Thiel, W. R. New Hexanuclear Group 11 Pyrazolate Complexes: Synthesis and Photophysical Features. *Chem. - Eur. J.* **2011**, *17*, 3384−3389.
(44) Gao, G.-F.; Li, M.; Zhan, S.-Z.; Lv, Z.; Chen, G.-H.; Li, D. Confined Metallophilicity Within a Coordination Prism. *Chem. - Eur. J.* **2011**, *17*, 4113−4117.
(45) Grzywa, M.; Bredenkötter, B.; Denysenko, D.; Spirkl, S.; Nitek, W.; Volkmer, D. A Metallosupramolecular Octahedron Assembled From Twelve Copper(I) Metal Ions and Six 4,4′-(1,2-Phenylene)Bis-(3,5-Dimethylpyrazol-1-ide) Ligands. *Z. Anorg. Allg. Chem.* **2013**, *639*, 1461−1471.
(46) Duan, P.-C.; Wang, Z.-Y.; Chen, J.-H.; Yang, G.; Raptis, R. G. Trigonal Prismatic Cu(I) and Ag(I) Pyrazolato Nanocage Hosts: Encapsulation of S_8 and Hydrocarbon Guests. *Dalton Trans.* **2013**, *42*, 14951−14954.
(47) Wang, J.-H.; Li, M.; Zheng, J.; Huang, X.-C.; Li, D. A Dual-Emitting Cu_6−Cu_2−Cu_6 Cluster as a Self-Calibrated, Wide-Range Luminescent Molecular Thermometer. *Chem. Commun.* **2014**, *50*, 9115−9118.

(48) Li, L.-H.; Zhang, J.-X.; Jia, S.-K.; Yang, G. A Trigonal Prismatic Copper(I)−Bipyrazolato Cage: Synthesis, Crystal Structure and Luminescence. *Transition Met. Chem.* **2016**, *41*, 107−113.
(49) Veronelli, M.; Dechert, S.; Demeshko, S.; Meyer, F. 1,1′-Bis(Pyrazol-3-yl)Ferrocene: a Clip Ligand That Forms Supramolecular Aggregates and Prismatic Hexanuclear Coinage Metal Complexes. *Inorg. Chem.* **2015**, *54*, 6917−6927.
(50) Shi, Z.-C.; Zhang, D.-X.; Zhan, S.-Z.; Li, M.; Zheng, J.; Yang, H.; Zhou, X.-P.; Li, D. Trigonal Prismatic Cu_6L_3 Coordination Cage: Encapsulation of Aromatic Molecules and Tuned Photoluminescence. *Isr. J. Chem.* **2019**, *59*, 317−322.
(51) Zhan, S.-Z.; Li, J.-H.; Zhang, G.-H.; Liu, X.-W.; Li, M.; Zheng, J.; Ng, S. W.; Li, D. A Luminescent Edge-Interlocked Prismatic Heteroleptic Metallocage Assembled Through a Ligand Replacement Reaction. *Chem. Commun.* **2019**, *55*, 11992−11995.
(52) Shi, Z.-C.; Chen, W.; Zhan, S.-Z.; Li, M.; Xie, M.; Li, Y. Y.; Ng, S. W.; Huang, Y.-L.; Zhang, Z.; Ning, G.-H.; Li, D. Guest Effects on Crystal Structure and Phosphorescence of a Cu_6L_3 Prismatic Cage. *Inorg. Chem. Front.* **2020**, *7*, 1437−1444.
(53) He, J.; Yin, Y.-G.; Wu, T.; Li, D.; Huang, X.-C. Design and Solvothermal Synthesis of Luminescent Copper(I)-Pyrazolate Coordination Oligomer and Polymer Frameworks. *Chem. Commun.* **2006**, *38*, 2845−2847.
(54) Zhang, J.-P.; Horike, S.; Kitagawa, S. A Flexible Porous Coordination Polymer Functionalized by Unsaturated Metal Clusters. *Angew. Chem., Int. Ed.* **2007**, *46* (6), 889−892.
(55) Zhang, J.-P.; Kitagawa, S. Supramolecular Isomerism, Framework Flexibility, Unsaturated Metal Center, and Porous Property of Ag(I)/Cu(I) 3,3′,5,5′-Tetrametyl-4,4′-Bipyrazolate. *J. Am. Chem. Soc.* **2008**, *130*, 907−917.
(56) Zhang, J.-X.; He, J.; Yin, Y.-G.; Hu, M.-H.; Li, D.; Huang, X.-C. Novel Thermochromism Relating to Supramolecular Cuprophilic Interaction: Design, Synthesis, and Luminescence of Copper(I) Pyrazolate Trimer and Polymer. *Inorg. Chem.* **2008**, *47*, 3471−3473.
(57) Hou, L.; Shi, W.-J.; Wang, Y.-Y.; Wang, H.-H.; Cui, L.; Chen, P.-X.; Shi, Q.-Z. Trinuclear-Based Copper(I) Pyrazolate Polymers: Effect of Trimer π-Acid···Halide/Pseudohalide Interactions on the Supramolecular Structure and Phosphorescence. *Inorg. Chem.* **2011**, *50*, 261−270.
(58) Zhan, S.-Z.; Li, M.; Zhou, X.-P.; Li, D.; Ng, S. W. Excimer and Exciplex Formation in a Pair of Bright Phosphorescent Isomers Constructed from $Cu_3(Pyrazolate)_3$ And Cu_3I_3 Coordination Luminophores. *RSC Adv.* **2011**, *1*, 1457−1459.
(59) Zhan, S.-Z.; Li, M.; Zhou, X.-P.; Wang, J.-H.; Yang, J.-R.; Li, D. When Cu_4I_4 Cubane Meets $Cu_3(Pyrazolate)_3$ Triangle: Dynamic Interplay Between Two Classical Luminophores Functioning in a Reversibly Thermochromic Coordination Polymer. *Chem. Commun.* **2011**, *47*, 12441−12443.
(60) Grzywa, M.; Geßner, C.; Denysenko, D.; Bredenkötter, B.; Gschwind, F.; Fromm, K. M.; Nitek, W.; Klemm, E.; Volkmer, D. CFA-2 and CFA-3 (Coordination Framework Augsburg University-2 and −3); Novel MOFs Assembled From Trinuclear Cu(I)/Ag(I) Secondary Building Units and 3,3′,5,5′-Tetraphenyl-Bipyrazolate Ligands. *Dalton Trans.* **2013**, *42*, 6909−6921.
(61) Wei, Z.-W.; Yuan, D.-Q.; Zhao, X.-L.; Sun, D.-F.; Zhou, H.-C. Linker Extension Through Hard-Soft Selective Metal Coordination for the Construction of a Non-Rigid Metal-Organic Framework. *Sci. China: Chem.* **2013**, *56*, 418−422.
(62) Zhan, S.-Z.; Li, M.; Ng, S. W.; Li, D. Luminescent Metal-Organic Frameworks (MOFs) as a Chemopalette: Tuning the Thermochromic Behavior of Dual-Emissive Phosphorescence by Adjusting the Supramolecular Microenvironments. *Chem. - Eur. J.* **2013**, *19*, 10217−10225.
(63) Wang, J.-H.; Li, M.; Li, D. An Exceptionally Stable and Water-Resistant Metal-Organic Framework with Hydrophobic Nanospaces for Extracting Aromatic Pollutants from Water. *Chem. - Eur. J.* **2014**, *20*, 12004−12008.
(64) Zhang, J.-X.; Yan, T.-T.; Kou, J.-F.; Zhang, W.-H.; Yang, G. Two Copper(I) Complexes of Bi- (or Tri-)Pyrazolyl Ligands Featuring Cu_3Pz_3 Or Cu_4Pz_4 Motifs. *Z. Naturforsch., B: J. Chem. Sci.* **2015**, *70*, 59−64.
(65) Kivi, C. E.; Song, D. A Luminescent Cationic Metal−Organic Framework Featuring $[Cu-Pyrazolate]_3$ Units for Volatile Organic Compound Sensing. *Dalton Trans.* **2016**, *45*, 17087−17090.
(66) Zhan, S.-Z.; Li, M.; Zheng, J.; Wang, Q.-J.; Ng, S. W.; Li, D. Luminescent $Cu_4I_4-Cu_3(Pyrazolate)_3$ Coordination Frameworks: Postsynthetic Ligand Substitution Leads to Network Displacement and Entanglement. *Inorg. Chem.* **2017**, *56*, 13446−13455.
(67) Tu, B.; Pang, Q.; Xu, H.; Li, X.; Wang, Y.; Ma, Z.; Weng, L.; Li, Q. Reversible Redox Activity in Multicomponent Metal−Organic Frameworks Constructed from Trinuclear Copper Pyrazolate Building Blocks. *J. Am. Chem. Soc.* **2017**, *139*, 7998−8007.
(68) Zhan, S.-Z.; Feng, T.; Lu, W.; Razali, M. R.; Li, D. Substituent Influence on Structural and Luminescent Diversities of $Cu_3(Pyrazolate)_3$-Cu_nI_n Coordination Supramolecular Isomers. *Cryst. Growth Des.* **2018**, *18*, 7663−7673.
(69) Burini, A.; Mohamed, A. A.; Fackler, J. P., Jr. Cyclic Trinuclear Gold(I) Compounds: Synthesis, Structures and Supermolecular Acid-Base π-Stacks. *Comments Inorg. Chem.* **2003**, *24*, 253−280.
(70) Sartori, P.; Golloch, A. Darstellung Und Eigenschaften Von Tetrafluorphthalsäure-Derivaten. *Chem. Ber.* **1968**, *101*, 2004−2009.
(71) Shur, V. B.; Tikhonova, I. A. Perfluorinated Polymercuramacrocycles as Anticrowns. Applications in Catalysis. *Russ. Chem. Bull.* **2003**, *52*, 2539−2554.
(72) Taylor, T. J.; Burress, C. N.; Gabbaï, F. P. Lewis Acidic Behavior of Fluorinated Organomercurials. *Organometallics* **2007**, *26*, 5252−5263.
(73) Schmidbaur, H.; Graf, W.; Müller, G. Weak Intramolecular Bonding Relationships: the Conformation-Determining Attractive Interaction Between Gold(I) Centers. *Angew. Chem., Int. Ed. Engl.* **1988**, *27*, 417−419.
(74) Schmidbaur, H.; Scherbaum, F.; Huber, B.; Müller, G. Polyauriomethane Compounds. *Angew. Chem., Int. Ed. Engl.* **1988**, *27*, 419−421.
(75) Scherbaum, F.; Grohmann, A.; Huber, B.; Krüger, C.; Schmidbaur, H. Aurophilicity" as a Consequence of Relativistic Effects: the Hexakis(triphenylphosphaneaurio)methane Dication $[(Ph_3PAu)_6C]^{2\oplus}$. *Angew. Chem., Int. Ed. Engl.* **1988**, *27*, 1544−1546.
(76) Andris, E.; Andrikopoulos, P. C.; Schulz, J.; Turek, J.; Růžička, A.; Roithová, J.; Růlíšek, L. Aurophilic Interactions in [(L)AuCl]···[(L′)AuCl] Dimers: Calibration by Experiment and Theory. *J. Am. Chem. Soc.* **2018**, *140*, 2316−2325.
(77) Mehrotra, P. K.; Hoffmann, R. Copper(I)-Copper(I) Interactions. Bonding Relationships in d^{10}-d^{10} Systems. *Inorg. Chem.* **1978**, *17*, 2187−2189.
(78) Jiang, Y.; Alvarez, S.; Hoffmann, R. Binuclear and Polymeric Gold(I) Complexes. *Inorg. Chem.* **1985**, *24*, 749−757.
(79) Pyykkö, P.; Zhao, Y. Ab Initio Calculations on the $(ClAuPH_3)2$ Dimer with Relativistic Pseudopotential: Is the "Aurophilic Attraction" a Correlation Effect? *Angew. Chem., Int. Ed. Engl.* **1991**, *30*, 604−605.
(80) Li, J.; Pyykkö, P. Relativistic Pseudo-Potential Analysis of the Weak Au(I)···Au(I) Attraction. *Chem. Phys. Lett.* **1992**, *197*, 586−590.
(81) Pyykkö, P.; Li, J.; Runeberg, N. Predicted Ligand Dependence of the Au(I)···Au(I) Attraction in $(XAuPH_3)_2$. *Chem. Phys. Lett.* **1994**, *218*, 133−138.
(82) King, C.; Wang, J. C.; Khan, M. N. I.; Fackler, J. P., Jr. Luminescence and Metal-Metal Interactions in Binuclear Gold(I) Compounds. *Inorg. Chem.* **1989**, *28*, 2145−2149.
(83) Che, C.-M.; Kwong, H.-L.; Poon, C.-K.; Yam, V. W.-W. Spectroscopy and Redox Properties of the Luminescent Excited State of $[Au_2(dppm)_2]^{2+}$ (dppm = $Ph_2PCH_2PPh_2$). *J. Chem. Soc., Dalton Trans.* **1990**, *11*, 3215−3219.
(84) Bauer, J.; Braunschweig, H.; Dewhurst, R. D. Metal-Only Lewis Pairs with Transition Metal Lewis Bases. *Chem. Rev.* **2012**, *112*, 4329−4346.
(85) Wang, S.-G.; Schwarz, W. H. E. Quasi-Relativistic Density Functional Study of Aurophilic Interactions. *J. Am. Chem. Soc.* **2004**, *126*, 1266−1276.

https://dx.doi.org/10.1021/acs.chemrev.0c00011
Chem. Rev. 2020, 120, 9675−9742

(86) Brands, M. B.; Nitsch, J.; Guerra, C. F. Relevance of Orbital Interactions and Pauli Repulsion in the Metal−Metal Bond of Coinage Metals. *Inorg. Chem.* **2018**, *57*, 2603−2608.
(87) Antony, J.; Sure, R.; Grimme, S. Using Dispersion-Corrected Density Functional Theory to Understand Supramolecular Binding Thermodynamics. *Chem. Commun.* **2015**, *51*, 1764−1774.
(88) Bondi, A. van der Waals Volumes and Radii. *J. Phys. Chem.* **1964**, *68*, 441−451.
(89) Caramori, G. F.; Piccoli, R. M.; Segala, M.; Muñoz-Castro, A.; Guajardo-Maturana, R.; Andrada, D. M.; Frenking, G. Cyclic Trinuclear Copper(I), Silver(I), and Gold(I) Complexes: a Theoretical Insight. *Dalton Trans.* **2015**, *44*, 377−385.
(90) Ghimire, M. M.; Nesterov, V. N.; Omary, M. A. Remarkable Aurophilicity and Photoluminescence Thermochromism in a Homoleptic Cyclic Trinuclear Gold(I) Imidazolate Complex. *Inorg. Chem.* **2017**, *56*, 12086−12089.
(91) Rawashdeh-Omary, M. A.; Omary, M. A.; Fackler, J. P., Jr.; Galassi, R.; Pietroni, B. R.; Burini, A. Chemistry and Optoelectronic Properties of Stacked Supramolecular Entities of Trinuclear Gold(I) Complexes Sandwiching Small Organic Acids. *J. Am. Chem. Soc.* **2001**, *123*, 9689−9691.
(92) Mohamed, A. A.; Pérez, L. M.; Fackler, J. P., Jr Unsupported Intermolecular Argentophilic Interaction in the Dimer of Trinuclear Silver(I) 3,5-Diphenylpyrazolates. *Inorg. Chim. Acta* **2005**, *358*, 1657−1662.
(93) García, F.; Hopkins, A. D.; Kowenicki, R. A.; McPartlin, M.; Rogers, M. C.; Wright, D. S. Synthesis of the $[MeAl(2\text{-}Py)_3]^-$ Anion and Its Application as a Stable and Mild Pyridyl-Transfer Reagent (2-Py = 2-Pyridyl). *Organometallics* **2004**, *23*, 3884−3890.
(94) Wang, X.-L.; Zheng, J.; Li, M.; Weng Ng, S.; Chan, S. L.-F.; Li, D. Curved Cyclic Trimers: Orthogonal Cu−Cu Interaction Versus Tetrameric Halogen Bonding. *Cryst. Growth Des.* **2016**, *16*, 4991−4998.
(95) Mohamed, A. A.; Burini, A.; Fackler, J. P., Jr Mixed-Metal Triangular Trinuclear Complexes: Dimers of Gold−Silver Mixed-Metal Complexes from Gold(I) Carbeniates and Silver(I) 3,5-Diphenylpyrazolates. *J. Am. Chem. Soc.* **2005**, *127*, 5012−5013.
(96) Muñiz, J.; Sansores, L. E.; Rojano, A.; Martínez, A.; Salcedo, R. Theoretical Study of Au(I)−Ag(I) Metallophilic Attractions and Luminescence of $[Au_2(carb)_2Ag(\mu\text{-}3,5\text{-}Ph_2Pz)]$ (with Ph = Phenyl, Pz = Pyrazolate) and $[Au(im)CH_3(Pz)Ag_2(\mu\text{-}3,5\text{-}H_2Pz)_2]$ (with im = Imidazole). *J. Mol. Struct.: THEOCHEM* **2009**, *901*, 232−242.
(97) Groom, C. R.; Bruno, I. J.; Lightfoot, M. P.; Ward, S. C. The Cambridge Structural Database. *Acta Crystallogr., Sect. B: Struct. Sci., Cryst. Eng. Mater.* **2016**, *B72*, 171−179.
(98) Yang, G.; Raptis, R. G. Supramolecular Assembly of Trimeric Gold(I) Pyrazolates Through Aurophilic Attractions. *Inorg. Chem.* **2003**, *42*, 261−263.
(99) Hu, B.; Gahungu, G.; Zhang, J. Optical Properties of the Phosphorescent Trinuclear Copper(I) Complexes of Pyrazolates: Insights from Theory. *J. Phys. Chem. A* **2007**, *111* (23), 4965−4973.
(100) Yang, C.; Messerschmidt, M.; Coppens, P.; Omary, M. A. Trinuclear Gold(I) Triazolates: a New Class of Wide-Band Phosphors and Sensors. *Inorg. Chem.* **2006**, *45*, 6592−6594.
(101) Perdew, J. P.; Burke, K.; Ernzerhof, M. Generalized Gradient Approximation Made Simple. *Phys. Rev. Lett.* **1996**, *77*, 3865−3868.
(102) Perdew, J. P.; Burke, K.; Ernzerhof, M. Generalized Gradient Approximation Made Simple [Phys. Rev. Lett. 77, 3865 (1996)]. *Phys. Rev. Lett.* **1997**, *78*, 1396.
(103) Hay, P. J.; Wadt, W. R. Ab Initio Effective Core Potentials for Molecular Calculations. Potentials for the Transition Metal Atoms Sc to Hg. *J. Chem. Phys.* **1985**, *82*, 270−283.
(104) Hariharan, P. C.; Pople, J. A. Accuracy of AH_n equilibrium Geometries by Single Determinant Molecular Orbital Theory. *Mol. Phys.* **1974**, *27*, 209−214.
(105) Tsipis, A. C.; Stalikas, A. V. Molecular and Electronic Structure, Magnetotropicity and Absorption Spectra of Benzene−Trinuclear Copper(I) and Silver(I) Trihalide Columnar Binary Stacks. *Inorg. Chem.* **2012**, *51*, 2541−2559.
(106) Tsipis, A. C.; Stalikas, A. V. Face-to-Face Stacks of Trinuclear Gold(I) Trihalides with Benzene, Hexafluorobenzene, and Borazine: Impact of Aromaticity on Stacking Interactions. *Inorg. Chem.* **2013**, *52*, 1047−1060.
(107) Pandolfo, L.; Pettinari, C. Trinuclear Copper(II) Pyrazolate Compounds: a Long Story of Serendipitous Discoveries and Rational Design. *CrystEngComm* **2017**, *19*, 1701−1720.
(108) Aullón, G.; Laguna, A.; Filippov, O. A.; Oliva-Enrich, J. M. Trinuclear Gold-Carborane Cluster as a Host Structure. *Eur. J. Inorg. Chem.* **2019**, *2019*, 18−22.
(109) Sansores, L. E.; Salcedo, R.; Martínez, A.; Mireles, N. Electronic Structure of Triangular Trigold(I) Complexes. a Theoretical Study. *J. Mol. Struct.: THEOCHEM* **2006**, *763*, 7−11.
(110) Wang, L.; Xu, J.; Kira, M.; Yan, L.; Xiao, X. Q.; Li, Z. A Stable Cyclic $(R_2SnAu)_3$ Anion Having in-Plane σ-Möbius Aromaticity. *Angew. Chem., Int. Ed.* **2020**, *59*, 1980−1984.
(111) Hayashi, A.; Olmstead, M. M.; Attar, S.; Balch, A. L. Crystal Chemistry of the Gold(I) Trimer, $Au_3(NC_5H_4)_3$: Formation of Hourglass Figures and Self-Association Through Aurophilic Attraction. *J. Am. Chem. Soc.* **2002**, *124*, 5791−5795.
(112) Bonati, F.; Burini, A.; Pietroni, B. R.; Bovio, B. Reactions of C-Imidazolyllithium Derivatives with Group IB Compounds: Tris[μ-(1-Alkylimidazolato-N^3,C^2)]Tri-Gold(I) and -Silver(I). Crystal Structure of Bis(1-Benzylimidazolin-2-yliden)Gold(I) Chloride. *J. Organomet. Chem.* **1989**, *375*, 147−160.
(113) Ruiz, J.; Sol, D.; Mateo, M. A.; Vivanco, M.; Badía-Laiño, R. A New Approach to the Synthesis of Trinuclear Gold(I) Imidazolate Complexes and Their Silver(I)-Induced Photoluminescence Behavior. *Dalton Trans.* **2020**, *49*, 6561−6565.
(114) Minghetti, G.; Bonati, F. Trimeric 1-(Cyclohexylimino)-Methoxymethylgold(I), a New Type of Organometallic Compound. *Angew. Chem., Int. Ed. Engl.* **1972**, *11*, 429.
(115) Bartolomé, C.; Carrasco-Rando, M.; Coco, S.; Cordovilla, C.; Espinet, P.; Martín-Alvarez, J. M. Structural Switching in Luminescent Polynuclear Gold Imidoyl Complexes by Intramolecular Hydrogen Bonding. *Organometallics* **2006**, *25*, 2700−2703.
(116) Bovio, B.; Bonati, F.; Banditelli, G. X-Ray Crystal Structure of Tris[μ-3,5-Bis(Trifluoromethyl)Pyrazolato-*N*,*N*′]Trigold(I), a Compound Containing an Inorganic Nine-Membered Ring. *Inorg. Chim. Acta* **1984**, *87*, 25−33.
(117) Woodall, C. H.; Fuertes, S.; Beavers, C. M.; Hatcher, L. E.; Parlett, A.; Shepherd, H. J.; Christensen, J.; Teat, S. J.; Intissar, M.; Rodrigue-Witchel, A.; Suffren, Y.; Reber, C.; Hendon, C. H.; Tiana, D.; Walsh, A.; Raithby, P. R. Paul R. Raithby, P. R. Tunable Trimers: Using Temperature and Pressure to Control Luminescent Emission in Gold(I) Pyrazolate-Based Trimers. *Chem. - Eur. J.* **2014**, *20*, 16933−16942.
(118) Raptis, R. G.; Fackler, J. P., Jr Structure of Tris(μ-3,5-Diphenylpyrazolato-*N*,*N*′)Tricopper(I). Structural Comparisons with the Silver(I) and Gold(I) Pyrazolate Trimers. *Inorg. Chem.* **1988**, *27*, 4179−4182.
(119) Murray, H. H.; Raptis, R. G.; Fackler, J. P., Jr. Syntheses and X-Ray Structures of Group 11 Pyrazole and Pyrazolate Complexes. X-Ray Crystal Structures of Bis(3,5-Diphenylpyrazole)Copper(II) Dibromide, Tris(μ-3,5-Diphenylpyrazolato-*N*,*N*′)Trisilver(I)-2-Tetrahydrofuran, Tris(μ-3,5-Diphenylpyrazolato-*N*,*N*′)Trigold(I), and Hexakis-(μ-3,5-Diphenylpyrazolato-*N*,*N*′)Hexagold(I). *Inorg. Chem.* **1988**, *27*, 26−33.
(120) Galassi, R.; Ricci, S.; Burini, A.; Macchioni, A.; Rocchigiani, L.; Marmottini, F.; Tekarli, S. M.; Nesterov, V. N.; Omary, M. A. Solventless Supramolecular Chemistry via Vapor Diffusion of Volatile Small Molecules Upon a New Trinuclear Silver(I)-Nitrated Pyrazolate Macrometallocyclic Solid: an Experimental/Theoretical Investigation of the Dipole/Quadrupole Chemisorption Phenomena. *Inorg. Chem.* **2013**, *52*, 14124−14137.
(121) Bertolotti, F.; Maspero, A.; Cervellino, A.; Guagliardi, A.; Masciocchi, N. Bending by Faulting: a Multiple Scale Study of Copper and Silver Nitropyrazolates. *Cryst. Growth Des.* **2014**, *14*, 2913−2922.

https://dx.doi.org/10.1021/acs.chemrev.0c00011
Chem. Rev. 2020, 120, 9675−9742

(122) Yang, G.; Baran, P.; Martínez, A. R.; Raptis, R. G. Substituent Effects on the Supramolecular Aggregation of Ag^{I}-Pyrazolato Trimers. *Cryst. Growth Des.* **2013**, *13*, 264−269.
(123) Chen, J.-H.; Liu, Y.-M.; Zhang, J.-X.; Zhu, Y.-Y.; Tang, M.-S.; Ng, S. W.; Yang, G. Halogen-Involving Weak Interactions Manifested in the Crystal Structures of Silver(I) or Gold(I) 4-Halogenated-3,5-Diphenylpyrazolato Trimers. *CrystEngComm* **2014**, *16*, 4987−4998.
(124) Yamada, S.; Ishida, T.; Nogami, T. Supramolecular Triangular and Linear Arrays of Metal−Radical Solids Using Pyrazolato-Silver(I) Motifs. *Dalton Trans.* **2004**, *22*, 898−903.
(125) Masciocchi, N.; Moret, M.; Cairati, P.; Sironi, A.; Ardizzoia, G. A.; La Monica, G. The Multiphase Nature of the Cu(Pz) and Ag(Pz) (Hpz = Pyrazole) Systems: Selective Syntheses and *Ab-Initio* X-Ray Powder Diffraction Structural Characterization of Copper(I) and Silver(I) Pyrazolates. *J. Am. Chem. Soc.* **1994**, *116*, 7668−7676.
(126) Gong, F.; Wang, Q.; Chen, J.; Yang, Z.; Liu, M.; Li, S.; Yang, G.; Bai, L.; Liu, J.; Dong, Y. Exploring Intertrimer Cu···Cu Interactions and Further Phosphorescent Properties of Aryl Trimer Copper(I) Pyrazolates via Substituent Changing and External Pressure. *Inorg. Chem.* **2010**, *49*, 1658−1666.
(127) Ardizzoia, G. A.; Cenini, S.; La Monica, G.; Masciocchi, N.; Maspero, A.; Moret, M. Syntheses, Structures, and Reactivity of Polynuclear Pyrazolato Copper(I) Complexes, Including an Ab-Initio XRPD Study of $[Cu(dmnpz)]_3$ (Hdmnpz = 3,5-Dimethyl-4-Nitropyrazole). *Inorg. Chem.* **1998**, *37*, 4284−4292.
(128) Singh, K.; Long, J. R.; Stavropoulos, P. Ligand-Unsupported Metal−Metal (M = Cu, Ag) Interactions Between Closed-Shell d^{10} Trinuclear Systems. *J. Am. Chem. Soc.* **1997**, *119*, 2942−2943.
(129) Singh, K.; Long, J. R.; Stavropoulos, P. Polynuclear Complexes of Copper(I) and the 2-(3(5)-Pyrazolyl)-6-Methylpyridine Ligand: Structures and Reactivity Toward Small Molecules. *Inorg. Chem.* **1998**, *37*, 1073−1079.
(130) Enomoto, M.; Kishimura, A.; Aida, T. Coordination Metallacycles of an Achiral Dendron Self-Assemble via Metal−Metal Interaction to Form Luminescent Superhelical Fibers. *J. Am. Chem. Soc.* **2001**, *123*, 5608−5609.
(131) Barberá, J.; Elduque, A.; Giménez, R.; Oro, L. A.; Serrano, J. L. Pyrazolate "Golden" Rings: Trinuclear Complexes That Form Columnar Mesophases at Room Temperature. *Angew. Chem., Int. Ed. Engl.* **1996**, *35*, 2832−2835.
(132) Barberá, J.; Elduque, A.; Giménez, R.; Lahoz, F. J.; López, J. A.; Oro, L. A.; Serrano, J. L. (Pyrazolato)Gold Complexes Showing Room-Temperature Columnar Mesophases. Synthesis, Properties, and Structural Characterization. *Inorg. Chem.* **1998**, *37*, 2960−2967.
(133) Kim, S. J.; Kang, S. H.; Park, K.-M.; Kim, H.; Zin, W.-C.; Choi, M.-G.; Kim, K. Trinuclear Gold(I) Pyrazolate Complexes Exhibiting Hexagonal Columnar Mesophases with Only Three Side Chains. *Chem. Mater.* **1998**, *10*, 1889−1893.
(134) Torralba, M. C.; Ovejero, P.; Mayoral, M. J.; Cano, M.; Campo, J. A.; Heras, J. V.; Pinilla, E.; Torres, M. R. Silver and Gold Trinuclear Complexes Based on 3-Substituted or 3,5-Disubstituted Pyrazolato Ligands. X-Ray Crystal Structure of Cyclo-Tris{μ-[3,5-Bis(4-Phenoxyphenyl)-1*H*-Pyrazolato-κN^1 : κN^2]Trigold Dichloromethane ($[Au(\mu\text{-}Pz^{PP2})]_3{\cdot}CH_2Cl_2$). *Helv. Chim. Acta* **2004**, *87*, 250−263.
(135) Rasika Dias, H. V.; Polach, S. A.; Wang, Z. Coinage Metal Complexes of 3,5-Bis(Trifluoromethyl)Pyrazolate Ligand. *J. Fluorine Chem.* **2000**, *103*, 163−169.
(136) Hettiarachchi, C. V.; Rawashdeh-Omary, M. A.; Korir, D.; Kohistani, J.; Yousufuddin, M.; Dias, H. V. R. Trinuclear Copper(I) and Silver(I) Adducts of 4-Chloro-3,5-Bis(Trifluoromethyl)Pyrazolate and 4-Bromo-3,5-Bis(Trifluoromethyl)Pyrazolate. *Inorg. Chem.* **2013**, *52*, 13576−13583.
(137) Dias, H. V. R.; Singh, S.; Campana, C. F. Toluene-Sandwiched Trinuclear Copper(I) and Silver(I) Triazolates and Phosphine Adducts of Dinuclear Copper(I) and Silver(I) Triazolates. *Inorg. Chem.* **2008**, *47*, 3943−3945.
(138) Chen, X.-M.; Tong, M.-L. Solvothermal in Situ Metal/Ligand Reactions: a New Bridge Between Coordination Chemistry and Organic Synthetic Chemistry. *Acc. Chem. Res.* **2007**, *40*, 162−170.
(139) Minghetti, G.; Bonati, F.; Massobrio, M. A New Type of σ-Bonded Organosilver Compound: $[Ag{-}C(OR){=}NAr]_3$. *J. Chem. Soc., Chem. Commun.* **1973**, No. 7, 260.
(140) Minghetti, G.; Bonati, F.; Massobrio, M. Isocyanide Complexes and (Alkoxy)(N-alkylimino)methyl Derivatives of Silver and Their Reactions. *Inorg. Chem.* **1975**, *14*, 1974−1977.
(141) Ardizzoia, G. A.; Cenini, S.; La Monica, G.; Masciocchi, N.; Moret, M. Synthesis, X-Ray Structure, and Catalytic Properties of the Unprecedented Tetranuclear Copper(I) Species $[Cu(dppz)]_4$ (Hdppz = 3,5-Diphenylpyrazole). *Inorg. Chem.* **1994**, *33*, 1458−1463.
(142) Yang, G.; Raptis, R. G. Synthesis, Structure and Properties of Tetrameric Gold(I) 3,5-di-*tert*-butyl−Pyrazolate. *Inorg. Chim. Acta* **2003**, *352*, 98−104.
(143) Yang, G.; Raptis, R. G. Synthesis and Crystal Structure of Tetrameric Silver(I) 3,5-di-*tert*-butyl-Pyrazolate. *Inorg. Chim. Acta* **2007**, *360*, 2503−2506.
(144) Maspero, A.; Brenna, S.; Galli, S.; Penoni, A. Synthesis and Characterisation of New Polynuclear Copper(I) Pyrazolate Complexes and Their Catalytic Activity in the Cyclopropanation of Olefins. *J. Organomet. Chem.* **2003**, *672*, 123−129.
(145) Fujisawa, K.; Ishikawa, Y.; Miyashita, Y.; Okamoto, K.-I. Pyrazolate-Bridged Group 11 Metal(I) Complexes: Substituent Effects on the Supramolecular Structures and Physicochemical Properties. *Inorg. Chim. Acta* **2010**, *363*, 2977−2989.
(146) Barberá, J.; Lantero, I.; Moyano, S.; Serrano, J. L.; Elduque, A.; Giménez, R. Silver Pyrazolates as Coordination-Polymer Luminescent Metallomesogens. *Chem. - Eur. J.* **2010**, *16*, 14545−14553.
(147) Minghetti, G.; Banditelli, G.; Bonati, F. Metal Derivatives of Azoles. 3. the Pyrazolato Anion (and Homologs) as a Mono- or Bidentate Ligand: Preparation and Reactivity of Tri-, Bi-, and Mononuclear Gold(I) Derivatives. *Inorg. Chem.* **1979**, *18*, 658−663.
(148) Yang, G.; Martínez, J. R.; Raptis, R. G. Dinuclear Gold(III) Pyrazolato Complexes − Synthesis, Structural Characterization and Transformation to Their Trinuclear Gold(I) and Gold(I/III) Analogues. *Inorg. Chim. Acta* **2009**, *362*, 1546−1552.
(149) Ehlert, M. K.; Rettig, S. J.; Storr, A.; Thompson, R. C.; Trotter, J. Synthesis and X-Ray Crystal Structure of the 3,5-Dimethylpyrazolato Copper(I) Trimer, $[Cu(Pz'')]_3$. *Can. J. Chem.* **1990**, *68*, 1444−1449.
(150) Ehlert, M. K.; Rettig, S. J.; Storr, A.; Thompson, R. C.; Trotter, J. Polynuclear Pyrazolate Complexes of Copper. Crystal and Molecular Structures of $[Cu(tmpz)]_3$, $[Cu(3\text{-}CO_2dmpz)(tmpzH)]_2Cu$, and $[Cu(4\text{-}Br\text{-}3\text{-}CO_2Mepz)(4\text{-}Br\text{-}dmpzH)_2]_2$ (Where Mepz = Methylpyrazolate, dmpz = Dimethylpyrazolate, and tmpz = Trimethylpyrazolate) and Magnetic Susceptibility Studies on the Dinuclear Complex. *Can. J. Chem.* **1992**, *70*, 2161−2173.
(151) Krishantha, D. M. M.; Gamage, C. S. P.; Schelly, Z. A.; Dias, H. V. R. Structures of Silver Pyrazolates in Hydrocarbon Solutions via Vapor-Pressure Osmometry. *Inorg. Chem.* **2008**, *47*, 7065−7067.
(152) Mahadevi, A. S.; Sastry, G. N. Cooperativity in Noncovalent Interactions. *Chem. Rev.* **2016**, *116*, 2775−2825.
(153) Ni, W.-X.; Qiu, Y.-M.; Li, M.; Zheng, J.; Sun, R. W.-Y.; Zhan, S.-Z.; Ng, S. W.; Li, D. Metallophilicity-Driven Dynamic Aggregation of a Phosphorescent Gold(I)−Silver(I) Cluster Prepared by Solution-Based and Mechanochemical Approaches. *J. Am. Chem. Soc.* **2014**, *136*, 9532−9535.
(154) Burini, A.; Galassi, R.; Pietroni, B. R.; Burini, A.; Fackler, J. P., Jr.; Galassi, R.; Staples, R. J. The First Sandwich Silver Cluster of a Trinuclear Cyclic Gold(I) Complex. *Chem. Commun.* **1998**, 95−96.
(155) Burini, A.; Bravi, R.; Fackler, J. P., Jr.; Galassi, R.; Grant, T. A.; Omary, M. A.; Pietroni, B. R.; Staples, R. J. Luminescent Chains Formed from Neutral, Triangular Gold Complexes Sandwiching Tl^{I} and Ag^{I}. Structures of $\{Ag([Au(\mu\text{-}C^2,N^3\text{-}BzIm)]_3)_2\}BF_4{\cdot}CH_2Cl_2$, $\{Tl([Au(\mu\text{-}C^2,N^3\text{-}BzIm)]_3)_2\}PF_6{\cdot}0.5THF$ (BzIm = 1-Benzylimidazolate), and $\{Tl([Au(\mu\text{-}C(OEt){=}NC_6H_4CH_3)]_3)_2\}PF_6{\cdot}THF$, with MAu_6 ($M = Ag^+$, Tl^+) Cluster Cores. *Inorg. Chem.* **2000**, *39*, 3158−3165.
(156) Osuga, T.; Murase, T.; Ono, K.; Yamauchi, Y.; Fujita, M. [M × *n*] Metal Ion Arrays Templated by Coordination Cages. *J. Am. Chem. Soc.* **2010**, *132*, 15553−15555.

https://dx.doi.org/10.1021/acs.chemrev.0c00011
Chem. Rev. 2020, 120, 9675−9742

(157) Osuga, T.; Murase, T.; Fujita, M. Triple-Decker Au_3-Ag-Au_3-Ag-Au_3 Ion Cluster Enclosed in a Self-Assembled Cage. *Angew. Chem., Int. Ed.* **2012**, *51*, 12199−12201.
(158) Osuga, T.; Murase, T.; Hoshino, M.; Fujita, M. A Tray-Shaped, PdII-Clipped Au_3 Complex as a Scaffold for the Modular Assembly of $[3 \times n]$ Au Ion Clusters. *Angew. Chem., Int. Ed.* **2014**, *53*, 11186−11189.
(159) Fujii, S.; Kanae, S.; Iwane, M.; Nishino, T.; Osuga, T.; Murase, T.; Fujita, M.; Kiguchi, M. Effect of Ag Ion Insertion on Electron Transport Through Au Ion Wires. *Chem. Lett.* **2016**, *45*, 764−766.
(160) Olmstead, M. M.; Jiang, F.; Attar, S.; Balch, A. L. Alteration of the Aurophilic Interactions in Trimeric Gold(I) Compounds Through Charge Transfer. Behavior of Solvoluminescent $Au_3(MeN{=}COMe)_3$ In the Presence of Electron Acceptors. *J. Am. Chem. Soc.* **2001**, *123*, 3260−3267.
(161) Tiripicchio, A.; Camellini, M. T.; Minghetti, G. The Crystal Structure of Tris-μ-[(ethoxy)(*N*-*p*-Tolylimino)methyl-*N*,*C*]Trigold-(I), $[(EtO)(MeC_6H_4N =)CAu]_3$. *J. Organomet. Chem.* **1979**, *171*, 399−406.
(162) Rasika Dias, H. V.; Palehepitiya Gamage, C. S. R.; Palehepitiya Gamage, C. S. Arene-Sandwiched Silver(I) Pyrazolates. *Angew. Chem., Int. Ed.* **2007**, *46*, 2192−2194.
(163) Jayaratna, N. B.; Hettiarachchi, C. V.; Yousufuddin, M.; Rasika Dias, H. V. Isolable Arene Sandwiched Copper(I) Pyrazolates. *New J. Chem.* **2015**, *39*, 5092−5095.
(164) Zhan, S.-Z.; Ding, F.; Liu, X.-W.; Zhang, G.-H.; Zheng, J.; Li, D. White Light from Blue Fluorescence and Sensitized Yellow Long-Afterglow Phosphorescence of *o*-Terphenyl in Its π-Acid···Base Adduct with Ag_3Pz_3. *Inorg. Chem.* **2019**, *58*, 12516−12520.
(165) Liu, R.; Zhang, W.; Wei, D.; Chen, J.-H.; Ng, S. W.; Yang, G. Adducts of Triangular Silver(I) 3,5-Bis(Trifluoromethyl)Pyrazolate with Thiophene-Derivatives: a Weak Interaction Model of Desulfurization. *Dalton Trans.* **2019**, *48*, 16162−16166.
(166) Ghimire, M. M.; Simon, O. C.; Harris, L. M.; Appiah, A.; Mitch, R. M.; Nesterov, V. N.; Macchioni, A.; Zuccaccia, C.; Rabaâ, H.; Galassi, R.; Omary, M. A. Binary Donor−Acceptor Adducts of Tetrathiafulvalene Donors with Cyclic Trimetallic Monovalent Coinage Metal Acceptors. *Inorg. Chem.* **2019**, *58*, 15303−15319.
(167) Dias, H. V. R.; Diyabalanage, H. V. K.; Gamage, C. S. P. Neutral Cu_4N_{12} And Ag_4N_{12} Metallacycles with a *para*-Cyclophane Framework Assembled from Copper(I) and Silver(I) Pyrazolates and Pyridazine. *Chem. Commun.* **2005**, 1619−1621.
(168) Yang, C.; Elbjeirami, O.; Gamage, C. S. P.; Dias, H. V. R.; Omary, M. A. Luminescence Enhancement and Tuning via Multiple Cooperative Supramolecular Interactions in an Ion-Paired Multinuclear Complex. *Chem. Commun.* **2011**, *47*, 7434−7436.
(169) Parasar, D.; Almotawa, R. M.; Jayaratna, N. B.; Ceylan, Y. S.; Cundari, T. R.; Omary, M. A.; Rasika Dias, H. V. Synthesis, Photophysical Properties, and Computational Analysis of Di- and Tetranuclear Alkyne Complexes of Copper(I) Supported by a Highly Fluorinated Pyrazolate. *Organometallics* **2018**, *37*, 4105−4118.
(170) Parasar, D.; Ponduru, T. T.; Noonikara-Poyil, A.; Jayaratna, N. B.; Dias, H. V. R. Acetylene and Terminal Alkyne Complexes of Copper(I) Supported by Fluorinated Pyrazolates: Syntheses, Structures, and Transformations. *Dalton Trans.* **2019**, *48*, 15782−15794.
(171) Peng, S.-K.; Lu, Z.; Xie, M.; Huang, Y.-L.; Luo, D.; Wang, J.-N.; Zhu, X.-W.; Li, X.; Zhou, X.-P.; Li, D. Unexpected Structural Transformation Into Noria-Like Ag_{13} Metal Clusters and a Copper-Doping Induced Boost in Photoluminescence. *Chem. Commun.* **2020**, *56*, 4789−4792.
(172) Titov, A. A.; Filippov, O. A.; Bilyachenko, A. N.; Smol'yakov, A. F.; Dolgushin, F. M.; Belsky, V. K.; Godovikov, I. A.; Epstein, L. M.; Shubina, E. S. Complexes of Trinuclear Macrocyclic Copper(I) and Silver(I) 3,5-Bis(Trifluoromethyl)Pyrazolates with Ketones. *Eur. J. Inorg. Chem.* **2012**, *2012*, 5554−5561.
(173) Titov, A. A.; Filippov, O. A.; Smol'yakov, A. F.; Godovikov, I. A.; Shakirova, J. R.; Tunik, S. P.; Podkorytov, I. S.; Shubina, E. S. Luminescent Complexes of the Trinuclear Silver(I) and Copper(I) Pyrazolates Supported with Bis(diphenylphosphino)methane. *Inorg. Chem.* **2019**, *58*, 8645−8656.
(174) Burini, A.; Fackler, J. P., Jr.; Galassi, R.; Grant, T. A.; Omary, M. A.; Rawashdeh-Omary, M. A.; Pietroni, B. R.; Staples, R. J. Supramolecular Chain Assemblies Formed by Interaction of a π Molecular Acid Complex of Mercury with π-Base Trinuclear Gold Complexes. *J. Am. Chem. Soc.* **2000**, *122*, 11264−11265.
(175) Burini, A.; Fackler, J. P., Jr.; Galassi, R.; Macchioni, A.; Omary, M. A.; Rawashdeh-Omary, M. A.; Pietroni, B. R.; Sabatini, S.; Zuccaccia, C. ^{19}F, ^{1}H-HOESY and PGSE NMR Studies of Neutral Trinuclear Complexes of Au^{I} and Hg^{II}: Evidence for Acid−Base Stacking in Solution. *J. Am. Chem. Soc.* **2002**, *124*, 4570−4571.
(176) Mohamed, A. A.; Galassi, R.; Papa, F.; Burini, A.; Fackler, J. P., Jr. Gold(I) and Silver(I) Mixed-Metal Trinuclear Complexes: Dimeric Products from the Reaction of Gold(I) Carbeniates or Benzylimidazolates with Silver(I) 3,5-Diphenylpyrazolate. *Inorg. Chem.* **2006**, *45*, 7770−7776.
(177) Yang, C.; Arvapally, R. K.; Tekarli, S. M.; Salazar, G. A.; Elbjeirami, O.; Wang, X.; Omary, M. A. Formation of a Fluorous/Organic Biphasic Supramolecular Octopus Assembly for Enhanced Porphyrin Phosphorescence in Air. *Angew. Chem., Int. Ed.* **2015**, *54*, 4842−4846.
(178) Zhan, S.-Z.; Jiang, X.; Zheng, J.; Huang, X.-D.; Chen, G.-H.; Li, D. A Luminescent Supramolecular $Cu_2I_2(NH_3)_2$-Sandwiched $Cu_3(Pyrazolate)_3$ Adduct as a Temperature Sensor. *Dalton Trans.* **2018**, *47*, 3679−3683.
(179) Tsupreva, V. N.; Titov, A. A.; Filippov, O. A.; Bilyachenko, A. N.; Smol'yakov, A. F.; Dolgushin, F. M.; Agapkin, D. V.; Godovikov, I. A.; Epstein, L. M.; Shubina, E. S. Peculiarities of the Complexation of Copper and Silver Adducts of a 3,5-Bis(Trifluoromethyl)Pyrazolate Ligand with Organoiron Compounds. *Inorg. Chem.* **2011**, *50*, 3325−3331.
(180) Titov, A. A.; Smol'yakov, A. F.; Filippov, O. A.; Godovikov, I. A.; Muratov, D. A.; Dolgushin, F. M.; Epstein, L. M.; Shubina, E. S. Supramolecular Design of the Trinuclear Silver(I) and Copper(I) Metal Pyrazolates Complexes with Ruthenium Sandwich Compounds via Intermolecular Metal−π Interactions. *Cryst. Growth Des.* **2017**, *17*, 6770−6779.
(181) Titov, A. A.; Filippov, O. A.; Guseva, E. A.; Smol'yakov, A. F.; Dolgushin, F. M.; Epstein, L. M.; Belsky, V. K.; Shubina, E. S. Role of Basic Sites of Substituted Ferrocenes in Interaction with the Trinuclear 3,5-Bis(Trifluoromethyl)Pyrazolates: Thermodynamics and Structure of Complexes. *RSC Adv.* **2014**, *4*, 8350−8359.
(182) Filippov, O. A.; Titov, A. A.; Guseva, E. A.; Loginov, D. A.; Smol'yakov, A. F.; Dolgushin, F. M.; Belkova, N. V.; Epstein, L. M.; Shubina, E. S. Remarkable Structural and Electronic Features of the Complex Formed by Trimeric Copper Pyrazolate with Pentaphosphaferrocene. *Chem. - Eur. J.* **2015**, *21*, 13176−13180.
(183) Jayaratna, N. B.; Olmstead, M. M.; Kharisov, B. I.; Dias, H. V. R. Coinage Metal Pyrazolates $[(3,5\text{-}(CF_3)_2Pz)M]_3$ (M = Au, Ag, Cu) as Buckycatchers. *Inorg. Chem.* **2016**, *55* (17), 8277−8280.
(184) Ulloa, C. O.; Ponce-Vargas, M.; Muñoz-Castro, A. Formation of Coinage-Metal···Fullerene Adducts. Evaluation of the Interaction Nature Between Triangular Coinage Metal Complexes (M_3 = Cu, Ag, and Au) and C_{60} Through Relativistic Density Functional Theory Calculations. *J. Phys. Chem. C* **2018**, *122*, 25110−25117.
(185) Jahnke, A. C.; Pröpper, K.; Bronner, C.; Teichgräber, J.; Dechert, S.; John, M.; Wenger, O. S.; Meyer, F. A New Dimension in Cyclic Coinage Metal Pyrazolates: Decoration with a Second Ring of Coinage Metals Supported by Inter-Ring Metallophilic Interactions. *J. Am. Chem. Soc.* **2012**, *134*, 2938−2941.
(186) Balch, A. L.; Doonan, D. J. Mixed Valence Gold Chemistry: Stepwise Oxidation of a Cyclic Trigold(I) Complex. *J. Organomet. Chem.* **1977**, *131*, 137−146.
(187) Vickery, J. C.; Balch, A. L. X-Ray Crystallographic Studies of the Products of Oxidative Additions of Iodine to Cyclic Trinuclear Gold(I) Complexes: Directional Effects for Au−I···I−Au Interactions. *Inorg. Chem.* **1997**, *36*, 5978−5983.
(188) Winkler, K.; Wysocka-Żołopa, M.; Rećko, K.; Dobrzyński, L.; Vickery, J. C.; Balch, A. L. Formation of a Partially Oxidized Gold

https://dx.doi.org/10.1021/acs.chemrev.0c00011
Chem. Rev. 2020, 120, 9675−9742

Compound by Electrolytic Oxidation of the Solvoluminescent Gold(I) Trimer, $Au_3(MeN{=}COMe)_3$. *Inorg. Chem.* **2009**, *48*, 1551−1558.
(189) Raptis, R. G.; Fackler, J. P., Jr. Synthesis and Crystal Structure of a Mixed-Valence, Au^I_2/Au^{III}, Pyrazolato Complex Stable in Aqua Regia. X-Ray Photoelectron Study of Homo- and Heterovalent Gold-Pyrazolato Trimers. *Inorg. Chem.* **1990**, *29*, 5003−5006.
(190) Raptis, R. G.; Murray, H. H.; Fackler, J. P., Jr The Structure of $[Au\text{-}\mu\text{-}\{3,5\text{-}(C_6H_5)_2C_3HN_2\}]_3Cl_2$: A Trinuclear Mixed-Valence Gold Pyrazolate Complex. *Acta Crystallogr., Sect. C: Cryst. Struct. Commun.* **1988**, *44*, 970−973.
(191) Yang, G.; Raptis, R. G. Oxidation of Gold(I) Pyrazolates by Aqua Regia. X-Ray Crystal Structures of the First Examples of Trinuclear Au^{III}_3 And $Au^IAu^{III}_2$ Pyrazolato Complexes. *J. Chem. Soc., Dalton Trans.* **2002**, *21*, 3936−3938.
(192) Bonati, F.; Burini, A.; Rosa Pietroni, B.; Bovio, B. Rosa Pietroni, B.; Bovio, B. Reactions of Symmetric C-Imidazolylgold(I) Leading to Au^I Carbene Complexes or Mixed Valence or AuIII Imidazolyl Derivatives. Crystal Structure of [1-Benzyl-3-(carboethoxy)-imidazolin-2-yliden]chlorogold(I). *J. Organomet. Chem.* **1991**, *408*, 271−280.
(193) Bovio, B.; Burini, A.; Pietroni, B. R. Reactions of Trimeric 1-Benzyl-2-Gold(I)Imidazole Leading to AuI Carbene Complexes. Crystal Structure of [1-Benzyl-3-benzoyl-imidazolin-2-yliden]-chlorogold(I). *J. Organomet. Chem.* **1993**, *452*, 287−291.
(194) Bovio, B.; Calogero, S.; Wagner, F. E.; Burini, A.; Pietroni, B. R. A ^{197}Au Mössbauer Study of Reaction Products of Trimeric 1-Benzyl-2-Gold(I)-Imidazole Leading to Au^I Carbene or Au^I Imidazoline Complexes and Trinuclear Au^{III} Imidazolyl Derivatives. X-Ray Crystal Structure of $[\{(\mu\text{-}1\text{-Benzylimidazolato-}N^3,C^2)Au\}_3I_2]$. *J. Organomet. Chem.* **1994**, *470*, 275−283.
(195) Ardizzoia, G. A.; Angaroni, M. A.; La Monica, G.; Cariati, F.; Cenini, S.; Moret, M.; Masciocchi, N. Reaction of Dioxygen with Poly[(3,5-dimethylpyrazolato)copper]. Crystal Structure, Reactivity, and Catalytic Properties of $[Cu_8(dmpz)_8(OH)_8]$. *Inorg. Chem.* **1991**, *30*, 4347−4353.
(196) Butler, I. S.; Harrod, J. F. *Inorganic Chemistry: Principles and Applications*; Benjamin/Cummings: Redwood City, CA, 1989
(197) Masciocchi, N.; Cairati, P.; Sironi, A. Crystal Structure Determination of Molecular Compounds from Conventional Powder Diffraction Data: Trimeric Silver(I) 3,5-Dimethylpyrazolate. *Powder Diffr.* **1998**, *13*, 35−40.
(198) Li, R. Bis{tris[μ-2-(1*H*-Pyrazol-3-yl-κN^1:κN^2)pyridinato-κN]-Trisilver(I)}(2 *Ag*—*Ag*). *Acta Crystallogr., Sect. E: Struct. Rep. Online* **2007**, *63*, m1640.
(199) An, Z.; Zhou, R.-J. *Cyclo*-Tris[μ-5-(2-Pyridyl)Pyrazol-1-ido-κ^3N^1,N^5:N^2]Trisilver(I). *Acta Crystallogr., Sect. E: Struct. Rep. Online* **2009**, *65*, m1335.
(200) Xing, L.-R.; Lu, Z.; Li, M.; Zheng, J.; Li, D. Revealing High-Lying Intersystem Crossing in Brightly Luminescent Cyclic Trinuclear Cu^I/Ag^I Complexes. *J. Phys. Chem. Lett.* **2020**, *11*, 2067−2073.
(201) Dias, H. V. R.; Diyabalanage, H. V. K. Trimeric Silver(I) Pyrazolates with Isopropyl, Bromo, and Nitro Substituents: Synthesis and Characterization of $\{[3,5\text{-}(i\text{-}Pr)_2Pz]Ag\}_3$, $\{[3,5\text{-}(i\text{-}Pr)_2,4\text{-}(Br)Pz]\text{-}Ag\}_3$, And $\{[3,5\text{-}(i\text{-}Pr)_2,4\text{-}(NO_2)Pz]Ag\}_3$. *Polyhedron* **2006**, *25*, 1655−1661.
(202) Yang, G.; Wang, Y.-L.; Li, J.-P.; Zhu, Y.; Wang, S.-M.; Hou, H.-W.; Fan, Y.-T.; Ng, S. W. Anion-Dependent Structural Diversity in Silver(I) Complexes of 4-Amino-3,5-Diisopropyl-1,2,4-Triazole. *Eur. J. Inorg. Chem.* **2007**, *2007*, 714−719.
(203) Wang, Z.; Begum, S.; Krautscheid, H. Solid-State Ring-Opening Structural Transformation in Triazolyl Ethanesulfonate Based Silver Complexes. *Cryst. Growth Des.* **2016**, *16*, 5836−5842.
(204) Balch, A. L.; Olmstead, M. M.; Vickery, J. C. Gold(I) Compounds Without Significant Aurophilic Intermolecular Interactions: Synthesis, Structure, and Electronic Properties of $Ph_3PAuC(O)NHMe$ and $Au_3(PhCH_2N{=}COMe)_3$: Comparative Monomeric and Trimeric Analogues of the Solvoluminescent Trimer, $Au_3(MeN{=}COMe)_3$. *Inorg. Chem.* **1999**, *38*, 3494−3499.
(205) White-Morris, R. L.; Olmstead, M. M.; Attar, S.; Balch, A. L. Intermolecular Interactions in Polymorphs of Trinuclear Gold(I) Complexes: Insight into the Solvoluminescence of $AuI_3(MeN{=}COMe)_3$. *Inorg. Chem.* **2005**, *44*, 5021−5029.
(206) Fujisawa, K.; Yamada, S.; Yanagi, Y.; Yoshioka, Y.; Kiyohara, A.; Tsutsumi, O. Tuning the Photoluminescence of Condensed-Phase Cyclic Trinuclear Au(I) Complexes Through Control of Their Aggregated Structures by External Stimuli. *Sci. Rep.* **2015**, *5*, 7934.
(207) Chilukuri, B.; McDougald, R. N., Jr.; Ghimire, M. M.; Nesterov, V. N.; Mazur, U.; Omary, M. A.; Hipps, K. W. Polymorphic, Porous, and Host−Guest Nanostructures Directed by Monolayer−Substrate Interactions: Epitaxial Self-Assembly Study of Cyclic Trinuclear Au(I) Complexes on HOPG at the Solution−Solid Interface. *J. Phys. Chem. C* **2015**, *119*, 24844−24858.
(208) Elbjeirami, O.; Rashdan, M. D.; Nesterov, V.; Rawashdeh-Omary, M. A. Structure and Luminescence Properties of a Well-Known Macrometallocyclic Trinuclear Au(I) Complex and Its Adduct with a Perfluorinated Fluorophore Showing Cooperative Anisotropic Supramolecular Interactions. *Dalton Trans.* **2010**, *39*, 9465−9468.
(209) Molčanov, K.; Kojić-Prodić, B. Towards Understanding π-Stacking Interactions Between Non-Aromatic Rings. *IUCrJ* **2019**, *6*, 156−166.
(210) Dias, H. V. R.; Gamage, C. S. P.; Keltner, J.; Diyabalanage, H. V. K.; Omari, I.; Eyobo, Y.; Dias, N. R.; Roehr, N.; McKinney, L.; Poth, T. Trinuclear Silver(I) Complexes of Fluorinated Pyrazolates. *Inorg. Chem.* **2007**, *46*, 2979−2987.
(211) Schmidbaur, H. Ludwig Mond Lecture. High-carat Gold Compounds. *Chem. Soc. Rev.* **1995**, *24*, 391−400.
(212) Pyykkö, P. Strong Closed-Shell Interactions in Inorganic Chemistry. *Chem. Rev.* **1997**, *97*, 597−636.
(213) Katz, M. J.; Sakai, K.; Leznoff, D. B. The Use of Aurophilic and Other Metal−Metal Interactions as Crystal Engineering Design Elements to Increase Structural Dimensionality. *Chem. Soc. Rev.* **2008**, *37*, 1884−1895.
(214) Grosu, Y.; Li, M.; Peng, Y.-L.; Luo, D.; Li, D.; Faik, A.; Nedelec, J.-M.; Grolier, J.-P. A Highly Stable Nonhysteretic $\{Cu_2(tebpz)$ MOF +Water$\}$ Molecular Spring. *ChemPhysChem* **2016**, *17*, 3359−3364.
(215) Lowe, A.; Tsyrin, N.; Chorazewski, M.ła.; Zajdel, P.ł; Mierzwa, M.ł; Leao, J. B.; Bleuel, M.; Feng, T.; Luo, D.; Li, M.; Li, D.; Stoudenets, V.; Pawlus, S.; Faik, A.; Grosu, Y. Effect of Flexibility and Nanotriboelectrification on the Dynamic Reversibility of Water Intrusion Into Nanopores: Pressure-Transmitting Fluid with Frequency-Dependent Dissipation Capability. *ACS Appl. Mater. Interfaces* **2019**, *11*, 40842−40849.
(216) Turro, N. J. *Modern Molecular Photochemistry*; University Science Books, 1991.
(217) Ovejero, P.; Mayoral, M. J.; Cano, M.; Lagunas, M. C. Luminescence of Neutral and Ionic Gold(I) Complexes Containing Pyrazole or Pyrazolate-Type Ligands. *J. Organomet. Chem.* **2007**, *692*, 1690−1697.
(218) Zhang, M.; Mang, C.; Wu, K. Ab Initio Study on Luminescent Properties of Triangular Au(I) Complexes. *J. Mol. Struct.: THEOCHEM* **2006**, *759*, 35−39.
(219) Haneline, M. R.; Tsunoda, M.; Gabbaï, F. P. π-Complexation of Biphenyl, Naphthalene, and Triphenylene to Trimeric Perfluoro-*ortho*-Phenylene Mercury. Formation of Extended Binary Stacks with Unusual Luminescent Properties. *J. Am. Chem. Soc.* **2002**, *124*, 3737−3742.
(220) Muñoz-Castro, A.; MacLeod Carey, D.; Arratia-Pérez, R. Calculated Molecular Properties of Triangular Tribenzo and Perfluoro-Tribenzo Trimercuronin Macrocycles. *J. Phys. Chem. A* **2010**, *114*, 666−672.
(221) Xiao, Q.; Zheng, J.; Li, M.; Zhan, S.-Z.; Wang, J.-H.; Li, D. Mechanically Triggered Fluorescence/Phosphorescence Switching in the Excimers of Planar Trinuclear Copper(I) Pyrazolate Complexes. *Inorg. Chem.* **2014**, *53*, 11604−11615.
(222) Earl, L. D.; Nagle, J. K.; Wolf, M. O. Tuning the Extended Structure and Electronic Properties of Gold(I) Thienyl Pyrazolates. *Inorg. Chem.* **2014**, *53*, 7106−7117.

https://dx.doi.org/10.1021/acs.chemrev.0c00011
Chem. Rev. 2020, 120, 9675−9742

(223) Tian, Y.; Wang, Z.-Y.; Zang, S.-Q.; Li, D.; Mak, T. C. W. Luminescent Cyclic Trinuclear Coinage Metal Complexes with Aggregation-Induced Emission (AIE) Performance. *Dalton Trans.* **2019**, *48*, 2275−2279.
(224) Hofbeck, T.; Monkowius, U.; Yersin, H. Highly Efficient Luminescence of Cu(I) Compounds: Thermally Activated Delayed Fluorescence Combined with Short-Lived Phosphorescence. *J. Am. Chem. Soc.* **2015**, *137*, 399−404.
(225) Föller, J.; Kleinschmidt, M.; Marian, C. M. Phosphorescence or Thermally Activated Delayed Fluorescence? Intersystem Crossing and Radiative Rate Constants of a Three-Coordinate Copper(I) Complex Determined by Quantum-Chemical Methods. *Inorg. Chem.* **2016**, *55*, 7508−7516.
(226) Aguiló, E.; Moro, A. J.; Outis, M.; Pina, J.; Sarmento, D.; Seixas de Melo, J. S.; Rodríguez, L.; Lima, J. C. Deactivation Routes in Gold(I) Polypyridyl Complexes: Internal Conversion vs Fast Intersystem Crossing. *Inorg. Chem.* **2018**, *57*, 13423−13430.
(227) Hamze, R.; Jazzar, R.; Soleilhavoup, M.; Djurovich, P. I.; Bertrand, G.; Thompson, M. E. Phosphorescent 2-, 3- and 4-Coordinate Cyclic(Alkyl)(Amino)Carbene (CAAC) Cu(I) Complexes. *Chem. Commun.* **2017**, *53*, 9008−9011.
(228) Gernert, M.; Müller, U.; Haehnel, M.; Pflaum, J.; Steffen, A. A Cyclic Alkyl(Amino)Carbene as Two-Atom-π-Chromophore Leading to the First Phosphorescent Linear Cu(I) Complexes. *Chem. - Eur. J.* **2017**, *23*, 2206−2216.
(229) Shi, S.; Jung, M. C.; Coburn, C.; Tadle, A.; Sylvinson, M. R. D.; Djurovich, P. I.; Forrest, S. R.; Thompson, M. E. Highly Efficient Photo- and Electroluminescence from Two- Coordinate Cu(I) Complexes Featuring Nonconventional N-Heterocyclic Carbenes. *J. Am. Chem. Soc.* **2019**, *141*, 3576−3588.
(230) Hamze, R.; Peltier, J. L.; Sylvinson, D.; Jung, M.; Cardenas, J.; Haiges, R.; Soleilhavoup, M.; Jazzar, R.; Djurovich, P. I.; Bertrand, G.; Thompson, M. E. Eliminating Nonradiative Decay in Cu(I) Emitters: > 99% Quantum Efficiency and Microsecond Lifetime. *Science* **2019**, *363*, 601−606.
(231) Hamze, R.; Shi, S.; Kapper, S. C.; Ravinson, D. S. M.; Estergreen, L.; Jung, M. C.; Tadle, A.; Haiges, R.; Djurovich, P. I.; Peltier, J. L.; Jazzar, R.; Bertrand, G.; Bradforth, S. E.; Thompson, M. E. Quick-Silver" From a Systematic Study of Highly Luminescent, Two-Coordinate, d^{10} Coinage Metal Complexes. *J. Am. Chem. Soc.* **2019**, *141*, 8616−8626.
(232) Li, T.-Y.; Ravinson, D. S. M.; Haiges, R.; Djurovich, P. I.; Thompson, M. E. Enhancement of the Luminescent Efficiency in Carbene-Au(I)-Aryl Complexes by the Restriction of Renner−Teller Distortion and Bond Rotation. *J. Am. Chem. Soc.* **2020**, *142*, 6158−6172.
(233) Mohamed, A. A.; Rawashdeh-Omary, M. A.; Omary, M. A.; Fackler, J. P., Jr. External Heavy-Atom Effect of Gold in a Supramolecular Acid−Base π Stack. *Dalton Trans.* **2005**, *41*, 2597−2602.
(234) Omary, M. A.; Elbjeirami, O.; Gamage, C. S. P.; Sherman, K. M.; Dias, H. V. R. Sensitization of Naphthalene Monomer Phosphorescence in a Sandwich Adduct with an Electron-Poor Trinuclear Silver(I) Pyrazolate Complex. *Inorg. Chem.* **2009**, *48*, 1784−1786.
(235) Vickery, J. C. Solvoluminescence. Remarkable Photophysical and Structural Properties of Inorganic Complexes Displaying Long-Range Au···Au, Ir···Ir, and I···I Interactions; Ph.D. Thesis; University of California, Davis, CA, USA, 1998.
(236) Zink, J. I. Triboluminescence. *Acc. Chem. Res.* **1978**, *11*, 289−295.
(237) Zink, J. I.; Chandra, B. P. Light Emission During Growth and Destruction of Crystals. Crystalloluminescence and Triboluminescence. *J. Phys. Chem.* **1982**, *86*, 5−7.
(238) Reynolds, G. T. Lyoluminescence. *J. Lumin.* **1992**, *54*, 43−69.
(239) Zhu, L.; Coropceanu, V.; Yi, Y.; Chilukuri, B.; Cundari, T. R.; Brédas, J.-L. Electronic and Charge-Transport Properties of the $Au_3(CH_3N = COCH_3)_3$ Crystal: a Density Functional Theory Study. *J. Phys. Chem. Lett.* **2013**, *4*, 2186−2189.
(240) Rabaâ, H.; Omary, M. A.; Taubert, S.; Sundholm, D. Insights Into Molecular Structures and Optical Properties of Stacked $[Au_3(RN = CR')_3]_n$ Complexes. *Inorg. Chem.* **2018**, *57*, 718−730.
(241) Greiner, J.; Valiev, R. R.; Sundholm, D. Photophysical Properties of the Triangular $[Au(HN = COH)]_3$ Complex and Its Dimer. *Phys. Chem. Chem. Phys.* **2020**, *22*, 10314−10321.
(242) Hardt, H. D.; Pierre, A. Fluorescence Thermochromism of Pyridine Copper Iodides and Copper Iodide. *Z. Anorg. Allg. Chem.* **1973**, *402*, 107−112.
(243) Hardt, H. D.; Pierre, A. Fluorescence Thermochromism and Symmetry of Copper(I) Complexes. *Inorg. Chim. Acta* **1977**, *25*, L59−L60.
(244) Ford, P. C.; Cariati, E.; Bourassa, J. Photoluminescence Properties of Multinuclear Copper(I) Compounds. *Chem. Rev.* **1999**, *99*, 3625−3647.
(245) De Angelis, F.; Fantacci, S.; Sgamellotti, A.; Cariati, E.; Ugo, R.; Ford, P. C. Electronic Transitions Involved in the Absorption Spectrum and Dual Luminescence of Tetranuclear Cubane $[Cu_4I_4(Pyridine)_4]$ Cluster: a Density Functional Theory/Time-Dependent Density Functional Theory Investigation. *Inorg. Chem.* **2006**, *45*, 10576−10584.
(246) Perruchas, S.; Tard, C.; Le Goff, X. F.; Fargues, A.; Garcia, A.; Kahlal, S.; Saillard, J.-Y.; Gacoin, T.; Boilot, J.-P. Thermochromic Luminescence of Copper Iodide Clusters: the Case of Phosphine Ligands. *Inorg. Chem.* **2011**, *50*, 10682−10692.
(247) Wenger, O. S. Vapochromism in Organometallic and Coordination Complexes: Chemical Sensors for Volatile Organic Compounds. *Chem. Rev.* **2013**, *113*, 3686−3733.
(248) Zhang, X.; Li, B.; Chen, Z.-H.; Chen, Z.-N. Luminescence Vapochromism in Solid Materials Based on Metal Complexes for Detection of Volatile Organic Compounds (VOCs). *J. Mater. Chem.* **2012**, *22*, 11427−15.
(249) Chi, Y.; Lay, E.; Chou, T.-Y.; Song, Y.-H.; Carty, A. J. Deposition of Silver Thin Films Using the Pyrazolate Complex $[Ag(3,5\text{-}(CF_3)_2C_3HN_2)]_3$. *Chem. Vap. Deposition* **2005**, *11*, 206−212.
(250) Yaseen, W. K.; Sanders, S. F.; Almotawa, R. M.; Otten, B. M.; Bhat, S.; Alamo, D. C.; Marpu, S. B.; Golden, T. D.; Omary, M. A. Are Metal Complexes "Organic," "Inorganic," "Organometallic," or "Metal-Organic" Materials? a Case Study for the Use of Trinuclear Coinage Metal Complexes as "Metal-Organic Coatings" for Corrosion Suppression on Aluminum Substrates. *Comments Inorg. Chem.* **2019**, *39*, 1−26.
(251) Burress, C. N.; Bodine, M. I.; Elbjeirami, O.; Reibenspies, J. H.; Omary, M. A.; Gabbaï, F. P. Enhancement of External Spin−Orbit Coupling Effects Caused by Metal−Metal Cooperativity. *Inorg. Chem.* **2007**, *46*, 1388−1395.
(252) Fraga, S.; Karwowski, J.; Saxena, K. M. S. *Handbook of Atomic Data*; Elsevier, 1976.
(253) Benton, E. N.; Marpu, S. B.; Omary, M. A. A Ratiometric Phosphorescent Silver Sensor: Detection and Quantification of Free Silver Ions Within a Silver Nanoparticles Medium. *ACS Appl. Mater. Interfaces* **2019**, *11*, 15038−15043.
(254) Anderson, P. W.; Lee, P. A.; Saitoh, M. Remarks on Giant Conductivity in TTF-TCNQ. *Solid State Commun.* **1973**, *13*, 595−598.
(255) Soria, L.; Cano, M.; Campo, J. A.; Torres, M. R.; Lodeiro, C. Silver Compounds Based on *N,N,N*-Tridentate Pyridylpyrazolate Ligands. an Opportunity to Build Cyclic Trimetallic and Oligomeric Luminescent Liquid Crystals. *Polyhedron* **2017**, *125*, 141−150.
(256) Giménez, R.; Crespo, O.; Diosdado, B.; Elduque, A. Liquid Crystalline Copper(I) Complexes with Bright Room Temperature Phosphorescence. *J. Mater. Chem. C* **2020**, *8*, 6552−6557.
(257) Kishimura, A.; Yamashita, T.; Yamaguchi, K.; Aida, T. Rewritable Phosphorescent Paper by the Control of Competing Kinetic and Thermodynamic Self-Assembling Events. *Nat. Mater.* **2005**, *4*, 546−549.
(258) Lintang, H. O.; Kinbara, K.; Tanaka, K.; Yamashita, T.; Aida, T. Self-Repair of a One-Dimensional Molecular Assembly in Mesoporous Silica by a Nanoscopic Template Effect. *Angew. Chem., Int. Ed.* **2010**, *49*, 4241−4245.

https://dx.doi.org/10.1021/acs.chemrev.0c00011
Chem. Rev. 2020, 120, 9675−9742

(259) den Boer, D.; Krikorian, M.; Esser, B.; Swager, T. M. STM Study of Gold(I) Pyrazolates: Distinct Morphologies, Layer Evolution, and Cooperative Dynamics. *J. Phys. Chem. C* **2013**, *117*, 8290−8298.
(260) Zaraiskii, A. P.; Kachurin, O. I.; Velichko, L. I.; Tikhonova, I. A.; Furin, G. G.; Shur, V. B.; Vol'pin, M. E. Cyclic Trimeric Perfluoro-*o*-Phenylenemercury as the Phase Transfer Catalyst for Nitration with Dilute Nitric Acid. *Russ. Chem. Bull.* **1994**, *43*, 507−508.
(261) Zaraisky, A. P.; Kachurin, O. I.; Velichko, L. I.; Tikhonova, I. A.; Furin, G. G.; Shur, V. B. Cyclic Trimeric Perfluoro-*o*-Phenylenemercury: a Highly Efficient Phase Transfer Catalyst for Nitration of Aromatic Substrates with Dilute Nitric Acid. *J. Mol. Catal. A: Chem.* **2005**, *231*, 103−111.

https://dx.doi.org/10.1021/acs.chemrev.0c00011
Chem. Rev. 2020, 120, 9675−9742